Systems Level Characterizations of Single and Combination Drug Mechanisms of Action *in vitro* and *in vivo*

By

Justin Pritchard

B.S. Biology

University of California Los Angeles, 2006

SUBMITTED TO THE DEPARTMENT OF BIOLOGY IN PARTIAL FULFILLMENT

OF THE REQUIREMENTS FOR THE DEGREE OF:

DOCTOR OF PHILOSOPHY IN BIOLOGY

AT THE

MASSACHUSETTS INSTITUTE OF TECHNOLOGY

June 2012

Signature of Author……..Justin Pritchard

Thesis Advisor……..Michael T. Hemann

Thesis Advisor……..Douglas A. Lauffenburger

Graduate Chair……Stephen Bell

Systems Level Characterizations of Single and Combination Drug Mechanisms of Action *in vitro* and *in vivo*

Justin Pritchard

Submitted to the Department of Biology on April 30, 2012 in partial fulfillment of the requirements for the degree of Doctor of Philosophy in Biology

Abstract

Small molecule characterization is a critical limiting step in cancer drug development. At the present time, high throughput screens of natural products and combinatorial synthesis libraries generate more pharmaceutical leads than can be characterized in detail. Lead optimization further generates many derivatives of these cytotoxic hits in an attempt to generate optimized compounds with better physical or chemical properties. This leaves many promising agents stranded in drug development and poorly characterized. In addition, most small molecules interact biochemically with a diverse set of proteins. While characterizing the diversity of biochemical interactions that can occur is important to understanding function, only a subset are likely to be necessary or sufficient for therapeutic efficacy. In light of this diversity, the functional characterization of the mechanisms of cell death by cytotoxic agents should improve drug discovery by allowing for the early prioritization of cytotoxic leads, derivatized compounds, and targeted inhibitors on the basis of the mechanisms by which they cause death in intact cells. Using RNAi mediated suppression of key mediators of apoptosis; we found that we could predict the functional mechanisms of drug action in lymphoma cells across many categories of cytotoxic therapeutics with as few as 8 shRNAs.

Beyond single drug mechanisms, most drugs used in cancer are used as drug combinations. These combinations were largely formulated on two principles: compounds must have a unique mechanism of action so that more cumulative drug can be dosed with non-overlapping toxicity, and they must have statistically independent mechanisms of drug resistance. However, beyond clinical efficacy, the basic mechanisms of combination therapy have never been examined. Thus, in light of the central role of apoptosis in guiding mammalian cell death to cancer therapy, we sought to examine the functional signatures of cell death in the face of combination therapy. Surprisingly we find that RNAi mediated suppression of cell death mediators in response to common cytotoxic regimens, averages both sensitivity and resistance to therapy and neutralizes the effects of genetic variation. This suggests that common cytotoxic regimens are intrinsically depersonalized and difficult to genetically stratify.

Thesis Supervisors: Michael Hemann and Douglas Lauffenburger

Titles: Associate Professor of Biology and Professor of Biological Engineering, and Biology

Acknowledgements

I would like to thank my mentors Mike Hemann and Doug Lauffenburger. The collaboration between the labs was a fortunate but unexpected turn of events and I learned a great deal from both of them. Furthermore, I thank them for their patience and guidance throughout the process.

I'd like to thank all members of both labs, but especially those who I had more extensive collaborations and conversations with. Specifically, Ben Cosgrove, Luke Gilbert, Hyung-Do Kim, Corbin Meacham, Shannon Alford, Jason Doles, Christian Pallasch, Peter Bruno, Miles Miller, Joel Wagner, Pam Kreeger, and Holly Criscione. I'd also like to thank my committee members: David Housman and Frank Gertler for their guidance and support.

I am also happy for the opportunity to thank the friends and family who have supported me throughout my years at MIT. First I would like to thank my parents for always encouraging me, and enduring a string of change of major forms in college until I finally settled on biology. I would like to thank my girlfriend Beth for her support, and her comprehensive thoughts on the genre of peer review[1] , as a specialist in the field, her insights are of immense relevance to the scientific peer review process. I would also like to thank my brother Tyler for terrific scientific discussions and technical support, whether it is data analysis or scientific computing he always had an informative perspective.

1. Parfitt, Elizabeth. Establishing the Genre of Peer Review to Create New Rhetorical Knowledge. *Compendium 2* Vol. 5 (2012)

Table of Contents

I. Introduction

Current clinical practice in combination chemotherapy is guided by a historically successful set of principles that were developed by basic and clinical researchers 50-60 years ago. In order to approach the creation of new therapeutic combinations, it is critical to understand the classic combination therapy principles and the original experimental rationales behind them. A commonly accepted principle is that combination therapies with statistically independent mechanisms of action can minimize drug resistance. A second is that in order to kill enough cancer cells to cure a patient, multiple drugs must be delivered at their maximum tolerated dose. This allows for more cancer cell killing and manageable toxicity. In light of these models, we aim to explore recent genomic evidence of what makes cancers resistant to current combination chemotherapy regimens that were built on these principles. Interestingly, much of this genomic evidence does not agree with the initial rationales of early practitioners, and while targeted therapies deviate from combination therapies in their mechanisms of clinical resistance, they have yet to be consistently incorporated into combination regimens. We suggest that systems biology approaches used to examine the responses to therapy in targeted settings have an immense opportunity to make a translational impact by developing approaches to characterize the distinctions between single and combination drug mechanisms in cancer therapy. Understanding combinations in multivariate ways should empower the next generation of combination therapies by giving a thorough understanding of cellular context and resistance.

II. Historical perspectives on cancer chemotherapy

Origins of cancer chemotherapy

The overwhelming majority of cures in cancer chemotherapy have come from the application of conventional cytotoxic chemotherapies. While some cytotoxics have been the product of serendipity, and some the product of large scale screening, others were part of the first wave of "rational" targeted therapies that were developed in the 1940's and were specifically aimed at targeting cancer cells on the basis of the nutritional properties that made them distinct from normal cells[1,2]. The history of these early successes illustrates the serendipity, and important insights that led to potentially curative regimens that we have for some forms of cancers today. It was this success that still guides a large amount of clinical practice and clinical trials.

In 1946 Goodman and Gilman published a landmark study in cancer chemotherapy. Nitrogen mustard agents that were serendipitously discovered to have drastic lymphoid cell reductions upon accidental or wartime exposure were shown to produce remarkable responses in human tumors from a variety of tissue origins [3]. Two years later Sidney Farber took a more rational target based strategy for anti-cancer drug discovery. He reasoned that if folate deficiency inhibited normal hematopoesis, and the addition of folates accelerated leukemia in children, then anti-folates would make a promising anti-leukemia drug. In his landmark 1948 paper Sidney Farber [4] observed the first true remissions in a disease where the time from diagnosis to death was often measured in days. For the purpose of context, it is interesting to note the similarities between Farber's anti-folates and current targeted therapies. Like early clinical trials with EGFR and BRAF inhibitors, these early reports documented some striking but short lasting remissions in a subset of patients, .

Combination chemotherapy

In 1942 Luria and Delbruck's fluctuation analysis [5] combining an experimental and mathematical modeling framework, showed that heritable resistance to viruses was derived

from pre-viral-exposure genetic variation in a bacterial population. Later, Newcombe [6] extended this finding to chemotherapy in bacteria, and in 1952, Law extended it to the resistance to anti-folates in *in vivo* mouse models of cancer [7]. Taken together these experiments suggested to early chemotherapy researchers that there might be a benefit to giving drugs in combination [8,9]. If a drug provided a resistance rate of 1/m and a second statistically independent (non-cross resistant) drug provided resistance of 1/n then co-resistance would occur in 1/m*n cells.

In 1958, citing the above rationales, and the successful creation of combination therapies for tuberculosis, Emil Frei III published the first randomized control trial of a combination therapy in cancer [10]. It established clear combination efficacy over the efficacy of the single substituent agents. In the mid 1960's, Howard Skipper showed that in experimental mouse models, as few as one cancer cell could give rise to lethal disease, and that chemotherapy followed a logarithmic killing model . Specifically, the same dose killed the same proportion of cells, regardless of the total disease burden [11]**.** This suggested to Skipper and some others that to have any chance of curing a cancer, a physician would have to administer as large a tolerable drug dose as is possible to the patient.

The rapid success of Emil Frei's 1958 trial, advances in supportive care, and Howard Skipper's principles for curing experimental mouse models all led to the extraordinary but not experimentally controlled adoption of the 4 drug VAMP regimen [12]. Coupled with care that was able to ameliorate the side effects of therapy and effectively dose even higher cumulative drug doses into leukemia patients, the VAMP regimen was the first big step towards the large and potentially curative regimens that we have today. It is important to note that this type of study (in which combinations of drugs are combined at maximally tolerated doses) is not able to specify the mechanism of increased efficacy to increased drug dose, or the minimization of the outgrowth of resistance, but it can and did demonstrate large efficacy. It was this bold, but less carefully controlled strategy that led to the rapid and successful adoption of combination

chemotherapy for many cancers, and by 1973 [13] had revolutionized the treatment of cancer, and found cures for previously untreatable diseases. Thus, it is interesting to note that the biggest early successes of cancer therapy owe less to systematic controlled trials and more to bold and decisive attempts to cure very sick patients.

These early and impressive successes fostered a manner of thinking about care that still largely dictates current clinical practice in combination therapy, and many clinical trials using a similar process are still being improving the current standard of care [14],[15]. Next, we examine current genomic evidence of what makes cells resistant to combination therapy in a clinical setting in light of the models and rationales of early combination regimens.

III. Clinical efficacy and resistance of combination therapy

The initial rationales behind the first combination therapy regimens suggested that 1. The maximum possible cumulative dose of drug should be given, and 2. Independent drugs with non-overlapping mechanisms of action are important for minimizing the probability of therapeutic resistance. The ideas about resistance have only been tested in the context of cross resistance following the selection of single drug resistant cell lines in Luria-Delbruck fluctuation tests. However, the genomic evidence in relapsed cancers following clinical combination treatment in multiple systems suggests that this microbiology inspired rationale, while true in the context of infectious diseases like tuberculosis and HIV [16] [17], is very different in the context of relapsed human cancers that are initially sensitive to combination chemotherapy. In order to think about how systems biology might inform drug selection and the clinical trials process we must consider how current clinical combinations fail in patients.

Genomics of clinical relapse in leukemias suggests multidrug resistant cell states

To examine the true clinical nature of acquired drug resistance in cancer, one must examine pre and post treatment matched patient samples. The first study to analyze recurrent genomic alterations in cohorts of matched pre-treatment and post relapse patients performed copy number analysis on acute lymphoblastic leukemia samples [18]. Mullighan et al. had two striking results that speak to both the historic rationales for combination therapy and the current studies on therapeutic resistance. First, the majority of relapse clones are low frequency variants that were progenitors of the dominant diagnosis clone. Second, the majority of alterations that dominated at relapse did not include direct alterations in the known biochemical targets of common therapeutics that are used for leukemia treatment. The most common alterations tended to affect B-Cell development, and might be hypothesized to promote generally drug resistant cell states, or homing to developmental niches that promote therapeutic resistance. In a later study by the same group, the sequencing of selected exons in matched pre-treatment and post treatment samples, identified recurrent mutations in the same developmental pathways, as well as CREBBP and genes that induce transcriptional states that correlate with drug resistance [19]. Finally, most recently, matched AML samples were also found to contain mutations in genes that were not related to the direct drug targets of frontline chemotherapeutic action [20]. Though these studies employ single measurement methodologies (sequencing or CNA), taken together they suggest that relapsed leukemias treated with multi-agent regimens develop resistance profiles that favor the development of a multi-drug resistant cell state. This state appears to be broad in its definition, but includes the alteration of apoptotic, epigenetic, and developmental cell states.

Clinical drug resistance to targeted therapy is pathway specific

Drug resistance to targeted single agent therapy is qualitatively distinct from drug resistance to combination regimens. Following the treatment of CML with Imatinib, it was noted that resistant cells harbored a spectrum of resistance mutations in the Bcr-Abl kinase domain.

Notably, some of these resistance mutations could be overcome by a distinct drug, Dasatinib. While still competitively inhibiting BCR-Abl, Dasatinib was found to have improved efficacy over Imatinib for most Imatinib induced kinase domain mutations [21], [22].

But how might this discovery be used to make effective drug combinations? Surprisingly when used in a temporally distinct manner, these two kinase inhibitors, whose spectrum of mutations are somewhat distinct can be alternatingly dosed over the course of the disease to stave off resistance, as long as compound mutations or single mutations causing resistance to both drugs are not present, furthermore, they suggest that compound mutations and the T315I mutation may be sensitive to combination with an aurora kinase inhibitor [23].This most common resistance mutation, the T315I mutation is poorly treatable with current methods, but recently in pre-clinical studies, two other distinct combination strategies have emerged. In an attempt to independently inhibit the BCR-Abl protein directly, allosteric inhibitors that bind to the myristate binding groove of the Abl protein were recently developed, that in combination with kinase domain targeted therapies are capable of treating T315I positive disease in tumor bearing mice[24]. Another approach utilized combinations of conventional cytotoxic drugs (L-Asparaginase and Dexamethasone) to prevent T315I mediated resistance in a mouse model of BCR-Abl positive acute lymphoblastic leukemia [25]. These strategies illustrate the opposing paradigms in how chemotherapy researchers may attempt to create next generation regimens with targeted therapeutics. While both studies have examined the T315I allele in the resistant disease that emerges following treatment in pre-clinical models, an unbiased look at the genomic mechanisms of the relapse that does occur has not been investigated.

While these are the most advanced efforts to rationally build clinical regimens to circumvent targeted resistance, similar investigations into the modes of targeted resistance in the hedgehog pathway in medullablastoma confirms the prevalence of on target pathway mutations [26] in targeted therapy. Studies in EGFR treated lung cancers have identified

amplifications in the Met receptor tyrosine kinase, an example of a parallel pathway activation mechanism inducing resistance to targeted therapy [27]. Furthermore broader studies in BRAFV600E treated melanoma employed a targeted re-sequencing strategy to identify downstream mutations in Mek [28]. This data suggests that these resistance models (mutations directly in the pathways of drug action or parallel to drug action in drug sensitive cancers) could be generalized to many targeted therapeutics. With this in mind there is a rising call for the use of these agents in combination regimens. The rationale is highly similar to the original rationale for the first regimens i.e. that the addition of independent drugs stops targeted therapeutic resistance. Just like the initial regimens, in the context of combination therapy, it will be important to consider whether the therapeutic combinations adopted are actually able to shift mechanisms of therapeutic resistance, or whether they increase the effective amount of killing, or both. These and other distinctions will be critical in understanding and stopping the resistance that might develop.

Single dosed cytotoxic drugs can produce drug target mutations in model systems

The comparison between conventional regimen resistance and targeted therapeutic resistance is obscured by the fact that current regimens contain multiple drugs that are not specifically targeted at oncogenic pathways, and because targeted therapeutics are almost always dosed in combination. This makes it difficult to directly compare the clinical mechanisms of drug resistance following singular cytotoxic therapy. In spite of this, some pre-clinical evidence suggests that many classic chemotherapeutic agents, when dosed in isolation can harbor very similar modes of resistance to the targeted therapies.

Traditional chemotherapeutic agents are often generally thought of as being remarkably pleiotropic, however, this is not a good description of all cytotoxic chemotherapies. While nitrogen mustards and cisplatin are highly chemically reactive, and nucleoside analogs can

incorporate into DNA and RNA, other drugs such as methotrexate, camptothecin, doxorubicin,and dexamethasone [29-32] make direct and specific contacts with their enzymatic targets. An examination of the preclinical literature suggests that in the case of both camptothecin and methotrexate, resistance to these agents can result in direct modifications to their respective drug targets [33]. Though many selection experiments have also revealed the role of MDR in single agent cross resistance, if MDR is inhibited and anthracycline resistance is selected for, it can switch the resistance profile back to a target dependent (Topoisomerase II alpha) mechanism of drug resistance [34] This is in contrast to the clinical picture of multidrug resistance portrayed above. Thus in the absence of direct evidence, it is interesting to speculate that the direct target mediated resistance of specific inhibitors is difficult to select for in the face of current clinical combination therapy regimens, and that this is due to the combination of classic chemotherapeutic agents, and not the nature of the agents themselves.

Functional mechanisms of clinical efficacy in combination therapy

If a property of combination therapy in human cancers is that it causes multi-drug resistant cell states, the distinctions between infectious disease and cancer may be indicative of the complex biology behind cell death in mammalian cells [35], and cancer's sensitivity to perturbations in cell death pathways. Recently it has been shown that in patient clinical samples and primary tissues the proximity to the apoptotic threshold in cancer cells, as measured by the sensitivity of the mitochondria to pro-apoptotic peptides, is correlated with therapeutic response, and the size of the therapeutic window that a drug can achieve. Thus, the proximity of cancer cells to the apoptotic threshold is responsible for the therapeutic responsiveness in mammalian cancers [36]. If maximizing the therapeutic dosing across the apoptotic spectrum increases the effective dose of drug and maximally activates apoptosis as a therapeutic response, then it is interesting to speculate that the resistance patterns in targeted

therapies may be due to the fact that they haven't been formulated into potent and curative regimens.

Predicting phenotypic response to drug action in mammalian cells

Cancer cells exist in a multivariate landscape [37]. Beyond oncogene and tumor suppressor signaling, drugs activate and inhibit cellular pathways, as does the microenvironment. While there is an impressive complexity to drug response, a variety of modeling approaches, each requiring different levels of molecular detail, and each uniquely suited to different types of data have begun to make progress in predicting drug effects across different cellular contexts. Predictive *in vitro* models of cellular systems may be effective ways to predict the cellular context in which a small molecule or a combination of small molecules might be active. Though most often employed in the context of targeted therapeutic inhibition, the lessons and methods of these studies can be used to examine any cytotoxic combination.

In well-studied systems with well-characterized pathways, it is possible to use differential equations of biochemical reactions to describe the mechanisms by which pro/antiapoptotic signals are conveyed in biochemical networks. This approach has demonstrated that even non oncogenic signaling proteins can be targets for drug intervention. Schoerbel et al. showed that Erb3 inhibition decreases AKT phosphorylation across a broad range of initial conditions [38]. The utility of Erb3 inhibition across a range of initial conditions demonstrates the power of *in silico* modeling to identify drug targets that have low context dependence. Importantly from a methodological perspective, to make a useful model, all biochemical parameters do not have to be known a priori. They can be estimated by first discovering highly sensitive species in the set of biochemical reactions. Then, using simulated annealing, many parameters can be fit to cell

line data. With these fit parameters incorporated, novel understanding of signaling network function can emerge [39]. While these approaches have proven their effectiveness for targeted therapeutic discovery, they remain underutilized for conventional cytotoxic therapeutics. However, similar types of models of DNA damage have been built to describe other phenomena, and may be used in the future to inform the therapeutic efficacy for conventional therapies.

When biochemical reactions are less described, higher levels of model abstraction can be used to understand the effect that biochemical reactions have upon cell outcome, even if the reactions are not modeled explicitly. Using partial least squares regression modeling in mammalian cells, Janes et al. suggested that given TNF-alpha induced cell death and opposing growth factor stimuli, kinase pathway interventions could be accurately predicted in a colon cancer cell line [40,41]. Impressively, this method incorporated enough of the signaling network context that it allowed for the prediction of apoptotic responses in diverse cell lines of epithelial origin [42]. In isogenic models of RAS signaling, Kreeger et al. showed that a similar multipathway model could incorporate diverse effects on cell death that were mediated by different RAS proteins to accurately predict apoptotic response [43]. To examine questions of kinase inhibitor specificity and off target effects, Kumar et al. showed that models incorporating multivariate descriptions of signaling responses could accurately predict cellular outcomes in the presence of promiscuous kinase inhibitor activity [44]. Together these studies show that regression based models can incorporate cell type and oncogene specific network influences to estimate drug on and off target effects that contribute to therapeutic action.

While these efforts focused on predicting specific drug effects on particular species in multivariate models, drugs often have a broader spectrum of biochemical and genetic effects. This spectrum requires a drug-centric approach, utilizing profiling methods and high level

statistical modeling that can simultaneously assess multiple relevant cellular effects, and predict the most relevant alterations for cellular phenotypes.

Multivariate signatures characterizing drug action

In order to understand combinations of drugs we first have to understand single drug effects in a multivariate manner. Beyond simple drug-target biochemical interactions, most small molecules have many biochemical effects and genetic interactions; they act promiscuously on a variety of cellular enzymes and processes [45]. When considered in the context of large scale genetic screens, these same molecules harbor a diverse array of genetic interactions [464748]. Comprehensive characterization of small molecules should help establish mechanistic information on how similar two drugs effects are, and can help to identify the cellular backgrounds in which they will be more successful.

Biochemical Signatures

Most compounds exert multiple biochemical effects in cellular systems. In order to examine the pleiotropy of the enzymatic effects induced by several families of anticancer agents, many groups have begun to examine the systematic biochemical profiles of drug action. Using recombinant protein libraries, compound Kd's can be systematically measured for hundreds of kinase domains. This binding information can yield profiles of affinities that broadly describe kinase inhibitor specificity. When plotted on phylogenetic trees of kinase sequence similarity, selectivity profiles of kinase inhibitors can be easily visualized [49]. Because kinase inhibitors are competitive inhibitors of ATP binding, a recent effort has extended the analysis of the selectivity of kinase inhibitors to the measurement of kinase activity in the presence of high ATP concentrations to more closely approximate cellular effects. This allows for the clustering of drugs based upon their relative kinase activity and the discovery of new drug

targets/functions for known inhibitors [50]. Together these approaches offer broad biochemical readouts of kinase inhibitor action, and allow for the biochemical classification of kinase inhibitors.

Beyond kinase activity, proteomics approaches in cell lysates can be used to couple quantitative mass spectrometry with conventional biochemical characterization approaches. Using non-specific kinase or histone-deacetylase beads as a capture reagent, proteomic signatures that are capable of semi-comprehensively assessing inhibitor function at various concentrations are used to produce inhibitor signatures of phosphorylation/de-acetylation inhibition [51,52]. Together, these biochemical approaches offer a variety of strategies for comprehensively profiling the biochemical effects of small molecules in an attempt to understand specificity and mechanism of action.

Mammalian Cell based signatures

While drugs have typically been characterized biochemically, and this can elucidate a spectrum of enzymatic effects, these biochemical characterizations often lack functional information about how a drug is actually causing cytotoxicity within a cancer cell.

The first efforts towards large scale drug characterization in mammalian cell lines were performed on the NCI 60 panel of cell lines. This panel was formed in an attempt to accelerate drug discovery for many of the intractable solid tumors that did not benefit from the first generation of combination regimen building. As a consequence of this, a large amount of screening data on thousands of novel compounds was generated by the NCI in the 1980's [53]. Upon characterizing and examining the profiles of activity for these compounds across cell lines, the NCI proposed the COMPARE approach. COMPARE sought to rank-order lists of drugs with correlated patterns of response across the entire NCI-60 panel of cell lines. Following the annotation of the NCI-60 with genetic and biochemical data, impressive efforts were undertaken

to align and cluster the cell line response data with the molecular characterization data [54,55] using the discovery algorithm. These efforts highlighted the importance of p53 and MDR in predicting cellular response to many commonly used cytotoxic compounds. Recently, utilizing the NCI data and microarray expression data for the NCI 60 cell lines the Theordescu group has suggested that it is possible to use the NCI60 data to predict drug response in completely distinct cell lines and cancer subtypes using the CONEX algorithm[56]. However, while thousands of compounds have been screened in the NCI-60 cells, and comprehensive genomic data exists, it remains difficult to mine and interpret the data that are generated in these efforts.

In 2006, a large microarray compendium, termed the connectivity map, was generated to allow producers of novel compounds to query a large database of reference compounds for relationships to an investigational compound or a disease state [57]. These searches have been suggested to not only identify a compounds' mechanism of action [58]but also allow for the querying of target signatures to produce predictions for therapeutic intervention(based on the assumption that opposing drug gene expression patterns should effectively cancel out pathogenic disease states) [59]. Finally, this work has been used by other groups to reposition drugs with similar molecular profiles but different indications [60,61]. Importantly, while these efforts have produced new proofs of concept, the signatures that are generated can be very difficult to interpret from a functional perspective. Furthermore, the published efforts to validate predictions often focus on one of the top-ranked compounds, and have not at this point rigorously validated the predictive depth of these signature-based queries.

Recently in mammalian cells, functional perturbation has also been examined to measure the differential sensitivity of cells to drugs using targeted shRNA or chemical perturbations [62,63]. Both of these methods focused on targeted feature sets that were capable of discriminating between drugs that act upon distinct subsets of biology. While the chemical approach has added resolution over non apoptotic forms of cell death, the shRNA based

approach allows for quantitative boundaries and predictions to be made using an algorithmic add-on to conventional supervised machine learning approaches. The strength of both of these approaches is that they detail specific functional relationships that alter cellular responses to a given compound.

In silico approaches

A large distinction exists for efforts that seek to model drug mechanisms of action *in silico* using datasets of clinical information since these contain data from medical practice. Campillos et al. started with a database of side effects from the unified medical language system (UMLS) and used it to build a common side effects drug interaction network. They identified sets of compounds with modest structural similarity, but high correlations in overall side effect profiles. Finally, in *in vitro* biochemical assays they confirmed common target binding [64]. While this method cannot attribute a target to a specific side effect or prove a functional role for the interaction, it is the only method that uses actual clinical data to classify drugs by their mechanism of action. Furthermore, in the future this approach may be extended to predict the mechanisms of particular side effects, and it is also interesting to speculate that common side effects profiles would indicate bad combinations in a potential regimen, and that early dismissal of combinations with close network proximity might be prioritized.

The field of signature-based prediction has developed numerous approaches to simultaneously characterize drug action beyond cell death. Signatures of drug action can tell us about inhibitor selectivity/off target effects, transcriptional response similarity, function and toxicological action. All of these indications are valuable, but if used together they might be combined in the drug development process to simultaneously characterize investigational compounds and promote their more rational and safe use.

Systems perspectives in combination therapy

There are many innovative perspectives on how systems/network biology might inform targeted cancer therapy, [65-67]. A major articulated goal is to identify activated pathways that are druggable, compensatory pathways that account for single targeted treatment failure, or combinations of network nodes that give greater than additive benefits. Furthermore mass action kinetic models in well studied pathways (EGFR) have been suggested to be potentially capable of identifying combinations of molecular species with synergistic effects [67]. This is most often considered in the context of specific kinase inhibitors against oncogenic pathways. However, many cancers are currently treated with cytotoxic clinical regimens that have diverse cure rates [68], and some that respond well to therapy initially but rapidly develop resistance [68]. Less often considered [69], is the value of systems biology in examining classical chemotherapeutics. Chemotherapeutics activate downstream pathway signaling following treatment. Oncogene and tumor suppressor networks are known to alter similar signaling molecules as a result of oncogenic transformation. For instance: given a particularly responsive patient population, it may be desirable to use two drugs with the same mechanism of action but non overlapping toxicity. Furthermore, kinase inhibitors are often neither specific nor free of side effects[70]and as such signatures of their effects and models of their action could help guide regimen building, even if the assumptions present in modeling efforts (inhibition of one key node) are not valid. Applying systems and network biology to characterize the global alterations affecting therapeutic response, in the face of chemotherapy should promote the appropriate and enhanced use of current clinically used drugs.

Towards combination drug signatures

To integrate systems/network biology into the future of combination regimens, network approaches will have to delineate altered pathways, and understand how combinations of drugs

will interact with those pathways. If combination chemotherapy in cancer tends to select for drug resistant cell states, a couple of hypotheses might account for this effect. The first is that resistance to multiple drugs in a combination regimen is mediated by downstream network effects that are common to all drugs (a common effects/non independent action hypothesis), and second, combinations may co-opt distinct sub-networks downstream of drug targets to create combination specific effects. Understanding these distinctions will be critical to future regimen building. A good way to test these conflicting hypotheses and examine them with next generation therapeutics will be to develop combination therapy signatures. While this is an attractive and potentially useful idea, no current methods for signature-based drug prediction as detailed above have specifically addressed how, relative to single agents, combinations of drugs might function. This may be due to technical and/or conceptual limitations of certain approaches, but combination signatures will be critical to regimen design.

In examining combination network signatures, combinations may be a sum of their component drug networks, they may reinforce single component drug networks, or they may act on sub-networks that are not utilized by single drugs(combination off target effects). All of these effects may be desirable in different personalized medicine contexts with a diverse range of prior knowledge. If a combination promotes a single drug network, it will need to be dosed in people that are responsive to that single drug mechanism. While this would require single drug sensitizing networks to be well described, it provides for the combination of drugs that might increase the therapeutic window for a compound, while also increasing the relevant effects that a patient is known to be susceptible to.

If compounds are the sum of their component sensitivities and resistances, will conflicting genetic dependencies be cancelled out? If so, this might imply a striking paradox (could a genetic interaction in a single drug case be unimportant for a combination?). This possibility is an intriguing concept that will have to be explicitly investigated, because, although

it would suggest the minimization of resistance to one drug it would also minimize sensitivity to another. This dichotomy in a combination regimen, one drug sensitizing while the other promotes resistance to a particular legion could have a strong benefit in the absence of any genetic knowledge (a type of drug hedge betting). Thus, averaging sensitivities and resistances may arise in iterative randomized trials across diverse cohorts simply by the nature of the fact that success requires enhanced drug response.

Finally, we think that understanding the network biology of single and combination drugs could guide clinical practice across a diverse spectrum of knowledge about a patient's pathology. In the absence of any information as to the network pathology of the patient, broadly acting combinations that independently utilize diverse subnetworks may form an optimal therapeutic strategy. In an attempt to administer drug combinations with particularly potent combination action (i.e. synergy) it may be possible to identify the signatures of sub-networks that are functionally important for that drug combination and design companion diagnostics to target the right combination to the right patient. Finally in the presence of extensive pathological information, we may not only be able to pick the right combination for the right patient, i.e. match drugs to information about the bulk portion of a patient's tumor, but identify resistant subpopulations before they dominate a tumor and dose drug combinations that might minimize the growth of these subpopulations.

Molecular descriptions of patients with pathologically indistinguishable disease

The first efforts to molecularly classify cancers according to genomic signatures utilized microarray based approaches. These efforts first focused on accurately re-classifying current pathological distinctions in the absence of any prior biological knowledge [71]. Following these early efforts, researchers focused on diseases with very diverse clinical outcomes, but relatively homogenous pathology. These initial studies were performed in diffuse large b-cell lymphomas (DLBCL). DLBCL is a diverse disease with very heterogeneous outcomes (50% overall survival), making it an interesting test candidate for molecular profiling. Importantly, work in DLBCL did not just discover signatures of mRNAs, but identified biologically distinct subsets of cancers with similarity to distinct aspects of B-cell biology [72]. These distinct B-cell biologies correlated with prognosis and have been relatively reproducible in later gene sets and patient cohorts [73,74]. In addition, a variety of microarray signature based approaches have been proposed in a variety of other types of cancers. Specifically in breast cancer, a study from the Netherlands cancer institute was concerned with the problem of predicting metastasis in lymph node-negative breast cancer. In a clinical cohort of 117 patients Vant Veer et al. [75] identified a biologically coherent metastasis signature involving angiogenesis and cell cycle related genes that outperformed all contemporaneous clinical predictors. Later, a second breast cancer classification study [76]in a cohort of 76 similarly selected patients, was also able to identify a small and highly predictive mRNA expression signature, but the overlap with the 2002 study was 3 mRNAs. While many differences exist between the two studies, it appears that a large part of the lack of reproducibility between the studies could be the result of inadequate clinical cohort size, given the amount of noise in the microarray data.

Due to the fact that mRNA signature based approaches in the same disease pathology can suffer from data noise across institutions and studies, Chuang et al. have recently proposed a network based strategy to identify differentially activated pathways [77]. A search through nodes on a protein interaction network can identify network subsets with predictive capability across data sets. This network centric strategy allows protein-protein interaction data to filter gene expression data in a way that is relevant to the clinical phenotype. These network depictions also generalize better across patient datasets, suggesting that the biological network is less sensitive to noise than an individual mRNA signature.

In order to account for the effect of the tumor stroma, some groups have begun to specifically examine "stromal" signatures of disease prognosis. In hepatocellular carcinoma this approach identified liver stromal gene expression as a prognostic factor [78], and lenz et al. [74] demonstrated that a stromal signature involved in angiogenesis and monocyte infiltration was involved with response to the R-CHOP regimen. Thus, multivariate descriptions of the tumor microenvironment can also add descriptive and prognostic value to current diagnostic protocols.

Finally in the same manner that protein interaction networks have been used to generate greater prognostic power in tumor intrinsic mRNA measurements, these ideas might be combined with current information about cell-cell interactions and cytokine signaling newtworks to provide search scaffolds to add statistical power to micro-environment focused datasets. These searches could use literature search scaffolds, or cell-cell signaling pathways and would seek to integrate stromal and tumor signatures using intercellular signaling/interaction networks.

Cataloging pathways and networks

Early cancer sequencing efforts were the first to catalog the spectrum of mutations in single patient tumor samples [79-81]. These studies identified a surprising complexity, but striking patterns. The number of acquired mutations varies by cancer subtype (~20-200 SNPs).

However, in spite of patient to patient heterogeneity, there were commonly mutated genes, however, more striking was the tendency of alterations to be in different genes yet converge on known pathways at different points in the pathway. Though not formally incorporated into a pathway/network model, these commonalities in pathway alterations fit into canonical views of classic signaling pathways i.e. Ras-Raf-Mek-Erk. Later, sequencing efforts in lung cancer identified mutually exclusive alterations in ATM and TP53, also suggestive of a pathway interaction[82].

These observations of common mutational alterations and mutually exclusive pathways were dramatically extended by the cancer genome atlas, TCGA seeks to characterize large patient cohorts, with simulatanous analyses of the epigenome, the transcriptome, and the genome (mutations and copy number variations) [83], and integrate these data with literature knowledge to perform pathway analyses. Integrating multiple genome wide data sets with known pathway functional annotations, they were able to predict that as many as 22% of patients harbor defects in homologous recombination pathways(centered around BRCA1/2 meta data) and might be candidates for PARP inhibitor therapy. These integrated analyses demonstrate the potential power of integrating comprehensive data sets and functional annotations to make predictions about larger sets of patients harboring similar functional alterations. Furthermore the functional (in this case literature) basis for the pathway groupings may make the networks discovered in TCGA more interpretable (though also perhaps more canonical) than those discovered using protein interaction scaffolds in microarray data.

Functional annotation of genomic data.

The flood of genomic data by many sources has spurred large scale efforts to functionally annotate gene function. Large scale RNAi libraries exist for mouse and human

systems [84], and custom libraries targeting sets of genomic alterations can be rapidly generated for targeted studies in relevant cancer models [85].

Some RNAi screening efforts focused on genome scale analyses of cancer cell growth [86]. Following these initial successes groups began to focus on conditional genetic dependencies with oncogenes as targets i.e. Myc and Ras. Reasoning that conditional genetic dependencies in these cell lines might identify oncogene dependent therapeutic strategies, Several RAS synthetic lethal screens were performed concurrently utilizing very different approaches. The first, utilized panels of human cell lines with or without RAS mutations [87], the second utilized an isogenic approach in which synthetic lethality was examined in the context of a genetically engineered cell line [88]. This same isogenic approach was recently used to perform a Myc synthetic lethal screen [89]. Importantly, the first effort was not able to be validated in a study by a second group, suggesting that there might be experimental differences or hairpin off target effects. This stresses the importance of independent validation with multiple hairpins and/or small molecules in large scale screens if accurate functional networks are to be used in genome scale analysis.

RNAi screens for drug sensitivity and resistance genes

To understand which elements of the cancer genome are therapeutically important, genetic screens can also be performed in the presence of drugs. In order to assess the function of a variety of genes in response to the frontline chemotherapeutic cisplatin, Bartz et al performed an *in vitro* RNAi screen. In their screen Bartz et al. found BRCA1/2 and translesion polymerases to be key mediators of cisplatin response. Serial enrichment screens in mouse models of lymphoma led to *in vivo* demonstration that topoisomerase II and I genetically determine resistance to their respective poisoning agents(Doxorubicin and Camptothecin)[90], as well as taxol/vincristine specific modulation by a putative microtubule related protein. Taxol

has also been the subject of a large scale RNAi screen. Interestingly lung cancer cells that had lost key regulators of the mitotic spindle were dramatically sensitized to microtubule disrupting agents [46]. A more recent study has interpreted drug gene synthetic lethality in terms of interaction networks. These network based screens identify network properties of high scoring siRNAs and coherent subsets of biology that coordinate cellular processes. Importantly this study examined how overlapping an EGFR inhibitor network and an Irinotecan centered network are. This network based view clearly showed the enrichment for EGFR related information in the drug network, but it also discovered substantial overlap in therapy sensitizing genes. This suggests that EGFR inhibitors and classic chemotherapeutics have overlapping cellular sensitivities [91].

RNAi screens *in vivo*

Some functional mechanisms of mutated genes in cancer may require physiological niches to accurately characterize their function. Recently RNAi approaches to understanding the relevant mutations in physiologic contexts have been developed for hematopoetic cancers.

In vivo RNAi screens were initially performed in the context of tumorigenesis and tumor maintenance. *In vivo* tumorigenesis screens identified accelerators of both lymphoma and liver cancer progression[85,92]. While these initial screens were terrific proofs of concept for screening for tumor suppressors, Meacham et al. simultaneously examined 1000 shRNAs in the same mouse, and discovered *in vivo* specific drug targets[93]. They found that inhibiting Rac2 specifically *in vivo* enhanced response to a frontline chemotherapeutic by inhibiting migration of minimal residual disease burden to sites of terminal pathology. Thus, *in vivo* specific modifiers of therapeutic response, identify functional relationships that are specific to organismal and not cellular response.

References

1 Wall, M. E. & Wani, M. C. Camptothecin and taxol: discovery to clinic--thirteenth Bruce F. Cain Memorial Award Lecture. *Cancer research* **55**, 753-760 (1995).

2 Chabner, B. A. & Roberts, T. G., Jr. Timeline: Chemotherapy and the war on cancer. *Nature reviews. Cancer* **5**, 65-72, doi:10.1038/nrc1529 (2005).

3 Goodman, L. S. *et al.* Landmark article Sept. 21, 1946: Nitrogen mustard therapy. Use of methyl-bis(beta-chloroethyl)amine hydrochloride and tris(beta-chloroethyl)amine hydrochloride for Hodgkin's disease, lymphosarcoma, leukemia and certain allied and miscellaneous disorders. By Louis S. Goodman, Maxwell M. Wintrobe, William Dameshek, Morton J. Goodman, Alfred Gilman and Margaret T. McLennan. *Jama* **251**, 2255-2261 (1984).

4 Farber, S. & Diamond, L. K. Temporary remissions in acute leukemia in children produced by folic acid antagonist, 4-aminopteroyl-glutamic acid. *The New England journal of medicine* **238**, 787-793, doi:10.1056/NEJM194806032382301 (1948).

5 Luria, S. E. & Delbruck, M. Mutations of Bacteria from Virus Sensitivity to Virus Resistance. *Genetics* **28**, 491-511 (1943).

6 Newcombe, H. B. & Hawirko, R. Spontaneous Mutation to Streptomycin Resistance and Dependence in Escherichia Coli. *J Bacteriol* **57**, 565-572 (1949).

7 Law, L. W. Origin of the resistance of leukaemic cells to folic acid antagonists. *Nature* **169**, 628-629 (1952).

8 Law, L. W. Effects of combinations of antileukemic agents on an acute lymphocytic leukemia of mice. *Cancer research* **12**, 871-878 (1952).

9 Skipper, H. E., Thomson, J. R. & Bell, M. Attempts at dual blocking of biochemical events in cancer chemotherapy. *Cancer research* **14**, 503-507 (1954).

10 Frei, E., 3rd *et al.* A comparative study of two regimens of combination chemotherapy in acute leukemia. *Blood* **13**, 1126-1148 (1958).

11 Skipper, H. E., Schabel, F. M., Jr. & Wilcox, W. S. Experimental Evaluation of Potential Anticancer Agents. Xiii. On the Criteria and Kinetics Associated with "Curability" of Experimental Leukemia. *Cancer chemotherapy reports. Part 1* **35**, 1-111 (1964).

12 Freireich EJ, K. M., Frei E III *Quadruple combination therapy (VAMP) for acute lymphocytic leukemia of childhood.* (Catalogue No. 20, 1964).

13 DeVita, V. T. & Schein, P. S. The use of drugs in combination for the treatment of cancer: rationale and results. *The New England journal of medicine* **288**, 998-1006, doi:10.1056/NEJM197305102881905 (1973).

14 Pirker, R. *et al.* Cetuximab plus chemotherapy in patients with advanced non-small-cell lung cancer (FLEX): an open-label randomised phase III trial. *Lancet* **373**, 1525-1531, doi:10.1016/S0140-6736(09)60569-9 (2009).

15 Conroy, T. *et al.* FOLFIRINOX versus gemcitabine for metastatic pancreatic cancer. *The New England journal of medicine* **364**, 1817-1825, doi:10.1056/NEJMoa1011923 (2011).

16 Almeida Da Silva, P. E. & Palomino, J. C. Molecular basis and mechanisms of drug resistance in Mycobacterium tuberculosis: classical and new drugs. *J Antimicrob Chemother* **66**, 1417-1430, doi:10.1093/jac/dkr173 (2011).

17 Durant, J. *et al.* Drug-resistance genotyping in HIV-1 therapy: the VIRADAPT randomised controlled trial. *Lancet* **353**, 2195-2199 (1999).

18 Mullighan, C. G. *et al.* Genomic analysis of the clonal origins of relapsed acute lymphoblastic leukemia. *Science* **322**, 1377-1380, doi:10.1126/science.1164266 (2008).

19 Mullighan, C. G. *et al.* CREBBP mutations in relapsed acute lymphoblastic leukaemia. *Nature* **471**, 235-239, doi:10.1038/nature09727 (2011).

20 Ding, L. *et al.* Clonal evolution in relapsed acute myeloid leukaemia revealed by whole-genome sequencing. *Nature* **481**, 506-510, doi:10.1038/nature10738 (2012).

21 Shah, N. P. *et al.* Overriding imatinib resistance with a novel ABL kinase inhibitor. *Science* **305**, 399-401 (2004).

22 Talpaz, M. *et al.* Dasatinib in imatinib-resistant Philadelphia chromosome-positive leukemias. *The New England journal of medicine* **354**, 2531-2541, doi:10.1056/NEJMoa055229 (2006).

23 Shah, N. P. *et al.* Sequential ABL kinase inhibitor therapy selects for compound drug-resistant BCR-ABL mutations with altered oncogenic potency. *The Journal of clinical investigation* **117**, 2562-2569, doi:10.1172/JCI30890 (2007).

24 Zhang, J. *et al.* Targeting Bcr-Abl by combining allosteric with ATP-binding-site inhibitors. *Nature* **463**, 501-506, doi:10.1038/nature08675 (2010).

25 Boulos, N. *et al.* Chemotherapeutic agents circumvent emergence of dasatinib-resistant BCR-ABL kinase mutations in a precise mouse model of Philadelphia chromosome-positive acute lymphoblastic leukemia. *Blood* **117**, 3585-3595, doi:10.1182/blood-2010-08-301267 (2011).

26 Yauch, R. L. *et al.* Smoothened mutation confers resistance to a Hedgehog pathway inhibitor in medulloblastoma. *Science* **326**, 572-574, doi:10.1126/science.1179386 (2009).

27 Turke, A. B. *et al.* Preexistence and clonal selection of MET amplification in EGFR mutant NSCLC. *Cancer Cell* **17**, 77-88, doi:10.1016/j.ccr.2009.11.022 (2010).

28 Wagle, N. *et al.* Dissecting therapeutic resistance to RAF inhibition in melanoma by tumor genomic profiling. *Journal of clinical oncology : official journal of the American Society of Clinical Oncology* **29**, 3085-3096, doi:10.1200/JCO.2010.33.2312 (2011).

29 Matthews, D. A. *et al.* Dihydrofolate reductase: x-ray structure of the binary complex with methotrexate. *Science* **197**, 452-455 (1977).

30 Staker, B. L. *et al.* The mechanism of topoisomerase I poisoning by a camptothecin analog. *Proceedings of the National Academy of Sciences of the United States of America* **99**, 15387-15392, doi:10.1073/pnas.242259599 (2002).

31 Bledsoe, R. K. *et al.* Crystal structure of the glucocorticoid receptor ligand binding domain reveals a novel mode of receptor dimerization and coactivator recognition. *Cell* **110**, 93-105 (2002).

32 Pommier, Y., Leo, E., Zhang, H. & Marchand, C. DNA topoisomerases and their poisoning by anticancer and antibacterial drugs. *Chemistry & biology* **17**, 421-433, doi:10.1016/j.chembiol.2010.04.012 (2010).

33 Hashimoto, M. W. *et al.* A comparison of the propensity for gene amplification between near-tetraploid and near-diploid V79 clones resistant to 150 nM methotrexate. *Carcinogenesis* **17**, 389-394 (1996).

34 Beketic-Oreskovic, L., Duran, G. E., Chen, G., Dumontet, C. & Sikic, B. I. Decreased mutation rate for cellular resistance to doxorubicin and suppression of mdr1 gene activation by the cyclosporin PSC 833. *Journal of the National Cancer Institute* **87**, 1593-1602 (1995).

35 Letai, A. G. Diagnosing and exploiting cancer's addiction to blocks in apoptosis. *Nature reviews. Cancer* **8**, 121-132, doi:10.1038/nrc2297 (2008).

36 Ni Chonghaile, T. *et al.* Pretreatment mitochondrial priming correlates with clinical response to cytotoxic chemotherapy. *Science* **334**, 1129-1133, doi:10.1126/science.1206727 (2011).

37 Kreeger, P. K. & Lauffenburger, D. A. Cancer systems biology: a network modeling perspective. *Carcinogenesis* **31**, 2-8, doi:10.1093/carcin/bgp261 (2010).

38 Schoeberl, B. *et al.* Therapeutically targeting ErbB3: a key node in ligand-induced activation of the ErbB receptor-PI3K axis. *Sci Signal* **2**, ra31, doi:10.1126/scisignal.2000352 (2009).

39 Chen, W. W. *et al.* Input-output behavior of ErbB signaling pathways as revealed by a mass action model trained against dynamic data. *Mol Syst Biol* **5**, 239, doi:10.1038/msb.2008.74 (2009).

40 Janes, K. A. *et al.* A systems model of signaling identifies a molecular basis set for cytokine-induced apoptosis. *Science* **310**, 1646-1653, doi:10.1126/science.1116598 (2005).

41 Janes, K. A. *et al.* Cue-signal-response analysis of TNF-induced apoptosis by partial least squares regression of dynamic multivariate data. *J Comput Biol* **11**, 544-561, doi:10.1089/1066527041887258 (2004).

42 Miller-Jensen, K., Janes, K. A., Brugge, J. S. & Lauffenburger, D. A. Common effector processing mediates cell-specific responses to stimuli. *Nature* **448**, 604-608, doi:10.1038/nature06001 (2007).

43 Kreeger, P. K., Mandhana, R., Alford, S. K., Haigis, K. M. & Lauffenburger, D. A. RAS mutations affect tumor necrosis factor-induced apoptosis in colon carcinoma cells via ERK-modulatory negative and positive feedback circuits along with non-ERK pathway effects. *Cancer research* **69**, 8191-8199, doi:10.1158/0008-5472.CAN-09-1921 (2009).

44 Kumar, N., Afeyan, R., Kim, H. D. & Lauffenburger, D. A. Multipathway model enables prediction of kinase inhibitor cross-talk effects on migration of Her2-overexpressing mammary epithelial cells. *Molecular pharmacology* **73**, 1668-1678, doi:10.1124/mol.107.043794 (2008).

45 Xie, L., Kinnings, S. L. & Bourne, P. E. Novel computational approaches to polypharmacology as a means to define responses to individual drugs. *Annual review of pharmacology and toxicology* **52**, 361-379, doi:10.1146/annurev-pharmtox-010611-134630 (2012).

46 Whitehurst, A. W. *et al.* Synthetic lethal screen identification of chemosensitizer loci in cancer cells. *Nature* **446**, 815-819, doi:10.1038/nature05697 (2007).

47 Doles, J. & Hemann, M. T. Nek4 status differentially alters sensitivity to distinct microtubule poisons. *Cancer research* **70**, 1033-1041, doi:10.1158/0008-5472.CAN-09-2113 (2010).

48 Bartz, S. R. *et al.* Small interfering RNA screens reveal enhanced cisplatin cytotoxicity in tumor cells having both BRCA network and TP53 disruptions. *Mol Cell Biol* **26**, 9377-9386 (2006).

49 Karaman, M. W. *et al.* A quantitative analysis of kinase inhibitor selectivity. *Nature biotechnology* **26**, 127-132, doi:10.1038/nbt1358 (2008).

50 Anastassiadis, T., Deacon, S. W., Devarajan, K., Ma, H. & Peterson, J. R. Comprehensive assay of kinase catalytic activity reveals features of kinase inhibitor selectivity. *Nature biotechnology* **29**, 1039-1045, doi:10.1038/nbt.2017 (2011).

51 Bantscheff, M. *et al.* Chemoproteomics profiling of HDAC inhibitors reveals selective targeting of HDAC complexes. *Nature biotechnology* **29**, 255-265, doi:10.1038/nbt.1759 (2011).

52 Bantscheff, M. *et al.* Quantitative chemical proteomics reveals mechanisms of action of clinical ABL kinase inhibitors. *Nature biotechnology* **25**, 1035-1044, doi:10.1038/nbt1328 (2007).

53 Paull, K. D. *et al.* Display and analysis of patterns of differential activity of drugs against human tumor cell lines: development of mean graph and COMPARE algorithm. *Journal of the National Cancer Institute* **81**, 1088-1092 (1989).

54 Weinstein, J. N. *et al.* An information-intensive approach to the molecular pharmacology of cancer. *Science* **275**, 343-349 (1997).

55 Scherf, U. *et al.* A gene expression database for the molecular pharmacology of cancer. *Nature genetics* **24**, 236-244, doi:10.1038/73439 (2000).

56 Lee, J. K. *et al.* A strategy for predicting the chemosensitivity of human cancers and its application to drug discovery. *Proceedings of the National Academy of Sciences of the United States of America* **104**, 13086-13091, doi:10.1073/pnas.0610292104 (2007).

57 Lamb, J. *et al.* The Connectivity Map: using gene-expression signatures to connect small molecules, genes, and disease. *Science* **313**, 1929-1935 (2006).

58 Hieronymus, H. *et al.* Gene expression signature-based chemical genomic prediction identifies a novel class of HSP90 pathway modulators. *Cancer Cell* **10**, 321-330 (2006).

59 Wei, G. *et al.* Gene expression-based chemical genomics identifies rapamycin as a modulator of MCL1 and glucocorticoid resistance. *Cancer Cell* **10**, 331-342, doi:10.1016/j.ccr.2006.09.006 (2006).

60 Dudley, J. T. *et al.* Computational repositioning of the anticonvulsant topiramate for inflammatory bowel disease. *Sci Transl Med* **3**, 96ra76, doi:10.1126/scitranslmed.3002648 (2011).

61 Sirota, M. *et al.* Discovery and preclinical validation of drug indications using compendia of public gene expression data. *Sci Transl Med* **3**, 96ra77, doi:10.1126/scitranslmed.3001318 (2011).

62 Jiang, H., Pritchard, J. R., Williams, R. T., Lauffenburger, D. A. & Hemann, M. T. A mammalian functional-genetic approach to characterizing cancer therapeutics. *Nature chemical biology* **7**, 92-100, doi:10.1038/nchembio.503 (2011).

63 Wolpaw, A. J. *et al.* Modulatory profiling identifies mechanisms of small molecule-induced cell death. *Proceedings of the National Academy of Sciences of the United States of America* **108**, E771-780, doi:10.1073/pnas.1106149108 (2011).

64 Campillos, M., Kuhn, M., Gavin, A. C., Jensen, L. J. & Bork, P. Drug target identification using side-effect similarity. *Science* **321**, 263-266, doi:10.1126/science.1158140 (2008).

65 Pawson, T. & Linding, R. Network medicine. *FEBS letters* **582**, 1266-1270, doi:10.1016/j.febslet.2008.02.011 (2008).

66 Erler, J. T. & Linding, R. Network-based drugs and biomarkers. *J Pathol* **220**, 290-296, doi:10.1002/path.2646 (2010).

67 Fitzgerald, J. B., Schoeberl, B., Nielsen, U. B. & Sorger, P. K. Systems biology and combination therapy in the quest for clinical efficacy. *Nature chemical biology* **2**, 458-466, doi:10.1038/nchembio817 (2006).

68 Abeloff, M. D. *Abeloff's clinical oncology*. 4th edn, (Churchill Livingstone/Elsevier, 2008).

69 Tentner, A. R. *et al.* Combined experimental and computational analysis of DNA damage signaling reveals context-dependent roles for Erk in apoptosis and G1/S arrest after genotoxic stress. *Mol Syst Biol* **8**, 568, doi:10.1038/msb.2012.1 (2012).

70 Kantarjian, H. M. *et al.* Dasatinib or imatinib in newly diagnosed chronic-phase chronic myeloid leukemia: 2-year follow-up from a randomized phase 3 trial (DASISION). *Blood* **119**, 1123-1129, doi:10.1182/blood-2011-08-376087 (2012).

71 Golub, T. R. *et al.* Molecular classification of cancer: class discovery and class prediction by gene expression monitoring. *Science* **286**, 531-537 (1999).

72 Alizadeh, A. A. *et al.* Distinct types of diffuse large B-cell lymphoma identified by gene expression profiling. *Nature* **403**, 503-511, doi:10.1038/35000501 (2000).

73 Rosenwald, A. *et al.* The use of molecular profiling to predict survival after chemotherapy for diffuse large-B-cell lymphoma. *The New England journal of medicine* **346**, 1937-1947, doi:10.1056/NEJMoa012914 (2002).

74 Lenz, G. *et al.* Stromal gene signatures in large-B-cell lymphomas. *The New England journal of medicine* **359**, 2313-2323, doi:10.1056/NEJMoa0802885 (2008).

75 van 't Veer, L. J. *et al.* Gene expression profiling predicts clinical outcome of breast cancer. *Nature* **415**, 530-536, doi:10.1038/415530a (2002).

76 Wang, Y. *et al.* Gene-expression profiles to predict distant metastasis of lymph-node-negative primary breast cancer. *Lancet* **365**, 671-679, doi:10.1016/S0140-6736(05)17947-1 (2005).

77 Chuang, H. Y., Lee, E., Liu, Y. T., Lee, D. & Ideker, T. Network-based classification of breast cancer metastasis. *Mol Syst Biol* **3**, 140, doi:10.1038/msb4100180 (2007).

78 Hoshida, Y. *et al.* Gene expression in fixed tissues and outcome in hepatocellular carcinoma. *The New England journal of medicine* **359**, 1995-2004, doi:10.1056/NEJMoa0804525 (2008).

79 Wood, L. D. *et al.* The genomic landscapes of human breast and colorectal cancers. *Science* **318**, 1108-1113, doi:10.1126/science.1145720 (2007).

80 Mardis, E. R. *et al.* Recurring mutations found by sequencing an acute myeloid leukemia genome. *The New England journal of medicine* **361**, 1058-1066, doi:10.1056/NEJMoa0903840 (2009).

81 Jones, S. *et al.* Core signaling pathways in human pancreatic cancers revealed by global genomic analyses. *Science* **321**, 1801-1806, doi:10.1126/science.1164368 (2008).

82 Ding, L. *et al.* Somatic mutations affect key pathways in lung adenocarcinoma. *Nature* **455**, 1069-1075, doi:10.1038/nature07423 (2008).

83 Integrated genomic analyses of ovarian carcinoma. *Nature* **474**, 609-615, doi:10.1038/nature10166 (2011).

84 Paddison, P. J. *et al.* A resource for large-scale RNA-interference-based screens in mammals. *Nature* **428**, 427-431 (2004).

85 Zender, L. *et al.* An oncogenomics-based in vivo RNAi screen identifies tumor suppressors in liver cancer. *Cell* **135**, 852-864 (2008).

86 Schlabach, M. R. *et al.* Cancer proliferation gene discovery through functional genomics. *Science* **319**, 620-624 (2008).

87 Scholl, C. *et al.* Synthetic lethal interaction between oncogenic KRAS dependency and STK33 suppression in human cancer cells. *Cell* **137**, 821-834, doi:10.1016/j.cell.2009.03.017 (2009).

88 Luo, J. *et al.* A genome-wide RNAi screen identifies multiple synthetic lethal interactions with the Ras oncogene. *Cell* **137**, 835-848, doi:10.1016/j.cell.2009.05.006 (2009).

89 Kessler, J. D. *et al.* A SUMOylation-dependent transcriptional subprogram is required for Myc-driven tumorigenesis. *Science* **335**, 348-353, doi:10.1126/science.1212728 (2012).

90 Burgess, D. J. *et al.* Topoisomerase levels determine chemotherapy response in vitro and in vivo. *Proceedings of the National Academy of Sciences of the United States of America* **105**, 9053-9058, doi:10.1073/pnas.0803513105 (2008).

91 Astsaturov, I. *et al.* Synthetic lethal screen of an EGFR-centered network to improve targeted therapies. *Sci Signal* **3**, ra67, doi:10.1126/scisignal.2001083 (2010).

92 Bric, A. *et al.* Functional identification of tumor-suppressor genes through an in vivo RNA interference screen in a mouse lymphoma model. *Cancer Cell* **16**, 324-335 (2009).

93 Meacham, C. E., Ho, E. E., Dubrovsky, E., Gertler, F. B. & Hemann, M. T. In vivo RNAi screening identifies regulators of actin dynamics as key determinants of lymphoma progression. *Nat Genet* **41**, 1133-1137 (2009).

Chapter 1

A Reverse-Engineering Strategy for Multi-target Compounds

Contributions:

I performed the experiments and analyzed the data in this chapter**,** D. Lauffenburger and I wrote the manuscript, the other authors contributed helpful comments and useful reagents. A version of this chapter was previously published as:

Three-kinase inhibitor combination recreates multipathway effects of a geldanamycin analogue on hepatocellular carcinoma cell death. Pritchard JR, Cosgrove BD, Hemann MT, Griffith LG, Wands JR, Lauffenburger DA. Mol Cancer Ther. 2009 Aug;8(8):2183-92. Epub 2009 Aug 11.

Abstract

Multi-target compounds that act on a diverse set of regulatory pathways are emerging as a therapeutic approach for a variety of cancers. Toward a more specified use of this approach, we hypothesize that the desired efficacy can be recreated in terms of a particular combination of relatively more specific (i.e., ostensibly single-target) compounds. We test this hypothesis for the geldanamycin analog 17AAG in hepatocellular carcinoma (HCC) cells. The multi target drug,17AAG, inhibits HSP90 and is known to concomitantly deactivate kinase signaling(to kill cancer cells) and transcriptionally activate a stress response through HSF1 activation(to protect cellular homeostasis). Measuring critical phosphorylation levels that indicate the kinase pathway effects and correlating these with the apoptotic responsiveness of the Hep3B cell line in contrast to the apoptotic resistance of the Huh7 cell line, a principal components analysis constructed from time-course measurements of 7 phospho-protein signaling levels identified modulation of the AKT, IKK and STAT3 pathways by 17AAG treatment as most important for distinguishing these cell-specific death responses. The analysis correctly suggested from 17AAG-induced effects on these phospho-protein levels that the FOCUS cell line would show apoptotic responsiveness similarly to Hep3B. The PCA also guided the inhibition of three critical pathways and rendered Huh7 cells responsive to 17AAG. Strikingly, in all three HCC lines the three-inhibitor combination alone exhibited similar or greater efficacy to 17AAG. We conclude that: (a) the principal components analysis captures and clusters the multi-pathway phospho-protein timecourses with respect to their 17AAG-induced apoptotic responsiveness;(b) we can recreate, in a more specified manner, the pro-death cellular responses of a prospective multi-target cancer therapeutic.

Introduction

The fairly limited success of many targeted cancer therapeutics when used as single-agent treatments presents a challenging problem that has motivated studies seeking to: stratify failure-vs-success categories[1] or to combine targeted therapeutics with traditional chemotherapeutic regimes[2]. An alternative avenue generating growing interest is a new class of compounds known as multi-target drugs[3]. These compounds aim to improve therapeutic efficacy by producing a combined inhibition of diverse regulatory pathways that are important for cancer cell proliferation and survival.

At one end of the multi-target drug spectrum lies a class of Hsp90 inhibitors such as 17AAG, which were derived from the tumoricidal natural product Geldanamycin[4]. Hsp90 is a vital chaperone that, relative to other chaperones, interacts with a select but critical subset of cellular proteins including nuclear hormone receptors and components of signal transduction cascades[5]. Hsp90 inhibition appears to offer a promising anti-cancer strategy[6] but, compared to more traditional targeted therapeutics, an exceptionally pleiotropic effect. In a recent genome-wide study in *Saccharomyces cerevisiae*, Hsp90 was found to interact with roughly 10% of the ORFs investigated[7].

The nature of the effects of 17AAG in tumor cells relative to non-transformed cells appears to derive from the enhanced binding of 17AAG to Hsp90 in the former. Tumor cell Hsp90 is found more highly resident in multi-chaperone complexes with high rates of ATPase activity, constituting a distinctive molecular state exhibiting an approximately 10-fold greater binding affinity for 17AAG compared to that in the normal cells[8]. Hsp90 inhibition in a variety of tumor cell lines has been shown to affect the levels and/or activity of ErbB family receptors, Src, Ras, Raf, AKT, IKK, Janus kinase, Her2, p53, RIP, and cell cycle regulators, as well as increasing the levels of the anti-apoptotic chaperone Hsp70[5,9-14] . In addition to these long-term

effects on client protein levels and their associated downstream signaling effects, short-term effects of Hsp90 inhibitors have also been observed. Geldanamycin treatment has been found to yield increased phosphorylation of AKT in myocytes[15], increased PKR activity and phosphorylation of eIF-2α in HeLa cells[16], and transient early signaling in the Src, AKT, and ERK pathways in both MCF-7 and COS7 cells[17]. However, the contributions of these various pathways effects to cell death responses are unclear, and the manner by which these effects integrate to impact cell behavior is even more difficult to ascertain.

Our goal is to offer an effective approach based upon systematically extracting the critical effects of multi-target compounds, which could enable the rationale recreation of their effectiveness via designed combinations of more selectively targeted drugs. Since Hsp90 inhibition elicits contradictory effects: the degradation of proteins involved in cellular survival, as well as an increase in HSP70 levels, we reason that a rational recreation of its pro-apoptotic effects may potentially increase efficacy. Our approach is motivated by recent successes in computational characterization of the effects of diverse drug induced perturbations governing cellular phenotypes[18,19]. Data-driven computational modeling techniques such as principal components analysis (PCA) and partial least-square regression (PLSR) seek to find key vectors representing signal combinations that contain the most vital information for predicting – at least in correlative fashion – cell responses to various stimuli[19].

We test this hypothesis on quantitative experimental measurement of multiple phosphoprotein signaling pathways altered by 17AAG in a set of HCC cell lines. A principal components analysis of time-course data for 7 kinase signals reveals that early effects of 17AAG on the AKT, IKK and STAT3 pathways are predominantly critical for clustering cell-specific apoptotic death responses among the Hep3B, Huh7, and FOCUS lines. While individual inhibition of each of these three pathways had little effect on the cell responses,

combining all three kinase inhibitors rendered the 17AAG-resistant Huh7 line responsive and greater efficacy than 17AAG itself in two of our three cell lines.

Materials and Methods

Cell Lines and Culture

Hep3B, Huh7 and FOCUS cell lines[27] were obtained from the Wands Lab (Brown University, Providence RI). Cells were maintained in Minimal Essential Media (ATCC Manassas VA) with 10% FBS (HyClone, Omaha NE) at sub-confluent densities and 37°C, 5%CO_2. Apoptosis and signaling experiments were seeded at cell densities of 200,000, and 150,000 cells per well of a 6-well plate for Hep3B and Huh7/Focus cell lines respectively.

Inhibitors

All inhibitors were purchased from Calbiochem (San Diego, CA). 17AAG (cat# 100068) was reconstituted in methanol; all other compounds (BMS-345541 cat# 401480, JAK inhibitor 1, Pyridone 6 cat# 420099, PI103 cat# 528100,) were reconstituted in DMSO. PD98059 (Calbiochem cat #513000) reconstituted in DMSO is the MEK inhibitor used in the control combination study (Figure S2), and the JNK inhibitor is SP600125 (Calbiochem cat#420119).

Signaling Measurements

Signaling measurements were made using bead based ELISA kits manufactured by Bio-Rad. Bioplex assays were run according to all of the manufacture's recommendations. These Bioplex assays were used to measure p-AKT (Ser473), p-ERK1/2 (Thr202/Tyr204), p-STAT-3 (Tyr705), p-p38 (Thr180/Tyr182), p-JNK (Thr183/Tyr185), p-GSK-3α/β (Ser21/Ser9), p-IKb-□ (Ser32), AKT, p38, and ERK. All measurements are the mean of duplicates. Measurements were taken at 0, 1, 2, 4, and 24 hours after addition of 1 μM 17AAG, and were normalized to unstimulated controls on a cell line by cell line basis. This fold-change normalization created a relative value of 1 for all signals in all cell lines at the point of 17AAG addition. This allowed direct comparison of the fold change of 17AAG effects across cell lines.

Apoptosis Assays

Cells were harvested from 6 well plates and combined with the floating fraction. This sample was fixed in 3-4% Para-Formaldehyde , then permeabilized for antibody staining in methanol and stored at -20° C for up to 1 week. Cells were stained with antibodies for Cleaved (Activated) Caspase 3 (BD Pharmingen, San Jose, CA, cat# 559565) and Cleaved PARP (BD Pharmingen cat# 51-9000017) at a dilution of 1:300 (in PBS-0.1%Tween20-1%BSA). Secondary antibodies were IgG Alexa Flour 647 and Alexa Fluor 488 (Invitrogen cat # A21245 and A11029 respectively) at 1:300 in PBS-TB. A minimum 10,000 gated events were collected per sample. All measurements are the mean of triplicates +/- SEM. .

Data Analysis

Principal Components Analysis (PCA)(Jolliffe 2002) is was done using Simca-p++ v11.5 (L. Eriksson et al. 2001). All signals were mean centered and unit variance scaled before analysis. This centering and scaling allows all signaling variables to be considered on an equal scale in principal components space, based solely upon induced variation relative to the mean of a given signal and its position in the distribution. Principal Components Analysis finds directions of covariance in the original data set. These directions become the principal components onto which the original data set is collapsed. Our initial multi-dimensional data is condensed down into 2 principal components dimensions that capture the majority of the variance. Loadings plots are created by plotting the original time dimension in the 2 component graph. Scores plot are generated by plotting the original signaling data in the two component plot. Hotelling's criterion displays the distance in the model plane at which a given sample is behaving significantly different than the rest of the data with 95% confidence(ref 28). For an intuitive description of PCA see Supplementary Figure 1. In our dataset, we use a variation of Principle Components cluster analysis. Since all of our signaling variables cannot be

segmented into completely separable groups, we use a “dissection” or “segmentation” based technique (Jolliffe PCA 2002). Here we calculate a euclidean distance based upon the original variables (a contributions vector) to identify signals that are the most distinct between sensitive and resistant cell lines.

The appropriate threshold to interpret the PCA was decided upon by the small increase in goodness of fit that was provided by a third component. To determine whether or not the percentage of the cumulative variance explained by our model was significant, we generated 1000 data matrices of the same size as our original dataset. The data matrix entries were found by randomly sampling the column indices across a signaling row. This perturbation retains similar variance structure to the original signal. Our test statistic was the cumulative percentage of the variance explained by a 2 component model built in Matlabv7.0 (using the princomp.m) function on these 1000 data matrices. The test statistic was then plotted as a histogram, a normal distribution was fit to the data, and a p-value was calculated using the Cumulative Distribution Function (CDF).

0-4hr integrals were calculated using a 2^{nd} order polynomial curve fit followed by numerical integration using a 0.2 hr increment. Heat maps were made in Matlabv7.0. The analysis of synergy was coded using Matlab. Statistical comparisons of cell death were done using a Student’s t-test. P-values <0.05 were deemed significant.

Results

Conventional markers of 17AAG action cannot account for the differential cell death responses in Huh7 and Hep3B cells. The effect of 17AAG treatment on cell death in hepatocellular carcinoma cell lines was assessed by treating Huh7 and Hep3B with 17AAG at 0.1 and 1μM for 48 hours. A representative gating for a population staining double positive for active (cleaved) Caspase 3 and cleaved PARP was assessed via flow cytometry (Figure 1A). Double positive cells represent the population of cells within a well that are undergoing apoptosis. The same gating thresholds were used for all of the samples from a given cell line and are based upon the negative control. No single positive populations were noted at 48 hours during the duration of our study. 3 samples per cell line/condition were averaged using the values obtained from the plots in 1A and are plotted in Figure 1B. Hep3B cells were found to be sensitive to 1μM 17AAG induced cell death, whereas Huh7 cells were found to be resistant (Figure 1B). We then hypothesized that a difference in the levels of p-AKT (S473), t-AKT, p-ERK1/2(T202, Y204), and p-IκB-α (S32/S36) 24 hours after the addition of 17AAG might account for the difference in phenotype (Figure 1C). Lysates were collected both before and 24 hours after treatment with 17AAG. The relative decrease in these 4 measurements at 24 hours is identical in sensitive and resistant cell lines. These late-time measurements indicate that a simple explanation regarding the long-term signaling degradation arising from 17AAG treatment is not able to explain the disparate death responses of Hep3B and Huh7 cells.

A dynamic multi-pathway analysis can distinguish Huh7 resistance and Hep3B sensitivity to 17AAG. Since the degradation of PI3K-AKT, Ras/Raf/Mek/ERK, and IKK-NF-κB pathway signaling at 24 hours failed to distinguish Huh7 from Hep3B, we proposed that a

dynamic study including measurements of the shorter-term effects of 17AAG treatment might yield information that could distinguish the differential response behaviors of these cell lines. We thus measured the levels of the same signals at 0, 1, 2, 4, and 24 hours after treatment in both the Huh7 and Hep3B cells. These timepoints were initially chosen based upon the literature reports of early and late changes in phosphorylation levels in response to 17AAG. The measurements were not extended to times between 4 and 24 hours since it was clear that most signaling degradation that was evident at 24hours, had begun by 4 hours, and the changes between 1 and 4 hours were provided substantial correlations for further study. These measurements were normalized to an un-treated control for each cell line, and are plotted in Figure 2A as fold-change induced by 17AAG. Both Huh7 and Hep3B exhibited transient early p-JNK activation. However, relatively stronger transient activation and/or relatively weaker degradation was seen for most other signals (p-AKT, p-IκB-α, p-GSK3α/β, p-ERK1/2, p-p38 and p-STAT3) in Huh7 cells compared to Hep3B cells (Figure 2A). Strikingly, the integrated signal changes over the first 4 hours after 17AAG treatment are higher across many components in Huh7 cells than in Hep3B cells (Figure 2B). In order to more effectively interpret these data we employed principal components analysis, a technique that models multi-variate data in terms of key combinations of measurements exhibiting major co-variation in the data set. These combinations can be viewed geometrically as “directions” (or vectors) in the “space” of the signaling measurements defined by axes representing each of the measured time-points and the integral metric. The direction of greatest co-variation, incorporating the most important measurement combinations, is the principal component #1 (PC1); principal component #2 (PC2) then incorporates the next most important measurement combinations best capturing the residual co-variation, and so on. The principal components taken all together collapse the original 5 dimensional data into a reduced number of axes representing the most important underlying variables. In our case the 5 dimensional data set can be comprehended in 2 dimensional principal components space as early signaling (PC1) and late

signaling(PC2). These underlying variables are just combinations of the original variables that best comprehend the data within the entire signaling measurement 'vector space' (Supplementary Figure S1 offers an illustrative tutorial). Our model with 2 principal components effectively captures 91% of the cumulative variance. Our cutoff was easily established by the impressive drop in the variance captured by the third component(Figure 3A). Furthermore a re-sampling of our data set determined that our analysis captures significantly(p=0.0002) greater variance than one can capture with 1000 2-component models generated by randomly sampling the column index of the rows in our data set(Figure 3B). Our analysis visually distinguishes the behavior of both Huh7 and Hep3B cells, and interestingly the PCA loadings plot(not shown) indicated that short-time signals reside along PC1 and the late-time signals reside along PC2(Figure2C). A so-called 'scores plot', in which the various signal measurements are projected on the principal components axes, visualizes distinct regions where Huh7 signals reside differentially with respect to Hep3B signals (Figure 2C). These differences are quantitated in Figure 2D, in terms of 'contribution vectors', which quantify the disparities between cell line-specific signals(in units of standard deviation) relative to the average distance between all of the signals of the distinct cell lines. The calculated contributions vectors reveal that out of the 10 signaling measurements made at each of 5 time-points, the most important differences between the drug resistant Huh7 and drug sensitive Hep3B lie in the early time-points of four signals: p-AKT, p-IκB-α, p-STAT3, and p-p38. Because the experimental conditions for the elucidation of signaling effect grows very rapidly with the size of the hit set, the p-p38 signal measurements can be seen to reside as an outlier beyond the region of Hotelling's criterion[28], presented no clear biological hypothesis and was excluded from further analysis.

The principal components model accurately maps another 17AAG-sensitive HCC cell line, FOCUS, to the same region as Hep3B. In order to test our principal components analysis we utilized our previous approach in a third HCC cell line. A signaling time-course for FOCUS cells, analogous to Figure 2A, shows signal degradation and no transient activation (Figure 4B). Although certain signaling network differences between FOCUS and Hep3B signaling are evident by inspection, our principal components analysis shows that the FOCUS cells cluster in the same region as the similarly 17AAG sensitive Hep3B cells (Figure 4C). Indeed, we found that FOCUS cells are sensitive to 1μM 17AAG-induced cell death at 48 hours (Figure 4A). This result demonstrates that the principal components capture critical signal combinations associated with these cell death-vs-survival outcome

es.

A drug combination pretreatment based on inhibition of three key nodes partially sensitizes Huh7 to 17AAG. In Figure 3D we identified four signals (p-AKT, p- IκB-α, p-STAT3, and p-p38) to be most important in distinguishing Huh7 from Hep3B. We proposed to test whether a combination of drugs inhibiting these key signals in particular could recreate the 17AAG treatment responses. We selected p-AKT, p-STAT3, and p- IκB-α for this purpose, omitting p-p38 due to its notification by Hotelling's outlier criteria at a 95% confidence level[28]. Pre-treatment of Huh7 cells for 12 hours with targeted inhibitors of p-AKT (PI3Kinhibitor, PI-103, 5μM), p-STAT3 (JAK inhibitor 1, Pyridone 6,Calbiochem, 3μM) and p- IκB-α (IKK inhibitor, BMS-345541, 15μM) signaling failed to sensitize Huh7 cells to 1μM 17AAG at 48hours (Figure 5A). However, a combination pre-treatment using all three inhibitors together partially sensitized ($p<0.0001$) Huh7 cells to 17AAG-induced cell death (Figure 5A). Moreover, this inhibitor combination induced Huh7 cell death to a significantly greater ($p<0.0005$) degree than

did 17AAG (Figure 5A). In order to control for the possibility that any combination of three inhibitors can potentiate 17AAG induced cell death, inhibition of one critical signal (p-STAT3) was combined with inhibition of two non-critical signals (p-JNK, p–ERK) (Figure 3D). This control drug combination, comprising 3μM of the JAK inhibitor, 10μM of a MEK inhibitor (PD98059) and 10μM of a JNK inhibitor (SP600125), failed to sensitize Huh7 to 17AAG or induce cell death on its own at 48 hours. (Figure S2).

Decoupling pro-apoptotic effects from the overall context of 17AAG treatment creates a three-kinase inhibitor combination that works as well or better than 17AAG in all cell lines. 17AAG is known to have both pro and anti apoptotic effects. Assuming that 17AAG induces cell death through a combination of the pro-apoptotic consequences of the degradation of key signaling pathway nodes, we hypothesized that the previously identified critical nodes distinguishing sensitive and resistant cells could be key sites for selectively-targeted drug contributions in sensitive cells. To test this idea, FOCUS and Hep3B cells were pre-treated with the three-kinase drug combination, or control vehicle, for 12 hours before addition of 1μM 17AAG. The drug combination enhanced 17AAG induced cell death significantly ($p=0.050$, and $p<0.0001$ respectively) in both cases (Figure 5B). Yet more strikingly, the drug combination by itself induced cell death as strongly -- or more so -- than 17AAG in all HCC cell lines. FOCUS cells showed no significant difference between 17AAG and the drug combination induced cell death, whereas in Hep3B and Huh7 cells the drug combination at 48 hours worked significantly better than 17AAG (Figure 5A, B).

Decoupling the pro-apoptotic effects from their 17AAG context allows for cell line specific tuning of the therapeutic strategy. After finding a drug combination that works as

well or better than 17AAG, we wanted to test two hypotheses. First, that the decoupling of a specific pathway effect from the context of 17AAG allows for cell line specific therapeutic strategies. And, second, that the presence of additivity or synergy correlates with cell line-specific differences in the combination inhibitor efficacy relative to 17AAG. To address these questions, we undertook a set of experiments in a Jak inhibitor background, across a 4×4 matrix of PI3K and IKK inhibitor concentration combinations, covering 4 concentrations of each (0, Low, Medium, and High) (Figure 6). Inspection of the cell death responses reported in this matrix indicated distinct responses for the three cell lines tested. FOCUS cells appeared to primarily be sensitive to the IKK inhibitor in the JAK inhibitor background whereas Hep3B and Huh7 cells exhibited sensitivity to both IKK and PI3K inhibition (Figure 6A). Calculation of the fold increase in cell death of a double drugged entry in the 4×4 dosing matrix relative to linear additivity demonstrates that only Huh7 cells exhibit a drug combination synergy (Figure 6B). This finding of multi-drug nonlinear synergy in the Huh7 and multi-drug additivity in Hep3B but not FOCUS cells correlates with our observation that the kinase inhibitor combination could essentially duplicate the 17AAG effects on cell death in the latter whereas it could exceed the 17AAG effects on cell death in the former 2.

Discussion

Inhibition of the Hsp90 chaperone represents a prominent example of a highly complex multi-target therapeutic approach to cancer[5], and studies have explored the myriad of regulatory pathway alterations associated with its effects[9-17]. Although these studies have unveiled short-term and/or long-term changes in levels and/or activities of numerous cellular components with opposing effects on the downstream phenotype, there is currently inadequate understanding which set of pathway alterations can recapitulate drug efficacy. Our effort here aims to gain quantitative understanding of the key kinase signals underlying the effects of the geldanamycin analogue 17AAG on differential apoptotic death responses of three HCC cell lines: Hep3B, FOCUS, and Huh7. Our studies centered on 7 canonical kinase signals: p-AKT (Ser473), p-ERK1/2 (Thr202/Tyr204), p-STAT-3 (Tyr705), p-p38 (Thr180/Tyr182), p-JNK (Thr183/Tyr185), p-GSK-3α/β (Ser21/Ser9), and p-IKb-α (Ser32), with a goal of ascertaining whether a quantitative combination of a particular subset of these signals might be especially critical in clustering the HCC line responses to 17AAG.

We found that a PCA-based model consisting of 2 principal components explains 91% of the cumulative variance captured by the model. This variation can be classified as early variation (PC1) and late variation (PC2) (Figure 3). All cell lines and signals inhabit the same principal components space, implying that there is a general homology of response. This overall homology stresses that the drug is operating similarly in all cell lines tested, and that the phenotypic responses are not likely to be based upon the metabolic inactivation of 17AAG or a rapid cellular efflux. The early variation axis (PC1) best separates the cell lines with disparate responses, suggesting, that this previously documented early signaling phenomena[17] can be correlated with a cellular phenotype.

The PCA based visualization accurately maps the sensitive FOCUS cell line to the same region as Hep3B cells (Figure 4). This greatly improves our confidence that the variation captured in 2 dimensional principal components space is relevant to the disparate cell phenotypes, and that our analysis has captured important biological information. The success of our PCA mappings suggests that data-driven modeling can effectively reduce the dimensionality of multi-target perturbations, and provide a compact easy to interpret analytical method for determining the most phenotypically relevant parameters for further investigations.

In previous data-driven modeling efforts, Miller-Jensen et al. 2007 and Kemp et al. 2007 have shown that a systematic signaling analysis of growth factor and cytokine induced cellular phenotypes, captures enough signaling variation that the phenotypic effects of drug perturbations can be predicted *a priori*. Kumar et al. 2008 extended this analysis to show that multiple signals measuring the off target effects of inhibitors are necessary to predict drug effects upon EGF-induced migration. Our quantitative analysis of 17AAG leads to testable hypotheses about the targeting of early IKK, PI3K, JAK-STAT inhibition in 17AAG induced cell death (Figure 2). The individual targeted pharmacological pre-treatment of these three survival pathways, fails to abrogate the resistance phenotype, but the combined pretreatment is able to synergistically sensitize Huh7 to 17AAG (Figure 5A). This evidence suggests that cumulative early action of the IKK, PI3K, and JAK-STAT pathway families may be responsible for a portion of Huh7's drug resistance phenotype.

While the combination therapy potentiates 17AAG induced cell death in all cell lines tested, the most striking consequence of our study, is the ability of combination therapy alone to recapitulate 17AAG's cell death effect in a manner that is equal to, or greater than the singular effect of 17AAG. This effect has two distinct modalities. In Huh7 and Hep3B cells the combination treatment works approximately 5-fold and 3-fold better, respectively, than 17AAG alone. In contrast, the combination treatment is of similar efficacy to 17AAG alone in FOCUS

cells (Figure 5). These distinct modalities can be correlated with the spectrum of multiple drug interactions in the combination therapy (Figures 6). We speculate that these correlations may suggest a basis for future work on the cell specific nature of both 17AAG's pro-/anti-apoptotic function, and how synergy between nodes may play a role in the efficacy of multi-drug combinations and multi-target inhibitors.

By using principal components modeling of a drug perturbation to guide the recreation of a more specific therapeutic strategy we have shown that we can not only recreate the effect of a multi-target drug, but that the recreated effect can work better than the original drug. The existence of differences in the multi-drug interactions (Figure 6) underscores the value of recreating multi-target effects. In decoupling the effects from the context of 17AAG we find that the potential exists to allow for the individual adjustment of the elements of a combination therapy.

Our argument that a particular combination therapy produces a less pleiotropic effect than the multi-target compound that it has been rebuilt from is reliant upon the diversity of the cellular effects of the initial multi-target compound along with the off-target effects of the combination therapy. In our particular case, a relatively extreme example, Hsp90 in *Saccharomyces Cerevisiae* is known to interact with approximately 10% of the ORF's examined in a recent study[7]. Though a similar analysis is not available for the three compounds of our combination therapy, it seems very likely that our combination therapy is far more specific for several reasons. A systematic study of 317 kinases found that for PI103, approximately 10 cellular kinases had IC50's of less than 10μM in vitro[29]. BMS-345541 is an allosteric inhibitor of IKK and failed to significantly inhibit a panel of 15 related kinases at concentrations as high as 100μM[30]. Our Janus kinase inhibitor, Pyridone 6, while less well tested than the other two fails to inhibit the proliferation of cell lines that do not harbor activated JAK-STAT signaling[31]. Thus in-spite of the inevitable existence of some off-target effects, it seems highly unlikely that the

magnitude of these effects could approach the pleiotropy of 17AAG. Therefore, the generalizability of this approach to other forms of multi-target compounds will likely prove increasingly practical as more specific inhibitors become available.

Acknowledgements

The authors would like to thank Hyung-Do Kim, and Luke Gilbert for insightful discussions, and Pam Kreeger, Megan Palmer, Shannon Alford, Shan Wu, Matt Lazzara, and Arthur Goldsipe for excellent technical input.

References

1. Lynch TJ, Bell DW, Sordella R, et al. Activating mutations in the epidermal growth factor receptor underlying responsiveness of non-small-cell lung cancer to gefitinib. New. Eng. J. Med. 2004; 350: 2129-39.

2. Chabner BA, and Roberts TG Jr. Chemotherapy and the war on cancer. Nat. Rev. Cancer 2005; 5: 65-71.

3. Petrelli A, Giordano S. From single to multi-target drugs in cancer therapy: when aspecificty becomes an advantage. Curr. Med. Chem. 2008; 15: 422-32.

4. Uehara Y, Makoto H, Tomio T, and Umezawa H. Phenotypic change from transformed to normal induced by benzoquinonoid ansamycins accompanies inactivation of p60src in rat kidney cells infected with Rous sarcoma virus. Molecular Cell. Biol. 1986; 6: 2198-2206.

5. Whitesell L, and Lindquist S. Hsp90 and the chaperoning of cancer. Nat. Rev. Cancer 2005; 5: 761-72.

6. Whitesell L, Shifrin SD, Schwab G, and Neckers L. Benzoquinonoid ansamycins possess selective tumoricidal activity unrelated to src kinase inhibition. Cancer Res. 1992; 52: 1721-8.

7. Zhao R, Davey M, Hsu YC, et al. Navigating the chaperone network: an integrative map of physical and genetic interactions mediated by the Hsp90 chaperone. Cell 2005; 120: 715-27.

8. Kamal A, Thao L, Sensintaffar J, et al. A high-affinity conformation of Hsp90 confers tumour selectivity on Hsp90 inhibitors. Nature 2003; 425: 407-10.

9. Hostein I, Robertson D, DiStefano F, et al. Inhibition of signal transduction by the Hsp90 inhibitor 17-Allyamino-17-demethoxygeldanamycin results in cytostasis and apoptosis. Cancer Res. 2001; 61: 4003-09.

10. Bareng J, Jilani I, Gorre M, et al. A potential role for Hsp90 inhibitors in the treatment of Jak2 mutant-positive diseases as demonstrated using quantitative flow cytometry. Leukemia and Lymphoma 2007; 48: 2189-95.

11. Mitsiades CS, Mitsiades NS, McMullan CJ, et al. Antimyeloma activity of heat shock protein-90 inhibition. Blood 2006; 107: 1092-1100.

12. Garcia-Morales P, Carrasco-Garcia E, Ruiz-Rico P, et al. Inhibition of Hsp90 function by ansamycins causes downregulation of cdc2 and cdc25c and G2/M arrest in glioblastoma cell lines. Oncogene 2007; 26: 7185-93.

13. Solit DB, Ivy SP, Kopli C, et al. Phase 1 trial of 17-Allyamino-17-demethoxygeldanamycin in patients with advanced cancer. Clin. Cancer Res. 2007; 13: 1775-82.

14. Chandarlapaty S, Sawai A, Qing Y, et al. Snx2112 a synthetic heat shock protein 90 inhibitor has potent antitumor activity against HER kinase-dependent cancers. Clin Cancer Res 2008; 14: 240-48.

15. Yun BG, and Matts R. Hsp90 functions to balance the phosphorylation state of Akt during C2C12 myoblast differentiation. Cellular Signaling 2005; 17: 1477-85.

16. Donze O, Abbas-Terki T, and Picard D. The Hsp90 chaperone is both a facilitator and a repressor of the dsRNA-dependent kinase PKR. The EMBO J. 2001; 20: 3771-80.

17. Koga F, Xu W, Karpova TS, et al. Hsp90 inhibition transiently activates Src and promotes Src-dependent Akt and Erk activation. PNAS 2006; 103: 11318-22.

18. Kumar N, Afeyan R, Kim HD, and Lauffenburger DA. A multi-pathway model enables prediction of kinase inhibitor cross-talk effects on migration of Her2-overexpressing mammary epithelial cells. Mol Pharmacol. 2008; 73: 1668-78.

19. Janes KA, and Yaffe MB. Data-driven modeling of signal-transduction networks. Nat. Rev. Mol. Cell Biol. 2006; 7: 820-8.

20. Prudhomme W, Daley GQ, Zandstra P, and Lauffenburger DA. Multivariate proteomic analysis of murine embryonic stem cell self-renewal versus differentiation signaling. PNAS 2004; 101: 2900-5.

21. Gaudet S, Janes KA, Albeck JG, Pace EA, Lauffenburger DA, and Sorger PS. A compendium of signals and responses triggered by prodeath and prosurvival cytokines. Mol. Cell Proteomics 2005; 4: 15669-90.

22. Janes KA, Albeck JG, Gaudet S, Sorger PK, Lauffenburger DA, and Yaffe MB. A systems model of signaling identifies a molecular basis set for cytokine-induced apoptosis. Science 2005; 310: 1646-53.

23. Miller-Jensen K, Janes KA, Brugge JS, and Lauffenburger DA. Common effector processing mediates cell-specific responses to stimuli. Nature 2007; 448: 604-8.

24. Kemp ML, Wille L, Lewis CL, Nicholson LB and Lauffenburger DA. Quantitative network signal combinations downstream of TCR activation can predict IL-2 production response. J Immunol. 2007; 178: 4984-92.

25. Farazi PA, and DePinho RA. Hepatocellular carcinoma pathogenesis: from genes to environment. Nat. Rev. Cancer 2006; 6: 674-86.

26. Lim SO, Park SG, Yoo J-H, et al. Expression of heat shock proteins (Hsp27, Hsp60, Hsp70, Hsp90, Grp78, Grp 94) in hepatitis B virus-related hepatocellular carcinomas and dysplastic nodules. World J. Gastroenterol. 2005; 11: 2072-9.

27. Lee HC, Tian B, Sedivy J, Wands JR, and Kim M. Loss of Raf kinase inhibitor protein promotes cell proliferation and migration of human hepatoma cells. Gastroenterology 2006; 131: 1208-17.

28. K.V. Mardia, J.T. Kent, and J.M. Bibby (1979) *Multivariate Analysis*, Academic Press.

29. Karaman MW, Herrgard S, Treiber DK, et al. A quantitative analysis of kinase inhibitor selectivity. Nat. Biotechnol. 2008; 26: 127-32.

30. Karin M, Yamamoto Y, and Wang QM. The IKK NF-ΚB system: a treasure trove for drug development. Nat. Rev. Drug Disc. 2004; 3: 17-26.

31. Pedranzini L, Dechow T, Berishaj M, et al. Pyridone 6, A pan-Janus-Activated Kinase inhibitor induces growth inhibition of multiple myeloma cells. Cancer Res. 2006; 66: 9714-21.

32. Jolliffe I.T. Principal Components Analysis. 2nd Edition. Springer-Verlag. New York. 2002.

33. Eriksson L., Johansson E., Kettanel N., and Wold S. Multi and Mega-variate Data Analysis, Principles and Applications. UMETRICS A.B. Umea, Sweden. 2001.

Figure1

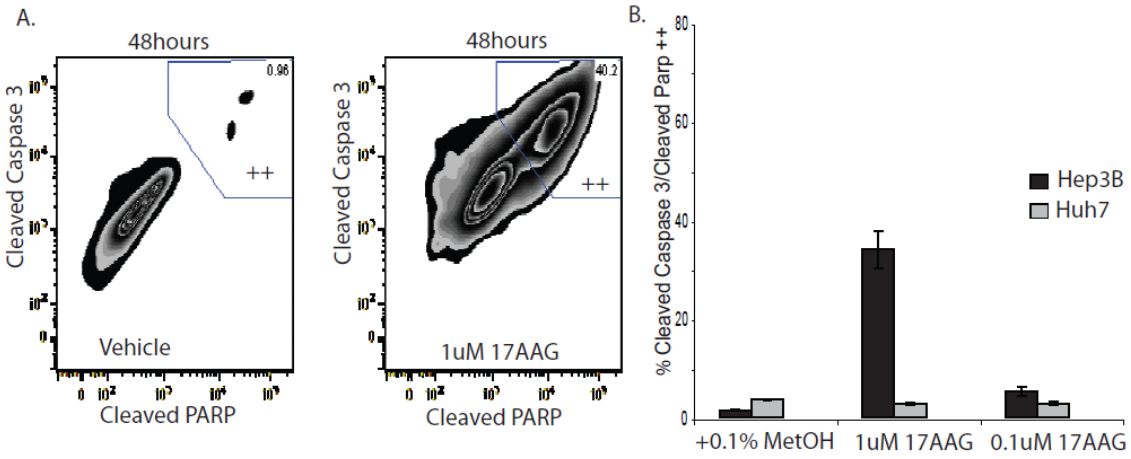

Figure 1. A plot for the Cleaved Caspase 3/Cleaved PARP double positive population at 48 hours measures the susceptibility of Hep3B and the resistance of Huh7 cells to 17AAG. Typical measurements of 24hr signaling degradation in response to 17AAG fail to correlate with this distinction. **A.** A representative flow cytometry scatter plot depicts Hep3B fixed and permeabilized cells, that are stained with antibodies for Active Cleaved Caspase 3 and Cleaved PARP at 48hrs after treatment with 1μM17AAG or 0.1% MetOH vehicle control. The double positive population is denoted by the gating in the upper right hand corner. Different gatings were used for Huh7 and Hep3B but the scatter plots looked very similar. **B.** The average size of the population of three replicates(+/-SEM) of Hep3B and Huh7 cells as gated in A. represents the percent of double positive apoptotic cells at 48hrs +/-SEM.

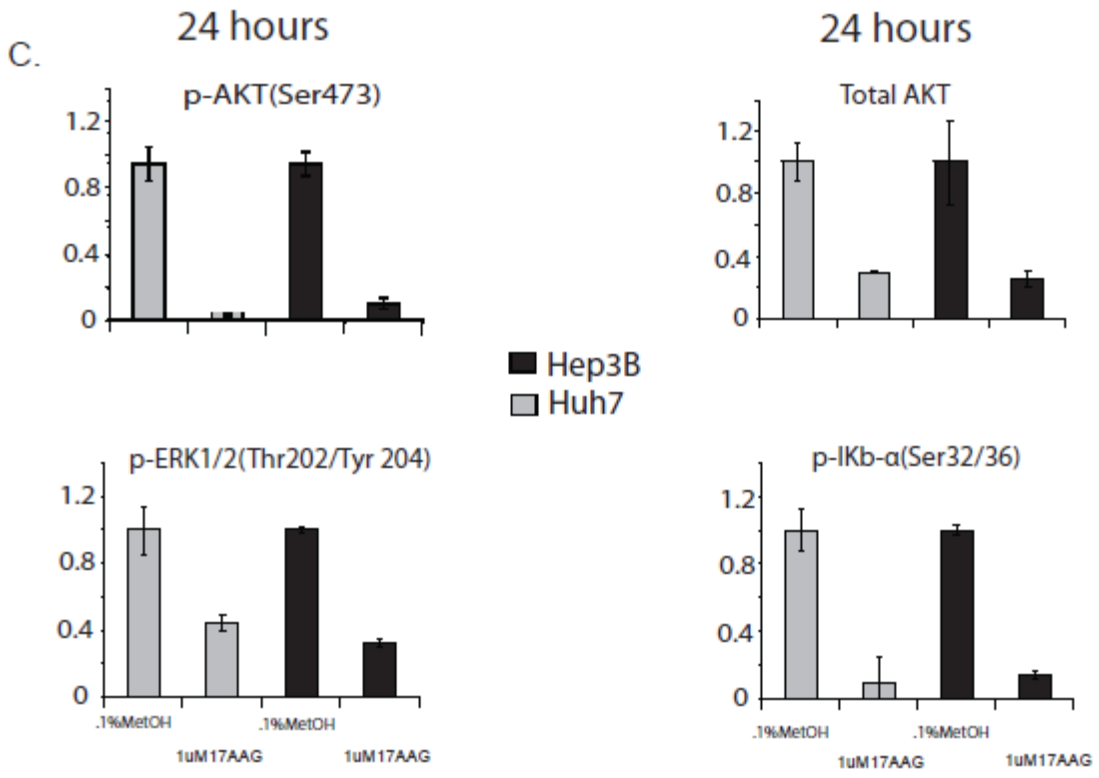

Figure 1 C. Late time signals do not correlate with 17AAG susceptibility**.** Measured at 24hours, the fold change of the mean of duplicates +/-SEM, treated with 1uM 17AAG, is normalized to a 0.1% MetOH control. p-AKT (Ser473), t-AKT, p-ERK1/2(Thr202/Tyr204), and p-IKB-α (Ser32/36) were measured by a bead based Bio-rad phospho-protein (Bioplex) assay.

Figure 2. A dynamic signaling timecourse reveals differences between Hep3B and Huh7. **A.** A signaling time-course in Hep3B and Huh7 cells depicts mean fold changes in phospho-protein signaling in response to 1uM 17AAG relative to the vehicle only (0.1%MetOH) control. **B.** The integral (discussed in methods) from 0-4hrs of 17AAG induced signaling shows the large cumulative difference in early signaling between Huh7 and Hep3B cells.

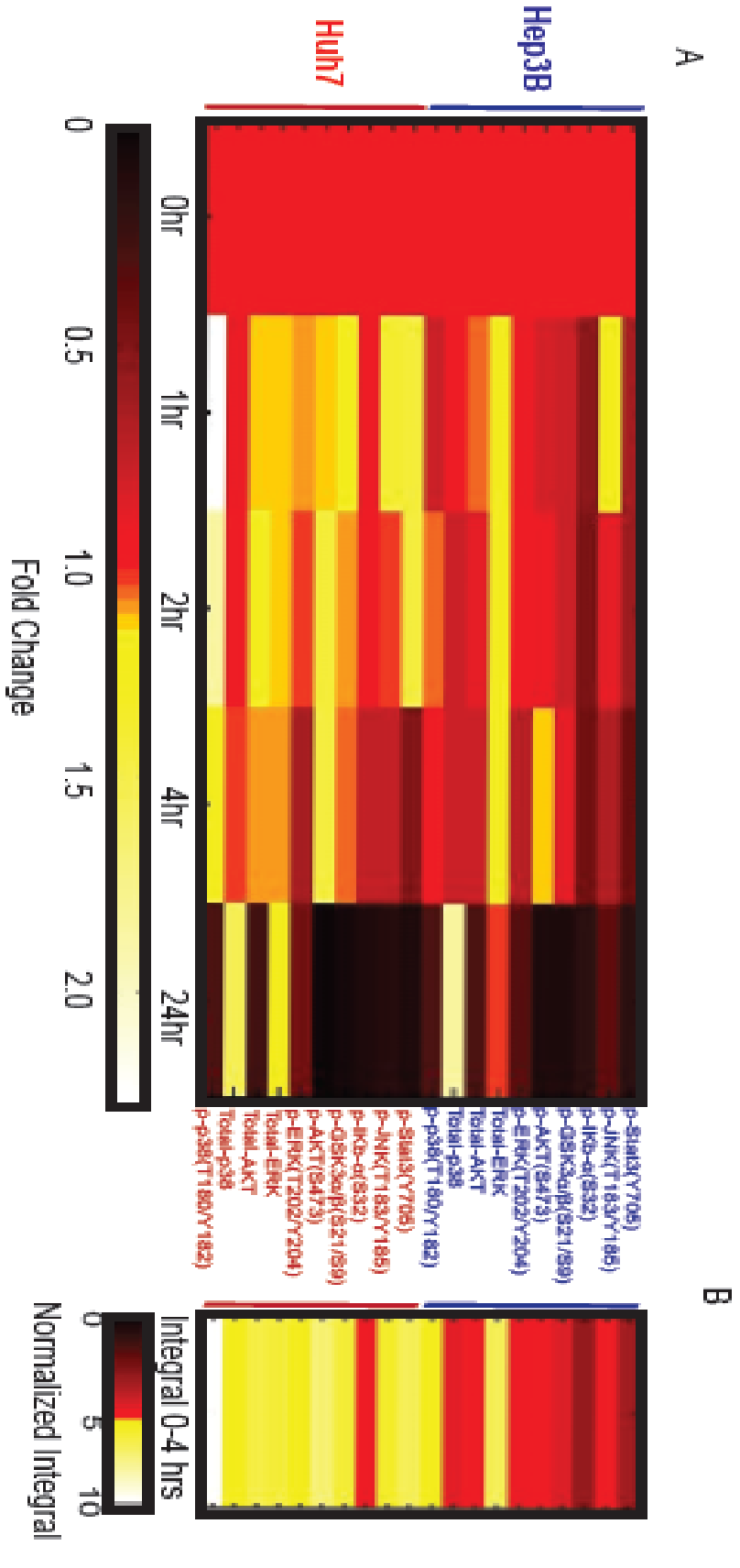

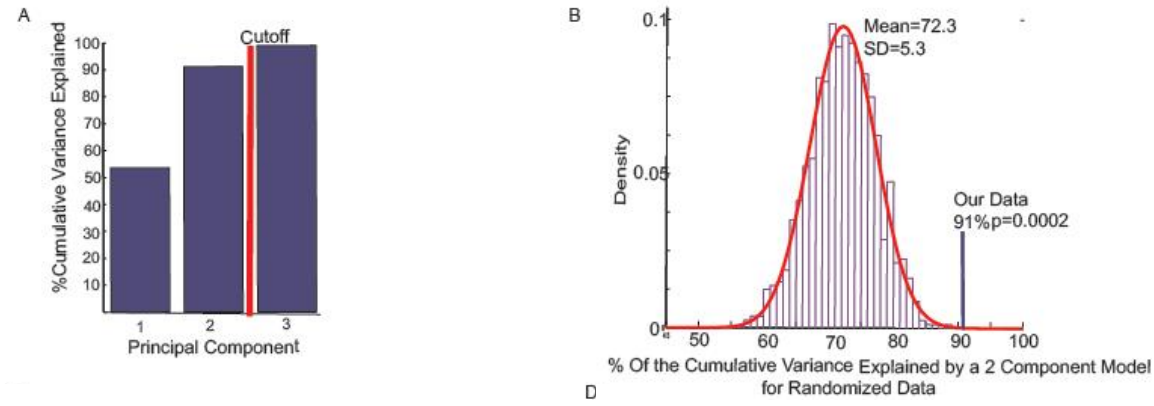

Figure 3. A Principal Components Analysis reduces data complexity and provides testable hypotheses. **A.** A bar graph depicts the percent of the total variance captured by a model consisting of 1,2,or 3 principal components. There is a marginal increase in the benefit of including principal component 3, indicating an obvious cutoff criterion. **B.** The % of total variance explained by two component models that are built upon 1000 perturbed data matrices(see methods). A histogram plots the data from the empirical 1000 matrix sampling. A normal distribution was fit to the histogram data and our model fit was calculated to have a highly significant p-value of 0.0002.

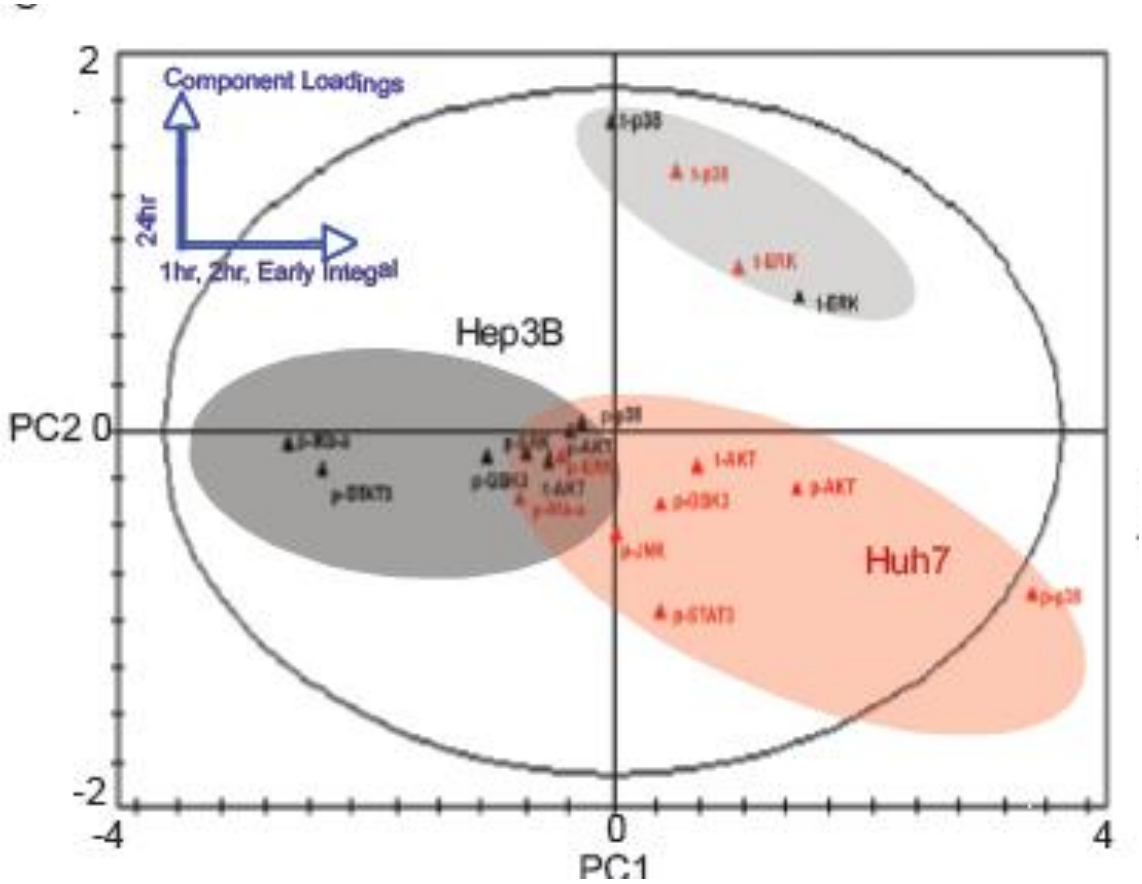

Figure3 C. A principal components analysis yielded a two component model that accurately explains 91% of the cumulative variance. Principal component 1 strongly captures variation at early time points, and in the 0-4hrs integral metric. Principal component 2 captures variation at 24hrs. These results from the loadings plot are summarized in the upper righthand corner of the plot. The ellipse represents Hotelling's outlier criteria at a 95% confidence level. The original signaling measurements are plotted in the principal components space. Principal component 1 visually appears to capture cell line variation. The colored ellipses are simply a visualization tool used to bring the readers attention to the distinct clusters in the scores plot.

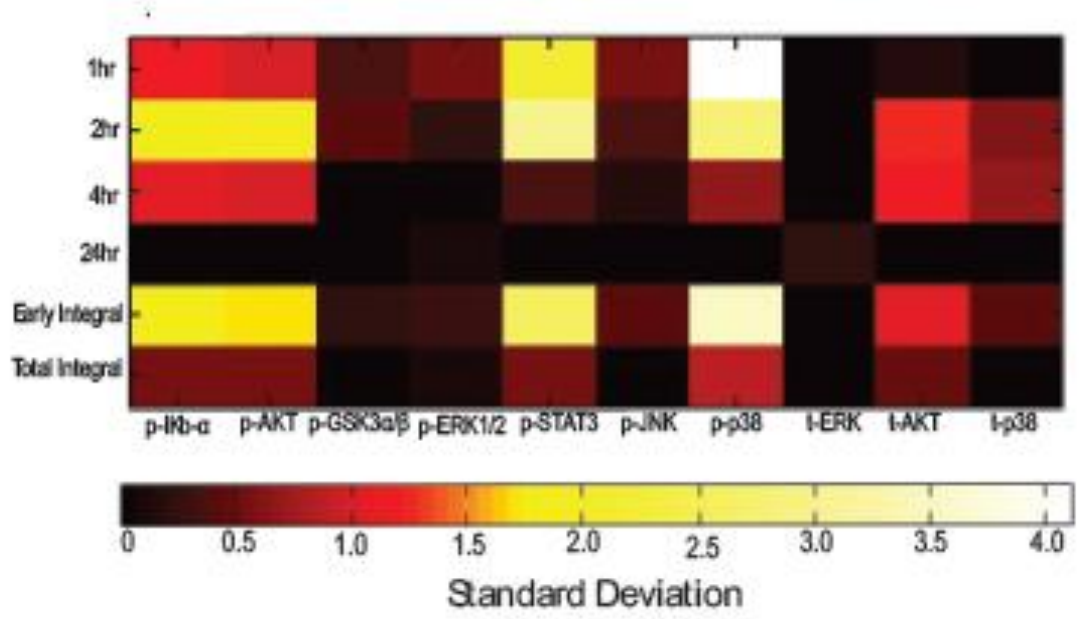

Figure3D. Contributions vectors describe how signals vary in principal components space, and, are derived computationally, by measuring the latent variable distance in terms of the measured variables between Huh7 and Hep3B for a given signal, then comparing that specific distance to an average distance (in units of standard deviation). This plot asks the question of how distinct are two signals between Huh7 and Hep3B cells relative to the average distance between the signals from the two cell lines. Quantitatively, D. affirms qualitative observations made in C.

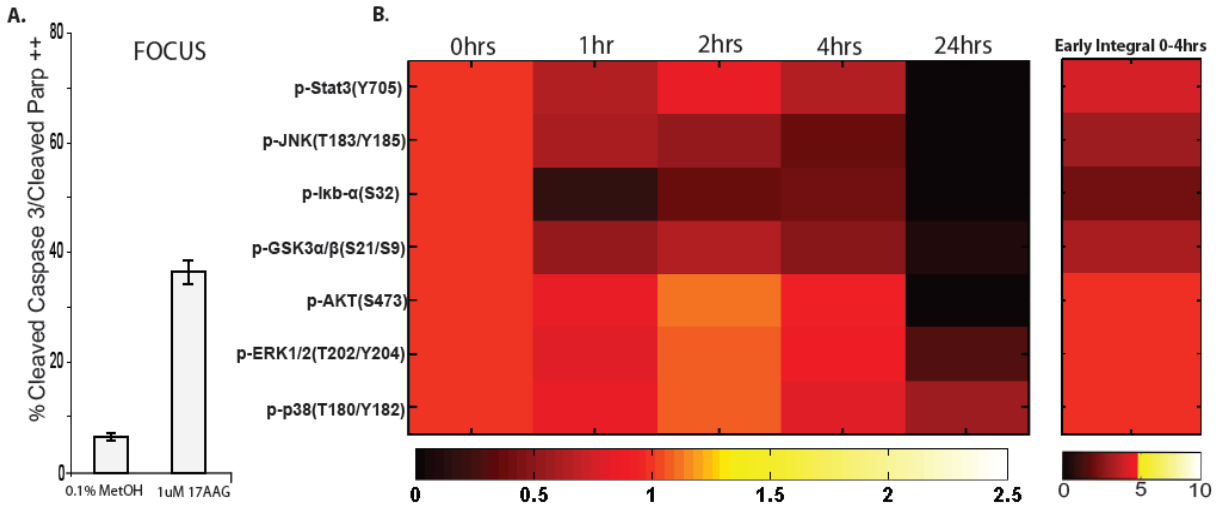

Figure 4. Adding signaling data from another HCC cell line (FOCUS) to the principal components analysis correctly clusters FOCUS cells with sensitive Hep3B cells. **A.** The mean of triplicate measurements of the percent of double positive FOCUS cells in response to 1uM 17AAG at 48 hrs. The gating strategy was the same as in 1A **B.** A signaling time-course of FOCUS cells in response to 1uM 17AAG. Time-point measurements are represented as mean signaling fold change relative to vehicle only controls.

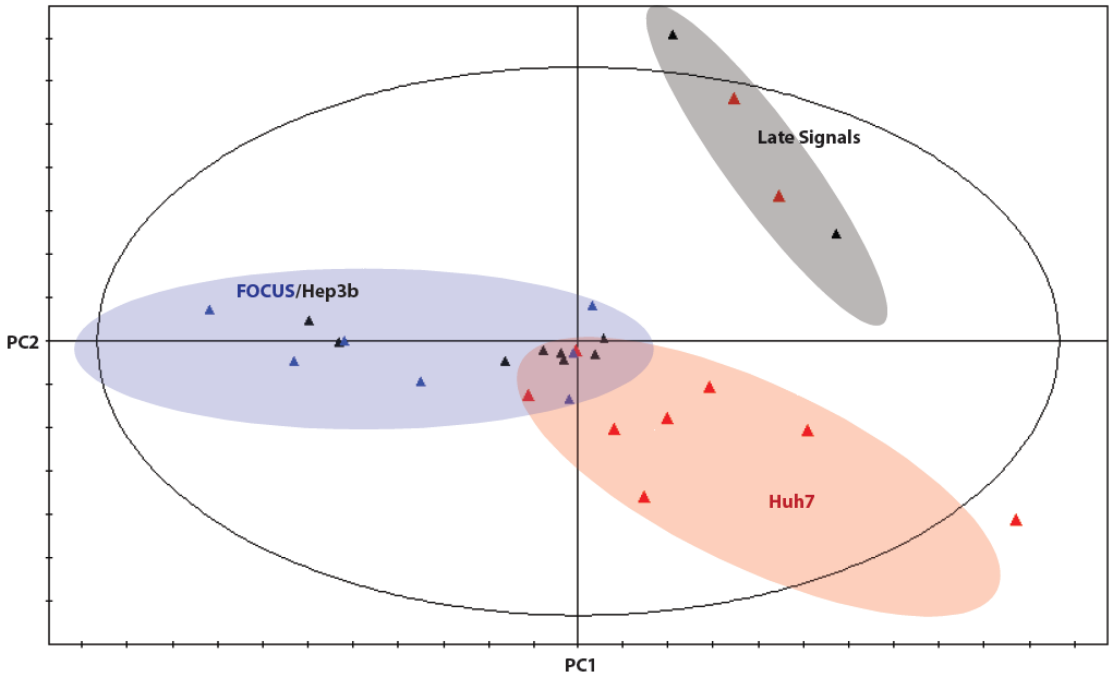

Figure 4C. A principal components plot, as in figure 2 correctly classifies FOCUS cells as sensitive to 17AAG in the 2-component model.

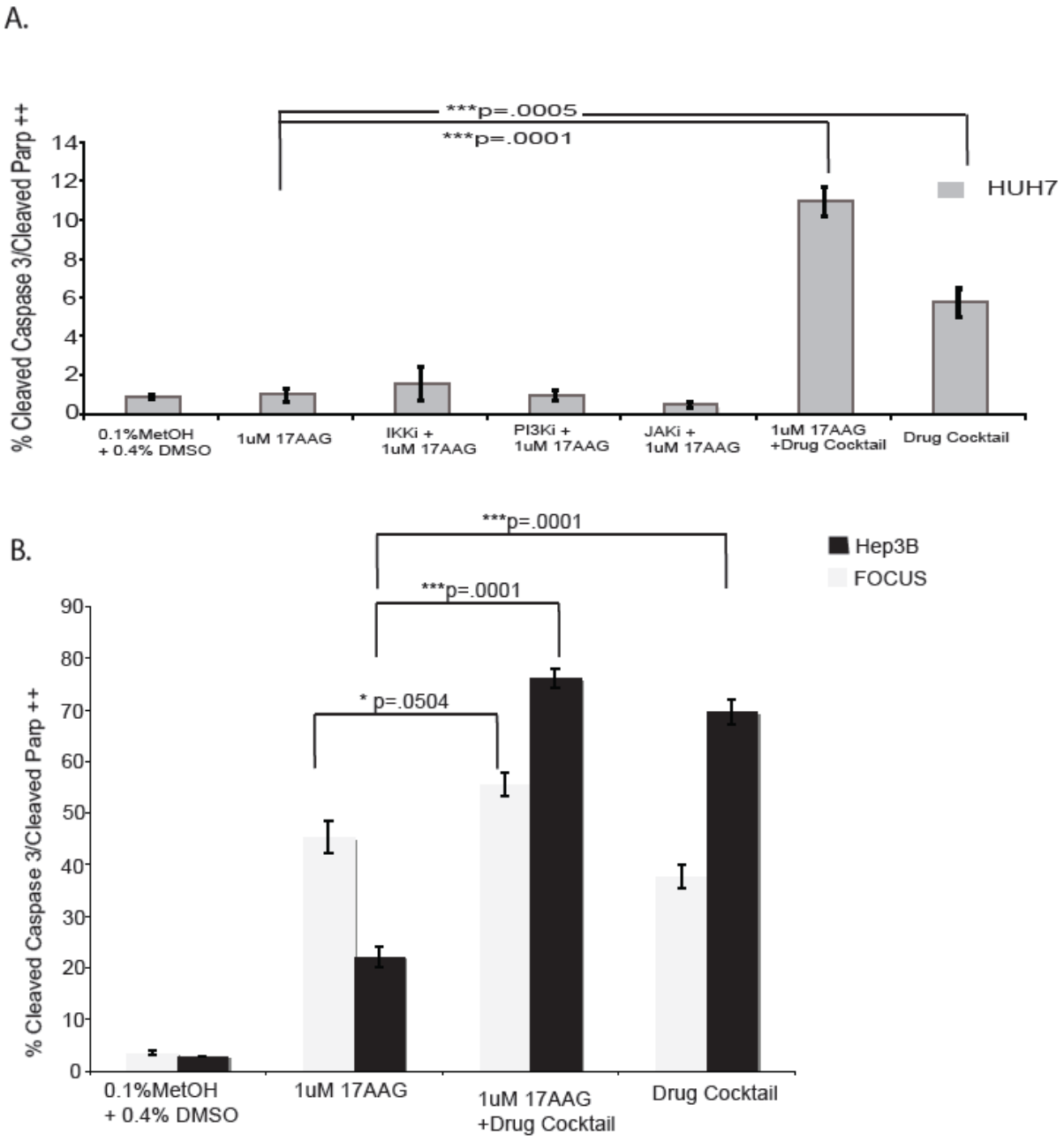

Figure 5. Where inhibition of singular nodes fails, pre-treatment with a combination therapy sensitizes Huh7 cells to 17AAG, and works as well or better than 17AAG in all cell lines tested. **A.** Double positive populations of Huh7 cells (mean of triplicate+/-SEM as gated in 1A) in response to different treatments at 48hours. The IKK inhibitor is BMS-345541 and was used at

15uM, the PI3K inhibitor is PI103 and was used at 5μM, the JAK inhibitor is Calbiochem JAK inhibitor 1: Pyridone 6, and was used at 3μM. The P-values were obtained by a T-test **B.** The double-positive populations for the listed treatments of Hep3B and FOCUS cells (mean of triplicates +/-SEM) at 48 hours. The P-values were obtained by a T-test. The drug combination is the same as in A.

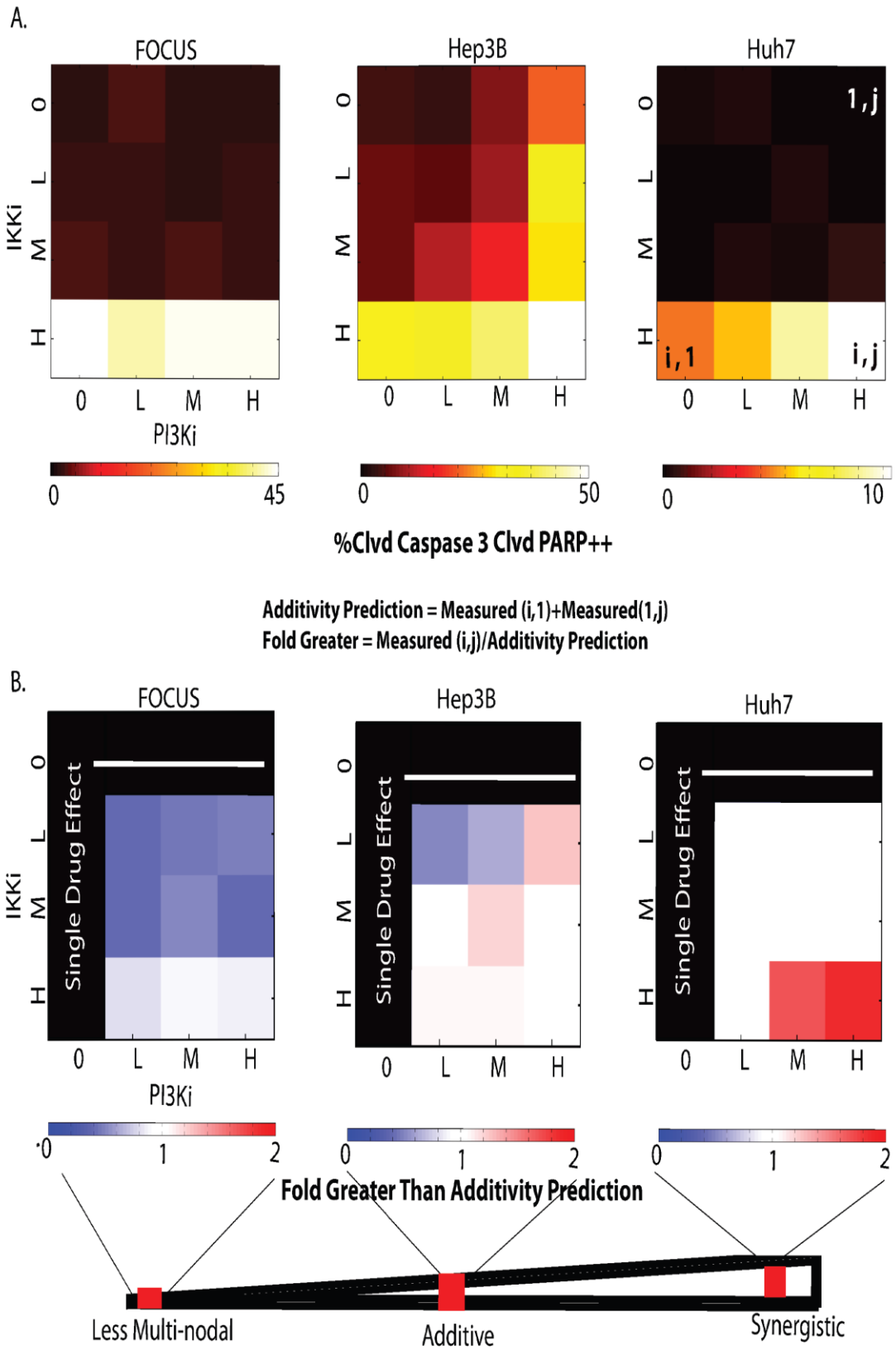
A.
FOCUS
Hep3B
Huh7
IKKi
PI3Ki
0
L
M
H
1,j
i,1
i,j
0
45
50
10
%Clvd Caspase 3 Clvd PARP++
Additivity Prediction = Measured (i,1)+Measured(1,j)
Fold Greater = Measured (i,j)/Additivity Prediction
B.
Single Drug Effect
Fold Greater Than Additivity Prediction
Less Multi-nodal
Additive
Synergistic

Figure 6. Focus, Huh7 and Hep3B cells exhibit different amounts of multi-node effects in a JAK inhibitor background. **A.** A matrix of the mean of duplicate measurements of the percent of double positive cells in response to varying concentrations of I-kappa-kinase inhibitor (IKKi) and PI3kinase inhibitor (PI3Ki) in a JAK (3μM) inhibitor background. The compounds are the same as in figure 4. Concentrations are as follows: (IKKi, H=20μM, M=6.66μM, L=2.22μM), (PI3Ki, H=5μM, M=1.66μM, L=0.55μM). **B.** The synergy plots display the fold deviation from predictions based on the assumption of additivity. Briefly, additivity predictions for any double-drugged entry (i,j) were calculated by adding the ith row of the first column (i.e. the singular IKK effect at that concentration) to the first row, jth column (i.e. the singular PI3k effect at that concentration). Then the measured value at the double-drugged entry (i,j) was divided by the additivity prediction. This created a metric that describes synergy versus additivity.

Chapter 2

A Mammalian RNAi Based Approach to Drug Characterization

Contributions:

Hai Jiang and Luke Gilbert cloned the initial 29 shRNA library. Hai Jiang performed the GFP enrichment assays for the first three figures. I developed all of the data analysis strategies and tools and contributed significantly to experimental design. I performed all ALL signature experiments and some of the later Myc GFP enrichment experiments. M. Hemann, H. Jiang, D. Lauffenburger and I all contributed to the writing on the paper. Much of this section was previously published as:

A mammalian functional-genetic approach to characterizing cancer therapeutics.

Jiang H, Pritchard JR, Williams RT, Lauffenburger DA, Hemann MT.

Nat Chem Biol. 2011 Feb;7(2):92-100. Epub 2010 Dec 26

Abstract

Identifying mechanisms of drug action remains a fundamental impediment to the development and effective use of chemotherapeutics. Here, we describe an RNA interference (RNAi)-based strategy to characterize small molecule function in mammalian cells. By examining the response of cells expressing short hairpin RNAs (shRNAs) to a diverse selection of chemotherapeutics, we could generate a functional shRNA signature that was able to accurately group drugs into established biochemical modes of action. This, in turn, provided a diversely sampled reference set for high-resolution prediction of mechanisms of action for poorly characterized small molecules. We could further reduce the predictive shRNA target set to as few as 8 genes, and by using a newly derived probability based nearest neighbors approach, could extend the predictive power of this shRNA set to characterize additional drug categories. Thus, a focused shRNA phenotypic signature can provide a highly sensitive and tractable approach for characterizing new anti-cancer drugs.

Introduction

Chemotherapy remains the front-line therapy for systemic malignancies. However, drug development has been severely hampered by an inability to efficiently elucidate mechanisms of drug action. This inability limits both the development of modified compounds with improved efficacy, as well as the capability to predict mechanisms of drug resistance and select optimal patient populations for a given agent. While drug-target interactions have traditionally been examined using biochemical approaches [1], a number of genetic strategies have been developed to identify pathways targeted by uncharacterized small molecules. A well-established genetic approach to drug classification is chemogenomic profiling in yeast [2-6]. In this approach, bar-coded yeast deletion strains are exposed to select agents, and genotype dependent drug sensitivity is used to identify genes and pathways affected by a given drug, as well as to develop a response signature that can be compared with other chemical or genetic perturbations [5, 7, 8]. This approach has proven quite powerful and has been broadly disseminated, however its efficacy in interrogating cancer chemotherapeutics is limited by the lack of conservation of certain drug targets from yeast to mammals. This is a particular problem in the context of targeted therapeutics, which are frequently directed towards alterations that are specific to mammalian tumors.

More recently, genetic approaches have been developed to examine drug action in mammalian settings. One such approach is to examine drug response in a diverse panel of tumor cell lines [9]. In this case, the pattern of cell line sensitivity and resistance can serve as a signature that defines drug mechanism. Additionally, drug response can be correlated with the presence of specific cancer-related alterations – although this analysis can be confounded by the large diversity of alterations present in a given tumor. An alternative approach is to compare

the global transcriptional changes induced by test compounds to those induced by known drugs or defined genetic alterations [10-13]. Here, gene expression changes are used as signatures that are characteristic of exposure to a given agent or the presence of a specific cellular state, and common expression changes can be used to cluster similar small molecules. While each of these approaches have yielded important new insights into drug action, these strategies retain a level of technical variability and resource requirement that limits both disseminated use and overall efficacy. Here, we report a tractable RNAi-based approach that represents a simple yet powerful platform for drug screening and characterization.

Results

Clustering drugs via shRNA-mediated phenotypes

We hypothesized that RNAi-mediated suppression of cell death regulators in mammalian cells would uniquely affect the cellular response to certain types of drugs, and that drugs with similar mechanisms of action would elicit similar shRNA-dependent responses. To test this strategy, we started with a cell line derived from tumors from a well-established mouse model of Burkitt's lymphoma [14, 15]. This cell line was chosen as an experimental system for two reasons. First, these cells are highly sensitive to a diverse set of chemotherapeutics, allowing small molecules to be used at pharmacologically relevant doses. Second, like many high-grade lymphomas, these cells undergo rapid apoptosis, as opposed to prolonged cell cycle arrest, following treatment. This common biological outcome following treatment allows for a systematic comparison of drugs.

In determining which genes to knock down for our studies, we chose two classes of genes known to be critical for cell fate decisions following drug treatment. The Bcl2 family of

genes includes both central mediators and inhibitors of cell death, and different members of this gene family are involved in the response to distinct cell death stimuli [16]. The transcription factor p53 functions upstream of components of the Bcl2 family and is another important cell death regulator [17]. Mutation or deletion of p53 has been shown to affect the cellular response to many types of chemotherapeutic drugs [18, 19]. Since the stabilization and activity of p53 is strongly regulated by phosphorylation, we also targeted a panel of p53 activating kinases, including ATM, ATR, Chk1, Chk2, DNA-PKcs, Smg-1, JNK1 and p38 [20, 21]. Importantly, aside from their roles as regulators of p53, these kinases are also involved in additional cellular responses to chemotherapy, such as DNA replication and repair, the activation of cell cycle checkpoints, regulation of RNA stability and stress signaling [22-26]. Thus, we generated shRNA vectors targeting the Bcl2 family, p53 and its activating kinases (Supplementary Fig. 1 and Supplementary Table 1).

To enable a quick and accurate analysis of how the suppression of a given gene affects drug-induced cell death, we utilized a single cell flow cytometry-based GFP competition assay. Lymphoma cells were infected with retroviruses co-expressing a given shRNA and green fluorescent protein (GFP) and subjected to 72 hours of drug treatment (Fig. 1a). In this assay, GFP negative cells in the same population serve as an internal control. Using this approach, we systematically investigated how suppression of individual genes affected drug-induced cell death. As an initial proof of principle, we chose 15 chemotherapeutics representing major categories of anti-cancer drugs in clinical use. To compare different drugs using an objective criterion, all drugs were used at their LD80-90 – a concentration at which 80 to 90 percent of uninfected lymphoma cells were killed (Supplementary Table 2). A control retrovirus lacking an shRNA or retroviruses expressing shRNAs targeting 29 genes were individually used to infect lymphoma cells. Each infected population was separately treated with 15 chemotherapeutic

drugs, and the effect of a particular gene knock down on therapeutic response was compiled as values of the GFP-determined “Resistance Index” (RI) (Fig. 1b). Drugs with similar mechanism of action were expected to have similar patterns of genetic dependence on these 29 genes, which would manifest as similar patterns of RI values. To test this hypothesis in an unbiased manner, we used an unsupervised agglomerative hierarchical clustering approach to compare the RI values of different drugs (Fig. 1b). The significance of this hypothesis was then evaluated using a Monte Carlo principal components analysis-based method [27]. Importantly, all 15 drugs tested in this initial experiment formed six distinct clusters that were consistent with their molecular mechanisms of action (Supplementary Fig. 2). Specifically, clear groupings were seen between topoisomerase II poisons doxorubicin (Dox) and etoposide (VP-16), DNA cross-linking agents cisplatin (CDDP), mitomycin C (MMC) and chlorambucil (CBL), single strand break-inducing agents camptothecin (CPT), 6-thioguanine (6-TG) and temozolomide (TMZ) [28, 29], nucleic acid synthesis inhibitors methotrexate (MTX), 5-Flurouracil (5-FU) and hydroxyurea (HU), and spindle poisons vincristine (VCR) and paclitaxel (Taxol). Taken together, these data showed that a simple comparison of drug response in cells expressing a small set of shRNAs could effectively categorize established chemotherapeutic drugs into subgroups that demarcate common target proteins and pathways.

To investigate whether this platform could be utilized to characterize mechanisms of drug action, we examined several recently developed chemotherapeutics: SAHA, decitabine and roscovitine. Although the immediate biochemical targets of these new chemotherapeutics are known, the mechanisms of cell death induced by these drugs are less well defined. Using our RNAi-based approach, we compiled RI values for each of these three drugs and compared them with the 15 reference drugs mentioned earlier. We observed that the CDK inhibitor roscovitine (Rosco) was most similar to the RNA polymerase inhibitor actinomycin D (ActD) (Fig. 1c and Supplementary Fig. 3a). This is consistent with the findings of several studies

showing that roscovitine inhibits CDK7, a component of the general transcription factor TFIIH, to inhibit RNA transcription [30-32]. Interestingly, the HDAC inhibitor SAHA and the DNA methyltransferase inhibitor decitabine (DAC) formed a distinct cluster outside of the 15 reference drugs (Fig. 1c), suggesting that these two drugs may share a similar mechanism of cell death. In order to extract the most relevant genes for distinguishing the SAHA-DAC cluster, shRNAs were ranked upon their ability to classify this cluster relative to the rest of the dataset. The most unique aspects of the new SAHA–DAC cell death signature were the: 1) p53-independence ($Log_2RI \approx 0$) and 2) Bim-dependence ($Log_2RI \approx 2$) of cell death, consistent with previous studies of SAHA treatment in mouse lymphoma models [33]. Indeed, both SAHA and DAC treatment resulted in an increase in the levels of the pro-apoptotic BH3-only protein Bim (Supplementary Fig. 3b). Furthermore, suppression of the Bim transcription regulator Chop, but not Foxo3a, resulted in resistance to both SAHA and DAC (Fig. 1d). Thus, the RI patterns of these newly established drugs could effectively identify their mechanism of action.

Functional characterization of derivitized compounds

A significant challenge in drug development is determining whether lead compound derivatives with enhanced efficacy share the same mechanism of action as the original small molecule. Theoretically, derivitized compounds could show enhanced efficacy, due to either the activation of additional cell death pathways or, alternatively, through altered pharmacodynamic properties. To examine whether our approach could be used to differentiate between these possibilities, we performed an shRNA-based functional analysis of CY190602, a chemical derivative of the nitrogen mustard bendamustine (Fig. 2a). Compared to the parental drug, CY190602 shows 20~100 fold enhanced toxicity towards cells from patients with multiple myeloma (Fig. 2b), an indication for which bendamustine is currently in clinical use. However, the mechanism underlying this increase in cytotoxicity remains unclear. Notably, CY190602's

modification on bendamustine occurs on a side chain well away from the nitrogen mustard functional group. To address whether CY190602's toxicity could still be attributed to the nitrogen mustard, or was a result of altered target specificity caused by the side chain modification moieties, we compiled the RI values of bendamustine and CY190602 and compared them to that of our 18 reference drugs. Notably, bendamustine and CY190602 exhibited highly similar patterns of RI values (Fig. 2c), despite a 100-fold lower dose of CY190602. Additionally, both drugs clustered together with chlorambucil, another nitrogen mustard (Fig. 2d), and a supervised K-nearest neighbors approach (see supplementary methods for a detailed rationale) predicted a chlorambucil-like mechanism for both drugs. This suggests that the increased efficacy of CY190602 is likely due to enhanced target engagement rather than an off-target effect conferred during drug optimization.

Screening for compounds based on shRNA signatures

Next, we asked whether this approach could be adapted to phenotype-based screens for novel drug candidates without well-established mechanisms of action. Suppression of ATM, Chk2 and p53 all led to significant resistance to genotoxic drugs such as Dox, VP-16, CPT, TMZ, 6TG, CDDP, MMC and CBL (Fig. 1b). This suggested that the shATM/Chk2/p53 "resistance signature" might be used to identify genotoxic drugs. In order to test this hypothesis quantitatively, we examined whether a supervised K-nearest neighbors approach could accurately characterize all of the drugs in our data set as either genotoxic, or non-genotoxic. Indeed, when a broad panel of chemotherapeutic drugs was tested, all 16 genotoxic chemotherapeutics, but none of 15 non-genotoxic chemotherapeutics, exhibited a distinct shATM/Chk2/p53 resistance signature (Fig. 3a). This three gene "resistance signature" was subsequently used to screen a small chemical library for genotoxic compounds. Two compounds, apigenin and NSC3852, were identified based on their strong shATM/Chk2/p53

resistance signature (Fig. 3b). We then compiled the full 29-gene RI values for these two compounds and compared them with reference drugs (Fig. 3c). Interestingly, the K-nearest neighbors approach predicted apigenin to be most similar to the topoisomerase II poisons doxorubicin and etoposide, and NSC3852 to be most like the single strand break-inducing agents. Subsequent clustering showed NSC3852 to be most similar to the topoisomerase I poison camptothecin. Our previous studies demonstrated that topoisomerase II poisons are ineffective in killing topoisomerase II deficient cells, while showing enhanced toxicity for cells lacking topoisomerase I [34]. Consistent with the clustering-based functional predictions, apigenin exhibited a pattern of shTopoII resistance and shTopoI sensitivity similar to the established topoisomerase II poisons doxorubicin, etoposide and mitoxantrone (Fig. 3d). Conversely, NSC3852 exhibited a characteristic pattern of shTopoI resistance, similar to established topoisomerase I poisons camptothecin and irinotecan (CPT11). Importantly, none of the other genotoxic drugs exhibited these resistance/sensitivity patterns with shTopoI and shTopoII (Fig. 3d). We also found that apigenin and NSC3852 failed to induce DNA damage in topoisomerase II and topoisomerase I deficient cells, respectively (Supplementary Fig. 4). Moreover, in a long-term survival assay, topoisomerase II deficiency resulted in significant protection from apigenin, whereas topoisomerase I deficiency significantly protected cells from NSC3852 (Fig. 3e). Taken together, these assays confirmed our classification of apigenin and NSC3852 as topoisomerase II and topoisomerase I poisons, respectively. Thus, small shRNA signatures can be used to screen chemical libraries to identify and characterize novel compounds with particular target specificities.

An 8-shRNA set for accurate drug mechanism predication

Given that a three-gene signature could effectively predict and classify genotoxic drugs, we hypothesized that the combined resistance/sensitivity pattern of a small number of genes

may be sufficient to accurately characterize most of our chemotherapeutic drugs in this cell line. To test this hypothesis, we examined the seven drug clusters demarcated in our secondary analysis (Figure 1c), and asked which smaller sets of shRNAs could similarly define these groupings. Here, we used a K-nearest neighbors cross validation based approach and a randomized search through 50,000 potential gene subsets. While most smaller shRNA sets showed a significant loss in resolution relative to the reference set, we found that a set of 8 shRNAs, targeting p53, ATR, Chk1, Chk2, Smg-1, DNA-PKcs, Bok and Bim, was able to classify the reference dataset with 100% accuracy and was highly correlated (r^2=0.81) with the original 29 shRNA signature (Fig. 4a and Supplementary Fig. 5a and b). While several other sets of 8 shRNAs could also classify chemotherapeutics with 100% accuracy, this 8-shRNA signature had the highest range of measurement across all drugs. Importantly, this 8-shRNA signature could also correctly classify bendamustine, CY190602, Apigenin, and NSC3852 - drugs that were not included in the feature reduction and cross-validation of the 8-shRNA signature (Supplementary Fig. 5c).

Given the known off-target potential of RNAi, we next sought to determine whether the functional signature derived from these 8 shRNAs was attributable to the specific effect of shRNA target gene suppression on therapeutic response. To do this, we used a second set of shRNAs targeting the same 8 genes to generate an independent drug response signature. Comparison of shRNA pairs revealed a high correlation between drug response signatures (r^2=0.86) in cells transduced with distinct shRNAs targeting the same gene, suggesting that the major effects of these shRNAs are “on target” (Fig. 4b). Additionally, unsupervised hierarchical clustering of the first 8-shRNA response signature or the combined response signatures generated using the first and second 8-shRNAs sets revealed the same 7 drug classes identified with the original 29-shRNA signature (Figure 4c). Notably, however, the second set of

8-shRNAs could independently predict only 5 out of 7 drug classes. This loss of resolution in the second shRNA set may represent trace “off-target” shRNA activity in either 8-shRNA set. Alternatively, these differences may be attributable to small differences in the degree of target gene knock down conferred by distinct hairpins. Consistent with the latter argument, shRNAs in the second set frequently showed reduced target gene suppression (Supplementary Fig. 1 and Supplementary Table 1) and yielded more subtle biological effects as evidenced by the relative RI values seen in shRNA pairwise comparisons (Fig. 4b).

In order to extend our 8-shRNA signature approach in a scalable and stringent manner, we re-visited a common problem in machine learning. A non-parametric classification method like K-nearest neighbors will classify any test compound according to its closest neighbor(s), even if the two compounds are quite distinct. Thus, it becomes difficult to determine how distantly a given compound can reside from a reference category of drugs and still be considered to share a similar mechanism of action (Fig. 5a). To overcome this problem, we took advantage of the carefully selected mechanistic diversity of our training set to create specific empirical cumulative distribution functions (CDFs) for each drug category (Fig. 5b). This allowed us to determine if a test compound was likely to belong to either an existing or a novel drug category – a process critical to the broader applicability of this approach.

To determine whether this methodology could correctly categorize chemotherapeutics absent from our initial reference set, we examined a set of 16 additional anti-cancer drugs (Table 1 and Supplementary Fig. 6). In each case, the 8-shRNA approach successfully grouped drugs according to their mechanism of action. Importantly, when compounds that represent novel drug categories were examined, they were not misclassified into the “nearest” drug category. Rather, they were identifiable as distinct agents that were significantly different

from all other drug categories. Consequently, although this 8-shRNA panel was assembled based on responses to seven drug classes, it was also successful in predicting other classes of chemotherapeutics when the training set was updated with new reference compounds. For example, the 8-shRNA signature accurately predicted that the proteasome inhibitor gliotoxin belonged to a drug category not represented by any of the existing reference drugs. However, when the proteasome inhibitors bortezomib (PS341) and MG132 were used to update the training set, the 8-shRNA signature was able to successfully classify gliotoxin and epoxomycin as proteasome inhibitors (Table 1). The 8-shRNA set could be similarly trained to identify two entirely distinct drug categories - Hsp90 inhibitors and EGFR inhibitors - neither of which was used to create the 8-shRNA reference set. Importantly, the 8-shRNA signature could also distinguish functional drug sub-classes within larger targeted classes of therapeutics. For example, the HER2 inhibitors Lapatinib and AEE788 and the multi-kinase inhibitor Sunitinib clustered in distinct categories relative to EGFR inhibitors (Supplementary Fig. 7), despite all of these drugs belonging to the broader category of tyrosine kinase inhibitors. While the use of more optimized sets of shRNAs may be necessary to probe fine details of certain drug categories, these data suggest that this 8-shRNA set has resolution over a broad range of cytotoxic activities.

While the cells used in this study are responsive to a number of targeted chemotherapeutics, like EGFR inhibitors, a potential limitation of this approach is that it lacks resolution for certain compounds requiring cellular targets not present in lymphoma cells. To determine whether this approach could be adapted to cell lines expressing targetable genetic lesions, we examined the performance of the 8 shRNA signature in cells derived from a BCR-Abl driven model of acute B cell leukemia (B-ALL) [35]. Strikingly, a robust functional signature for alkylating agents could be generated in these cells using the same 8-shRNA set (Fig. 6).

Importantly, however, the response signature in B-ALL cells differed from that in lymphoma cells. For example, leukemia cells showed distinct genetic dependencies on ATR, DNA-PKcs and Bok. Thus, informative signatures can be derived in distinct cell lines, even if the signatures differ between cell types. Notably, this 8-shRNA signature may not be optimal for B-ALL cells, as feature reduction from the 29-shRNA signature was not performed in this context. Additionally, this signature may not have the same resolution as in lymphoma cells. However, these data suggest that even sub-optimal signatures may provide resolution sufficient to cluster classes of chemotherapeutics.

Discussion

The functional genetic approach described here has similarities to well-characterized chemogenomic profiling strategies in lower organisms. However, this approach also has notable advantages over existing genetic approaches for examining drug mechanisms of action and identifying drug targets. First, this approach is sufficiently sensitive to differentiate drugs with distinct targets but common downstream signaling pathways. For example, topoisomerase I and II poisons produce distinct shRNA sensitivity profiles, yet both ultimately engage common transcriptional networks. Microarray approaches that focus on downstream changes in gene expression are, consequently, less able to distinguish between conventional anti-cancer agents. In fact, previous microarray studies have shown limited resolution over a number of front-line chemotherapeutics (Supplementary Table 3). Second, this approach is unaffected by pharmacodynamic variability, such as distinctions in drug efflux or detoxification, that obscures comparisons between different cancer cell lines. Finally, and most importantly, this approach is both simple and tractable. While microarray studies suffer from significant variability between experiments and laboratories, RNAi-based functional arrays are highly reproducible and can be widely disseminated.

Perhaps the most unanticipated aspect of this work lies in the surprising quantity of information that can be derived from of a small set of mammalian loss of function phenotypes. This focused shRNA signature can characterize a diverse range of drug categories at high resolution and is extendable to completely novel drug categories and distinct cell types, suggesting that such signatures might serve as a tractable approach to screen chemical libraries for diverse functional classes of small molecules in a high throughput manner. While this specific set of shRNAs may not provide optimal resolution for all cell types or small molecules, these data also suggest that alternative small sets of shRNAs may yield similar information content. For example, while this work focuses on cell viability, it is likely that – given appropriate phenotypic resolution - bioactive compounds affecting diverse aspects of biology can similarly be interrogated with distinct targeted sets of shRNAs.

Acknowledgments

The MM1S cell line was a generous gift from Dr. Steve Rosen. CY190602 and Hsp90 inhibitors were kindly provided by Nextwave Biotech. We thank Luke Gilbert, Holly Criscione, Stephanie Wu, Shannon Alford and Shan Wu for their experimental or analytical assistance. We are grateful to Leona Samson, Christian Pallasch and Corbin Meacham for critically reading the manuscript and the entire Hemann lab for helpful discussions. M.T.H. is a Rita Allen Fellow and the Latham Family Career Development Assistant Professor of Biology, and M.T.H. and H.J. are supported by NIH RO1 CA128803-03. J.R.P. is supported by the MIT Department of Biology training grant. RTW is the recipient of an AACR Career Development Award. Additional funding was provided by the Integrated Cancer Biology Program grant 1-U54-CA112967 to D.A.L. and M.T.H.

Author Contributions

H.J., J.R.P., and M.T.H. designed experiments. H.J. and J.R.P. performed RNAi knock down and treatment studies. J.R.P. developed the computational approaches and performed all of the computational analyses. R.T.W. developed and characterized the B-ALL cell line. H.J., J.R.P., D.A.L and M.T.H. analyzed the data and wrote the manuscript.

We declare that the authors have no competing interests as defined by Nature Publishing Group, or other interests that might be perceived to influence the results and discussion reported in this paper.

Methods

Cell lines and drugs: *Eμ-Myc p19$^{Arf-/-}$* mouse lymphoma cells were cultured in B cell medium as described [15]. MM1S and RPMI8226 cells were cultured in RPMI medium supplemented with glutamate and 10% FBS. Drugs were obtained from Sigma, Tocris, Calbiochem, VWR, LC labs and other suppliers. shRNA vectors were generated as described [36, 37]. *p185+ p19$^{Arf-/-}$* acute lymphoblastic leukemia cells were obtained from the Williams laboratory and cultured according to the procedures outlined in [35].

Drug treatment and flow cytometry: *Eμ-Myc p19$^{Arf-/-}$* cells were counted and seeded at 1 million cells/ml in 48 well plates, and treated with various concentrations of drugs. To approximate therapeutic situations in which drug dose decreases over time, half of the volume

from each experiment was removed and replenished with fresh medium every 24 hours. Cells were analyzed by FACS, with PI as a viability marker. LD80~90 of drugs are defined as concentrations at which the lowest viability reading out of three FACS time points (24, 48 and 72 hours) is between 10% and 20%. After determining drug dose, *Eμ-Myc p19*$^{Arf-/-}$ cells were infected with retroviruses encoding shRNAs targeting particular genes. Individual infected cell populations were counted and seeded at 1 million cells/ml in 48 well plates, and treated with drugs using afore-mentioned protocol. At 72 hours, treated and untreated cells were analyzed by flow cytometry. GFP percentages of live (PI negative) cells were recorded and used to calculate relative resistance index. To avoid outgrowth of untreated control cells, we typically seed them at 0.25 million/ml, and 75% of medium was replaced at 24 and 48 hours.

Calculation of relative resistance index (X): To compare the relative level of chemoresistance and sensitization conferred by each gene knockdown, we introduced "relative resistance index", or **RI**, to more accurately analyze the GFP competition results. We define the value of "relative resistance index (**RI**)" as **X**. The biological meaning of this factor "**X**" is that, in a mixture of uninfected and infected (knockdown) cells, the infected (knockdown) cells will be **X** fold as likely to survive drug treatment when compared to uninfected cells. By our definition of relative resistance index (**X**), if 1 out of N uninfected cells survives a drug treatment, then **X** our of N infected cells should survive. If we define the total number of uninfected and infected cells as T, and the GFP percentage of untreated population as G1, then the number of surviving, uninfected cells can be defined as **N-un**=T*(1-G1)*1/N, and the number of surviving, infected cells can be defined as **N-in**=T*G1*__X__/N. Hence, the GFP percentage of the treated, surviving population (G2) can be calculated as G2=**N-in**/(**N-un** + **N-in**). From this equation, we can derive that **X**= (G2-G1*G2)/(G1-G1*G2). This equation was used in our studies to compute RI values.

Enhanced K-nearest neighbors methods: K-nearest neighbors (KNN) modeling is a weighted-voting methodology where the proximity to the training set is used to predict drug class membership. We include this analysis for four reasons: 1) It provides independent validation of the clustering result. 2) It allows us to quantify the predictive power of the reference set through Leave-one-out cross-validation. 3) Leave-one-out cross-validation allows us to perform a feature reduction to discover smaller gene sets. 4) It provides an objective prediction of classes for novel compounds.

K-nearest neighbors predictions were performed using a correlation based metric, and a consensus voting scheme. The matlab knnclassify.m function was used as a basis for the feature reduction search, as well as cross-validation and predictions. The cross-validation for the KNN approach was done by systematically leaving out one of the 18 drugs at a time in the final dataset (Fig. 1c) and using the remaining 17 to predict the left out drugs identity.

In order to reduce the size of the feature set to a smaller group of key genes we randomly searched a subset of 2000 unique gene sets of size of increasing size. Sampled subsets were scored based upon their ability to cross-validate. We then performed a much more extensive search (>50,000 subsets) of 8 gene signatures that would be able to correctly classify all of the drugs in our reference set. The gene subsets that cross-validated at 100% were then ranked by their least-squares correlation with the distances between drugs in the 29 gene signature, and the 8 gene set with the highest correlation score was chosen for later experiments.

A K-nearest neighbors based approach will always yield a prediction of drug class based upon proximity. Therefore, in order to evaluate the similarity of a novel drug to its predicted class we developed a linkage ratio p-value test Briefly, we calculated the initial cluster size of each of the 7 drug groups (Fig. 1c) by evaluating the average of all pairwise linkage distances amongst all members of a drug group. When a test compound was predicted to belong to a drug group based upon proximity, then the cluster size of that particular drug group was calculated again with the new test drug included. A linkage ratio was then calculated by comparing the cluster size with and without the tested compound. A linkage ratio of less than 1 indicated that the addition of the drug to a cluster made the average distance between drugs in that category smaller, whereas a linkage ratio greater than 1 indicated that the cluster expanded. An obvious tradeoff exists between cluster expansion to accommodate modestly distinct compounds with highly homologous mechanism, and expanding the definition to a point where one masks the existence of a completely novel compound. This tradeoff varies amongst drug classes as a function of the inter-class distances. In order to estimate the significance of a K-nearest neighbors prediction, as well as to determine whether a compound has a mechanism of action different from those of our original 7 drug groups, we sampled the negative control distributions of drug classifications. This was done on a class by class basis by taking the previously studied compounds and forcing them to erroneously classify. We then calculated a linkage ratio for all of these erroneous classifications. On a class-by-class basis we fit a normal distribution to the range of misclassified linkage ratios. The value of the cumulative distribution function (CDF) was used to calculate the p-value of the novel classifications in Fig. 5c, utilizing the null hypothesis that the linkage ratio for a prediction is identical to the linkage ratios of the negative control distribution.

References

1. Sato, S., Murata, A., Shirakawa, T. & Uesugi, M. Biochemical target isolation for novices: affinity-based strategies. *Chem Biol* **17**, 616-623 (2010).

2. Giaever, G. et al. Genomic profiling of drug sensitivities via induced haploinsufficiency. *Nat Genet* **21**, 278-283 (1999).

3. Giaever, G. et al. Chemogenomic profiling: identifying the functional interactions of small molecules in yeast. *Proc Natl Acad Sci U S A* **101**, 793-798 (2004).

4. Lum, P. Y. et al. Discovering modes of action for therapeutic compounds using a genome-wide screen of yeast heterozygotes. *Cell* **116**, 121-137 (2004).

5. Parsons, A. B. et al. Integration of chemical-genetic and genetic interaction data links bioactive compounds to cellular target pathways. *Nat Biotechnol* **22**, 62-69 (2004).

6. Hillenmeyer, M. E. et al. The chemical genomic portrait of yeast: uncovering a phenotype for all genes. *Science* **320**, 362-365 (2008).

7. Parsons, A. B. et al. Exploring the mode-of-action of bioactive compounds by chemical-genetic profiling in yeast. *Cell* **126**, 611-625 (2006).

8. Hillenmeyer, M. E. et al. Systematic analysis of genome-wide fitness data in yeast reveals novel gene function and drug action. *Genome Biol* **11**, R30 (2010).

9. Shoemaker, R. H. The NCI60 human tumour cell line anticancer drug screen. *Nat Rev Cancer* **6**, 813-823 (2006).

10. Hughes, T. R. et al. Functional discovery via a compendium of expression profiles. *Cell* **102**, 109-126 (2000).

11. Gardner, T. S., di Bernardo, D., Lorenz, D. & Collins, J. J. Inferring genetic networks and identifying compound mode of action via expression profiling. *Science* **301**, 102-105 (2003).

12. Lamb, J. et al. The Connectivity Map: using gene-expression signatures to connect small molecules, genes, and disease. *Science* **313**, 1929-1935 (2006).

13. Hieronymus, H. et al. Gene expression signature-based chemical genomic prediction identifies a novel class of HSP90 pathway modulators. *Cancer Cell* **10**, 321-330 (2006).

14. Adams, J. M. et al. The c-myc oncogene driven by immunoglobulin enhancers induces lymphoid malignancy in transgenic mice. *Nature* **318**, 533-538 (1985).

15. Schmitt, C. A., McCurrach, M. E., de Stanchina, E., Wallace-Brodeur, R. R. & Lowe, S. W. INK4a/ARF mutations accelerate lymphomagenesis and promote chemoresistance by disabling p53. *Genes Dev* **13**, 2670-2677 (1999).

16. Youle, R. J. & Strasser, A. The BCL-2 protein family: opposing activities that mediate cell death. *Nat Rev Mol Cell Biol* **9**, 47-59 (2008).

17. Lu, C. & El-Deiry, W. S. Targeting p53 for enhanced radio- and chemo-sensitivity. *Apoptosis* **14**, 597-606 (2009).

18. Lowe, S. W., Ruley, H. E., Jacks, T. & Housman, D. E. p53-dependent apoptosis modulates the cytotoxicity of anticancer agents. *Cell* **74**, 957-967 (1993).

19. Lowe, S. W. et al. p53 status and the efficacy of cancer therapy in vivo. *Science* **266**, 807-810 (1994).

20. Bode, A. M. & Dong, Z. Post-translational modification of p53 in tumorigenesis. *Nat Rev Cancer* **4**, 793-805 (2004).

21. Brumbaugh, K. M. et al. The mRNA surveillance protein hSMG-1 functions in genotoxic stress response pathways in mammalian cells. *Mol Cell* **14**, 585-598 (2004).

22. Lavin, M. F. Ataxia-telangiectasia: from a rare disorder to a paradigm for cell signalling and cancer. *Nat Rev Mol Cell Biol* **9**, 759-769 (2008).

23. Cimprich, K. A. & Cortez, D. ATR: an essential regulator of genome integrity. *Nat Rev Mol Cell Biol* **9**, 616-627 (2008).

24. Bartek, J. & Lukas, J. Chk1 and Chk2 kinases in checkpoint control and cancer. *Cancer Cell* **3**, 421-429 (2003).

25. Reinhardt, H. C., Aslanian, A. S., Lees, J. A. & Yaffe, M. B. p53-deficient cells rely on ATM- and ATR-mediated checkpoint signaling through the p38MAPK/MK2 pathway for survival after DNA damage. *Cancer Cell* **11**, 175-189 (2007).

26. Pearce, A. K. & Humphrey, T. C. Integrating stress-response and cell-cycle checkpoint pathways. *Trends Cell Biol* **11**, 426-433 (2001).

27. Pritchard, J. R. et al. Three-kinase inhibitor combination recreates multipathway effects of a geldanamycin analogue on hepatocellular carcinoma cell death. *Mol Cancer Ther* **8**, 2183-2192 (2009).

28. Swann, P. F. et al. Role of postreplicative DNA mismatch repair in the cytotoxic action of thioguanine. *Science* **273**, 1109-1111 (1996).

29. Mojas, N., Lopes, M. & Jiricny, J. Mismatch repair-dependent processing of methylation damage gives rise to persistent single-stranded gaps in newly replicated DNA. *Genes Dev* **21**, 3342-3355 (2007).

30. Akhtar, M. S. et al. TFIIH kinase places bivalent marks on the carboxy-terminal domain of RNA polymerase II. *Mol Cell* **34**, 387-393 (2009).

31. Ljungman, M. & Paulsen, M. T. The cyclin-dependent kinase inhibitor roscovitine inhibits RNA synthesis and triggers nuclear accumulation of p53 that is unmodified at Ser15 and Lys382. *Mol Pharmacol* **60**, 785-789 (2001).

32. MacCallum, D. E. et al. Seliciclib (CYC202, R-Roscovitine) induces cell death in multiple myeloma cells by inhibition of RNA polymerase II-dependent transcription and down-regulation of Mcl-1. *Cancer Res* **65**, 5399-5407 (2005).

33. Lindemann, R. K. et al. Analysis of the apoptotic and therapeutic activities of histone deacetylase inhibitors by using a mouse model of B cell lymphoma. *Proc Natl Acad Sci U S A* **104**, 8071-8076 (2007).

34. Burgess, D. J. et al. Topoisomerase levels determine chemotherapy response in vitro and in vivo. *Proc Natl Acad Sci U S A* **105**, 9053-9058 (2008).

35. Williams, R. T., Roussel, M. F. & Sherr, C. J. Arf gene loss enhances oncogenicity and limits imatinib response in mouse models of Bcr-Abl-induced acute lymphoblastic leukemia. *Proc Natl Acad Sci U S A* **103**, 6688-6693 (2006).

36. Dickins, R. A. et al. Probing tumor phenotypes using stable and regulated synthetic microRNA precursors. *Nat Genet* **37**, 1289-1295 (2005).

37. Jiang, H. et al. The combined status of ATM and p53 link tumor development with therapeutic response. *Genes Dev* **23**, 1895-1909 (2009).

Figure 1 - Functional characterization of chemotherapeutic drugs according to patterns of shRNA-conferred drug resistance or sensitivity.

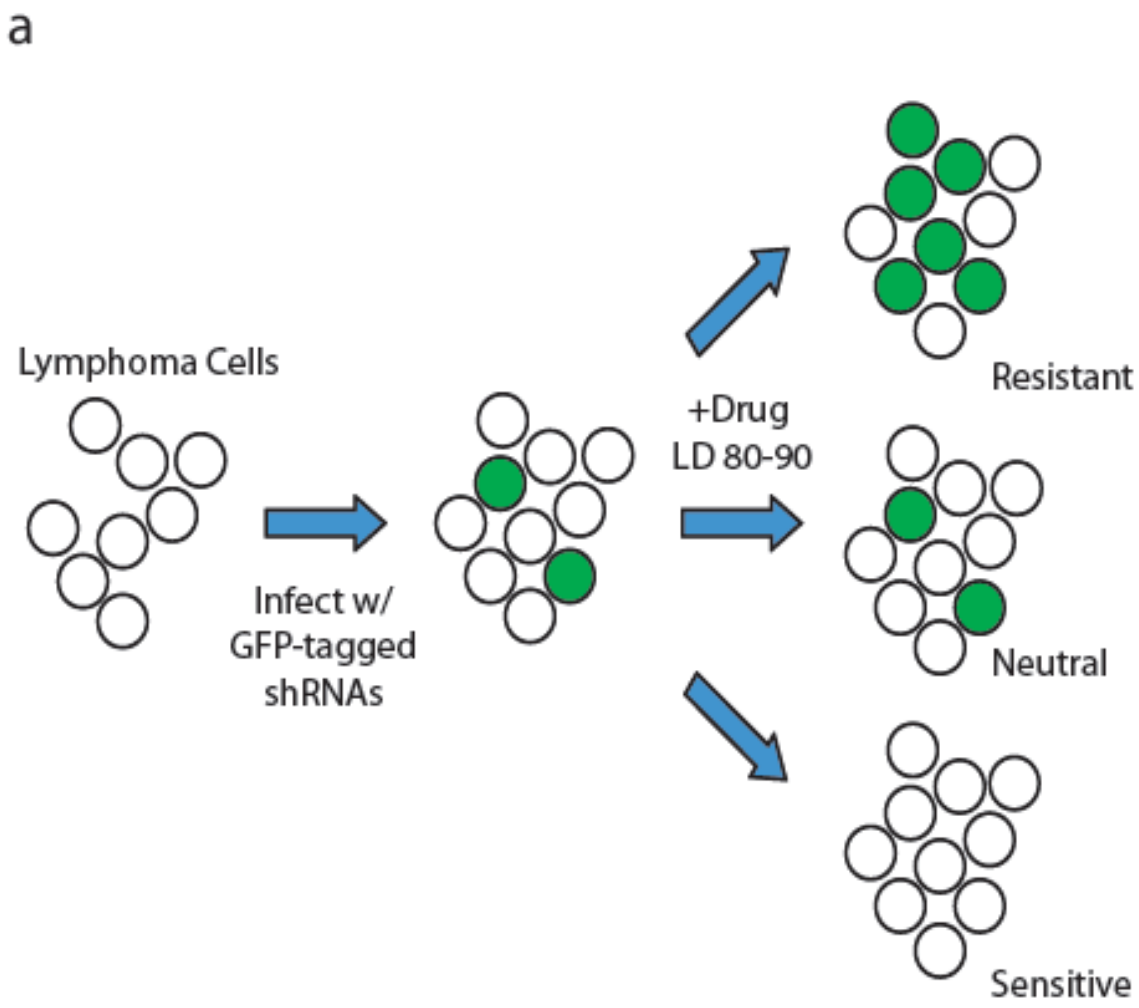

Figure1 a, A diagram showing the principle of GFP-based competition assays. Suppression of genes that alter drug sensitivity leads to changes in the percentage of GFP-positive cells after treatment, which can be used to calculate the relative “resistance index” (RI - see methods).

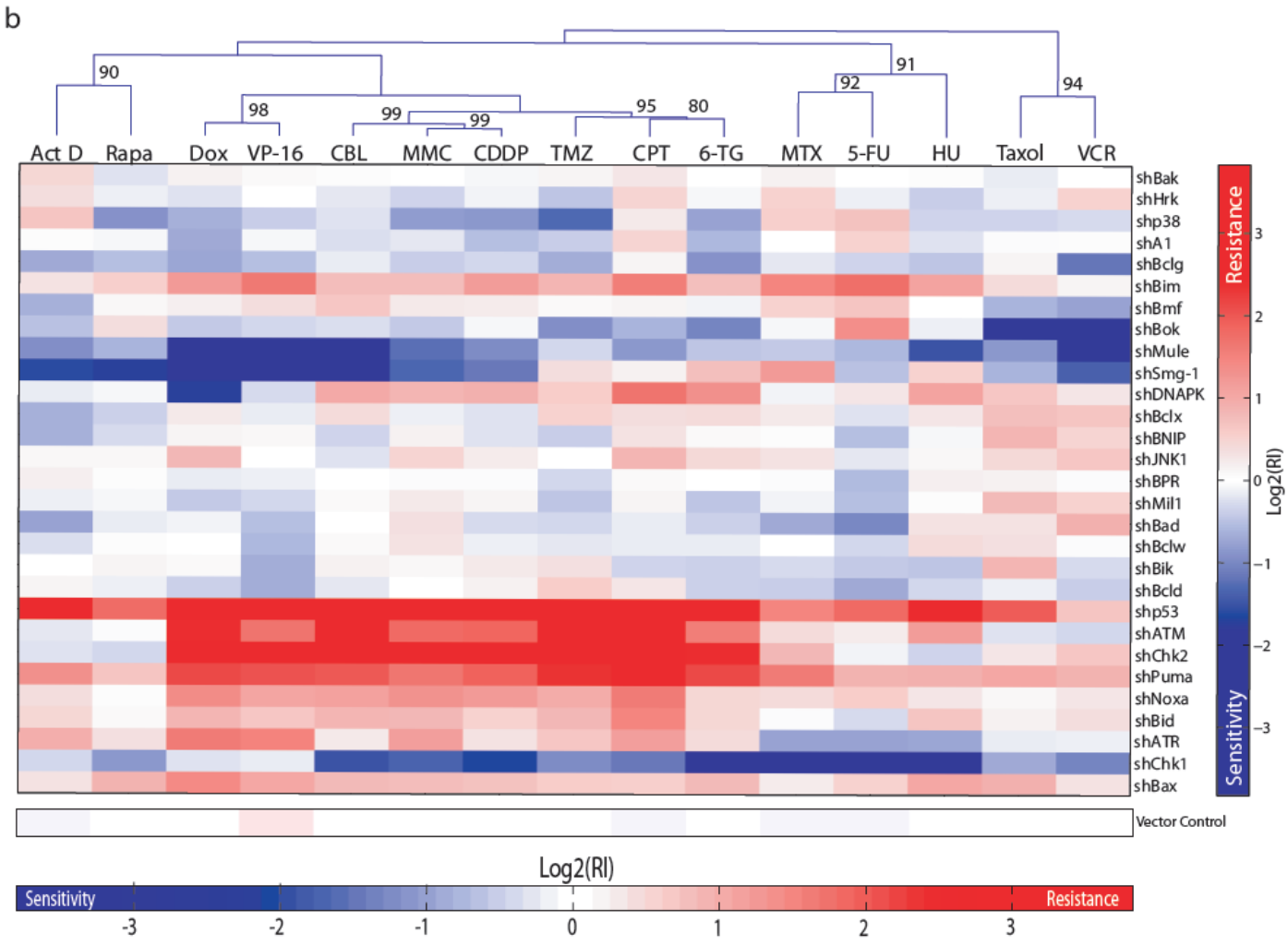

Figure 1b, Unsupervised clustering of RI values of 15 reference compounds. Agglomerative hierarchichal clustering was performed on log transformed RI values for the initial 15 reference drugs, using a correlation metric and centroid linkage. Bootstrapping data is shown to indicate

clustering robustness. AU values from the PVclust function are indicated next to the relevant branches in the clustergram.

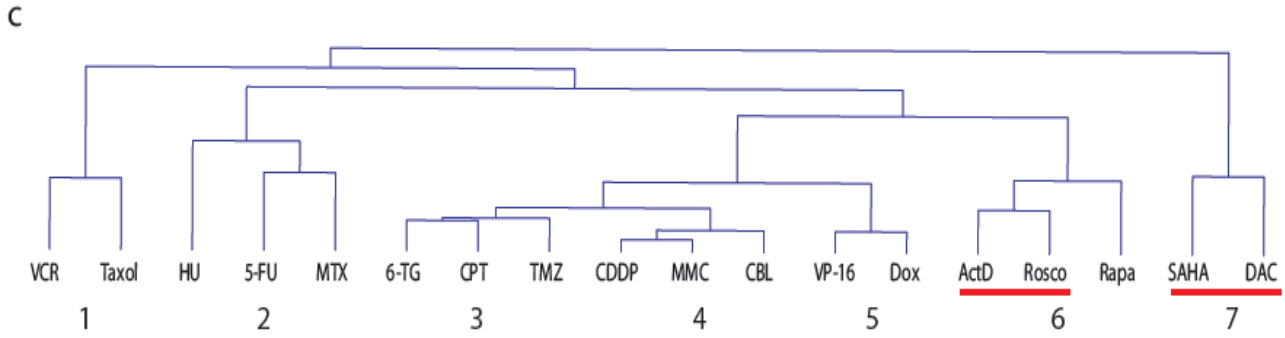

Figure 1c, The branching pattern for SAHA, DAC and Rosco and the 15 reference chemodrugs. Numbers below the dendogram demarcate drug categories

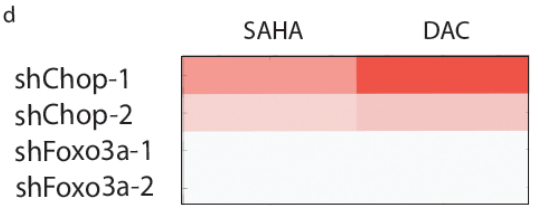

Figure. 1**d,** A heat map showing the response of cells expressing shRNAs targeting the Bim transcriptional regulator Chop and Foxo3a to SAHA and DAC. Log transformed RI values are shown.

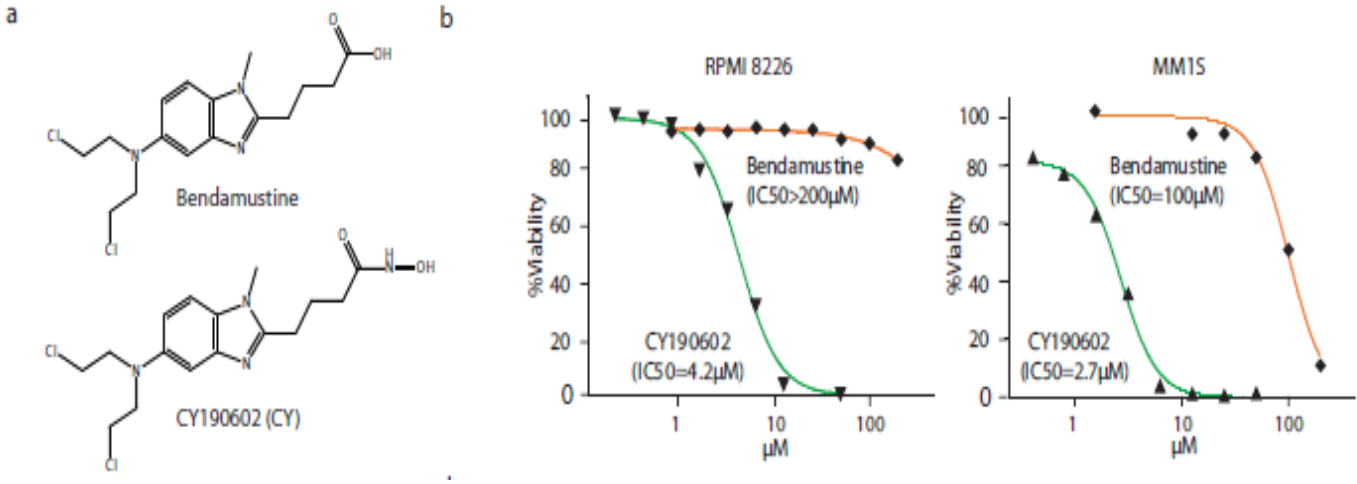

Figure 2 – RNAi-based characterization of a compound derivative of bendamustine. a, The chemical structures of bendamustine and a chemical derivative, CY190602. **b,** Dose response curves comparing the viability of the multiple myeloma cell lines RPMI-8226 (left) and MM1S (right) following treatment with bendamustine or CY190602.

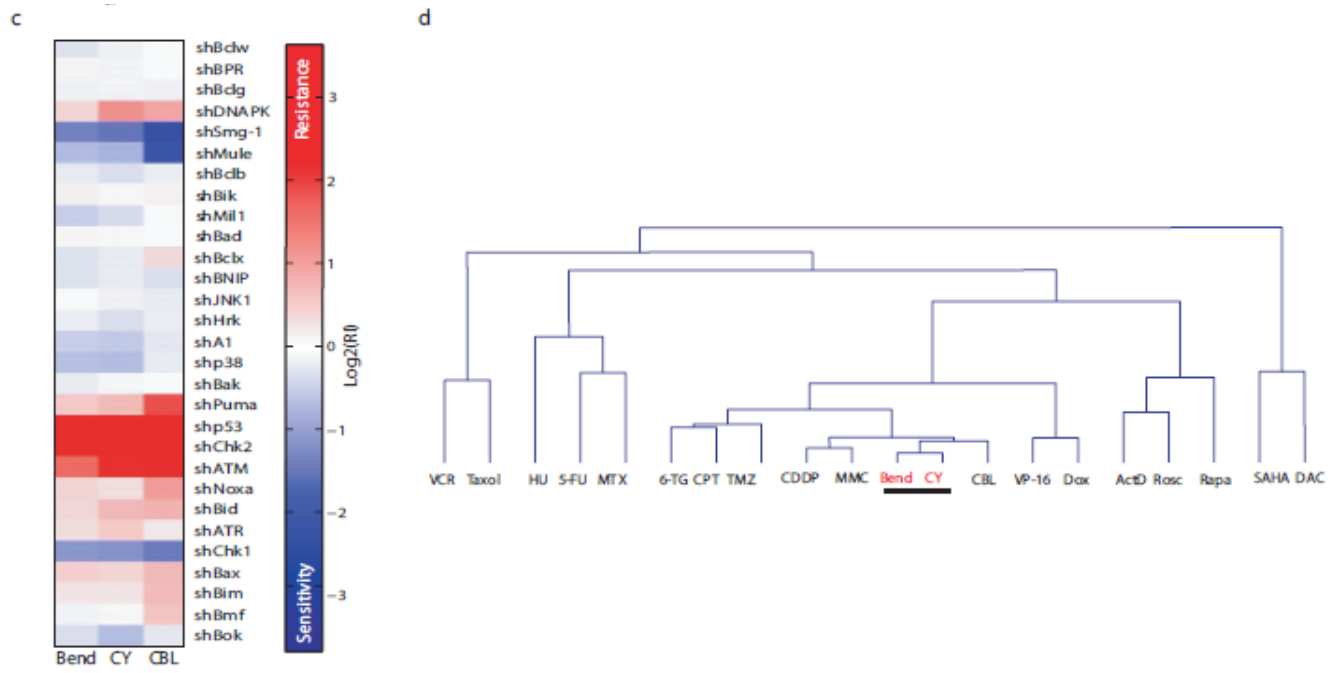

Figure 2 c, RI patterns for bendamustine, CY190602 and a related compound, chlorambucil (CBL). Bendamustine and CY190602 were used at LD80-90 of 110μM and 1.4μM, respectively. **d,** The branching pattern for the 18 reference drugs plus bendamustine and CY190602.

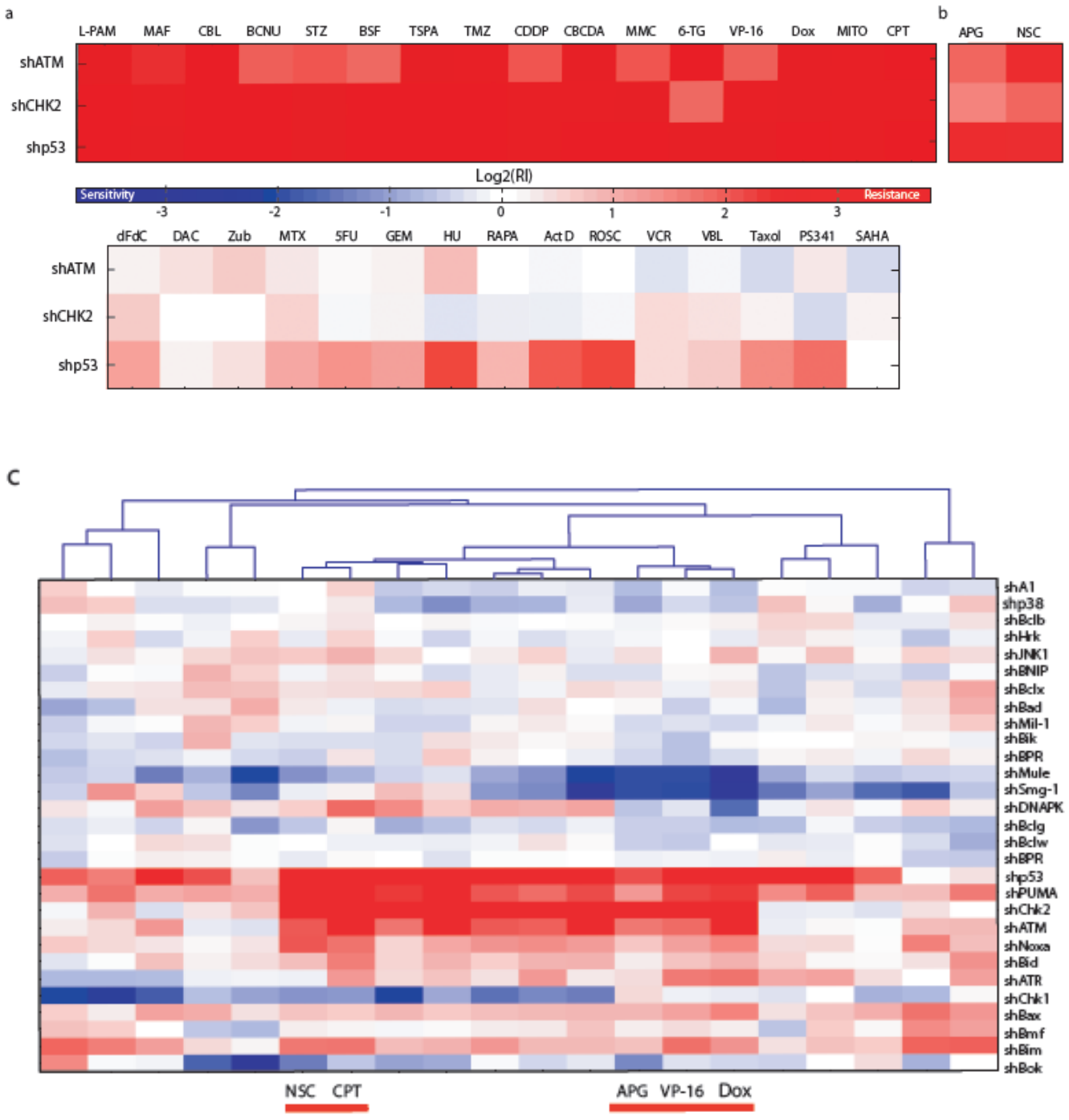

Figure 3 – Identification and functional characterization of ill-defined genotoxic drugs. a, A heat map showing the reponse of cells expressing shATM, shChk2 or shp53 to 16 genotoxic (upper panel) and 15 non-genotoxic (lower panel) chemotherapeutics (see table S2 for drug abbreviations). **b,** The shATM/Chk2/p53 response signature for apigenin (APG) and NSC3852 (NSC). **c,** The branching pattern for the 18 reference compounds plus APG and NSC. APG clusters with the TopoII poisons Dox and VP-16, whereas NSC clusters with the TopoI poison CPT.

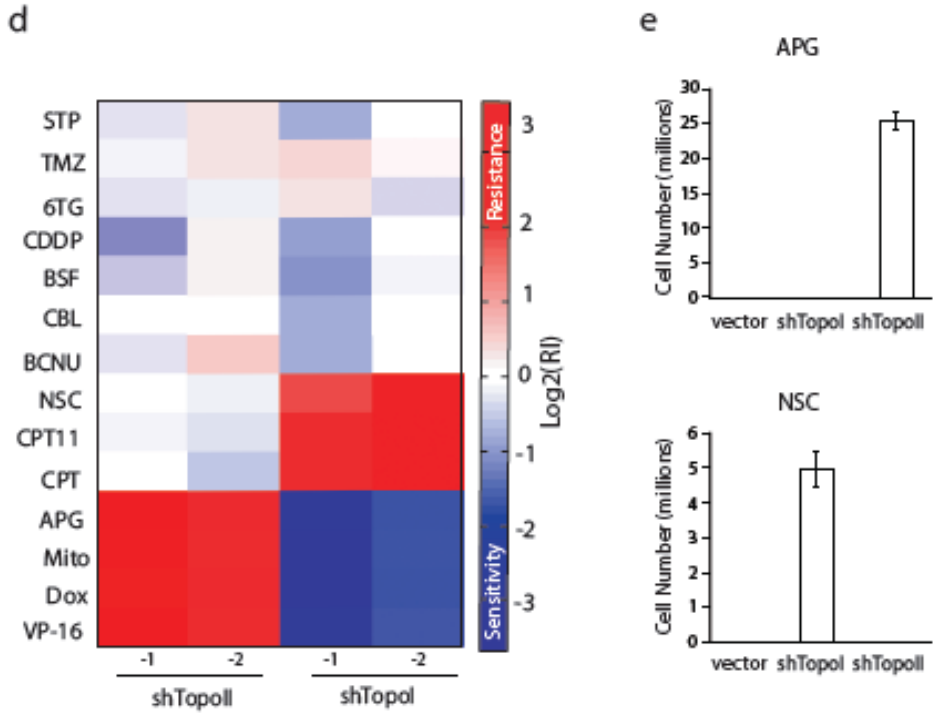

Figure 3 d, A comparison of the shTopoI and shTopoII response signatures for APG and NSC3852 with response signatures derived from established TopoI (CPT and CPT11) and TopoII poisons (Dox, Mito and VP-16). While NSC3852 and APG show response patterns characteristic of TopoI and TopoII poisons, respectively, none of the other genotoxic drugs exhibited either of these resistance/sensitivity patterns. **e,** A graph showing the number of surviving shTopo II, shTopo I or vector control expressing cells 12 days after drug treatment

with APG or NSC3852. In each case, one million cells were plated prior to treatment. Data shown are mean ± SEM from three independent experiments.

Figure 4

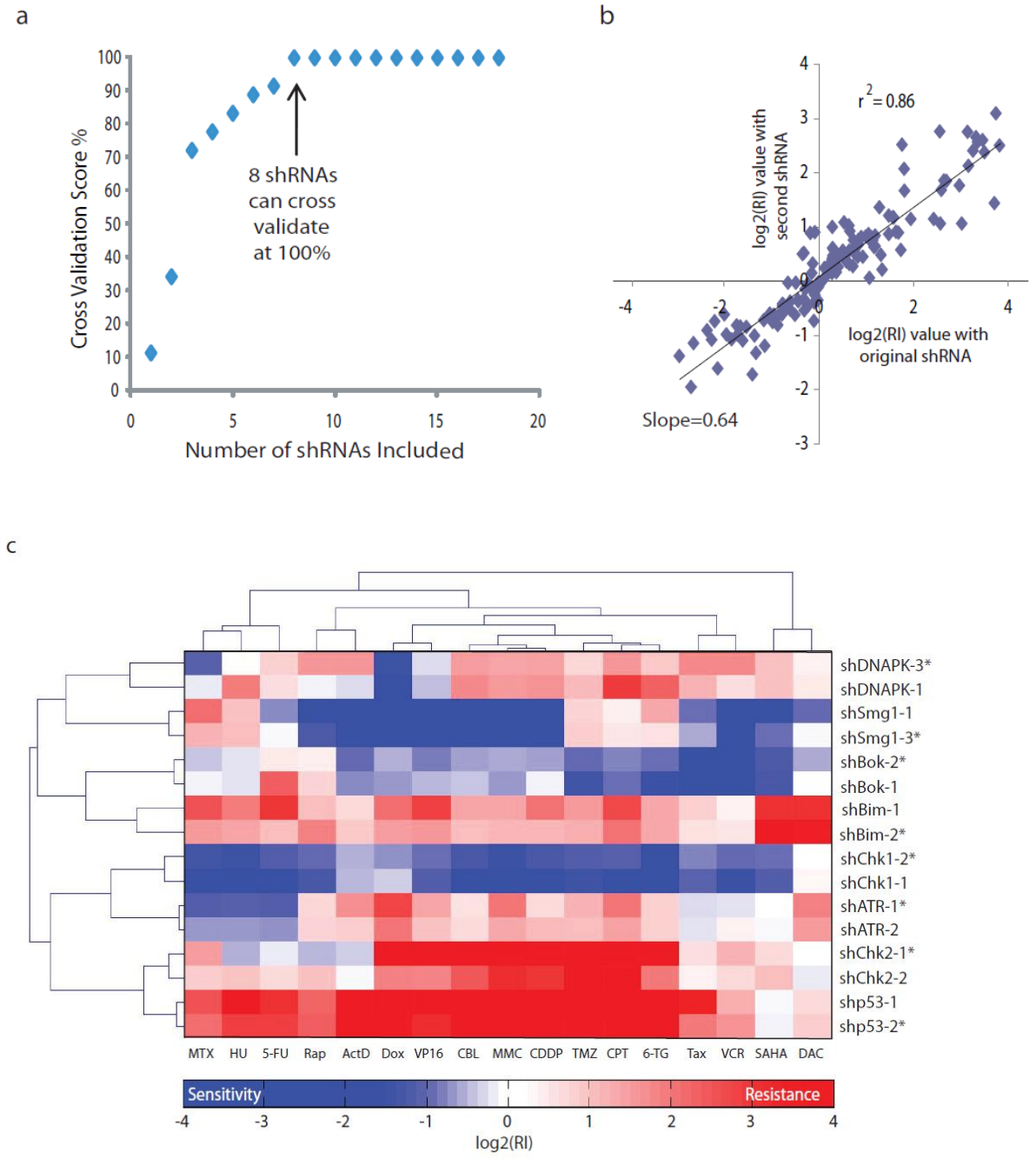

Figure 4 - A feature reduction identifies a reduced "8-shRNA set". a, Analysis of the data set used for Fig. 1c, using a randomized search strategy. The graph shows the relative efficacy of drug prediction as a function of increasing shRNA subset size. The maximum predictability for 2000 iterations at each shRNA subset size is shown. **b,** A table showing "8-shRNA signatures" that exhibit a 100% cross-validation rate. The columns show the composition of each 8-shRNA set that cross validates at 100%. Grey boxes indicate the presence of an shRNA in a particular 8-shRNA set. **c,** A heat map showing the relative enrichment (red) or depletion (blue) of a second set of shRNAs (labeled with asterisks) targeting each of the genes in the 8-shRNA signature. The associated dendograms show clustering between shRNA pairs, as well as clustering of small molecules into the same 7 categories predicted from the 29-shRNA signature. **d,** A graph showing the correlation between enrichment or depletion of cells expressing shRNAs from the original 8 shRNA set and cells expressing shRNAs from the additional 8 shRNA set following drug treatment. Each square represents the $\log_2$RI values following single drug treatment of cells expressing an original shRNA (x-axis) or the second shRNA targeting the same gene (y-axis). The slope of the best-fit line is 0.64, indicating that the absolute RI values are consistently lower in cells expressing hairpins from the second 8-shRNA set.

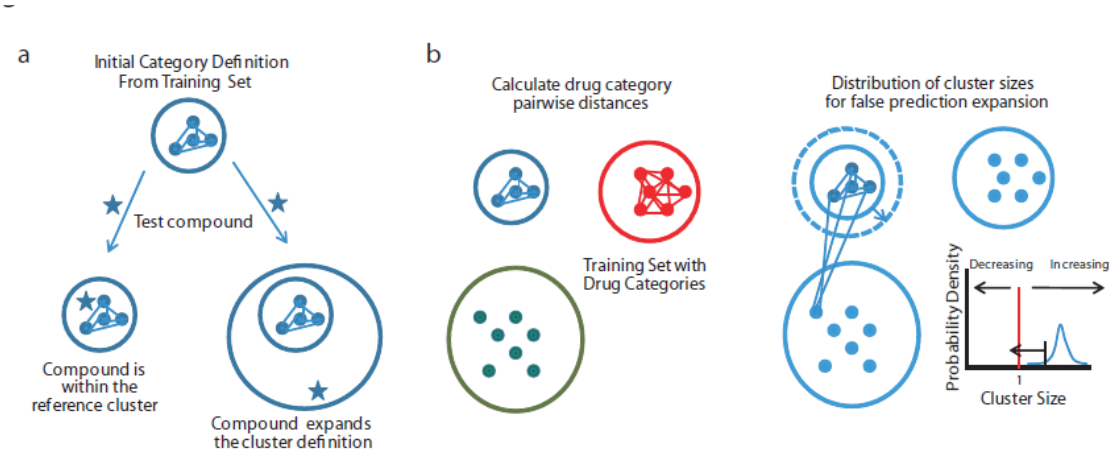

Figure 5 – A reduced shRNA signature can accurately predict drug mechanism of action. **a,** A diagram of the possible outcomes for a test compound when it is compared to the training set. A test compound could be interpolated within the definition of a drug category that is provided by the training set (Left). Alternatively, a test compound could be outside of the drug category (Right). Our probabalistic nearest-neighbors algorithm attempts to define an "acceptable" category extension. **b,** A schematic depicting the methodology behind probabilistic nearest neighbors predictions. An initial training set with empirically validated drug categories, is used to calculate the drug category specific cluster sizes. This same methodology is utilized for compounds whose known mechanism of action is distinct from a particular drug category. The increase in the drug category definition that is observed by forcing these empirically derived negative controls to cluster in an erroneous category is used to build a null distribution, and an empirical cumulative distribution function (CDF).

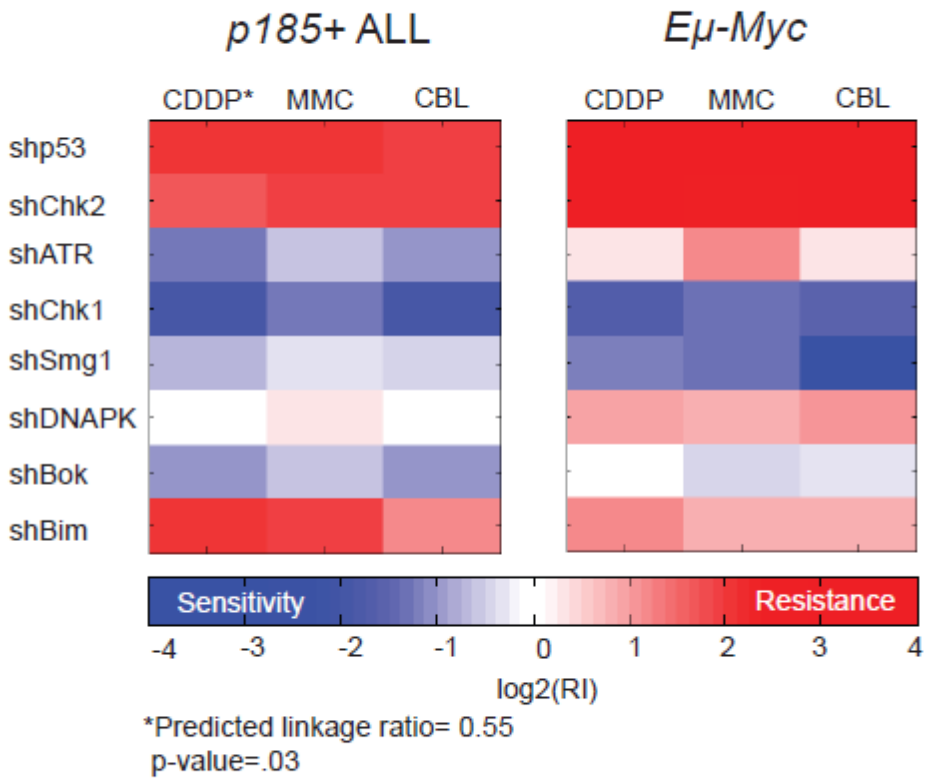

Figure 6 – Adaptation of the 8-shRNA signature to a distinct cell line. A heat map comparing the 8-shRNA response signatures of *Myc p19*$^{Arf-/-}$ lymphoma cells and *p185+ BCR-Abl* leukemia cells following treatment with alkylating agents in a model of acute lymphoblastic leukemia. The 8-shRNA signature from *p185+ BCR-Abl p19*$^{Arf-/-}$ leukemia cells can identify CDDP as an alkylating agent when CBL and MMC are used as a reference set.

Table 1 – Using the 8-shRNA signature to predict drug mechanism

a

Compounds	Prediction	Linkage Ratio	p-value	Correct Prediction
Daunorubicin	TopoII Poison	0.83	0.0004	yes
Zebularine	HDAC/DNMT inhibitor	0.82	0.002	yes
Busulfan	DNA Crosslinking	0.97	0.007	yes
2-Methoxyestradiol	Anti-Microtubule	1.08	0.009	yes
Vinblastine	Anti-Microtubule	0.95	0.001	yes
Scriptaid	HDAC/DNMT inhibitor	0.85	0.004	yes
Carmustine	DNA Crosslinking	0.95	0.005	yes
Mitoxantrone	TopoII Poison	0.94	0.002	yes
Thiotepa	DNA Crosslinking	0.92	0.003	yes
Gemcitabine	Nucleotide Synthesis Inhibitor	0.93	0.002	yes
Melphalan	DNA Crosslinking	0.91	0.002	yes
Carboplatin	DNA Crosslinking	0.86	0.0008	yes
Streptozocin	SSB inducer	1.03	0.02	yes
Maphosphamide	DNA Crosslinking	0.93	0.003	yes
Irinotecan	SSB inducer	0.88	0.002	yes
Noscapine	Anti-Microtubule	0.83	0.0002	yes
Cantharidin	Novel mechanism	1.27	0.10	Negative control
AA2	Novel mechanism	1.39	0.3	Negative control
Gliotoxin	**Novel mechanism**	**1.11**	**0.09**	**Negative control**
AG1478	**Novel mechanism**	**1.08**	**0.06**	**Negative control**

b

Updated training set with new categories:

New Category	Reference Drugs Added	New Compound	Class Prediction	Linkage Ratio	p-value	Correct Prediction
Proteasome inhibitor	PS341 and MG132	Epoxomycin	Proteasome	1.02	0.03	Yes
Proteasome inhibitor	PS341 and MG132	Gliotoxin	Proteasome inhibitor	1.22	0.05	Yes
Hsp90 inhibitor	17AAG and	VER-50589	Hsp90 inhibitor	1.09	0.0002	Yes
Hsp90 inhibitor	17AAG and	BIIB021	Hsp90 inhibitor	0.80	<0.0001	Yes
Hsp90 inhibitor	17AAG and	Neopentylamine -42	Hsp90 inhibitor	0.75	<0.0001	Yes
EGFR inhibitor	Erlotinib and Gefitinib	AG1478	EGFR inhibitor	0.88	0.002	Yes
Negative control	All	PD173074 (FGFR inhibitor)	Novel mechanism	1.30	0.2	Negative control

Negative control	All	GDC0941 (PI3K inhibitor)	Novel mechanism	1.13	0.2	Negative control

Table 1 - a, A table showing the predictive power of the 8-shRNA signature on a set of drugs that were not used to derive the signature. The “Prediction” column indicates the mechanism of action of the compound as predicted by a nearest neighbors approach. The linkage ratio describes the proximity of a test compound to a particular class of compounds and defines the observed increase (or decrease) in drug category size. For example, a linkage ratio of 1.1 indicates that the addition of a new drug expands the drug category by 10%. The p-value describes whether the proximity of a compound to a given drug category is significant when compared to a negative control distribution for that drug category. Cantharidin (a protein phosphatase inhibitor), apoptosis activator 2 (AA2, a direct activator of the apoptosome), gliotoxin (a proteasome inhibitor) and AG1478 (an EGFR inhibitor) were used as negative controls and were predicted to be distinct from any of the existing reference drugs. **b**, Category predictions and significance levels upon adding 3 new drug categories (proteasome, Hsp90 and EGFR inhibitors) that were not used to develop the initial 8-shRNA signature. PU-H71-Br is a chemical derivative of the benzyladenine-based Hsp90 inhibitor PU-H71. VER-50589 and Neopentylamine-42 are Hsp90 inhibitors. PD 173074 (a FGFR inhibitor) and GDC 0941 (a PI3K inhibitor) were used as negative controls to test the stringency of predictions after the incorporation of these new drug categories.

Supplementary Figure 1

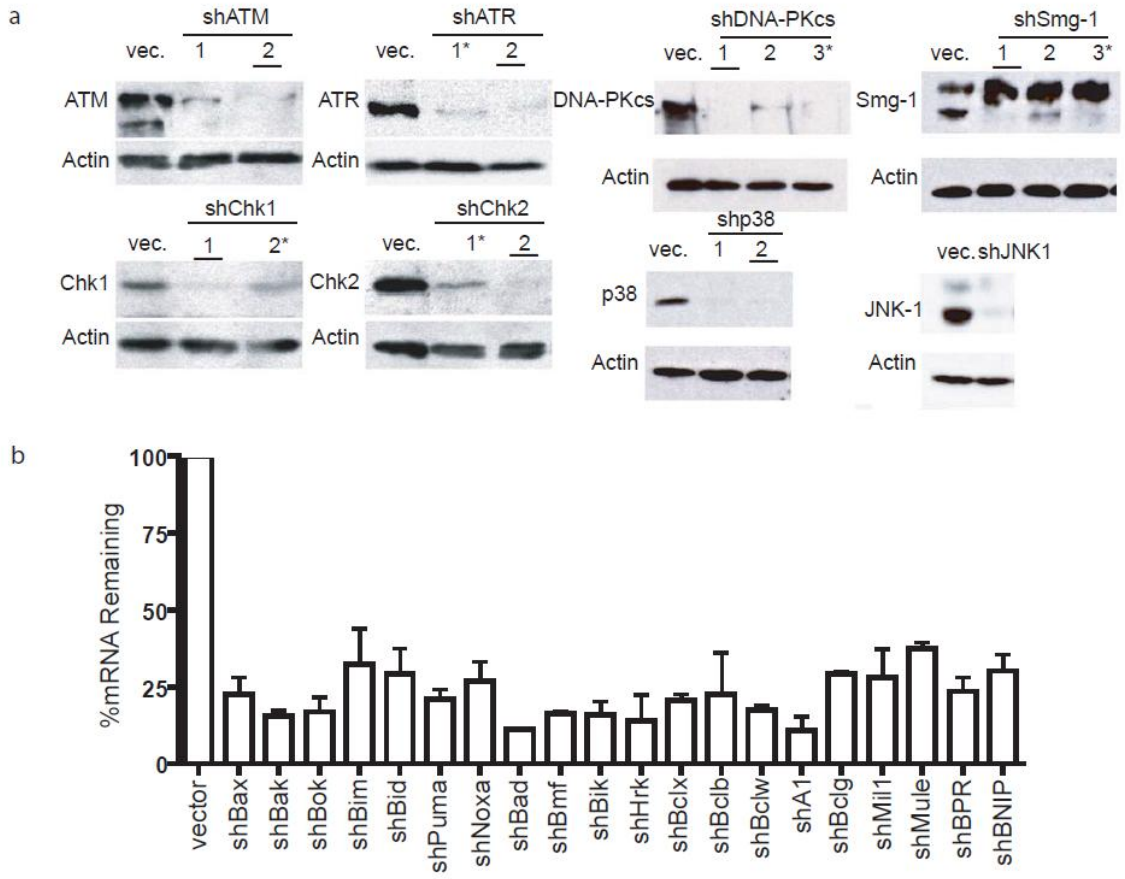

Supplementary Figure 1. shRNAmir-mediated stable suppression of drug response genes. a, Western blot image showing knockdown of p53-activating kinases. Underlined lanes demarcate shRNAs used in subsequent studies. Starred lines demarcate shRNAs used in Figure 4c as additional shRNAs. b, QPCR data showing knockdown of Bcl2 family genes. Data represent the results from two independent experiments. Bcl2 and Mcl1 were omitted from this study, as we could not establish Bcl2 and Mcl1 stable knockdown cells. Western blots were performed by Hai Jiang, qPCR was performed by Luke Gilbert.

a

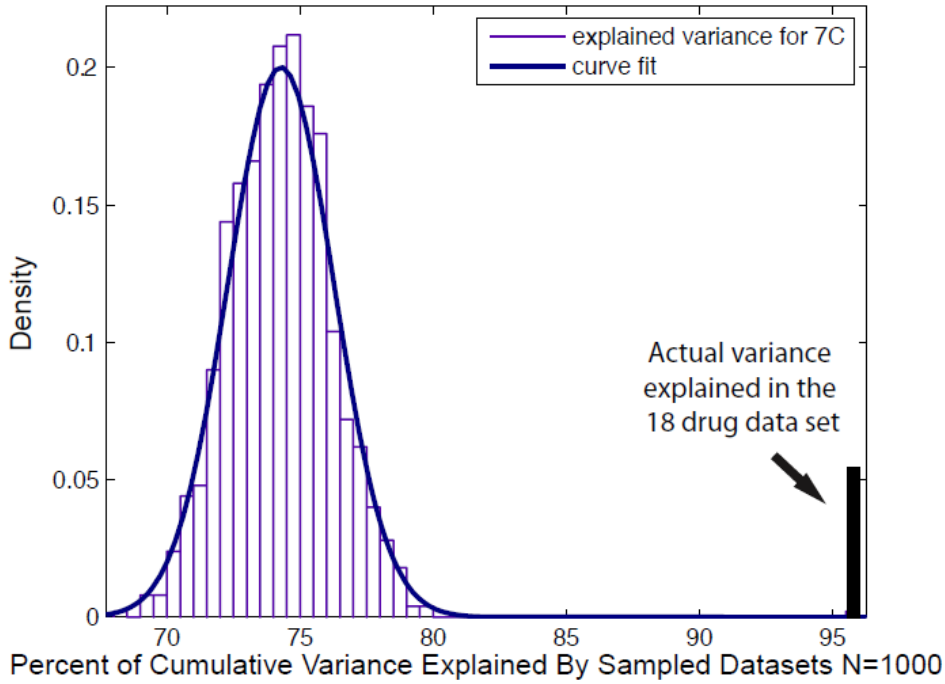
explained variance for 7C
curve fit
Actual variance explained in the 18 drug data set
Density
0.2
0.15
0.1
0.05
0
70
75
80
85
90
95
Percent of Cumulative Variance Explained By Sampled Datasets N=1000

b

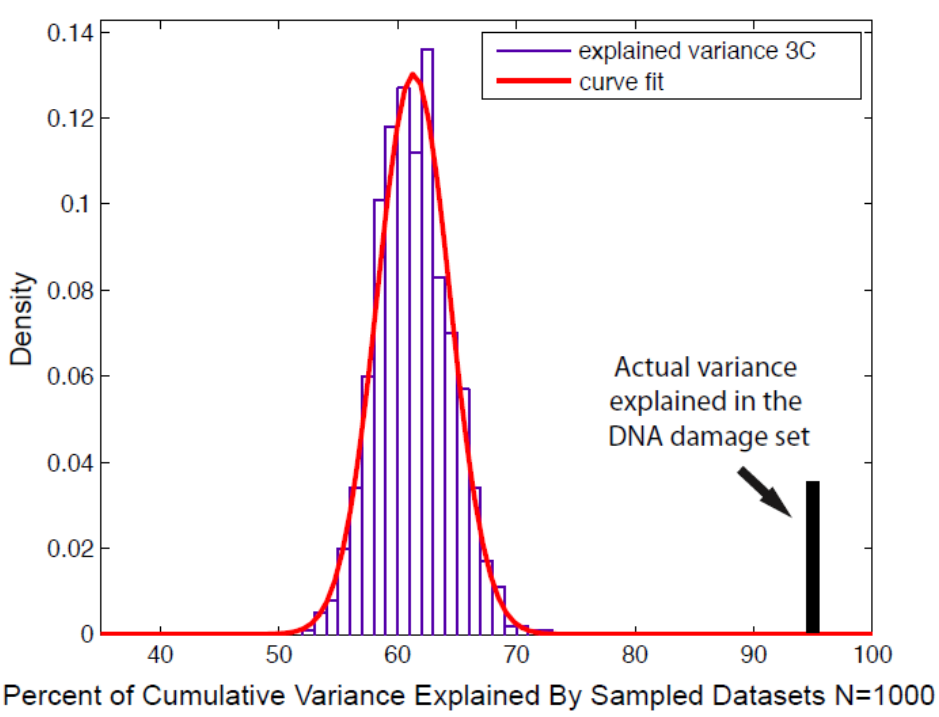
explained variance 3C
curve fit
Actual variance explained in the DNA damage set
Density
0.14
0.12
0.1
0.08
0.06
0.04
0.02
0
40
50
60
70
80
90
100
Percent of Cumulative Variance Explained By Sampled Datasets N=1000

Supplementary Figure 2. Significance analysis of the 18 drug and DNA damage subcategory clustering. a, PCA Monte Carlo analysis comparing the percent variance explained in the actual 7 category (7C) decomposition of the 18-drug set versus 7C decomposition of 1000 randomized data sets. b, PCA Monte Carlo analysis comparing the percent variance explained in the actual 3 category (3C) decomposition of the DNA damage set versus 3C decompsition of 1000 randomized data sets.

Supplementary Figure 3

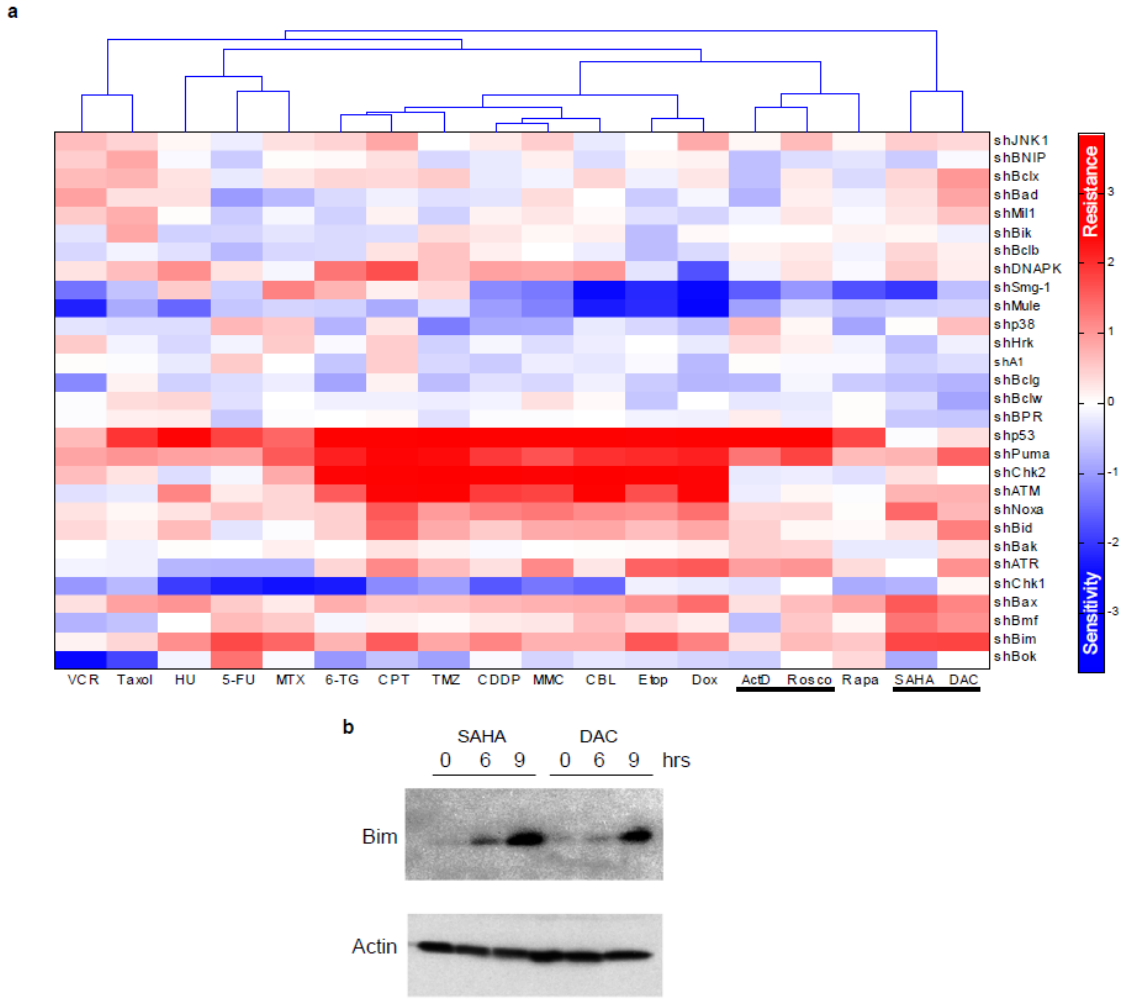

Supplementary Figure 3. a, Unsupervised clustering of RI values of the 15 reference compounds, SAHA, decitabine (DAC),and roscovitine (Rosco). Agglomerative hierarchichal clustering was performed on log transformed RI values for these 18 drugs, using a correlation metric and centroid linkage. Their cluster position is underlined in red. b, Lymphoma cells were treated with SAHA or DAC for 6 or 9 hours. Bim expression level was analyzed by western blot. The western blot was performed by Hai Jiang.

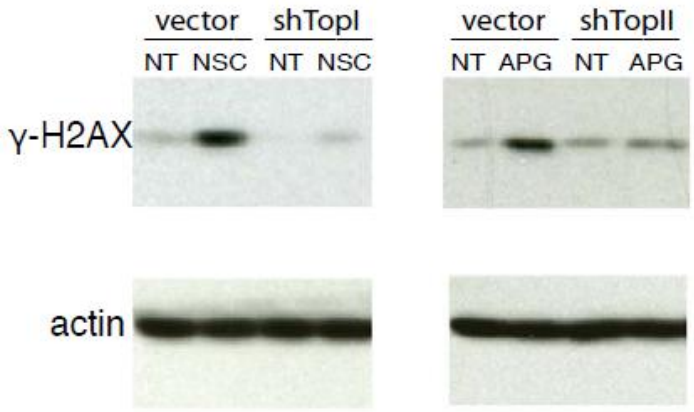

Supplementary Figure 4. The effect of TopoI and TopoII deficiency on NSC3852 and APG induced DNA damage. Vector control, TopoI and TopoII knockdown cells were treated with NSC3852 and APG, respectively. Cells were monitored by western blot for activation of a DNA damage response, as indicated by γ-H2AX phosphorylation. Hai Jiang performed this western blot.

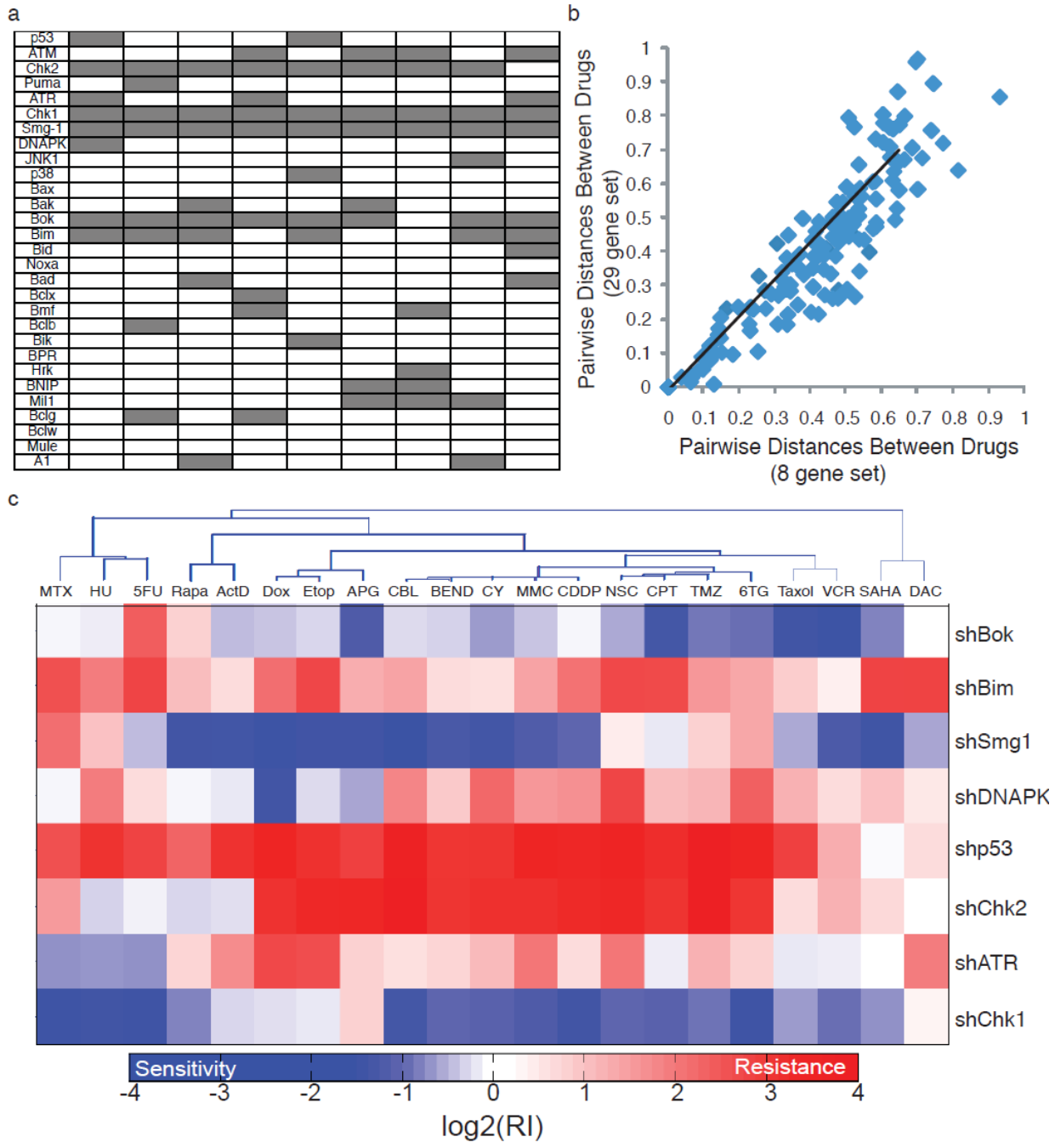

Supplementary Figure 5. a, "8-shRNA signatures" that exhibit a 100% cross-validation rate. The columns show the composition of each 8-shRNA set that cross validates at 100%. Grey boxes indicate the presence of an shRNA in a particular 8-shRNA set. b, A scatter plot of the correlation between the pairwise distances in the reference drug set for the original 29 shRNA

set versus the reduced 8 shRNA set (r2=0.81). c, A clustergram of 17 references drug plus APG, NSC3852, bendamustine and CY190602 using 8 shRNAs.

Supplementary Figure 6

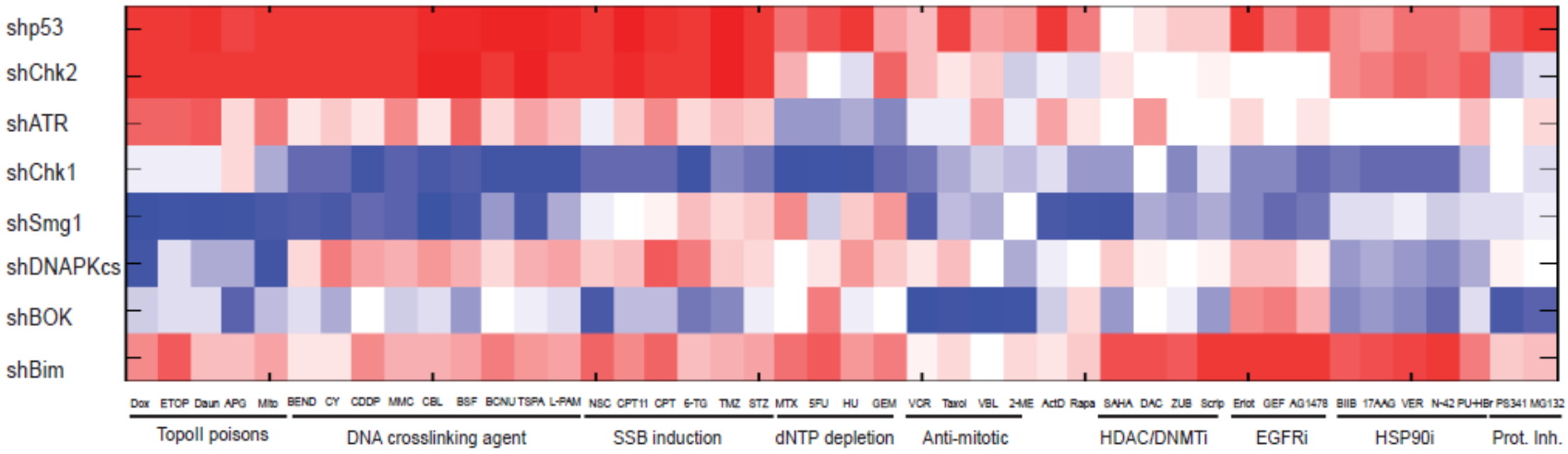

Supplementary Figure 6. A heat map showing the 8 shRNA resistance and sensitivity patterns of all chemotherapeutics examined.

Supplementary Figure 6. A heatmap of the 8 shRNA signature for all of the drugs used in this study. Colors correspond to RI values from the GFP enrichments experiments.

Supplementary Figure 7

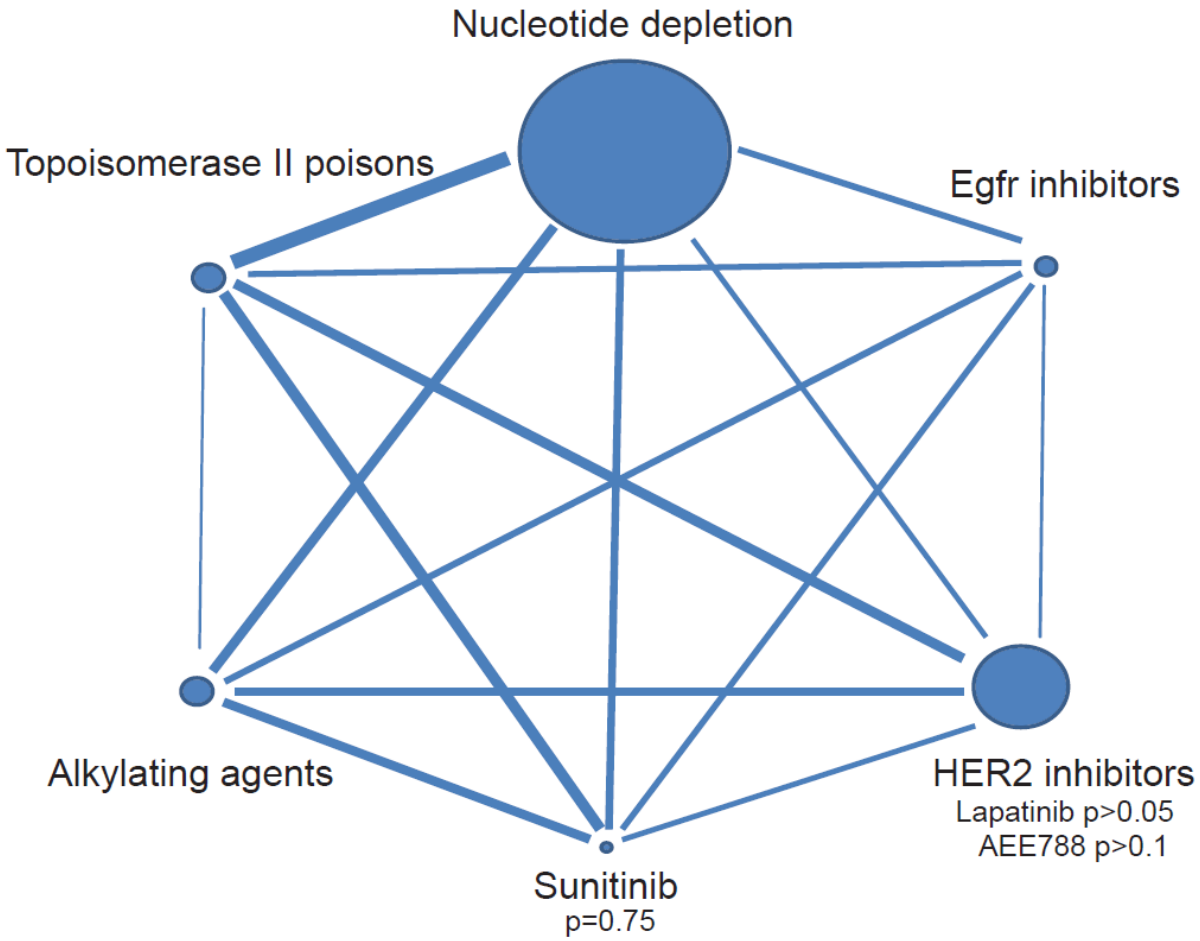

Supplementary Figure 7. A diagram showing the relative correlation distances within and between clusters. The bubble size represents the intracategory average linkage distance between drugs. The line thickness represents the average intercategory distances between the drugs of distinct categories. P values show how significantly HER2 inhibitors and Sunitinib cluster with EGFR inhibitors.

Gene	Gene Function	Gene ID	shRNA Target Sequences *
p53	sequence-specific transcription factor, pro-apoptotic	22059	CCACTACAAGTACATGTGTAA TGGAGAGTATTTCACCCTCAA (18%)
ATM	DNA damage response, checkpoint signaling, DNA repair, phosphorylation of p53	11920	CACGAAGTCCTCAATAATCTA
Chk2	DNA damage response, checkpoint signaling, DNA repair, phosphorylation of p53	50883	CAGAAACACATAATCATTAAA CACTTTCACTATGTAGAAATA
ATR	DNA damage response, checkpoint signaling, DNA repair, DNA replication, phosphorylation of p53	2E+05	ACCCATGTTCTTGACATTGAA ACCTTTAATGAGTGTCTTAAA
Chk1	DNA damage response, checkpoint signaling, DNA repair, DNA replication, phosphorylation of p53	12649	CAGGAATATTCTGATTGGAAA AAGGGCTTGACCAATTATAAA
Smg1	nonsense-mediated mRNA decay, DNA damage response, checkpoint signaling, phosphorylation of p53	2E+05	CAGGATAGCAATAAAGATGAA CAGGCTGCATTCAATAACTTA
DNA-PKcs	DNA damage response, DNA repair, phosphorylation of p53	19090	CAGGCCTATACTTACAGTTAA CTCCAACATGTAGAGAACAAA
JNK1	DNA damage response, stress signaling, phosphorylation of p53	26419	TCAGAGCATAACAAACTTAAA
p38	DNA damage response, checkpoint signaling, stress signaling, phosphorylation of p53	26416	CAGGTCTTGTGTTTAGGTCAA
A1	Bcl-2 family gene, anti-apoptotic	12044	GGAAGATGGCTTCATAAAGAA
Bclb	Bcl-2 family gene, anti-apoptotic	12049	AAGGAATCCCTTGAAACCTAA
Bclw	Bcl-2 family gene, anti-apoptotic	12050	GGCTATAAGCTGAGGCAGAAG
Bclx	Bcl-2 family gene, anti-apoptotic (long form), pro-apoptotic (short form)	12048	GGAGAGCGTTCAGTGATCTAA (targets both long and short forms of Bclx)
Bad	Bcl-2 family gene, pro-apoptotic	12015	CGCGAGAAACGTGCTTTATAA

Bak	Bcl-2 family gene, pro-apoptotic	12018	CCGGAACCTATGATTACTTGA
Bax	Bcl-2 family gene, pro-apoptotic	12028	CCGCGTGGTTGCCCTCTTCTA
Bid	Bcl-2 family gene, pro-apoptotic	12122	CACAGAAGATTCCATATCAAA
Bik	Bcl-2 family gene, pro-apoptotic	12124	CCGGACAGGTGTCAGAGGTAT
Bim	Bcl-2 family gene, pro-apoptotic	12125	TAGGAACAGAGAAATATGCAA CACCCTCAAATGGTTATCTTA (22%)
Bmf	Bcl-2 family gene, pro-apoptotic	2E+05	CGCAGAGCCCTGGCATCACAA
Bnip3l	Bcl-2 family gene, pro-apoptotic	12177	GGTATCAGACTGGTCCAGTAG
Bclg	Bcl-2 family gene, less defined	66813	TCCAAACAGCATAGAGTTCAA
Bok	Bcl-2 family gene, less defined	51800	CTGGCCTCTGTGACTGCTCTA TCGGTGTCCAGCCCTAGAGAA (25%)
BPR	Bcl-2 family gene, less defined	75736	CCCAGCCTCTTCCGAGTTCTA
Hrk	Bcl-2 family gene, pro-apoptotic	12123	CAGCAGGGAGTGTCTACTTTA
Mil1	Bcl-2 family gene, pro-apoptotic	94044	CCTGAAGAAGTGAAGAGCTTA
Mule	Bcl-2 family gene, E3 ligase for Mcl-1 and p53	59026	CCACCTCAGCTACTTCAAGTT
Noxa	Bcl-2 family gene, pro-apoptotic	58801	CAGATTGAATAGTATGTGATA
Puma	Bcl-2 family gene, pro-apoptotic	2E+05	CTGTAGATATACTGGAATGAA

* Underlined are the additional shRNA sequences showed in Supp. Fig. For these additional shRNAs, target suppression were comfirmed by western blot (ATR, Chk1, Chk2, Smg1, DNA-PKcs as shown in Supp. Fig. 1) or by QPCR (p53, Bok, Bim: listed as % mRNA remaining after their hairpin sequences).

Supplementary Table 1. This table includes the sequences for all of the hairpins used in this study.

Supplementary Table 2 - Compounds tested

Drug Name	Abbreviation	Mechanism of Action	Drug Category	Concentration used*
Chlorambucil	CBL	DNA crosslinking	Alkylating agent	6.6 uM
Bendamustine		DNA crosslinking	Alkylating agent	110 uM
CY-190602	CY-B	DNA crosslinking	Alkylating agent	1.4 uM
Melphalan	L-PAM	DNA crosslinking	Alkylating agent	3.9 uM
Maphosphamide	MAF	DNA crosslinking	Alkylating agent	6.9 uM
Carmustine	BCNU	DNA crosslinking	Alkylating agent	26.7 uM
Busulfan	BSF	DNA crosslinking	Alkylating agent	40.6 uM
ThioTEPA	TSPA	DNA crosslinking	Alkylating agent	2.1 uM
Carboplatin	CDDPC	DNA crosslinking	Platinum	16.4 uM
Cisplatin	CDDP	DNA crosslinking	Platinum	3.3 uM
Mitomycin C	MMC	DNA crosslinking	Anti-tumor antibiotic	90 nM
Camptothecin	CPT	Induction of SSBs	Topo I poison	0.4 nM
Irinotecan	CPT11	Induction of SSBs	Topo I poison	2.1 uM
NSC3852	NSC3852	Induction of SSBs	Topo I poison	1.7 uM
Doxorubicin	Dox	Induction of DSBs	Topo II poison	16.2 nM
Etoposide	VP16	Induction of DSBs	Topo II poison	34 nM
Mitoxantrone	MITO	Induction of DSBs	Topo II poison	0.4 nM
Apigenin	APG	Induction of DSBs	Topo II poison	100 nM
Daunorubicin	Dau	Induction of DSBs	Topo II poison	22.5 nM
6-Thioguanine	6TG	DNA methylation memetic	Antimetabolite	54 nM
Temozolomide	TMZ	DNA methylation	Alkylating agent	23.2 uM
Streptozocin	STZ	DNA methylation	Alkylating agent	83 uM
17 AAG		HSP90 inhibition	HSP90 inhibitor	2.6 uM
BIIB021		HSP90 inhibition	HSP90 inhibitor	0.79 uM
PU-H71-Br		HSP90 inhibition	HSP90 inhibitor	0.53 uM
Neopentylamine 42		HSP90 inhibition	HSP90 inhibitor	1.1 uM
VER-50589		HSP90 inhibition	HSP90 inhibitor	0.16 uM
Vorinostat	SAHA	HDAC inhibition	HDAC inhibitor	0.2 uM
Scriptaid		HDAC inhibition	HDAC inhibitor	0.5 uM
Decitabine	DAC	DNMT inhibition	Antimetabolite	0.6 uM
Zebularine		DNMT inhibition	Antimetabolite	30 uM
PD 173074		FGFR inhibition	FGFR inhibitor	4.2 uM
AG1478		EGFR inhibition	EGFR inhibitor	19 uM
Gefitinib		EGFR inhibition	EGFR inhibitor	12.5uM
Erlotinib		EGFR inhibition	EGFR inhibitor	6.5 uM
GDC 0941		PI3K inhibition	PI3K inhibitor	5.4 uM
Actinomycin D	ActD	RNA syn. inhibition	Anti-tumor antibiotic	1.2 nM
Roscovitine	Rosco	CDK inhibition	Kinase inhibitor	26.7 uM
Rapamycin	RAPA	Protein syn. inhibition	Anti-tumor antibiotic	15 uM
Bortezomib	PS341	Proteasome inhibition	Proteasome inhibitor	13 nM
Epoxomicin		Proteasome inhibition	Proteosome inhibitor	45 nM
Gliotoxin		Proteasome inhibition	Proteosome inhibitor	0.3 uM
Vinblastine	VLB	Disruption of mitosis	Antimicrotuble agent	2.5 nM
Paclitaxel	Taxol	Disruption of mitosis	Antimicrotuble agent	8 nM
Vincristine	VCR	Disruption of mitosis	Antimicrotuble agent	1.5 nM
Noscapine		Disruption of mitosis	Antimicrotuble agent	58.1 uM
2-Methoxyestradiol		Disruption of mitosis	Antimicrotuble agent	1.8 uM
Methotrexate	MTX	nucleic acid syn. inhibition	Antimetabolite	33 nM
5-Fluorouracil	5FU	nucleic acid syn. inhibition	Antimetabolite	30.5 nM
Hydroxyurea	HU	nucleic acid syn. inhibition	Antimetabolite	78 uM
Fludarabine	dFdC	nucleic acid syn. inhibition	Antimetabolite	3.8 uM
Gemcitabine	GEM	nucleic acid syn. inhibition	Antimetabolite	100 nM
Cantharidin		Phophatase inhibition	Phophatase inhibitor	10.7 uM
Apoptosis Activator 2	AA2	Direct activation of apoptosome	Activator of apoptosis	1.9 uM

* Listed are concentrations of drugs that cause between 80 and 90% of maximal killing. For every set of experiments, cell death was monitored using uninfected cells to ensure proper IC80-90s.

a

Vorinostat query

Rank	cmap name	Mean	n	Enrichment	p	Specificity	Percent non-null	Known Mechanism/Target
1	vorinostat	0.743	12	0.976	0	0.0151	100	HDACi
2	trichostatin A	0.631	182	0.898	0	0.0095	97	HDACi
3	resveratrol	0.275	9	0.757	0	0.0343	100	HDACi
4	15-delta prostaglan	0.16	15	0.589	0	0.1173	86	PPAR-gamma agonist
5	thioridazine	0.169	20	0.588	0	0.1324	75	Seratonin antagonist
6	geldanamycin	0.203	15	0.587	0	0.0924	86	HSP90i
7	LY-294002	0.202	61	0.578	0	0.0134	85	PI3Ki
8	sirolimus	0.143	44	0.515	0	0.0361	68	mTOR
9	valproic acid	0.206	57	0.512	0	0	70	HDACi
10	tanespimycin	0.172	62	0.503	0	0.0725	80	HSP90i

Geldanamycin query

Rank	cmap name	Mean	n	Enrichment	p	Specificity	Percent non-null	Known Mechanism/Target
1	withaferin A	0.345	4	0.969	0	0.0211	100	Heat shock response inducer
2	lomustine	0.311	4	0.941	0	0.0118	100	Alkylating agent
3	geldanamycin	0.522	15	0.925	0	0	100	HSP90i
4	tanespimycin	0.438	62	0.827	0	0.0052	98	HSP90i
5	alvespimycin	0.394	12	0.802	0	0.0058	100	HSP90i
6	vorinostat	0.263	12	0.742	0	0.1759	91	HDACi
7	monorden	0.302	22	0.719	0	0.0054	100	Poorly characterized in mammals
8	15-delta prostaglan	0.282	15	0.71	0	0.0335	93	PPAR-gamma agonist
9	trifluoperazine	0.177	16	0.631	0	0.0529	68	Dopamine D1, D2 receptor
10	thioridazine	0.123	20	0.599	0	0.1279	50	Anti-cholinergic

b

Chlorambucil query

Rank	cmap name	Mean	n	Enrichment	p	Specificity	Percent non-null	Known Mechanism/Target
1	monensin	-0.337	6	-0.831	0.00006	0	50	Ionophore
2	nialamide	0.223	4	0.909	0.00008	0	100	MAOI
3	quinethazone	0.206	4	0.877	0.00034	0	100	Anti-hypertensive
4	capsaicin	0.161	4	0.86	0.0005	0	100	VR1 agonist
5	fluocinonide	0.14	5	0.774	0.00134	0.0075	80	Glucocorticoid
6	Prestwick-983	-0.732	3	-0.905	0.00162	0.0069	100	Poorly characterized
7	biperiden	-0.55	5	-0.751	0.00174	0.0748	80	Anti-cholinergic
8	bendroflumethiazide	0.157	6	0.705	0.00175	0	83	Anti-hypertensive
9	cefamandole	-0.345	4	-0.805	0.00282	0.0083	50	Beta-lactam antibiotic
10	ikarugamycin	-0.467	3	-0.885	0.00296	0.0152	66	Endocytosis inhibitor
90	semustine	0.103	4	0.568	0.09445	0.3051	75	Alkylating agent

Vinblastine query

Rank	cmap name	Mean	n	Enrichment	p	Specificity	Percent non-null	Known Mechanism/Target
1	methotrexate	-0.473	8	-0.679	0.00044	0.0069	87	Nucleotide depletion
2	nifedipine	0.061	7	0.696	0.00056	0	71	Calcium channels
3	doxylamine	-0.273	5	-0.796	0.00074	0.0267	60	Anti-histamine
4	Prestwick-642	0.148	4	0.844	0.00097	0	100	Poorly characterized
5	meptazinol	-0.635	4	-0.828	0.00165	0.0054	100	Opioid receptor agonist
6	pirenperone	0.089	5	0.758	0.00194	0	60	5-HT2A receptor
7	valinomycin	0.119	4	0.811	0.00241	0.0349	100	K+ Carrier
8	cinnarizine	0.12	4	0.805	0.00269	0	100	Anti-histamine
9	(-)-atenolol	0.12	4	0.8	0.00302	0	100	Beta blocker
10	urapidil	0.114	4	0.798	0.0032	0	100	Alpha-1 adrenergic receptor
271	podophyllotoxin	0.079	4	0.434	0.32889	0.7286	50	Microtubule assembly

c

Connectivity Map Comparison Criteria	Out of 14
Top hit is either a replicate of the same compound or a compound with the same mechanism	6
At least one of the top 5 is the same mechanism	10
At least one of the top 10 is the same mechanism	10

A summary of small molecule queries using the Connectivity Map. a, Tables showing results in which compounds - Vorinostat (above), and Geldanamycin (below) were queried against the connectivity map. These compounds show clear mechanistic signatures characteristic of their molecular drug class. Analogous compounds present in the top 10 search

results are shown in red. **b**, Tables showing results in which the queried compounds are vinblastine and chlorambucil. The red text indicates the first compound with a known mechanistic relationship. Notably, while the 8-shRNA can effectively classify these compounds, the Connectivity Map lacks resolution for either agent. All data was obtained at: http://www.broadinstitute.org/cmap/. **c**, Connectivity Map analysis of 14 compounds categorized in this study. The drugs examined were Mitoxantrone, Doxorubicin, Daunorubicin, Camptothecin, Irinotecan, Carmustine, Vinblastine, Paclitaxel, Methotrexate,Vorinostat, Geldanamycin, Lomustine, MG132, and Rapamycin.

Supplementary methods

Clustering:

Agglomerative Hierarchical Clustering was performed in Matlab v7.0. All RI values were Log2 transformed to represent depletion and enrichment data on the same scale. To measure the distance between clusters, we used an inverse correlation based metric: get equation. After all drug pairwise distances were calculated, we used centroid linkage to compute the distance between cluster groups. Several forms of significance calculations were performed. To estimate the overall number of significant underlying drug groups in our data set, we looked at the number of latent variables that could explain the majority of the variance in the data set via a principal components analysis. However, Random Matrix Theory for small data sets suggests that small noisy data sets may have large eigenvalues based upon chance. Therefore, in order to estimate the significance of our categorization of underlying drugs, we also performed a Monte Carlo analysis on our dataset. Briefly, we sampled 1000 data matrices from our drug-gene data. We then plotted the distribution of the cumulative variance explained by our 7-component model relative to randomized matrices.

This Monte Carlo analysis estimates the significance of the number of components that one uses to interpret the PCA model.

In an idealized scenario where the distances between and within drug clusters are similar across drug types, a uniform cutoff at a single branch length should guide interpretation of the clusters. However, in stratified datasets like ours, where considerable variation exists within and between clusters, a more stratified approach becomes appropriate. Our DNA damage drug set contained extraordinarily close correlations between distinct drugs relative to the rest of our dataset. To determine whether we could confirm sub-categories of drugs within this cluster, we extended the PCA sampling approach to this subset of data. Utilizing this stratified approach to cluster interpretation, we were able to support a hypothesis of three distinct DNA damage sub-clusters. This variegated approach to cluster interpretation was also evaluated by doing Bootstrapping analysis in R using the PVClust function 1. This approach was used to complement the PCA data. The PCA data tells us how many significant underlying drug variables we can interpret from the data, and the bootstrapping can tell us whether particular branches are significant.

Comparison of shRNA's to miRNA's

Local sequence alignments were performed in matlab using the localalign.m function. Briefly, each shRNA in the 8 shRNA signature was pairwise aligned to every miRNA in the *Mus musculus* genome.

Reference

1. Suzuki, R. & Shimodaira, H. Pvclust: an R package for assessing the uncertainty in hierarchical clustering. *Bioinformatics* **22**, 1540-1542 (2006)

Chapter 3

Defining Genetic Principles of Combination Drug Action

Contributions:

I performed the majority of experiments and data analysis in this chapter. Peter Bruno assisted with the primary cell line experiments. Kelsey Capron, a UROP, performed the pairwise drug synergy screen. M. Hemann, D. lauffenburger, and I wrote the paper. A version of this manuscript has been submitted for publication at Cell.

Abstract

Combination chemotherapies have been a mainstay in the treatment of disseminated malignancies for almost 60 years, yet even successful regimens fail to cure many patients. Though their single drug components are well studied, the mechanisms by which drugs work together in clinical combination regimens is poorly understood. Here, we combine RNAi based functional signatures with complementary informatics tools to examine drug combinations. This approach seeks to bring to combination therapy what the knowledge of biochemical targets has brought to single drug therapy and creates a statistical and experimental definition of "combination drug mechanisms of action". We show that highly synergistic drug combinations function as a more potent version of a *single* drug. Conversely, unlike highly synergistic combinations, most drugs *average* extant single drug variations in therapeutic response. When combined to form multi-drug regimens, averaging combinations form averaging regimens that homogenize - genetic variation in mouse models of cancer and in clinical genomics datasets. We suggest surprisingly simple and predictable combination mechanisms of action that are independent of biochemical mechanism and have implications for biomarker discovery, and the development of regimens with defined genetic dependencies.

Introduction

Current rationales for the design of combination chemotherapy regimens were developed in the 1940's-1950's (1-5) and, remarkably, were concurrent with the identification of DNA as the genetic material. The development of these regimens in the absence of any knowledge of cancer genetics was a remarkable achievement. However, while our knowledge of the genetic drivers of cancer and the mechanisms of drug action has increased dramatically over the last 30 years, this information has been difficult to adapt to clinical practice. As such, even very successful combination regimens often fail to cure many patients (6) (7). We hypothesize that part of this failure is due to the absence of mechanistic information about how drugs in regimens interact to promote combination effects (we term these effects "combination mechanisms of action"). We sought to address this gap by investigating specific hypotheses concerning the "mechanisms of action" of combination therapy.

The classic term "drug mechanism of action" refers to the description of a specific biochemical event - often the activation or inhibition of an enzymatic effect. However, in recent years, "signature" based prediction has provided a powerful new strategy for examining drug mechanism. In signature-based approaches, a series of drug-induced molecular/phenotypic measurements are made in an experimental system. Collections of measurements from many small molecules form multivariate signatures that aim to fingerprint drugs based upon their relative signature similarity (8-13). In several landmark studies using *S. cerevesiae*, gene expression compendia (8), and later barcoded loss of function/ORF libraries (9, 10), large signatures were shown to effectively characterize individual small molecule mechanisms of action. Similar work utilizing the NCI-60 cell lines (14) showed that signatures comprised of the

inhibitory concentrations of cytotoxic drugs across diverse cancer cell lines could provide sufficient resolution to predict a novel small molecule's mechanism of action. Additionally, mammalian transcriptional data has also been used to determine the mechanisms of small molecule action (15, 16). However, in spite of their broad use in single agent drug studies, these molecular/phenotypic signatures have not been adapted to the examination of multi-drug combinations. Signatures are a uniquely attractive methodology to characterize combination drug mechanisms of action, providing a higher-level phenotype beyond simple measures of cell viability. Signatures allow for a simple comparison of controlled combination drug molecular and phenotypic information with component single drug information.

While attempts have been made to quantify combinatorial drug effects (17), no existing methodology has a demonstrated ability to resolve combination mechanisms of action. To create a platform that is capable of resolving between differing hypotheses about combination mechanisms of action, we turned to high-resolution RNAi signatures of mammalian cell death genes. Specifically, we recently developed an approach to use patterns of drug sensitivity or resistance conferred by sets of shRNAs to develop "signatures" that are characteristic of specific classes of compounds. This signature-based approach compares the signature of a test compound to a reference set of single drug signatures that possess known mechanisms of action. It then examines the similarity of a predicted drug for its predicted target drug class relative to the likelihood that the negative controls in the data set would produce the same result. We were able to use this approach to classify uncharacterized drugs based on well-described compounds that showed similar signatures. Informative patterns of resistance and sensitivity could be revealed with as few as 8 shRNAs (shp53, shChk2, shChk1, shATR, shATX, shDNAPKcs, shBok and shBim), with high quantitative resolution across the diverse training drug categories that included most established cytotoxic agents. Surprisingly, these signatures

were scalable, such that the addition of 8-shRNA signatures for as few as two drugs from entirely new mechanistic categories (Hsp90 inhibitors, kinase inhibitors and others) was sufficient to classify a third structurally unrelated drug from that category (18). We reasoned that this signature-based platform, with validated resolution over a breadth of drug categories, might resolve important hypotheses as to the nature of multi-drug combinations.

Potential mechanisms of combination drug action.

Combination therapies might be hypothesized to interact in two general ways: [a] one agent may simply reinforce the action of another agent; or [b] the two drugs may combine to exert effects that are distinct from either individual compound. Correspondingly, the combination drug shRNA signature would either [a] resemble that of one individual drug, or [b] exhibit distinct genetic dependencies. With respect to the latter possibility, a combination signature could be distinct from that of the individual component drugs in one of at least three ways: [i] it could average, or "homogenize", individual drug signatures; [ii] it could mimic a compound not present in the combination; or [iii] it could adopt an entirely novel (neomorphic) signature (Figure 1A). To extend our functional genomic signature-based framework to combination drug dosing, we created shRNA signatures of resistance or sensitivity in response to combinations of drugs that were controlled for dose level effects. All signatures in the single drug reference set were obtained at concentrations of single drugs that induce 80-90% cell death (LD80-90) in *Eμ-Myc*$^{p19arf-/-}$ lymphoma cells, a well-characterized model of human Burkitt's lymphoma(19). To allow for reference set comparisons, combination dosings were dosed at 80-90% cell death. The cumulative LD80-90 of the combination was achieved by dosing single drugs such that each drug contributed equally to an LD80-90 combination cell death. (Figure 1B). These

combinations were then quantitatively compared using probabilistic nearest neighbors analysis (Figure 1C).

While combination therapies are the standard of care for nearly all disseminated human cancers, to our knowledge, only the interaction of 5-fluorouracil (5-FU) and leucovorin has a well-characterized combination mechanism of action. Leucovorin (which on its own is non-toxic) exerts a synergistic effect by enhancing the inhibition of thymidylate synthase by the nucleoside analog 5-FU (20); this inhibition depletes cellular nucleotide levels and induces apoptosis. Thus, we reasoned that we could use this drug combination as a proof of principal for our combination signature approach. Specifically, a signature of leucovorin plus 5-FU should resemble the single drug 5-FU signature but at a lower 5-FU concentration. We observed that dosing lymphoma cells with leucovorin elicited no cell death at 1μM but the addition of 1μM leucovorin potentiated 5-FU action (Figure 1D). Moreover, the 8-shRNA signature for 5-FU plus leucovorin closely resembled 5-FU and was significantly ($p<0.0001$) predicted by probabilistic nearest neighbors analysis to be a nucleotide depletion agent. This indicates that the known biochemical mechanism of 5-FU and leucovorin is the relevant mechanism of cell death induction in *Eμ-Myc*$^{p19arf-/-}$lymphoma cells, and suggests that our signature based approach can offer resolution for combination drug mechanisms.

Signatures of synergistic combination therapies.

In order to take a non-biased approach to the study of combination drug mechanisms, we examined all pairwise interactions between distinct functional categories of cytotoxic agents upon which our 8-shRNA signature has established resolution (Figure 2A). Since little is known about the nature of combination drug mechanisms of action, quantifying the amount of drug

interaction allows us to do two things: [i.] We can quantify the single drug doses that give rise to combination LD80-90s, and thus allow for the controlled comparison of drug combination signatures to single drug signatures. [ii.] We can examine combination signatures of combinations with distinct modes of drug interaction i.e. synergy versus additivity. Initially, we chose to examine the two most synergistic combinations from our pairwise interaction screen: 17AAG (an Hsp90 inhibitor) combined with Taxol (a spindle poison), and 17AAG combined with chlorambucil (abbreviated CBL, a DNA alkylating agent) (Figures 2A and 2B). Specifically, concentrations of single drugs that individually induced single drug cell death (as assessed by PI+) in ~15% of the population (for both 17AAG and Taxol) and ~20% (for both 17AAG and CBL) of the population were sufficient to elicit a combination LD of 80-90% (Figure 2B). Consistent with this high level of synergy, control signatures taken at the respective single drug LD15s and LD20s exhibited little to no shRNA-mediated resistance or sensitivity (Figure 2C). However, upon combination, the LD80-90s of 17AAG-Taxol and 17AAG-CBL synergistically elicited robust phenotypic signatures. Comparison of 17AAG-Taxol's signature to our single drug reference set suggested that this combination exhibited a spindle poison-like mechanism of action ($p=0.003$) (Figure 2C). This evidence favors a model whereby 17AAG acts to enhance taxol-induced cytotoxicity. Similarly, the signature for the 17AAG and CBL combination matched a DNA damage-like mechanism of action ($p=0.00006$), suggesting that 17AAG synergizes with CBL by promoting CBL's genotoxic activity (Figure 2C).

To visually examine these mechanistic predictions regarding combination drug action, we performed Principal Components Analysis (PCA). In PCA, large dimensional datasets with many variables (here 8 variables,1 for each shRNA in the signature) are collapsed onto composite variables, termed principal components, which represent a weighted combination of the 8 original primary variables. Consequently, observations of single drugs and drug

combination behaviors can be replotted in 1, 2, or 3 dimensions to facilitate visual analysis and further interpretation of the statistical predictions. Replotting of Hsp90 inhibitors and spindle poisons alongside the 17AAG-Taxol combination revealed a clear separation of Hsp90 inhibitors from spindle poisons along a single composite variable: principal component 1 (PC1) (Figure 2D, top) and captured a large proportion of the variance explained by the model (Figure S1A). Furthermore, 17AAG-Taxol clearly mapped in the same region in PCA space, supporting the prediction that 17AAG reinforces a taxol-like action. A similar separation and fit (Figure S1B) along the first principal component was seen with Hsp90 inhibitors in relation to DNA damaging agents (Figure 2D). Plotting 17AAG-CBL, the closer proximity of the 17AAG-CBL to other DNA damaging agents indicates a genotoxic mechanism for this combination. Taken together, these data suggest that highly synergistic combinations act by potentiating a single drug's mechanism of action.

Examining the pairwise interaction of drugs within commonly used regimens.

We next examined pairwise combinations of drugs that are far less synergistic than the combinations of 17AAG/Tax, and 17AAG/CBL. Here we also aimed to use combinations that are used as the backbone of induction regimens for many hematopoetic and solid cancers (Table S1). First, we combined doxorubicin (Dox) and CBL to obtain a combination LD80-90 signature. Notably, unlike the synergistic drug combinations examined previously, the shRNA signature for this drug combination suggested a mechanism of action that was distinct from both of the component drugs that form the combination (Figure 3A). Specifically, PCA clearly separated topoisomerase II poisons like Dox from DNA alkylating-like agents along PC1. Furthermore, the Dox-CBL combination dosing clustered around the origin of the PCA plot. This indicated a relative averaging of the individual drug signatures – i.e., the remarkable elimination

of contrasting shRNA-conferred phenotypes exhibited by individual drugs. For example, the suppression of DNAPKcs levels yielded sensitivity to Dox and resistance to CBL, but had no consequence in the face of a combination drug dosing. Thus, DNAPK status is relevant to the drug response to single agents, but loses relevance in response to combination treatment.

To more thoroughly explore clinically relevant combinations (Table S1), we next examined the additive combination of Dox/Vincristine (Vin) (Figure 3B and Figure S2B) and CBL/Vin (Figure 3C and Figure 2C). Like Dox and CBL, both of these additive combinations were computationally predicted to be novel compounds (Figures 3B and C), which could be rationalized by examining the first 2 PCA component plots of single drug constituent categories alongside a scatter plot of the combination data (Figures 3B and C). Both drug combinations scattered adjacent to the origin and lay between the original single drug categories on principal component 1, essentially averaging both component drugs. Thus, many drug combinations average single drug genetic dependencies - even to the point of essential neutrality.

Distinct oncogenes or cell types may impart differences in drug signatures that are dependent upon their genetic context. To examine our averaging phenomena in a second genetic background, we turned to a model of BCR-Abl positive acute lymphoblastic leukemia (ALL) (21). Interestingly, p185+*BCR-Abl* $^{p19arf-/-}$ cells exhibited single drug RNAi signatures that were distinct from *Eμ-Myc* $^{p19arf-/-}$ cells (Figure 3D). However, in spite of these differences, extant dependencies between Dox and CBL treated cells followed an averaging model when exposed to a combination of the two agents. The averaging model fit was similar in magnitude to the additive combinations in the *Eμ-Myc* $^{p19arf-/-}$ cells (Figure 3E) and a significantly better ($p<0.0005$)

fit than the synergistic combinations. Thus, the averaging phenotype of this combination is independent of the driving oncogene.

Upon qualitative examination of the drug-gene dependencies in the BCR-Abl positive ALL, we noticed large and robust distinctions in the 8 shRNA signature phenotypes produced by the glucocorticoid receptor agonist dexamethasone (Dex) and Dox (Figure 3D). We reasoned that the large differences between Dex and Dox signatures in ALL would provide broad quantitative resolution to examine a variety of ratiometric mixtures of single drug contributions to combination LD80-90 killing. Specifically, we performed an experiment using a 5x5 dosing matrix of Dex and Dox combinations. Upon the examination of the heat maps for the 8 shRNA signatures (Figure 3F), we noted a linear drug ratio dependent effect upon the Dox/Dex combination signatures. When we used a simple weighted average model that was based upon the proportion of combination killing attributable to the individual drugs at the combination doses, we found that all of the p185+ ALL Dox/Dex mixtures followed an averaging model. Thus, not only could we extend this averaging hypothesis to a distinct cell type, but the analysis of combination therapy in this model also allowed us to rigorously examine the averaging model across numerous drug dose ratios.

Examining components of larger drug regimens.

The combinations tested in Figure 3 have broad relevance as components of diverse drug regimens that constitute the frontline treatment for many human cancers. (Table S1). This stands in contrast to synergistic combinations, where, for example, 17AAG and other Hsp90 inhibitors are not currently components of clinically established drug regimens (22). Thus, we were interested in expanding our analysis to examine larger combination regimens that are now

the standard of care for B cell malignancies. Given that the *Eμ-Myc*$^{p19Arf-/-}$ lymphoma cells are a well-established mouse model of high grade Non-Hodgkin's lymphoma, we chose to examine 3 and 4 drug combinations that are a large proportion of the CHOP and Hyper-CVAD regimens. The induction arm of both of these regimens utilizes cyclophosphamide (C), Vin (O or V), Dox (A or H), and a glucocorticoid receptor agonist (P or D). Since cyclophosphamide requires activation *in vivo*, we utilized another nitrogen mustard, CBL, which has shown similar *in vivo* efficacy in clinical trials of lymphoma chemotherapy (23). Surprisingly, in our pairwise synergy screen, drugs from the cytotoxic functional categories of CHOP/CVAD exhibited significantly less pairwise *in vitro* synergy than the dataset as a whole (p=0.018) (Figure 4A). Thus CHOP/CVAD's extensive clinical efficacy cannot be attributed to component drug synergy.

Since drug half-lives and dosing protocols for these combination therapies can result in the concurrent presence of all four drugs in patients, we examined a three drug CVA/CHO/CAV and a four drug CVAD/CHOP signature. Interestingly, a PCA plot with two principal components separates the four individual drugs into distinct quadrants (Figure 4B), and the sequential plotting of signatures resulting from the increasing combination complexity draws the combination projections toward the loci of the respective drug substituents (through vector addition) until the four-drug combination of CVAD reached the origin – i.e., an essentially neutral signature. This four-drug combination fit an averaging model, as well as the two drug and three drug components of CVAD tested (Figure 4C). Taken together, these data suggest that clinically utilized 3 and 4 drug combinations can homogenize single-agent genetic dependencies.

Given the extraordinary number of genetic and epigenetic changes typically present in human tumors, we next sought to further validate the broader relevance of this averaging effect. We performed a pooled, partial genome scale screen of a randomly selected set of 10,000 shRNAs, in which the 8-shRNA signature was added at a 1:10,000 ratio as an internal control. Single agent C, V, A, D were compared to combination CVAD for each shRNA in the pooled set. Of the initial pool, 6819 shRNAs (including 7 out of 8 of the 8 shRNA signature) were present at high enough abundance (>700 sequencing reads per shRNA) to be included in further analysis. To examine the robustness of this data set, we first confirmed that the 3 biological replicates of drug treatments clustered together (Figure 5A). Furthermore, representation of the 7/8 shRNAs from the 8 shRNA signature that were above the read number cutoff strongly correlated with single hairpin measurements (Figure S3). As a more stringent data threshold, we further filtered shRNAs based on the magnitude of shRNA enrichment and the reproducibility of the sequencing data (Figure 5B). This filter reduced the set of 6819 shRNAs to 93 putative shRNA "hits" that exhibited large and reproducible phenotypes (Figure 5C). We next examined whether these 93 shRNAs exhibited a genetic averaging mechanism following treatment with combination therapy. Using a cutoff of 2 standard deviations away from the control shRNAs, we found that 78/93 shRNAs produced an average of individual drug phenotypes when treated with CVAD (Figure 5D and Figure S4). Moreover, the majority of shRNAs that deviated from this average (12/15) were "over-neutralized", meaning that the shRNAs affected the response to combination therapy even less than the averaging mechanism predicts. Therefore, 90/93 shRNA phenotypes are homogenized by the combination of CHOP/CVAD, and the examples that deviate may represent the result of multiple hypothesis testing, and not a truly unique phenotype. This suggests that the vast majority of genetic dependencies (as modeled by shRNAs) are averaged in response to combination therapy.

Modeling single versus combinatorial drug regimens.

Since our shRNA signatures revealed an averaging mechanism in response to CVAD, we sought to model genetic dependencies even more explicitly in an isogenic mouse model of human lymphoma. These isogenic, spontaneous models develop stochastic secondary legions that overcome the stress of oncogene expression. We asked whether spontaneous heterogeneity in drug effectiveness evolving in individual mice during tumorigenesis (characterizing patient-to-patient variability) is diminished by combination therapy (Figure 6A). When independent *Eμ-Myc* primary tumor lines were examined for single versus combination drug effects *in vitro*, different primary lymphomas displayed distinct patterns of sensitivity or resistance to CVAD component drugs (Figures 6B and C). We again employed PCA analysis, now considering the tumor lines as variables. Examining each cell line's contribution to principal components 1 and 2, we found that individual cell line behaviors were more diverse following treatment with single agents, as evidenced by the higher variance and the requirement of multiple principal components to explain this variance. This complexity was diminished in the combination case, where principal component 1 could explain more than 93% of the cumulative variance. Thus, tumor-specific variation in the response to single agent treatment is homogenized in the presence of combination therapy. This decrease in the complexity of cell line dose response behaviors is further evidence in favor of an averaging model. In this case, cell lines harbor distinctions in their relative sensitivity to different CHOP components. They are not simply "resistant" cells and "sensitive" cells. This may suggest that subsets of patients could preferentially benefit from subsets of therapeutic agents. One of the most striking examples of this phenomena is primary cell line B. Cell line B exhibits a profound sensitivity to Dex in comparison to all other cell lines tested (Figure 6C) and is potently more resistant to the DNA damaging agents CBL and Dox. Because there is a potential utility in identifying this subset of tumors genetically, we characterized p53 and NR3C1 (the glucocorticoid receptor) in all of our

primary cell lines (Table S2). The two most resistant cell lines to both CBL and Dox (primary lines A and B) harbored p53 hotspot mutations. mRNA measurements of NR3C1 expression indicated that primary cell line B's dramatic sensitivity to Dex correlated with approximately 2.5-3 fold more glucocorticoid receptor mRNA expression than the other primary lines. Thus, p53 loss of function and NR3C1 overexpression may identify tumors that are hypersensitive to Dex and insensitive to DNA damaging agents. This lends support to the idea that averaging combinations mask genetic heterogeneity that might be better suited to treatment with altered subsets of established combinations.

Effects of combinatorial regimens on clinical genomic signatures.

A common approach towards personalized cancer therapy is to search for molecular differences between pathologically indistinguishable tumors that can serve as specific biomarkers of drug regimen efficacy. Since averaging diminishes resistance and sensitivity signatures, we wondered if the averaging phenotype between drugs in clinically utilized combination regimens might diminish the sensitivity of genetic biomarkers as clinical regimens gain greater drug diversity. To address this question, we made use of a publically available dataset that performed genome wide microarray analysis on large clinical cohorts of CHOP and R-CHOP treated diffuse large B-cell lymphomas (DLBCLs) (24). Specifically, we focused on a signature that was very clearly linked to tumor identity, the Germinal Center B-cell (GCB) signature. To see if there was a measurement resolution gap between CHOP and R-CHOP, we examined the magnitude of the expression values of the 36 mRNAs in the GCB signature in the "good" versus "poor" prognosis groups for the CHOP versus R-CHOP cohorts (Figure 6D). We observed that GCB mRNAs appeared to exhibit larger measurement differences between good and poor prognosis in the CHOP versus the R-CHOP cohort. To examine this observation quantitatively,

we examined the distribution of measurement quality (mRNA measured difference between the groups/mRNA standard error of the mean) of the GCB signature in the different cohorts (Figure 6E). When comparing the GCB signature relative to a background distribution, we found that CHOP samples had significantly greater measurement resolution between good and poor prognosis patients than the R-CHOP cohort. Thus, the addition of new agents to established drug regimens may further hinder the identification of biomarkers that stratify patient response.

Discussion

Predicting mechanisms of combination drug action

In deriving a strategy for defining combination drug mechanisms of action we have combined RNAi based interrogation of biological pathways, and multiple informatics techniques that together demonstrate a simple strategy to compare a signature of a combination of drug's relative to all other single drug signatures. We use this strategy to answer long-standing hypotheses about combination drug action, and we find that these comparisons yield strikingly simple mechanisms of action. Most notably, we show that combination mechanisms of action are weighted composites of single drug classes. In some combinations, the mechanistic contribution of a single drug component is negligible. For example, the extremely potent synergies identified in this study act like single component drugs. Conversely, drug combinations that comprise commonly used cytotoxic regimens show an average of single drug signatures. Thus, our data reveal a surprising simplicity in "combination drug mechanisms of action": either drug A potentiates the mechanism of drug B, or drug A plus B produce additive, yet distinguishable, effects. Additionally, these mechanisms hold true upon the introduction of additional compounds into complex drug regimens. These data have strong implications for the application of combination therapy. Specifically, we suggest that drugs interact via a defined set of relationships, such that a combination mechanism represents a solvable product of

component drug mechanisms. This is, perhaps, surprising given widely held ideas regarding drug synergy and combination therapy. For example, one might think that clinically co-administered agents are combined because they promote a neomorphic effect – one not seen in the presence of either agent alone. Alternatively, combination therapies may elicit synthetic signatures, in which the inhibition of parallel distinct pathways combine to kill target cells. Our data suggest that neither of these mechanisms is operative in the context of existing combination therapy, and that unexpected chemical or biochemical interactions play a minimal role in the cytotoxic effects of multi-drug regimens.

Current application of combination drug regimens

Numerous recent and ongoing large-scale efforts have sought to systematically delineate synergistic combinations of drugs for cancer therapy (25). Yet, despite the ability to identify synergy in cell-based studies, synergistic combinations have proven difficult to adapt for clinical use. Synergistic combinations might fail for multiple reasons. They may be synergistic in both tumor and normal cells, leading to toxicity and the absence of a therapeutic window. However, they may also be highly specific to the set of alterations present in a tumor cell (26). Our functional signatures support the latter conclusion. The synergistic combinations tested appear to polarize drug response, resulting in shRNA dependencies that favor the mechanism of action of a single drug. In contrast to an averaging result, we suggest that combinations that potentiate a single mechanism of action will often have fewer genetic dependencies, but those dependencies will be as potent as the single drug case. Therefore, in populations treated with a drug combination that potentiates a single drug's mechanism of action, functional biomarkers of the potentiated single drug mechanism will help large randomized clinical trials succeed in the face of the heterogeneity in patient populations.

Effective combination therapies have been argued to act via; the minimization of acquired resistance, the existence of cell intrinsic drug synergy, or the maximization of the cumulative drug dose. While increases in the tolerated cumulative drug dose have been demonstrated to be critical to combination success in a variety of cancers (27-29), it is impossible to distinguish dose effects from other proposed mechanisms of action in clinical settings.

The rationale that combination therapies minimize the acquisition of resistance in heterogeneous populations of cells has its roots in the Luria-Delbruck fluctuation experiments of the 1940's(1, 30) (2). If two drugs work independently through distinct mechanisms of action, then resistance requires the acquisition of mutations in distinct drug targets. Consistent with this idea, in tuberculosis and HIV, sequencing studies in drug resistant clinical isolates have shown that pathogens treated with clinical combination regimens tend to follow this path to drug resistance (Blanchard et. al. 1996,Broussier et. al. 2010). However, genomic and sequencing studies in pre-treatment and relapsed leukemias treated with conventional chemotherapeutic regimens suggest a distinct picture. Relapsed leukemias rarely harbor alterations in genes that are direct biochemical targets of drug action, and selection seems to favor multi-drug resistant cell states (31-33). In the context of our study, when the suppression of wildtype gene function by RNAi in single versus combination dosing leads to distinct therapeutic phenotypes, these distinctions are averaged. This averaging occurs for shRNAs that confer either resistance or sensitivity. Our data suggests that downstream mechanisms of cell death are often shared between "independent compounds" and combinations that average genetic dependencies minimize the relative resistance between two drugs, but they also minimize the relative sensitivities.

This basic averaging mechanism for combination regimens may represent an unintended consequence of clinical trial design. Genetically unstratified cohorts that are randomly assigned to experimental or control groups are often used to iteratively define combinations that perform better than the previous generation of treatment. While these regimens manifest some of the greatest success stories in decades of cancer research, the lack of relevant molecular information during their inception has served to shape regimens that are broadly useful across diverse patients rather than tailored to "driving" cancer lesions. We suggest that some subsets of patients may only respond to subsets of drug regimens. An implication of this is that averaging combinations may have a fundamental incompatibility with personalized medicine. This hypothesis is further supported by our analysis of microarray data from large clinical cohorts.

Importantly, we do not intend to devalue the clinical benefit of well-established combination therapies. In fact, our data highlights the strengths of diversity optimized combinatorial regimens in the absence of clinical biomarkers. However, we suggest that attempts to genetically stratify patients that are treated with combinations of drugs that exhibit an averaging mechanism will be fraught with diminishing returns as regimens gain greater mechanistic diversity.

Towards mechanism-based combination drug regimens

The principles governing combination action create entirely new opportunities in the design of combinatorial therapy. First, given the lack of neomorphic signatures or mechanisms emerging from drug combinations, small molecule combinations produce predictable outcomes. These outcomes represent a set of defined genetic stratifiers that can serve as biomarkers that inform

clinical application. This is particularly true of synergistic combinations, where our data suggests that the genetic determinants of single component efficacy determine the outcome following combination therapy. Second, drug combinations can be tailored to produce customized mechanistic outcomes that specify precise determinants of resistance. For example, agents could be combined such that the status of a single gene is of paramount importance to overall response. This approach would allow one to direct therapy towards a specific biomarker. In fact, given the predictable nature of signature interaction, numerous signatures could be mathematically combined using weighted averages to solve for a desired solution.

Finally, this approach to signature-based analysis may inform the treatment of cancers bearing intra-tumoral heterogeneity. A mixed population of tumor cells bearing distinct genetic alterations can be thought of as mixture of cells expressing distinct shRNAs. The ability to determine the precise impact of a given alteration/shRNA on the response to a combination therapy allows for the explicit calculation of the trajectory of a population of cancer cells in response to a combination therapy. Given equally potent drugs and a heterogeneous population of cancer cells with known single drug responses, we expect that it will be possible to compute solutions that can minimize drug resistance over all variants of that population, or that purposely select for a particular mode of resistance to combination therapy.

Acknowledgements

The authors would like to thank AJ Bhutkar for bioinformatics support, Corbin Meacham for reagents and advice, and Christian Braun, Joel Wagner, Michael Lee, Hai Jiang and Yadira Soto-Feliciano for their comments on this manuscript. J.R.P. was supported by a Poitras

Foundation Fellowship for Biomedical Engineering. M.T.H.is the Chang and Eisen Associate Professor of Biology, D.A.L. is the Ford Professor of Biological Engineering, L.A.G. is the recipient of a Ludwig graduate fellowship and K.A.C. was an ICBP summer research fellow. Funding was provided by ICBP #U54-CA112967-06(M.T.H. and D.A.L.) and NIH RO1-CA128803-04 (M.T.H.).

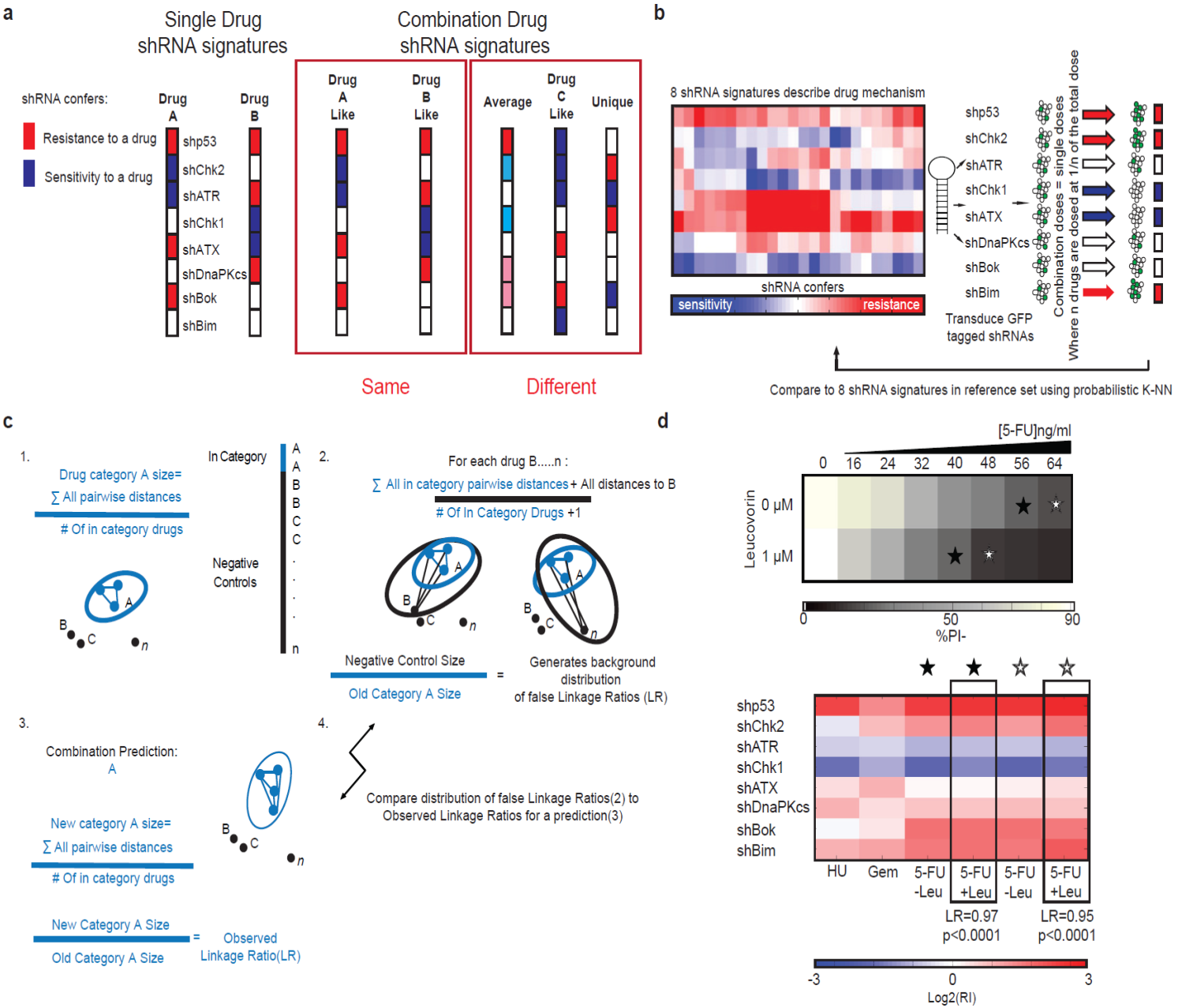
a
Single Drug shRNA signatures
Combination Drug shRNA signatures
shRNA confers:
Drug A
Drug B
Resistance to a drug
Sensitivity to a drug
shp53
shChk2
shATR
shChk1
shATX
shDnaPKcs
shBok
shBim
Drug A Like
Drug B Like
Average
Drug C Like
Unique
Same
Different
b
8 shRNA signatures describe drug mechanism
shRNA confers
sensitivity
resistance
Transduce GFP tagged shRNAs
Combination doses = single doses
Where n drugs are dosed at 1/n of the total dose
Compare to 8 shRNA signatures in reference set using probabilistic K-NN
c
1.
Drug category A size=
∑ All pairwise distances
Of in category drugs
In Category
Negative Controls
2.
For each drug B.....n :
∑ All in category pairwise distances + All distances to B
Of In Category Drugs +1
Negative Control Size
Old Category A Size
=
Generates background distribution of false Linkage Ratios (LR)
3.
Combination Prediction:
A
New category A size=
∑ All pairwise distances
Of in category drugs
New Category A Size
Old Category A Size
=
Observed Linkage Ratio(LR)
4.
Compare distribution of false Linkage Ratios(2) to Observed Linkage Ratios for a prediction(3)
d
[5-FU]ng/ml
0 16 24 32 40 48 56 64
Leucovorin
0 µM
1 µM
0 50 90
%PI-
shp53
shChk2
shATR
shChk1
shATX
shDnaPKcs
shBok
shBim
HU
Gem
5-FU -Leu
5-FU +Leu
5-FU -Leu
5-FU +Leu
LR=0.97 p<0.0001
LR=0.95 p<0.0001
-3 0 3
Log2(RI)

Figure 1. A strategy to define combination mechanisms of drug action. (A) An illustration of the competing hypotheses for single versus combination mechanisms. Squares denote a diagrammatic version of an shRNA signature with resistance shown in red and sensitivity in blue. A schematic of the potential results following the combinations of Drugs A and B is shown to the right. "same mechanism" refers to the idea that a combination signature could look similar to the individual drug signatures that are used to create the combination. The "different mechanism box" provides qualitative examples of how combination signatures might differ from component signatures. (B) An outline of the signature-based methodology. shRNAs targeting the 8 genes in our signature are retrovirally transduced in a mixed pool. These pools are subsequently treated with combinations of drugs and compared to a high-resolution single drug signature dataset. Combination killing is controlled at an LD80-90 to be comparable to single drug LD80-90 killing. Given a combination of n drugs, combinations are dosed such that 1/n of the LD80-90 comes from each of the n individual components. (C) A description of the process of comparing drug signatures to the drug categories in our reference set. (1) The initial drug category size in the reference set is defined. (2) Out of category drugs in the reference set are used as negative controls. These drugs are forced to belong to the wrong category. Iteration through all of the negative control categories for a given mechanism of action produces a background distribution of how unrelated control drugs affect a given drug mechanism's category size. (3) Given a category prediction for a drug signature by the nearest neighbors algorithm, the category size for the predicted drug mechanism that now includes the new category member is calculated. (4) This new category size is compared to the background distribution of negative controls from (2). (D) Top: A heat map of the dose response of *Eμ-Myc;p19*$^{arf-/-}$ to 5-FU with or without leucovorin. Bottom: an 8-shRNA signature for 5-FU and 5-FU plus leucovorin measured concurrently at the indicated (starred) doses of cell killing. Linkage ratios and p-values are indicated below. 8-shRNA signatures for gemcitabine (Gem)

and hydroxyurea (HU) are shown to aid interpretation. Leucovorin is not cytotoxic at micromolar concentrations.

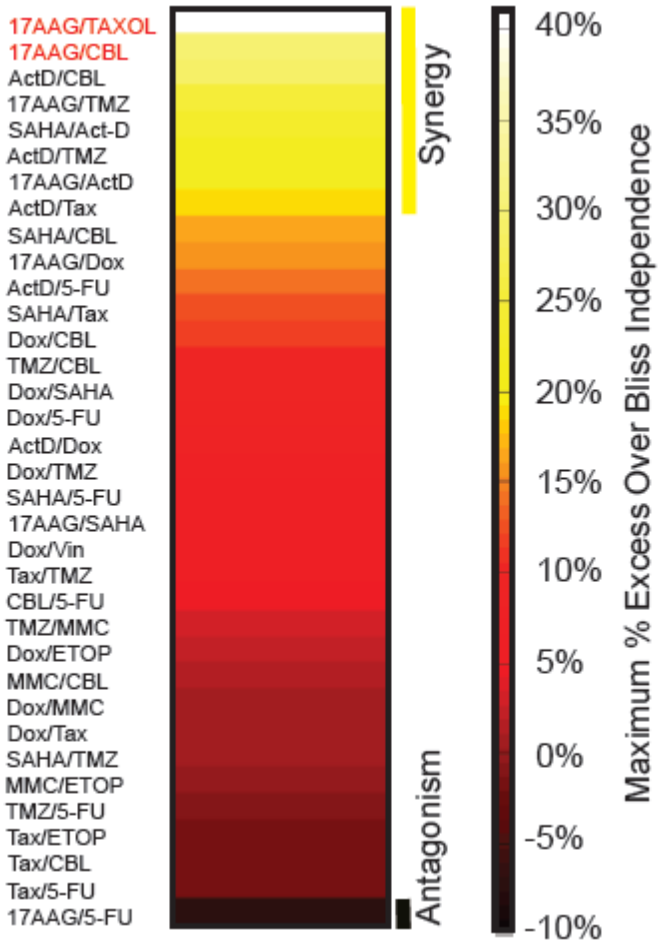

Figure 2. A pairwise drug interaction screen identifies highly synergistic combinations whose mechanism resembles single drug action. (A) The response to pairwise small molecule treatment using the indicated drugs is quantified by maximum % excess propidium iodide negative cells over a control additive model and rank ordered. Synergy and antagonism are indicated.

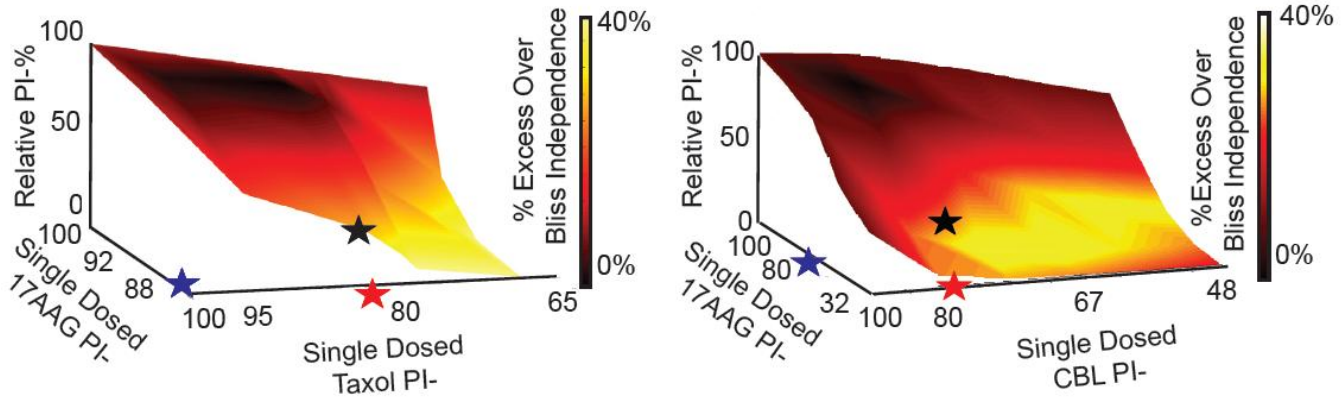

Figure 2. (B) Response surface diagrams of 17AAG in combination with Taxol and CBL. Surface color corresponds to the level of synergy. Colored stars indicate equivalent single drug LD dosings that combine to produce LD80-90 of the combination doses (demarcated by black stars).

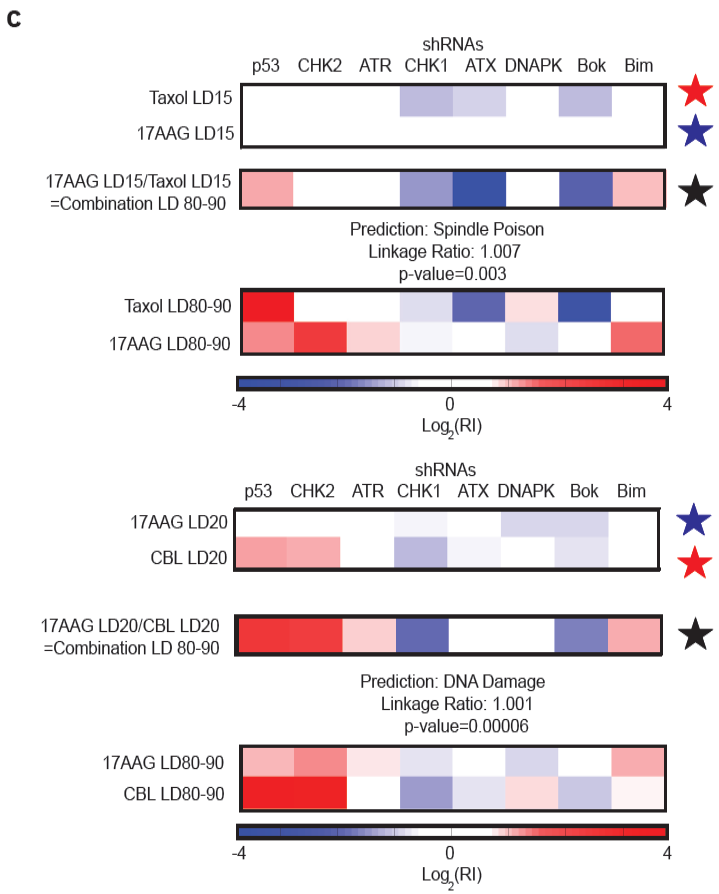
c
shRNAs
p53 CHK2 ATR CHK1 ATX DNAPK Bok Bim
Taxol LD15
17AAG LD15
17AAG LD15/Taxol LD15
=Combination LD 80-90
Prediction: Spindle Poison
Linkage Ratio: 1.007
p-value=0.003
Taxol LD80-90
17AAG LD80-90
-4
0
4
Log2(RI)
shRNAs
p53 CHK2 ATR CHK1 ATX DNAPK Bok Bim
17AAG LD20
CBL LD20
17AAG LD20/CBL LD20
=Combination LD 80-90
Prediction: DNA Damage
Linkage Ratio: 1.001
p-value=0.00006
17AAG LD80-90
CBL LD80-90
-4
0
4
Log2(RI)

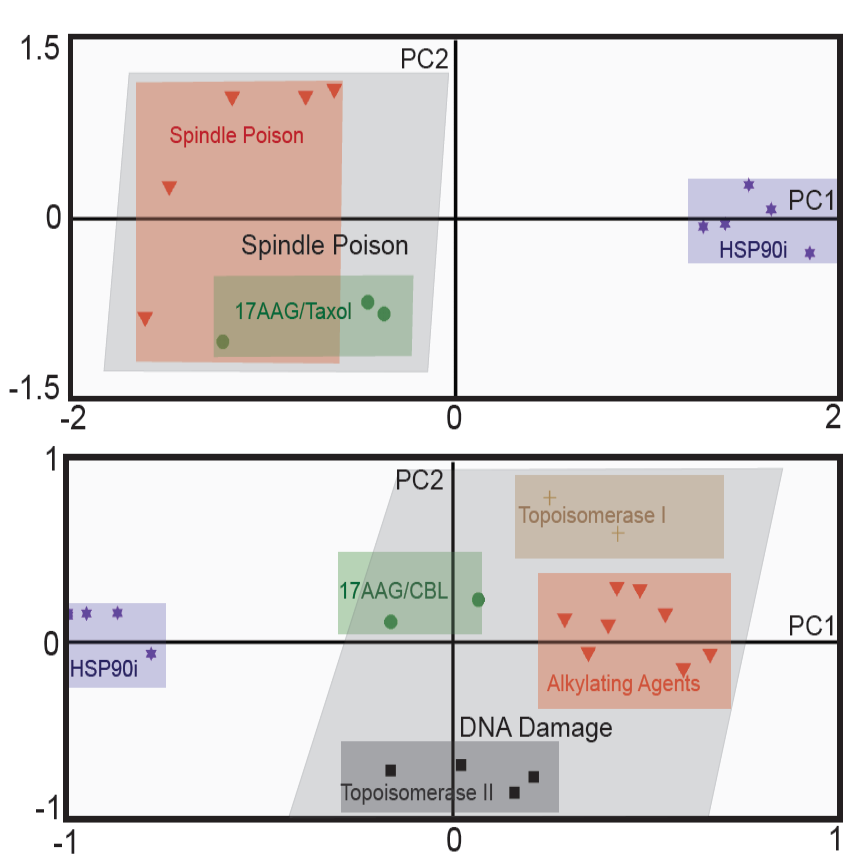
d
1.5
0
-1.5
-2
0
2
PC2
PC1
Spindle Poison
Spindle Poison
17AAG/Taxol
HSP90i
1
0
-1
-1
0
1
PC2
PC1
Topoisomerase I
17AAG/CBL
HSP90i
Alkylating Agents
DNA Damage
Topoisomerase II

Figure 2. (C) Signatures of 17AAG, Taxol, and CBL action at low single drug doses that combine to produce synergistic LD80-90 signatures, compared with single drug LD 80-90s. (D) PCA "scores" plots of single and combination drug action allow for the visualization of the 8-shRNA signature predictions.

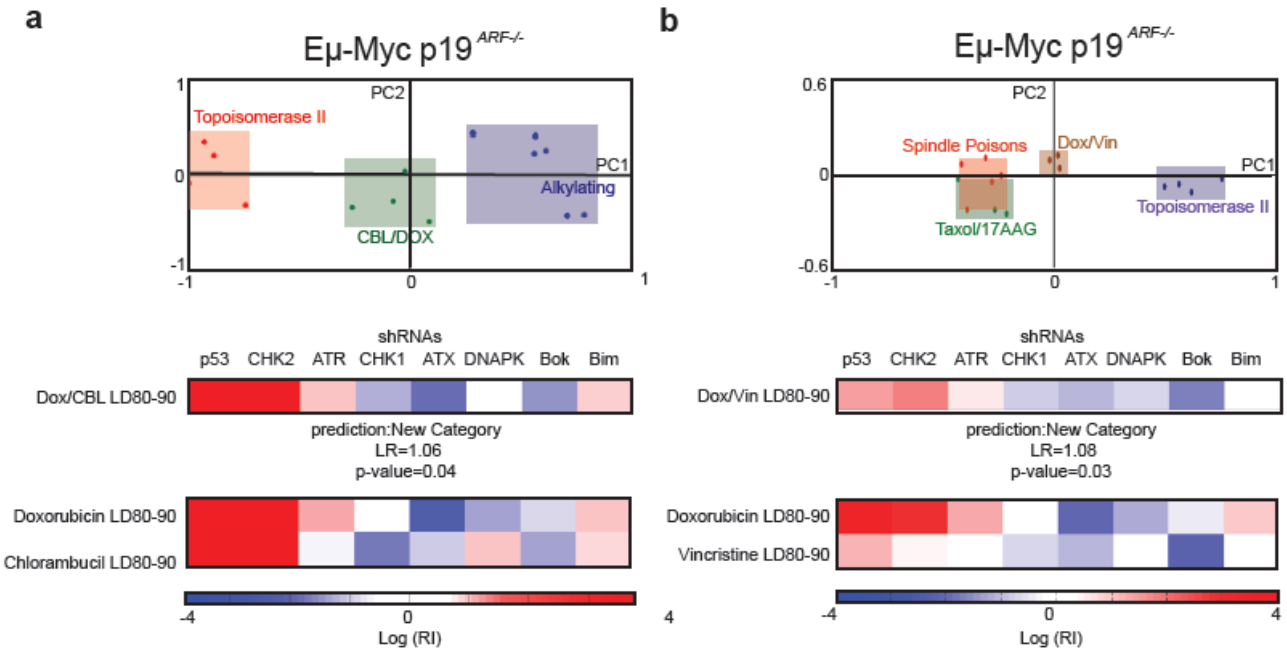

Figure 3. Additive combinations average extant genetic dependencies in diverse contexts. (A) Top: A PCA scores plot of Doxorubicin (Dox) and Clorambucil (CBL) in reference to an example from their respective categories. Bottom: Heat maps depict resistance and sensitivity to the indicated single or combination drug dosings. (B) Top: A PCA scores plot of Doxorubicin (Dox) and Vincristine (Vin) compared with examples from their respective categories. Bottom: Heat maps depict resistance and sensitivity to the indicated single or combination drug dosings.

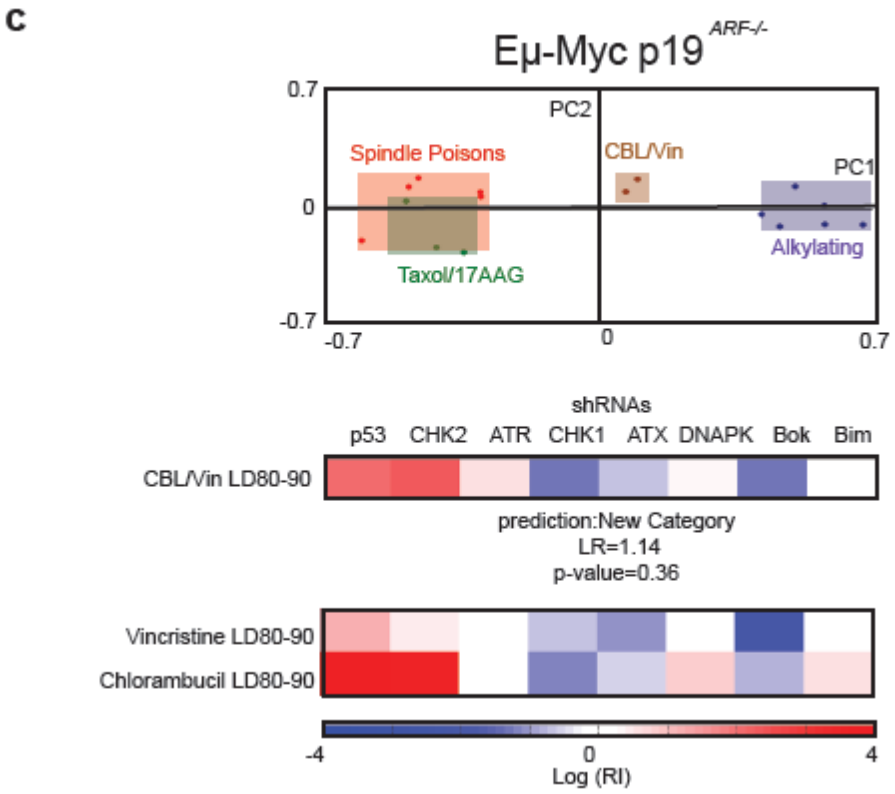

Figure 3. (C) Top: A PCA scores plot of Doxorubicin (Dox) and Chlorambucil (CBL) compared with an example from their respective categories. Bottom: Heat maps depict resistance and sensitivity to the indicated single or combination drug dosings.

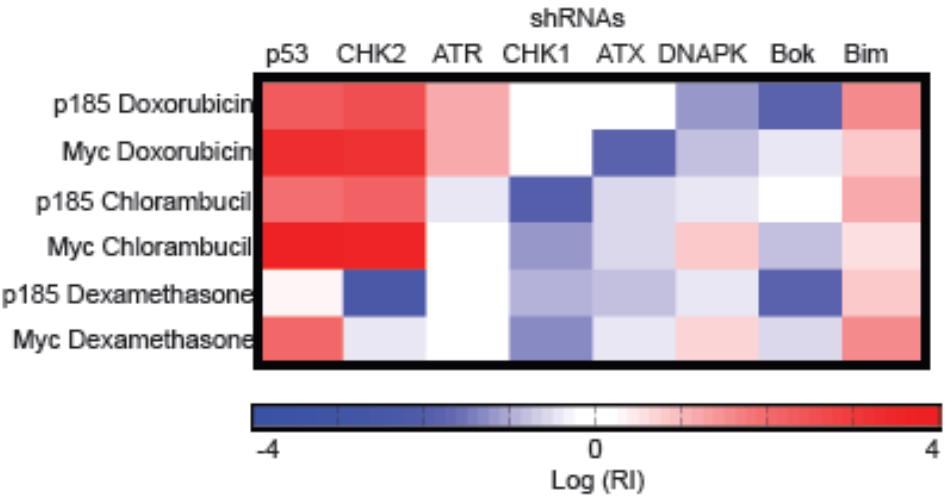

Figure 3. (D) A heat map comparing the cell line specific differences in 8-shRNA signatures.

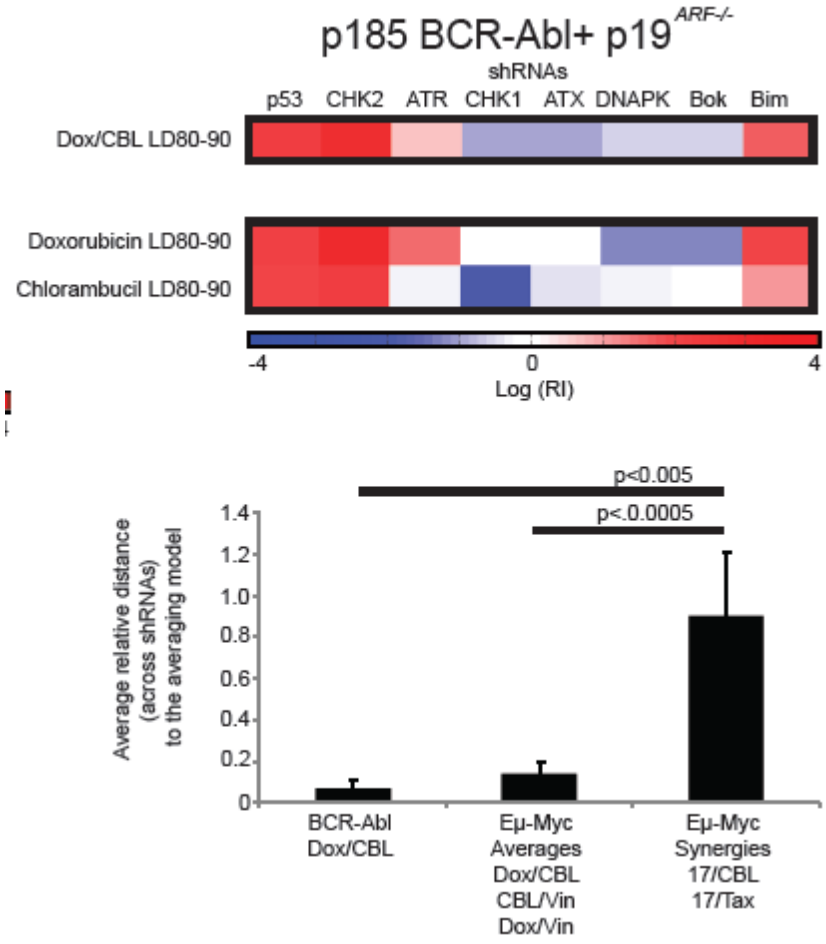

Figure 3. (E) Top: A Heat map of the responses of p185+ BCR-Abl cells harboring the 8-shRNA signature and treated with Dox and CBL and Dox/CBL. Bottom: A comparison of the fit of the BCR-Abl Dox/CBL combination and the three additive combinations to the synergistic combination of 17AAG/Taxol and 17AAG/CBL. A wilcoxon rank-sum test was used to obtain the p-values. Error bars show the SEM.

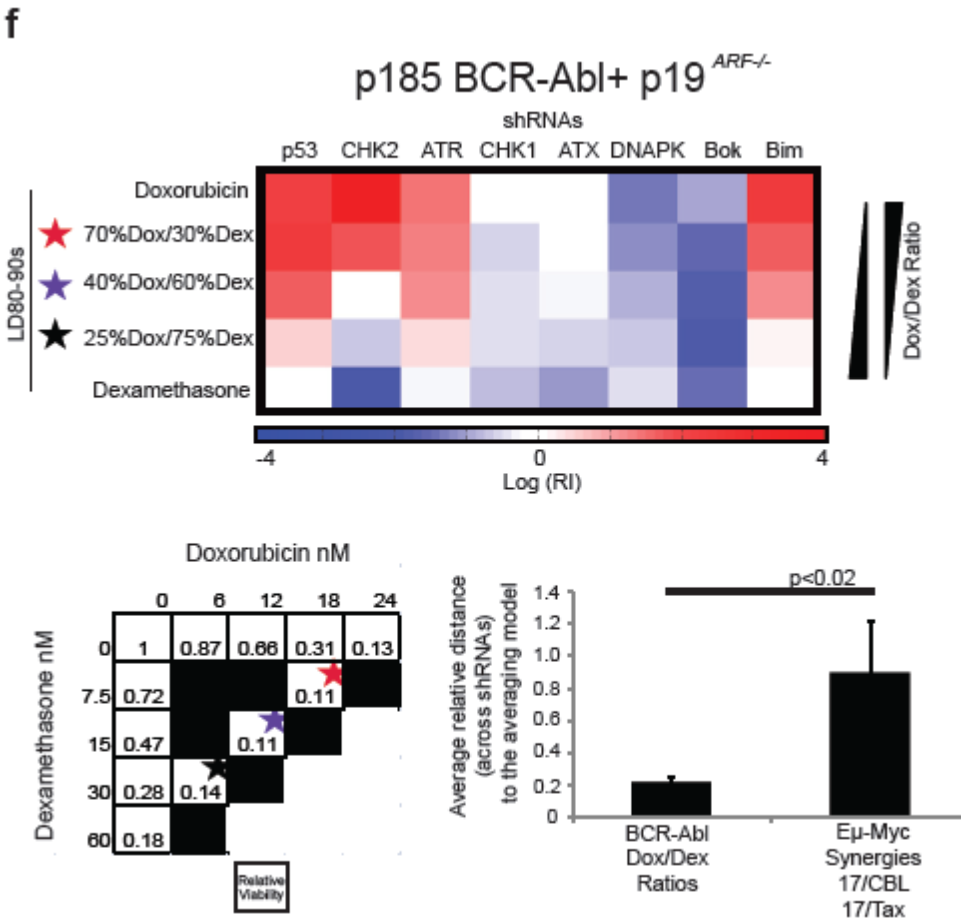

Figure 3. (F) Doxorubicin and dexamethasone combinations in BCR/Abl+ ALL cells. Top: A heat map showing the 8-shRNA signatures for the combinations versus single drugs from a dose response matrix of dexamethasone and doxorubicin. Stars indicate doses in the dose response matrix. Bottom: Dose response data and schematic for the heat map. Numbers indicate the relative viability of the BCR-Abl ALL cells at 48 hrs. Bottom right: A comparison of the Dox/Dex model fit for combination dosing in BCR-Abl cells relative to synergistic combinations. A wilcoxon rank-sum test was used to obtain the p-values. Error bars are the SEM.

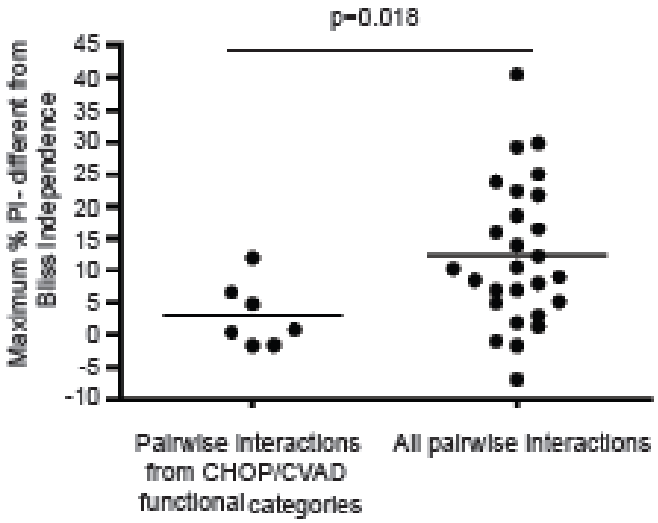

Figure 4. CHOP/CVAD components work via an averaging mechanism. (A) A scatter plot compares bliss independence values for the pairwise combinations of cytotoxic CVAD/CHOP components to the rest of the dataset. Significance was determined using a Mann-Whitney Utest.

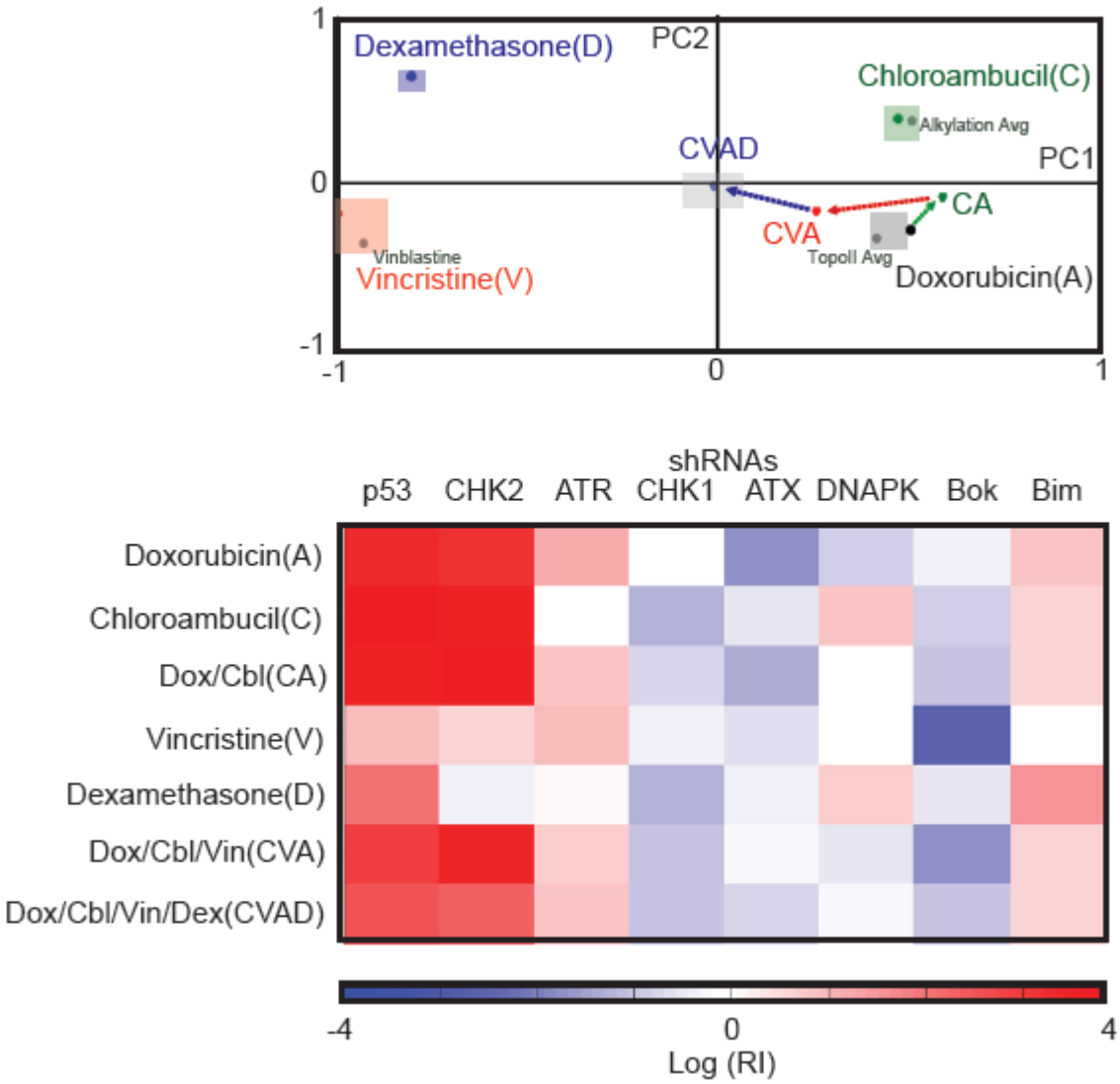

Figure 4. (B) Top: A PCA scores plot for a PCA performed on all four-component drugs and the combinations of (CA,CVA, and CVAD). The dexamethasone signature is taken at an LD70. The average trajectories of the combinations are indicated with vectors. Bottom: A heat map of the 8-shRNA signatures contained in the PCA. Greyed dots indicate the average of the other members of the drug category if they are available.

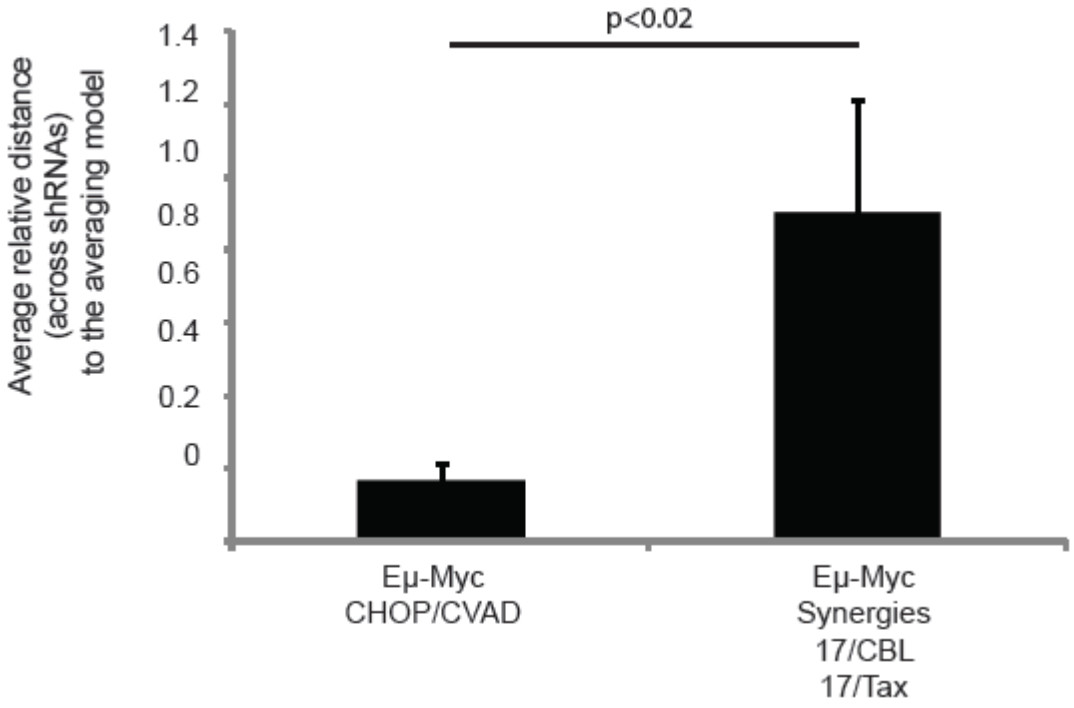

Figure 4. (C) A comparison of model fit for CVAD/CHOP versus synergistic combinations. A wilcoxon rank-sum test was used to obtain the p values. Error bars show the SEM.

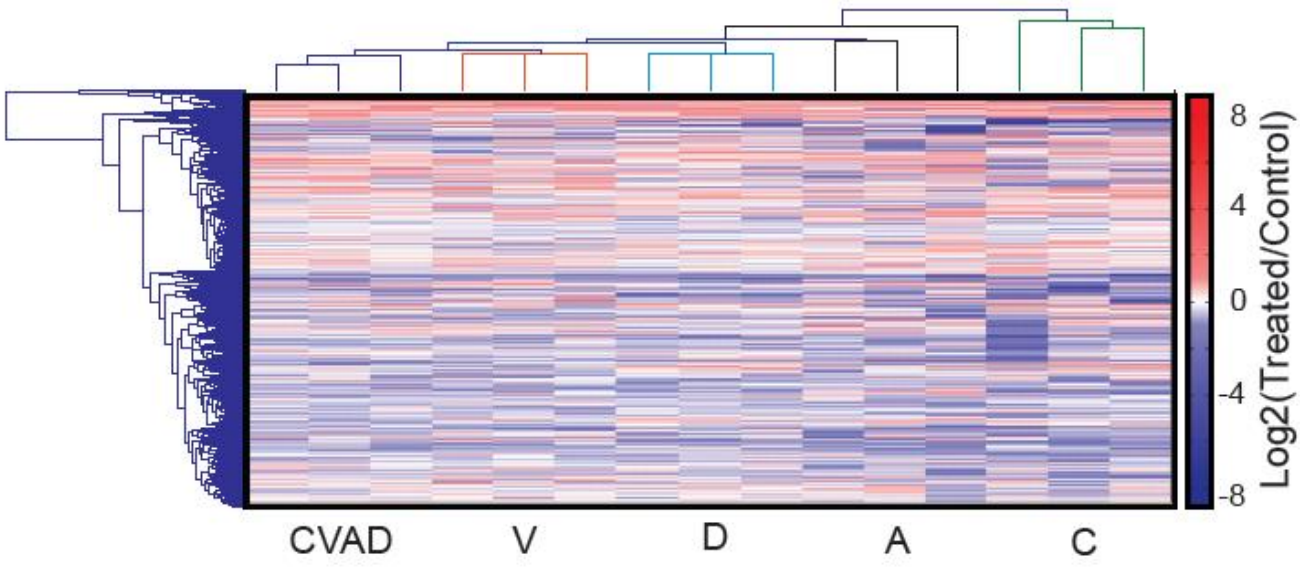

Figure 5. An unbiased screen suggests that CHOP/CVAD averages the phenotypes conferred by a diverse set of shRNAs. (A) A clustergram of 6819 shRNAs that were well represented (>700reads/sequencing lane) for biological replicates of cells treated with the indicated drugs.

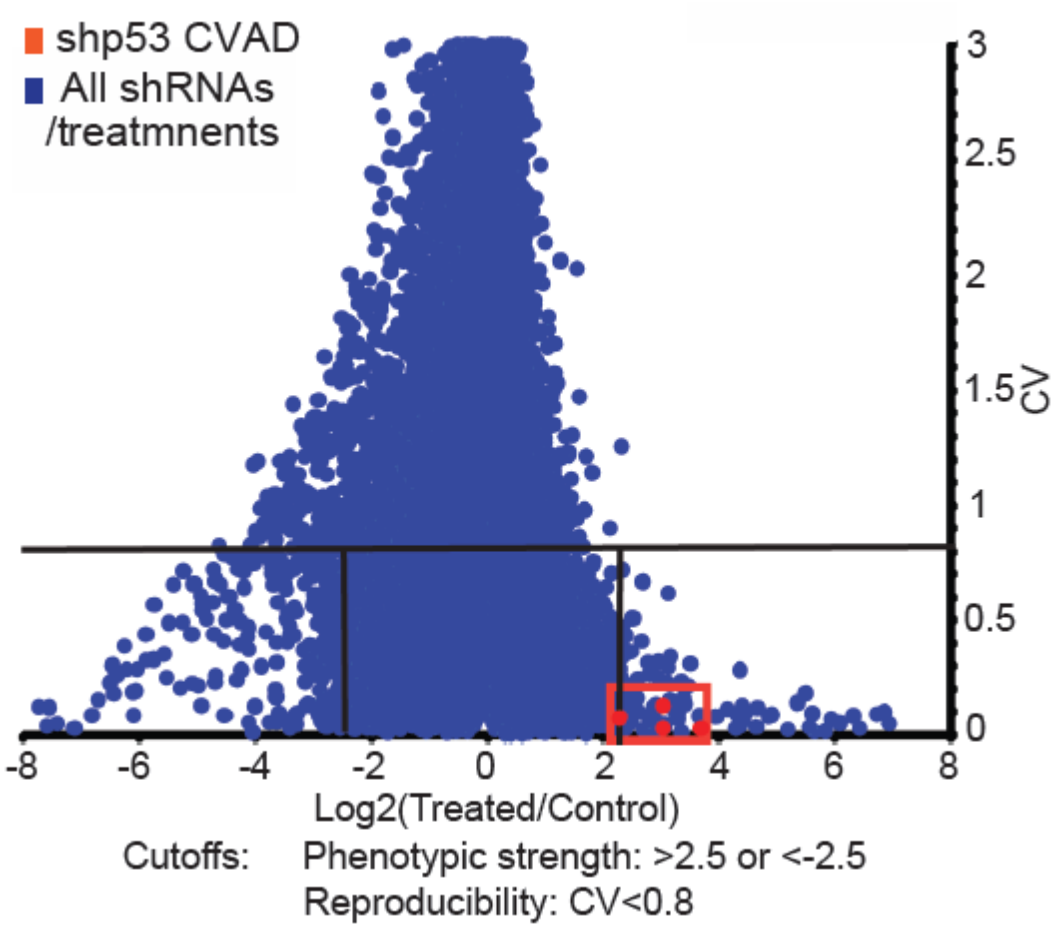

Figure 5. (B) A scatter plot of the data contained in a showing the average log enrichment across all drug biological replicates, versus the coefficient of variation. Each dot corresponds to one shRNA in one drug condition. This data was filtered according to a reproducibility and strength criterion (below), yielding 93 informative shRNAs. The CVAD shp53 data is indicated as a reference for the strength criterion in the distribution.

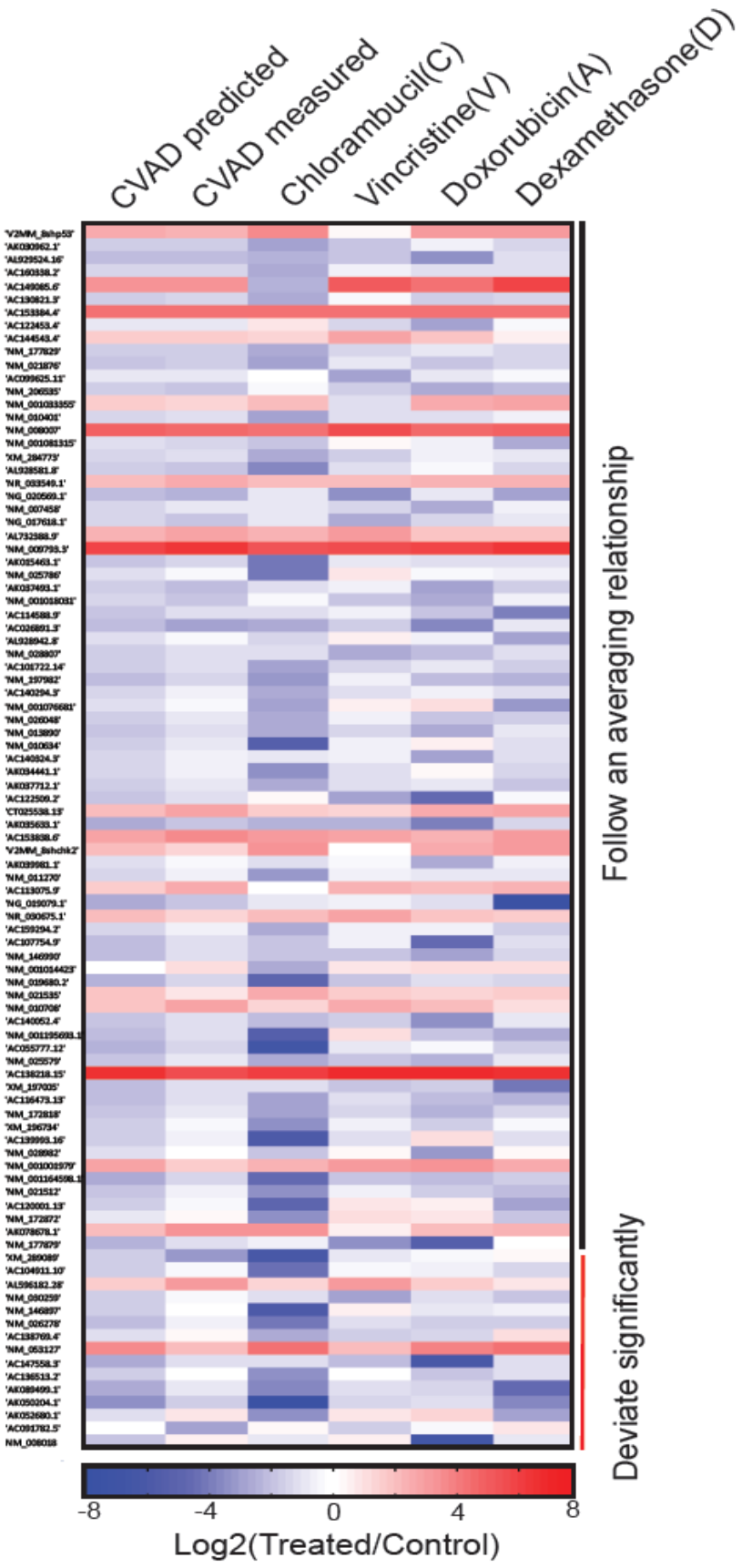
CVAD predicted
CVAD measured
Chlorambucil(C)
Vincristine(V)
Doxorubicin(A)
Dexamethasone(D)
Follow an averaging relationship
Deviate significantly
-8
-4
0
4
8
Log2(Treated/Control)

Figure 5. (C) A heat map of the indicated enrichment or depletion data for the 93 shRNAs, showing the range of phenotypes and their similarity to an averaging model.

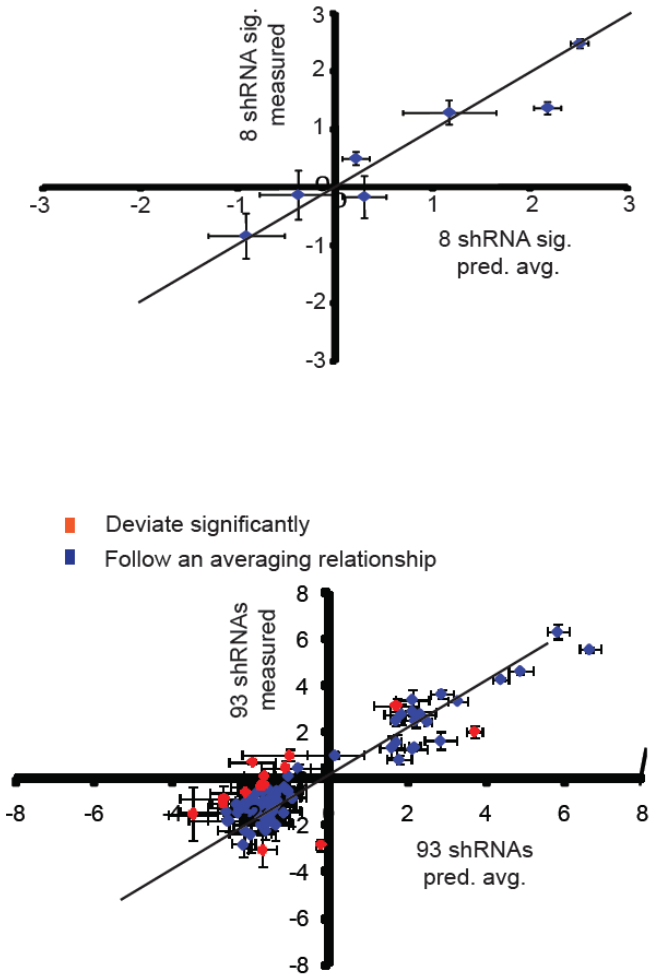

Figure 5. (D) Top: 7 of the 8 shRNAs in the 8-shRNA signature were contained among the filtered 6819 shRNAs. They are plotted as a scatter plot relative to the prediction of additivity. The line represents perfect model:data fit. Error bars depict the SEM. Bottom: The filtered 93 shRNAs are plotted as a scatter plot relative to the prediction of additivity. The line represents perfect model:data fit. The deviation from the model prediction (above) is used to produce a 0.05 significance threshold. The 15/93 that deviate are coded in red. Error bars depict the SEM.

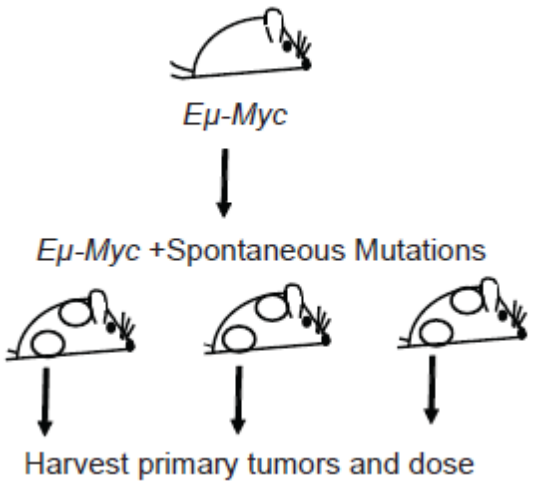

Figure 6. Spontaneous genetic variation in mouse models of lymphoma and clinical cohorts of microarray measurements from CHOP and R-CHOP treated patients is averaged. (A) A schematic showing the generation of distinct spontaneous lymphomas in mice.

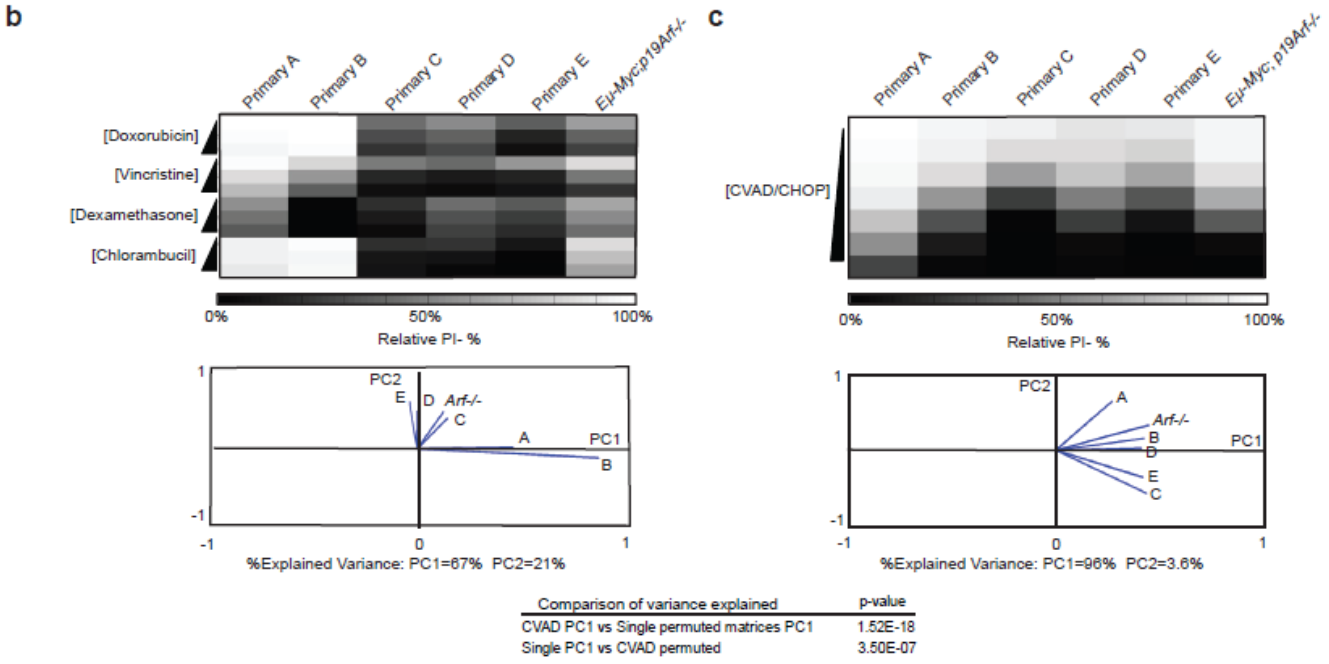

Figure 6. (B) Top: A heat map of the relative (to untreated) PI negative (%) values in distinct primary cell lines following treatment with increasing levels of single drugs. Bottom: A PCA

loadings plot for the PCA performed on the above data. The variance explained by the first two principal components is indicated below the plot. (C) Top: A heat map of the relative (to untreated) PI negative (%) values in distinct primary cell lines that result from increasing levels of combination (CVAD) dosing. To create the combination, the average LD50-60 of each of the individual drugs across all primary cell lines was combined and then the combination was serially diluted. Bottom: a PCA loadings plot for the PCA performed on the above data. The variance explained by the first two principal components is indicated below the plot. The significance of the variance explained is compared to permuted matrices to assess statistical significance.

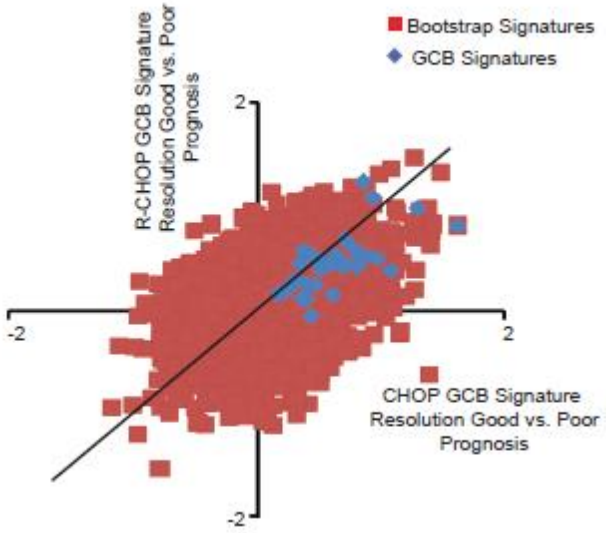

Figure 6. (D) Publically available microarray data from Lenz et al. 2008 was filtered into good and poor prognosis samples for CHOP and RCHOP treated patient samples on the basis of 2-year survival. We examined the measurement difference between CHOP and R-CHOP in their published Germinal Center B-cell signature (GCB signature) and 50,000 randomly chosen predictors. The measurement difference was calculated by subtracting the average relative mRNA expression for a signature gene in the “Poor” prognosis category from the average

mRNA expression signature in the “Good” prognosis category. This difference in the CHOP cohort is compared to the same measurement in the R-CHOP category. The line represents a perfect concordance between the measurement differences between “Good” and “Poor” prognosis groups.

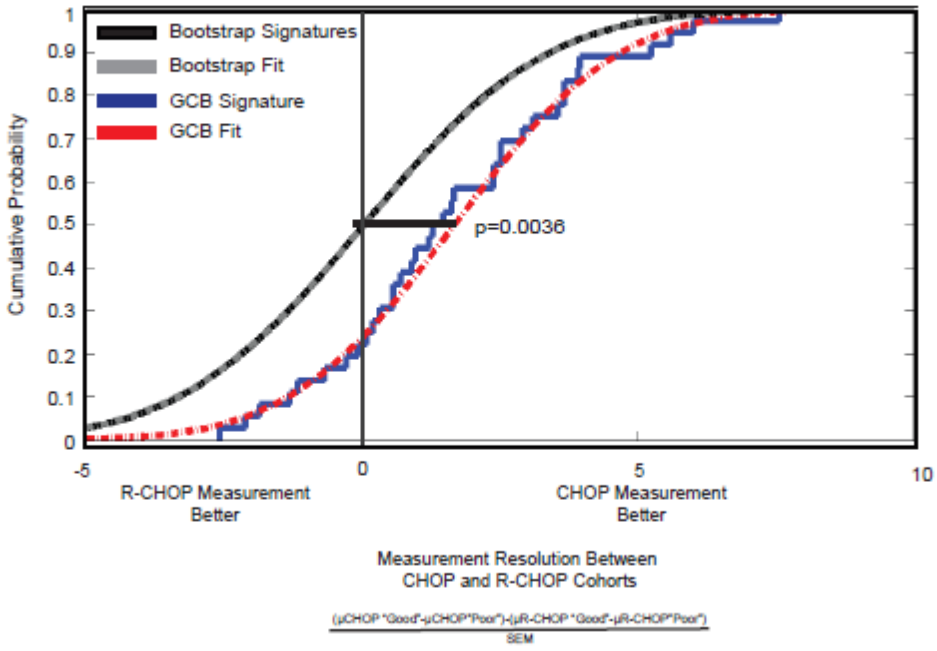

Figure 6. (E) The measurement difference between CHOP and R-CHOP divided by the SEM to account for measurement noise. Cumulative distribution functions were plotted and compared by a 2-sided KS test.

a.

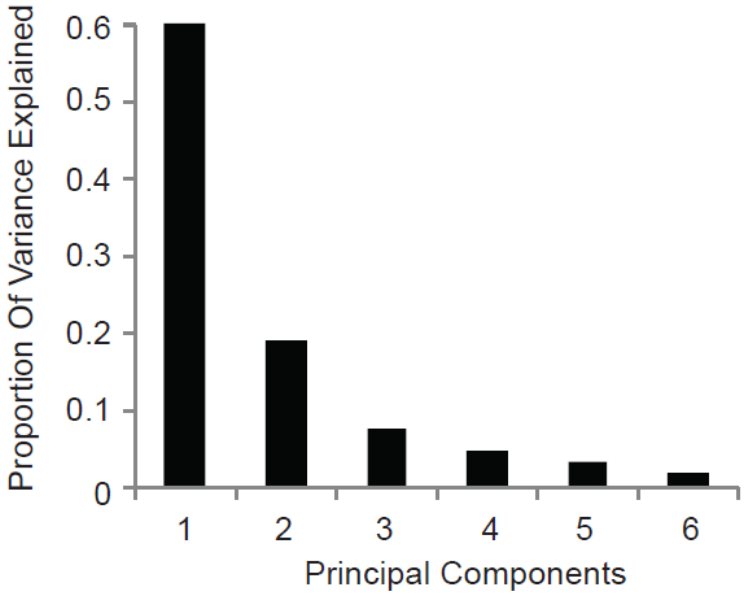

b.

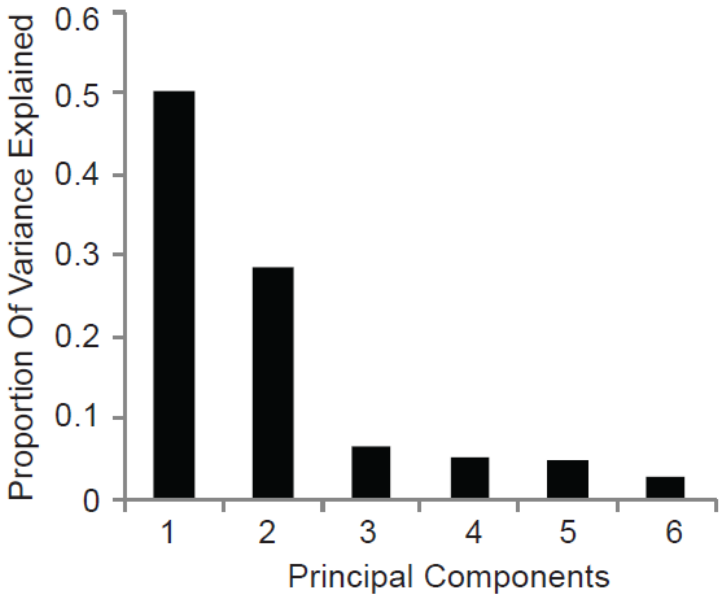

Supplementary Figure 1. PCA model fit across components. **a.** The proportion of variance explained across the first 6 principal components for 17AAG/Taxol. **b.** The proportion of variance

explained across the first 6 principal components for 17AAG/CBL.

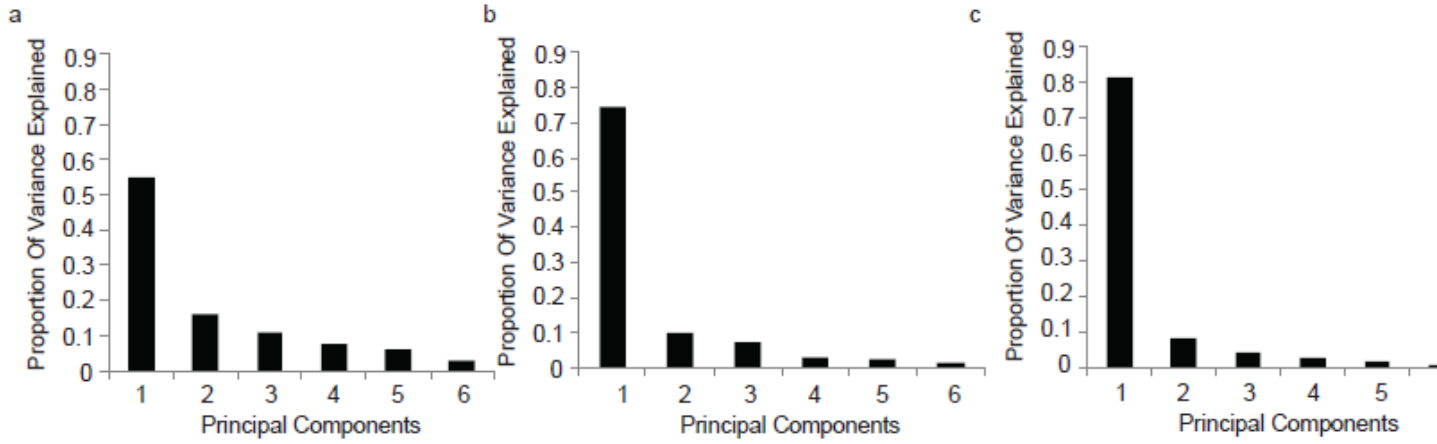

Supplementary Figure 2. PCA model fit across components. **a.** The proportion of variance explained across the first 6 principal components fo Doxorubicin and Chlorambucil. **b.** The proportion of variance explained across the first 6 principal components for Doxorubicin and Vincristine. **c.** The proportion of variance explained across the first 6 principal components for Chlorambucil and Vincristine.

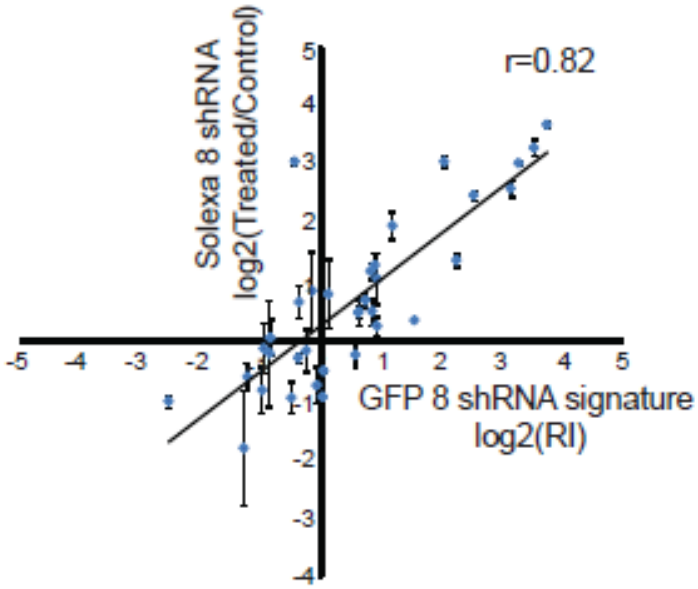

Supplementary Figure 2. Pooled Solexa sequencing measurements of 7 of the 8 shRNA (filtered>700 reads) signature hairpins are plotted relative to their 72 hour GFP enrichment

scores for C,V,A,D, and CVAD dosings. r is the pearson correlation coefficient between the two measurements.

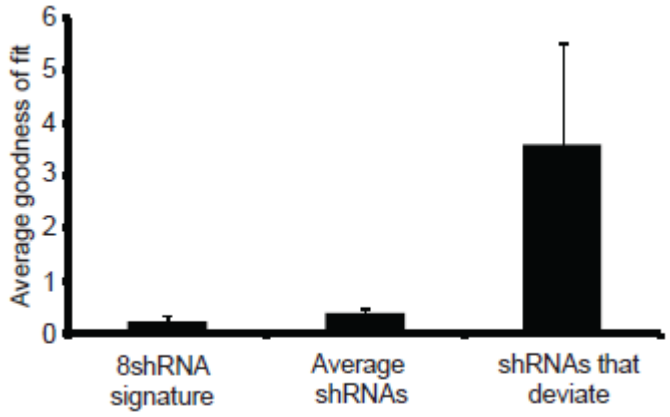

Supplementary Figure 4. The average fit to an averaging model for the solexa 8 shRNA signature data, the 78 hairpins that appear to be averages and the 15 hairpins that do not.

In vitro model combination	Relevant clinical regimens	Disease Indications
Chlorambucil/Doxorubicin	CHOP,Hyper-CVAD,CAV,AC	Non-Hodgkins lymphoma, Acute lymphoblastic leukemia, Small cell lung cancer, Breast cancer
Doxorubicin/Vincristine	CHOP,ABVD,CAV,ABVE	Non-Hodgkins lymphoma,Hodgkin's lymphoma, Small cell lung cancer, Childhood Hodgkin's lymphoma
Chlorambucil/Vincristine	CHOP,COPP,CAV	Non-Hodgkins lymphoma,Hodgkin's lymphoma, Small cell lung cancer
Doxorubicin/Dexamethasone	CHOP,ABVD,Hyper-CVAD	Non-Hodgkins lymphoma,Hodgkin's lymphoma,Acute lymphoblastic leukemia

Supplementary Table 1. A table displaying our *in vitro* models and their relevance to combination cancer chemotherapy regimens.

Characterization	A	B	C	D	E	EμMyc; $p19^{Arf-/-}$
p53 status	R210C	R270C	WT	WT	WT	WT
Relative glucocorticoid receptor expression	0.84 +/-0.49	2.83 +/-0.35	0.90 +/-0.12	1.32 +/-0.16	1.03 +/- 0.09	1

Supplementary Table 2. Characterization of spontaneous primary lines for p53 status and glucocorticoid receptor expression relative to the EμMyc; p19 *Arf-/-* control cells +/- the SEM n=3.

Materials and Methods

Cell Culture

Eμ-Myc$^{p19arf-/-}$ lymphoma cells and primary isolates from spontaneous *Eμ-Myc* primary tumor cells were cultured using established protocols (34). Cell death was measured using propidium iodide (PI).

shRNAs

All shRNAs were expressed in the MLS or MLP retroviral vector (35)and were previously validated for knockdown and single agent phenotypes (18). shRNA plasmids were packaged in phoenix cells, and viral supernatants were concentrated using the co-polymer precipitation method (36). $5x10^4$ initial cells were infected to between 10 and 20% of the total population. All signatures include replicates from at least two distinct infections. Combination vector control dosing was performed to rule out combination specific effects of the vector alone.

Pairwise Drug Interactions

Cytotoxic agents from distinct functional categories (18)were dosed in a pairwise fashion. Dosings were done in two dimensional dose response matrices. Dosings encompassed the single drug LD50 in all cases. At least one compound from each category was tested against all other functional categories. Cell death was normalized to 100% and the relative PI negative measurement was reported. Every point in the dosing matrix that contained a combination of drugs was used to estimate Bliss Independence at that point. A Mann-Whitney U-test was used to compare the pairwise drug interactions for combinations that came from a CHOP/CVAD functional category (Dox-CBL, Dox-Vin, CBL-Vin, Dox-Taxol, Etoposide-Taxol, Dox-Mitomycin C (MMC), Tax-MMC) with the remainder of the dataset. Drug dosing concentrations are provided in the supplemental data.

Combination dosing

Since absolute drug stock concentration can vary from stock to stock, and small changes in the exact number of live negative cells can bias genetic signature measurements, drug dosings were normalized by bioassay with PI. Bioassay LD values were monitored after every independent replicate dosing to ensure bioassay effect accuracy and reproducibility in control cells. Combination dosings for shRNA signature measurements were performed in a 4X4 dose response matrix form. The first row and the first column of every dosing assay include singly dosed controls. The matrix was assessed for the %PI negative population at 48 hours after treatment. The row/column matrix position for the combination signature measurements was determined by the bioassay PI values in control cells. All drugs, single or combination, must be dosed at levels that give equivalent bioassay effect levels i.e. kill 80-90% of cells by PI staining. Single drug doses from the first row and first column of the dosing matrix were used to identify similar levels of single drug toxicity (within 10% PI negative of each other). These equivalent single drug doses were required to define a combination dose at the row/column position in the matrix that caused 80-90% cell death with equivalent single drug contributions. If an exact value was not in the LD80-90 range, but values encompassed a range that included these values PI negative values were linearly interpolated. These dose-response trends are normalized to an interpolated LD85. Heat map inputs and drug concentrations as well as data quality metrics over time are provided as supplementary data.

CVAD/CHOP dosing

For the four drug dosing, all members of the combination were dosed such that they contributed 25% to the overall killing. Just as in single and double drug combinations, the four-drug combination was dosed at a cumulative LD80-90. Each drug contributed an approximate LD20 to the total level of killing. Because of the complexity of the four drug experiments full factorial

dose response matrices could not be done, so to control for day to day variability, the concentration of single drug added was monitored for PI staining to ensure that each of the 4 components was contributing equally. Heat map inputs and data are provided as supplementary data.

p185 BCR-Abl cells

These were cultured and maintained according to the method of Williams et al. 2006. Combination dosing protocols are performed identically. Heat map inputs are provided as supplementary data

p53 sequencing

cDNA was prepared from total RNA purified from cultured cells and Sanger sequenced using the primer 5' cacgtactctcctcccctca 3'.

NR3C1 qPCR

Total RNA was isolated and cDNA was prepared using standard methodologies. Samples were normalized between lanes for loading error-utilizing GAPDH. NR3C1 primers were 5' atgccgctatcgaaaatgtc 3' and 5' acagtgacaccagggtaggg 3'.

Primary tumor dosings

C57/BL6 *Eμ-Myc* transgenic mice were obtained from Jackson Labs (Bar Harbor, Maine) and were monitored for the spontaneous development of lymphoid tumors. Upon the onset of morbidity, mice were euthanized according to established MIT veterinary protocols. Tumors were harvested disassociated, and grown in culture. The fraction of primary tumors that were capable of growing in tissue culture was used to assess drug response. *Eμ-Myc*$^{p19arf-/-}$ mice were used as a control. For single drug treatments, cell lines were compared using a dose

response range that included the LD50 of *Eμ-Myc*$^{p19arf-/-}$ control cells. In order to create a combination that was fair to all cell lines we searched for single concentrations of single drugs that produced an average bioassay effect of an LD50-60 across all of the primary cell lines. For example a combination of drug that gives an LD 25, 50, and 75 across cell lines would be an acceptable concentration to add to a mixture for the combination dosing experiment. This mixture was then serially diluted to compare combination response across all of the primary lines. Heat map inputs are provided as supplementary data, and dose effect levels used in the combination are highlighted.

Combination probKNN analysis

The algorithm is as described in Jiang et al. 2011 and Figure 1C. Matlab code is available at the MIT ICBP center website. MAT files with training and test sets as well as group descriptions are included as supporting data and materials. Signatures values and quality control metrics are included as supplementary data.

Combination PCA analysis

Rows of the PCA input were individual drug experiments and the 8 columns correspond to the 8-shRNA signature genes. PCA was performed using the Matlab princomp.m function. Scores plots indicate the projection of drug observations onto the latent variable projections. All matrices used as the input for PCA contained only the observations that were plotted. MAT files containing eigenvalues, as well as loadings and scores are available in the supporting data.

Cell Line PCA analysis

Matrices were organized as shown in Figures 6b and c. Different drugs and drug dosings constituted experimental observations. Different cell lines were treated as variables. PCA was performed in Matlab using the Princomp.m function. As such, the loadings plots show the

contribution of each cell line “variable” to the meta-variable or principal component. The percent of the variance explained by the model is calculated by totaling the latent vector and dividing each PC’s value by the sum of the vector components. This tells how much of the total model fit is from each component. The significance of the percent of the variance explained by the principle components was determined by comparing the experimental results to 1,000 randomized matrices. These matrices were assembled by randomly drawing values for each column from the corresponding column of the experimental data, effectively reshuffling the rows of data within each column. PCA was executed on the 1000 randomized matrices and the percent of data explained by each principle component was determined. The mean and standard deviation of the percent of data explained by the 1st or the 2nd principle components for the 1,000 matrices was then used to execute z-tests.

Clinical Microarray Data Analysis

We filtered patient samples into CHOP and R-CHOP treated groups, of which, patients who were deceased upon a 2 year follow up were classified as having a “Poor” prognosis, and patients who were confirmed to be alive at a follow up appointment greater than 2 years after treatment were classified as having a “Good” prognosis. This left 140 CHOP patients and 171 R-CHOP patients from the original patient cohorts. To examine our hypothesis: that averaging in response to combination therapies might decrease the observed differences between groups with differential prognosis in clinical trials, we decided to examine the GCB signature from Lenz et al 2008. While this study also included two stromal signatures, we reasoned that cell extrinsic signatures might be the result of cell intrinsic alterations, or idiosyncratic immune responses. Therefore, we decided to examine a signature that was clearly the result of lymphoma cell intrinsic processes. For all mRNAs in the GCB signature or our bootstrapped control signatures (sampled with replacement) we examined the mean of the mRNA measurement from the reported data of Lenz et al in “Good” and “Poor” prognosis groups in the

CHOP and RCHOP cohorts. We compared these average prognosis differences between these two cohorts and divided by the standard error of the mean to correct for differences in error (which was less than 10% between cohorts, data not shown). Normal distributions were fit to the cumulative distribution function, and distributions were compared using the 2-sided KS test.

10k-pooled screen

The 8-shRNA set was added to a 10,000 shRNAmir30 retroviral library at a ratio 1:10000. Phoenix cells were used to package a mixed pool of retrovirus containing the 10k library. 3 million *Eμ-Myc*$^{p19arf-/-}$ were infected to 50% GFP+ (MOI=1) and expanded *in vitro* for 2 days. At that point cells were treated with an LD70-80 of single and combination drugs. A slightly lower drug dose was used to enhance pool representation. Cells were diluted 1:2 at 24 hours, %PI negativity was assessed at 48hours and dosings with the desired % of cell killing were resuspended in fresh media. Cells were allowed 2-3 day to recover to 80-90% viability, and frozen down for analysis. MAT files and excel files containing raw and processed data are provided as supplementary information.

Sequencing

Half hairpin barcodes were PCR amplified from genomic DNA(37). PCRs with distinct mutations in the 5' primer were used to barcode distinct drug treatments. This PCR product was then processed using the solexa genomic DNA preparation kit. Gel purified solexa input product was submitted to the Koch Institute genome analyzer. Data is included in three supplementary excel files.

Data Analysis

Raw sequence read numbers (for exact matches only) between lanes were normalized by the total reads per lane. Raw reads for all barcodes in a lane were normalized to be equal across

all barcodes. These normalized reads were then filtered for further analysis. A threshold of >700 reads per hairpin in all three lanes sequenced was used to filter out low abundance reads. This left us with 6819 shRNAs. Of these 6819 shRNAs, 7 shRNAs from our 8-shRNA signature were represented. Hierarchical clustering on this data set was done using a correlation based metric and complete linkage. Averages, standard deviations and coefficients of variation were calculated. shRNAs with an absolute value of the Log_2(treated reads/control reads) greater than 2.5 (CVAD shp53 value) for any drug/ combination treatment was used to filter for hairpins of high potency. This set was again filtered for reproducibility. A CV of 0.8 (a conservative estimate of the 8-shRNA signature variability at high levels of enrichment or depletion was used). This yielded a reproducible set of 93 hairpins for further analysis. In order to assess whether or not these 93 hairpins followed an averaging model, we used the 7 abundant shRNAs from the 8-shRNA signature as a set of positive controls. These 7 shRNAs are known to show an averaging effect in a GFP competition based experiment, so they were used to threshold our 93 shRNAs. shRNAs had to be two standard deviations different from the average deviation of the 8-shRNA signature set to be considered distinct from the averaging model.

References

References

1. Luria SE, Delbruck M. Mutations of Bacteria from Virus Sensitivity to Virus Resistance. Genetics. 1943;28:491-511.

2. Law LW. Origin of the resistance of leukaemic cells to folic acid antagonists. Nature. 1952;169:628-9.

3. Law LW. Effects of combinations of antileukemic agents on an acute lymphocytic leukemia of mice. Cancer research. 1952;12:871-8.

4. Skipper HE, Thomson JR, Bell M. Attempts at dual blocking of biochemical events in cancer chemotherapy. Cancer research. 1954;14:503-7.

5. Frei E, 3rd, Holland JF, Schneiderman MA, Pinkel D, Selkirk G, Freireich EJ, et al. A comparative study of two regimens of combination chemotherapy in acute leukemia. Blood. 1958;13:1126-48.

6. Cabanillas F. Front-line management of diffuse large B cell lymphoma. Curr Opin Oncol. 2010;22:642-5.

7. Bassan R, Hoelzer D. Modern therapy of acute lymphoblastic leukemia. Journal of clinical oncology : official journal of the American Society of Clinical Oncology. 2011;29:532-43.

8. Hughes TR, Marton MJ, Jones AR, Roberts CJ, Stoughton R, Armour CD, et al. Functional discovery via a compendium of expression profiles. Cell. 2000;102:109-26.

9. Parsons AB, Lopez A, Givoni IE, Williams DE, Gray CA, Porter J, et al. Exploring the mode-of-action of bioactive compounds by chemical-genetic profiling in yeast. Cell. 2006;126:611-25.

10. Ho CH, Magtanong L, Barker SL, Gresham D, Nishimura S, Natarajan P, et al. A molecular barcoded yeast ORF library enables mode-of-action analysis of bioactive compounds. Nature biotechnology. 2009;27:369-77.

11. Rihel J, Prober DA, Arvanites A, Lam K, Zimmerman S, Jang S, et al. Zebrafish behavioral profiling links drugs to biological targets and rest/wake regulation. Science. 2010;327:348-51.

12. Perlman ZE, Slack MD, Feng Y, Mitchison TJ, Wu LF, Altschuler SJ. Multidimensional drug profiling by automated microscopy. Science. 2004;306:1194-8.

13. Krutzik PO, Crane JM, Clutter MR, Nolan GP. High-content single-cell drug screening with phosphospecific flow cytometry. Nature chemical biology. 2008;4:132-42.

14. Weinstein JN, Myers TG, O'Connor PM, Friend SH, Fornace AJ, Jr., Kohn KW, et al. An information-intensive approach to the molecular pharmacology of cancer. Science. 1997;275:343-9.

15. Lamb J, Crawford ED, Peck D, Modell JW, Blat IC, Wrobel MJ, et al. The Connectivity Map: using gene-expression signatures to connect small molecules, genes, and disease. Science. 2006;313:1929-35.

16. Hieronymus H, Lamb J, Ross KN, Peng XP, Clement C, Rodina A, et al. Gene expression signature-based chemical genomic prediction identifies a novel class of HSP90 pathway modulators. Cancer Cell. 2006;10:321-30.

17. Geva-Zatorsky N, Dekel E, Cohen AA, Danon T, Cohen L, Alon U. Protein dynamics in drug combinations: a linear superposition of individual-drug responses. Cell. 2010;140:643-51.

18. Jiang H, Pritchard JR, Williams RT, Lauffenburger DA, Hemann MT. A mammalian functional-genetic approach to characterizing cancer therapeutics. Nature chemical biology. 2011;7:92-100.

19. Adams JM, Harris AW, Pinkert CA, Corcoran LM, Alexander WS, Cory S, et al. The c-myc oncogene driven by immunoglobulin enhancers induces lymphoid malignancy in transgenic mice. Nature. 1985;318:533-8.

20. Longley DB, Harkin DP, Johnston PG. 5-fluorouracil: mechanisms of action and clinical strategies. Nature reviews Cancer. 2003;3:330-8.

21. Williams RT, Roussel MF, Sherr CJ. Arf gene loss enhances oncogenicity and limits imatinib response in mouse models of Bcr-Abl-induced acute lymphoblastic leukemia. Proc Natl Acad Sci U S A. 2006;103:6688-93.

22. Ramalingam SS, Egorin MJ, Ramanathan RK, Remick SC, Sikorski RP, Lagattuta TF, et al. A phase I study of 17-allylamino-17-demethoxygeldanamycin combined with paclitaxel in patients with advanced solid malignancies. Clinical cancer research : an official journal of the American Association for Cancer Research. 2008;14:3456-61.

23. Carbone PP, Spurr C, Schneiderman M, Scotto J, Holland JF, Shnider B. Management of patients with malignant lymphoma: a comparative study with cyclophosphamide and vinca alkaloids. Cancer research. 1968;28:811-22.

24. Lenz G, Wright G, Dave SS, Xiao W, Powell J, Zhao H, et al. Stromal gene signatures in large-B-cell lymphomas. The New England journal of medicine. 2008;359:2313-23.

25. Borisy AA, Elliott PJ, Hurst NW, Lee MS, Lehar J, Price ER, et al. Systematic discovery of multicomponent therapeutics. Proceedings of the National Academy of Sciences of the United States of America. 2003;100:7977-82.

26. Lehar J, Krueger AS, Zimmermann GR, Borisy AA. Therapeutic selectivity and the multi-node drug target. Discov Med. 2009;8:185-90.

27. Frei E, 3rd, Elias A, Wheeler C, Richardson P, Hryniuk W. The relationship between high-dose treatment and combination chemotherapy: the concept of summation dose intensity. Clinical cancer research : an official journal of the American Association for Cancer Research. 1998;4:2027-37.

28. Budman DR, Berry DA, Cirrincione CT, Henderson IC, Wood WC, Weiss RB, et al. Dose and dose intensity as determinants of outcome in the adjuvant treatment of breast cancer. The Cancer and Leukemia Group B. Journal of the National Cancer Institute. 1998;90:1205-11.

29. Frei E, 3rd. Curative cancer chemotherapy. Cancer research. 1985;45:6523-37.

30. Newcombe HB, Hawirko R. Spontaneous Mutation to Streptomycin Resistance and Dependence in Escherichia Coli. J Bacteriol. 1949;57:565-72.

31. Mullighan CG, Phillips LA, Su X, Ma J, Miller CB, Shurtleff SA, et al. Genomic analysis of the clonal origins of relapsed acute lymphoblastic leukemia. Science. 2008;322:1377-80.

32. Mullighan CG, Zhang J, Kasper LH, Lerach S, Payne-Turner D, Phillips LA, et al. CREBBP mutations in relapsed acute lymphoblastic leukaemia. Nature. 2011;471:235-9.

33. Ding L, Ley TJ, Larson DE, Miller CA, Koboldt DC, Welch JS, et al. Clonal evolution in relapsed acute myeloid leukaemia revealed by whole-genome sequencing. Nature. 2012;481:506-10.

34. Burgess DJ, Doles J, Zender L, Xue W, Ma B, McCombie WR, et al. Topoisomerase levels determine chemotherapy response in vitro and in vivo. Proc Natl Acad Sci U S A. 2008;105:9053-8.

35. Dickins RA, Hemann MT, Zilfou JT, Simpson DR, Ibarra I, Hannon GJ, et al. Probing tumor phenotypes using stable and regulated synthetic microRNA precursors. Nat Genet. 2005;37:1289-95.

36. Landazuri N, Le Doux JM. Complexation of retroviruses with charged polymers enhances gene transfer by increasing the rate that viruses are delivered to cells. The journal of gene medicine. 2004;6:1304-19.

37. Pritchard JR, Gilbert LA, Meacham CE, Ricks JL, Jiang H, Lauffenburger DA, et al. Bcl-2 family genetic profiling reveals microenvironment-specific determinants of chemotherapeutic response. Cancer research. 2011;71:5850-8.

Chapter 4

Genetic profiling for *in vivo* microenvironment specific drug responses

Contributions:

Luke Gilbert and I performed the majority of the experiments in this paper. Hai Jiang provided western blots showing Bax and Bak knockdown. Jennifer Ricks performed the *in vivo* GFP enrichment experiment with Vincristine. I designed and validated the luminex assay, performed the screen, analysed the screen data. Luke performed the *in vivo* validation studies with the Bid hairpins. Mike Hemann, Luke Gilbert and I wrote the paper. A version of this chapter was published as:

Bcl-2 family genetic profiling reveals microenvironment-specific determinants of chemotherapeutic response. Pritchard JR*, Gilbert LA*, Meacham CE, Ricks JL, Jiang H, Lauffenburger DA, Hemann MT. Cancer Res. 2011 Sep 1;71(17):5850-8. Epub 2011 Jul 22.

*Indicates joint first author

Abstract

The Bcl-2 family represents a diverse set of pro and anti-apoptotic factors that are dynamically activated in response to a variety of cell intrinsic and extrinsic stimuli. While *in vitro* cell culture experiments have identified growth factor-, cytokine-, and drug-dependent effects on utilization of BCL-2 family members, *in vivo* studies have typically focused on the role of one or two particular members in development and organ homeostasis. Thus, the ability of complex physiologically relevant contexts to modulate canonical dependencies has yet to be systematically investigated. Here, we have developed a pool-based shRNA measurement assay to systematically interrogate the functional dependence of leukemia and lymphoma cells upon the various BCL-2 family members comprehensively across diverse *in vitro* and *in vivo* settings. Using this approach, we report the first *in vivo* loss of function screen for modifiers of response to a frontline chemotherapeutic. Notably, our data reveal an unexpected role for the extrinsic death pathway as a tissue specific modifier of therapeutic response. Our findings demonstrate that particular sites of tumor dissemination can play critical roles in demarcating cancer cell vulnerabilities and mechanisms of chemoresistance.

Introduction

Chemotherapy represents a major treatment modality for cancer, and numerous genetic screens have probed the mechanisms underlying cell-intrinsic resistance or sensitivity to front-line chemotherapy (1-6). However, these studies, while informative, have not been adapted to relevant tumor microenvironments, which may contain diverse stromal and/or immune cell types, are subject to immune surveillance, and harbor physical barriers to drug delivery (7). Additionally, the native tumor microenvironment comprises a diverse mixture of chemokines and cytokines that may impact responses to genotoxic agents (8, 9). Thus, the central determinants of therapeutic outcome may be highly dependent upon paracrine survival or stress signals. Indeed, it is well documented that gene function and relevance can vary dramatically when compared *in vivo* versus *in vitro* (8, 10). Consequently, studying the impact of defined genetic alterations on therapeutic response in native tumor microenvironments is critical for effective drug development, personalized cancer regimens, and the rational design of combination therapies.

Recent advances in the development of tractable mouse models of cancer have, for the first time, enabled the examination of complex sets of defined alterations in individual mice. For example, retroviral infection of murine hematopoietic stem cells or primary embryonic hepatocytes with small pools of short hairpin RNAs (shRNAs), followed by adoptive transfer into lethally-irradiated recipient mice, has been used to screen for suppressors of B cell lymphomagenesis or hepatocellular carcinoma (11, 12). Additionally, *ex vivo* manipulation of lymphoma cells followed by transfer into syngeneic recipient mice has permitted the interrogation of thousands of shRNAs for modulators of tumor growth and dissemination (13). These screens provide powerful proofs of principle that diverse alterations can be introduced in chimeric tumor models *in vivo* and that these systems might permit the simultaneous

examination of the relevance of a whole set of genes to therapeutic response in relevant physiological contexts.

Front-line cancer therapies generally exert their effects by modulating the proportion of pro- to anti- apoptotic death regulators, most notably members of the Bcl-2 family (14, 15). Thus, we reasoned that interrogating Bcl-2 family functionality might provide a high-resolution focus on a crucial facet of cytotoxic cellular responses to chemotherapy in a variety of distinct settings. Notably, previous studies using recombinant BH3 peptides in reconstituted mitochondrial suspensions have systematically identified cellular states associated with the loss of function of one of the BH3-only Bcl-2 family members, the loss of function of a multi-domain pro-apoptotic Bcl-2 family member, or the enhanced function of an anti-apoptotic family member; these states characterize the potential range of dysregulation that the Bcl-2 family can acquire during tumorigenesis and demarcate central cell fate decisions that are susceptible to therapeutic intervention (16, 17). However, this approach, while quite powerful, does not allow for the comprehensive examination of the role and relevance of individual Bcl-2 family members to cell death following chemotherapy. Here we describe a complementary *in vivo* screening approach that provides a detailed assessment of the role of each Bcl-2 family member in the response to chemotherapy in heterogeneous tumor environments.

Results

A bead-based assay for the direct measurement of pooled shRNA representation

The Bcl-2 family consists of 16 pro- and 6 anti-apoptotic proteins that regulate programmed cell death in response to a diverse set of intrinsic and extrinsic death stimuli (18, 19). To assess how these genes modulate chemotherapy-induced cell death across multiple *in vivo* contexts, as well as across diverse *in vitro* conditions in a multiplexed manner, we adapted

a validated set of shRNAs targeting all 22 Bcl-2 family members to Luminex bead-based analysis (Figure 1A and (20)). This technology has previously been used to quantify diverse sets of microRNAs in solution with improved accuracy relative to classic microarray approaches (21). Thus, we reasoned that this approach could be modified to perform reproducible quantification of sub-genome sized shRNA pools.

Briefly, we covalently coupled an amino modified oligonucleotide that is the reverse complement of the unique guide strand section of each shRNA to fluorescently labeled Luminex beads. Our PCR strategy uses a forward primer complementary to the microRNA loop sequence present in all hairpins and a biotinylated reverse primer complementary to the flanking microRNA sequence (Figure 1B). Thus, all shRNA guide strands can be amplified using common primers, and the quantity of individual shRNAs can be visualized with streptavidin-PE after bead hybridization. Notably, this approach is distinct from barcoded shRNA libraries, in which shRNAs are identifiable by a flanking DNA sequence. In this case, we used the unique portion of the shRNA, itself, as the barcode. This allows for multiplexed shRNA quantification in any vector backbone.

As an initial proof-of-principle experiment, we confirmed that each Bcl-2 shRNA could be quantified by Luminex bead hybridization when starting with similar concentrations of dsPCR product (Supp. Figure S1A). Importantly, while each PCR product with a cognate bead was readily detectable, a control probe exhibited no significant signal with any of the 22 shRNAs in the plasmid library. In fact, the average maximum signal for an shRNA present in the pool was approximately 100-fold higher than the control probe signal. While this negative control ruled out any large magnitude non-specific hybridization, we wanted to rule out smaller amounts of cross hybridization as the source of the variation in the maximum fluorescence intensity of the various probes (Supp. Figure S1B). To this end, we noted a strong relationship between probe GC content and maximum signal intensity. Oligonucleotides deviating from this relationship

were analyzed for local sequence alignments across the entire shRNA library utilizing the dynamic programming method of Smith-Waterman (22). The variation in the average local alignment bit scores for all "outlier" probes was highly similar (Supp. Figure S1C), indicating that cross-hybridization is an unlikely contributor to overall signal intensity. Thus, oligonucleotide sequences chosen for optimal siRNA performance are well suited for hybridization-based sequence identification.

We next performed mock enrichment experiments in which known concentrations of genomic DNA from single hairpin infected *Eμ-Myc p19*$^{Arf-/-}$ lymphoma cells were combined at distinct ratios (Supp. Figure S1D). These lymphoma cells were derived from a well-established pre-clinical mouse model of Burkitt's lymphoma and represent a tractable setting to investigate the genetics of therapeutic response (23, 24). Using these cells, we observed a linear and highly reproducible change in measured fluorescence intensity that tightly correlated with the known fold enrichment of the control sample across 8 fold changes in relative DNA abundance.

The BCL-2 family differentially modulates therapeutic response in distinct B-cell tumors

The initial validation of our measurement technology led us to benchmark this approach against an established single shRNA flow cytometry based assay. In this assay, GFP was used as a surrogate marker for the presence of each of 16 distinct Bcl-2 family member shRNAs, and the impact of gene suppression was determined by the relative change in the percent of GFP positive cells following treatment (20). In each case, we examined the effect of Bcl-2 family gene knockdown on the *in vitro* response of *Eμ-Myc p19*$^{Arf-/-}$ lymphoma cells to the front-line chemotherapeutic doxorubicin (Figure 1C). A linear relationship (r^2=0.89) was observed between multiplexed bead-based measurements and single shRNA flow cytometry measurements of shRNA enrichment and depletion following doxorubicin treatment. Thus, a

bead hybridization assay can rapidly and accurately measure shRNA pool composition following drug selection.

A key advantage of shRNA pool-based approaches lies in their inherent adaptability to diverse experimental systems and conditions. In order to test the flexibility of our system, we examined the effects of Bcl-2 family member suppression on doxorubicin response in a distinct cell line. In this case, we examined cells derived from a BCR-Abl driven murine model of B cell acute lymphoblastic leukemia (B-ALL) (25). As observed in the Burkitt's lymphoma model, we could identify a robust Bcl-2 family shRNA drug resistance and sensitivity profile in these cells. However, the shRNA signatures were distinct between cell types. The most obvious feature differentiating the two cell lines was the critical role for the BH3-only member Bim in doxorubicin-induced cell death in B-ALL (Figure 1D). Since Bim levels are known to increase in response to environmental but not genotoxic stress, the involvement of Bim in the response to a DNA damaging agent in this context was unexpected. In order to explore the mechanism of Bim induced cell death, we examined Bim levels in p185+ BCR-Abl ALL cells treated with genotoxic agents (doxorubicin and chlorambucil) and a histone deacetylase inhibitor known to promote significant Bim induction (SAHA) in B cell malignancies (26). Notably, protein levels of Bim were induced acutely following treatment with DNA damaging agents in B-ALL cells (Figure1E). These data highlight the potential of pool-based shRNA approaches to identify tumor cell-specific determinants of therapeutic response.

An *in vivo* screen for microenvironment specific modifiers of therapeutic response

A central challenge in the development of effective anti-cancer approaches is to understand the impact of the tumor microenvironment on therapeutic response. To test whether our system could be used to examine cancer therapy *in vivo*, we performed a screen to identify

Bcl-2 family members that modulate the response of lymphomas to doxorubicin. Here, all Bcl-2 family shRNAs were simultaneously co-transfected into viral packaging cells to produce a multi-construct viral pool (Figure 2A). The resulting pool was used to infect primary *Eμ-Myc p19*$^{Arf-/-}$ lymphoma cells *ex vivo*, and transduced cells were tail-vein injected into syngeneic recipient mice. A cohort of 8 mice was sacrificed following tumor onset, and a second cohort was treated with 8mg/kg doxorubicin. Following tumor relapse, lymphoma cells were harvested from lymph nodes and the thymus, two common sites of lymphoma manifestation in the *Eμ-Myc* mouse (23), and the relative shRNA content was compared between untreated and treated tumors in these distinct tumor microenvironments.

A striking feature of the resulting data was the mouse-to-mouse variability in hairpin composition following drug treatment. This suggests that the complexity of the *in vivo* microenvironment can substantially influence the measured effect of a relatively neutral shRNA. Further inspection of this variation suggested that a subset of shRNAs exhibited a level of variation comparable to the *in vitro* data while the remainder showed significantly higher fluctuation (Figure 2B). If otherwise neutral hairpins exhibit larger variation in *in vivo* datasets, the size of this variation may represent a meaningful discriminator to focus on hairpins whose effects are large and reproducible enough to overcome this variability. To determine whether such variation is a consistent feature of *in vivo* data sets, we made use of a comprehensive *in vivo* versus *in vitro* shRNA screening data set (13). Indeed, most shRNAs exhibited high mouse-to-mouse CVs *in vivo* (Figure 2C). However, when we focused on shRNAs shown to exert a biological effect in subsequent validation experiments, we saw a significant decrease in shRNA CVs ($p<0.01$). Thus, variation present in this established data set can be used to generate a CV threshold that identifies shRNAs with a high probability of exerting a relevant biological effect. This cutoff was then employed to filter data generated using our Luminex approach (Figure 2D). As a test of the relevance of this variation cutoff to other drug screens,

we examined the stochastic variation in the representation of vector control infected *Eμ-Myc* tumor cells following treatment with the microtubule poison vincristine *in vivo*. Here, we transplanted tumor cells into recipient mice at a defined infection efficiency, as monitored by GFP expression, and examined the variation in the percentage of GFP positive cells in distinct mice following treatment. Importantly, these controls exhibited an *in vivo* CV that was greater than the doxorubicin variation cutoff (Supp. Figure S2), suggesting that the CV threshold established in this study may be broadly applicable to other data sets.

As additional criteria for examining *in vivo* screening data, we required that shRNA target mRNAs be present in untransduced lymphoma cells and that the representation of a "scoring" shRNA be significantly enriched or depleted as a consequence of doxorubicin treatment (see methods). The resulting list of scoring shRNAs included Bcl-2 family members previously described to influence therapeutic response (17) (Figure 2D and Supp. Table S1). For instance, we found that suppression of the BH3-only protein Puma promoted doxorubicin resistance in both the lymph node and thymus compartments, consistent with previous reports examining either B lymphoma cells or thymocytes (24, 27). Thus, this approach can readily identify important regulators of drug-induced cell death.

The extrinsic death pathway is a thymus specific mediator of therapeutic response

Interestingly, in contrast with Puma and other general cell death regulators, we identified the pro-apoptotic Bcl-2 family member Bid as a specific mediator of doxorubicin cytotoxicity in the thymus but not in the lymph nodes. To validate and extend the genetic result in light of this finding, we performed an *in vivo* GFP competition assay in the spleen, bone marrow, peripheral lymph nodes and thymus. In this assay, GFP positivity is used as a surrogate marker for the presence of a Bid shRNA, and the impact of Bid suppression is determined by the relative

change in the percent of GFP positive tumor cells. Consistent with the initial screening data, Bid loss impaired lymphoma cell death in the thymic tumor microenvironment, but not other tumor microenvironments (Figure 3A and B). This tissue specificity was not due to the selective expression of these proteins in specific tumor microenvironments, as we observed similar levels of Bid and its upstream regulator Caspase 8 in the tumor-bearing lymph node and thymus (Supp. Figure S3A and B). Notably, Bid is unique among Bcl-2 family members in that it translocates to the mitochondria following extrinsic activation of death receptors (28, 29). Thus, these data are consistent with a mechanism whereby constitutively present Bid is activated following the release of secreted factors or tumor-stromal cell interactions that are specific to the treated thymic microenvironment.

The relevance of Bid to DNA damage-induced death remains a subject of debate (30, 31). To confirm the importance of Bid to doxorubicin-induced cell death *in vivo*, we injected three cohorts of syngeneic mice with *Eu-Myc p19*$^{Arf-/-}$ lymphoma cells expressing one of two validated shRNAs targeting Bid or a vector control. At tumor onset, all mice were treated with 10mg/kg doxorubicin and monitored for tumor regression and relapse. Suppression of Bid resulted in decreased tumor free survival and tumor cell clearance compared to control tumors (Figure 4A). Furthermore, in mice bearing shBid-transduced lymphomas, 50% of the mice showed no tumor free survival while 90% of control mice exhibited a period of tumor free survival. Notably, in the case of the lymphoma cells used in this study, suppression of Bid *in vitro* had minimal effect on lymphoma cell survival following doxorubicin treatment (Figure 4B). Thus, treatment of these tumors in their native microenvironment reveals genetic dependencies that are not present in cultured cells.

These data suggest that activation of components of the extrinsic cell death pathway potentiate chemotherapeutic efficacy in the thymus. To further interrogate the role of death receptor signaling in therapeutic response in this setting, we targeted Caspase 8, the direct

activator of Bid by generating hairpins targeting Caspase 8 (Supp. Figure S3C). Suppression of Caspase 8 in transplanted lymphomas phenocopied the effect of Bid silencing as measured by tumor free survival (Figure 5A), suggesting an upstream induction of death receptor signaling in the thymus following doxorubicin treatment.

Finally, to confirm the specificity of Bid-induced cell death in the thymus relative to whole organism chemotherapeutic response, we examined the effect of Bid suppression on tumor free survival following doxorubicin treatment in athymic mice. Pure populations of either shBid or vector control transduced lymphoma cells were transplanted into surgically thymectomized recipient mice. Upon the presentation of a palpable disease burden, mice were dosed with 10mg/kg of doxorubicin and monitored for tumor-free and overall survival. In this context, chemotherapeutic response was indistinguishable in the presence or absence of Bid (Figure 5B).

Discussion

We have presented a tractable methodology for pooled shRNA screens that can be rapidly adapted to diverse vector systems and gene families. The value of this system is exemplified by the rapid manner in which drug function can be interrogated in multiple cell types *in vitro* and in diverse anatomical contexts *in vivo*. Importantly, while numerous cell culture-based loss of function screens have been performed to identify modulators of therapeutic response, this is the first report to describe an *in vivo* loss of function therapy screen – the relevance of which is apparent in light of the discordant *in vitro* and *in vivo* phenotypes resulting from Bid suppression. While the set of shRNAs probed in this work is restricted to a particular aspect of cell biology, recent advances in bead-based DNA hybridization now permit the simultaneous resolution of as many as 500 distinct oligonucleotides so that multiple facets can

be explored simultaneously. We have recently shown that as many as 1000 distinct shRNAs can be introduced into individual mice (13), suggesting that large shRNA libraries can be combined with this technology to probe the impact of myriad genetic lesions in diverse pathophysiological contexts.

In this study we systematically examined shRNAs targeting the entire Bcl-2 family in multiple *in vitro* and *in vivo* settings. In all therapeutic contexts, we identified a specific BH3 "activator" gene essential for mediating the effects of frontline chemotherapy. Biochemical studies have previously defined critical roles for the BH3 only family members Bid, Puma and Bim. Furthermore, the recent development of a Bid, Puma, and Bim triple knockout mouse confirmed the essential role of these proteins in developmentally regulated apoptosis (32). Interestingly, our data suggests that the relevant "activator" protein can vary quite significantly in neoplastic cells. While an "activator" is always necessary for cell death, the cellular environment or driving oncogene can dramatically shift the precise BH3-only family member that is most relevant for therapy-induced apoptosis. This context-dependent relevance of apoptotic regulators may underlie the significant challenge in eradicating disseminated malignancies and highlights the need to understand the relationship between intrinsic and paracrine signals and Bcl-2 family regulation.

An unexpected finding from this work is that while Caspase 8 and Bid are expressed at similar levels in diverse tumor-bearing locations *in vivo*, they are specifically required for drug efficacy in the thymus. Examined in isolation, this result would suggest that the thymus is a pro-death microenvironment. However, previous studies in thymectomized mice have shown that the thymus can exert a net protective effect on tumor cells following doxorubicin treatment (9). This cytoprotective effect is mediated in a paracrine fashion by thymic endothelial cells that secrete multiple pro-survival cytokines in response to DNA damage. Cytokine induction subsequently upregulates BCL-xL and promotes the survival of target tumor cells. Thus, the

unique role of death receptor activity in this context may function to counterbalance unchecked survival signaling following cellular stress in the thymic microenvironment. Notably, however, the precise mechanism of death receptor engagement in this context remains to be determined. Addition of recombinant death receptor ligands, such as FASL, TNF, and TRAIL *in vitro* fails to induce lymphoma cell death. Consequently, the engagement of death receptor signaling, like survival signaling, may require a more complex concerted action of secreted factors and cell-cell or cell-stromal interactions.

Materials and Methods

shRNA generation

shRNAs targeting the Bcl-2 family (20) were designed using Biopredsi from Novartis. shRNAs were cloned into the MLS (33) retroviral vector containing a Mir30 expression cassette under the transcriptional control of the MSCV LTR and coexpressing GFP. Plasmids were verified for mRNA target knockdown using standard qRT-PCR techniques. Western blots were performed to analyze total protein knock down for a subset of Bcl-2 family members. Bim, Bax, and Bak knockdown are shown in Supp. Figure S4. The shRNA library was constructed by evenly pooling individual minipreps of each individual shRNA. This mixture was co-transfected into Phoenix retroviral packaging cells and pooled virus was collected.

Western Blots

SDS-PAGE was performed according to standard protocols, and gels were transferred to PVDF membranes. The antibodies used were as follows; Bid (polyclonal antisera from Honglin Li), BAX (Cell Signaling Technologies #2772), BAK (Upstate #06-536), BIM (Cell Signaling Technologies #C34C5), Casapase 8 (Cell Signaling Technologies #D35G2), beta-Actin (Cell Signaling Technologies #4967L), and Tubulin (ECM Biosciences #TM1541).

Luminex bead-based assay

Carboxylated Luminex beads were purchased from Mirai biosystems. Probe oligonucleotides comprised of the shRNA anti-sense strand modified with C12-amine were conjugated to the beads using EDC in a pH 4.5 MES hydrate buffer. Coupling efficiency was validated with sense oligonucleotides. 3500 beads were added to a 50μl reaction volume in a 3M Tetra-methyl ammonium chloride (TMAC) buffer to reduce the differences in T_m that accompany differences in GC content. DNA loading concentrations are as indicated (2-200ng

per well were added). Blocking oligos that corresponded to the biotinylated PCR product but lacked the sense portion of the shRNA were added at 100-fold molar excess to compete out the dsPCR product and reduce the preferential re-hybridization of the PCR product. Samples were denatured for 3 min at 95°C and hybridized for 30 minutes at 52°C. Streptavidin-PE (Invitrogen)/TMAC was then added to the wells and incubated for 5 minutes at 52°C. All samples were incubated at 52°C to ensure they stayed at equilibrium, and the PMT setting on the Luminex machine was approximately 520 volts (low calibration).

Polymerase Chain Reaction

Three individual 25μl PCR reactions were performed using a 5' primer targeting the constant hairpin loop region and a 3' primer targeting the vector backbone. The PCR buffer was 2x Failsafe Buffer B (Epicentre Biotechnologies) and we ran 35 cycles with an extension time of 1 minute at 72°C and a hybridization temperature of 52°C for 35 seconds. The 3' primer was biotinylated. Pooled PCR product was column purified and resuspended in 36μl water prior to serial dilution and subsequent measurement.

Cell culture

All lymphoma and leukemia cells were cultured at 5% CO2 at 37°C. *Eμ-Myc p19*$^{ARF-/-}$ cells were maintained as described (5). B-ALL cells were maintained as described (34). All *in vitro* viral transduction was performed by co-infecting 1 million cells per 10cm plate. Infection efficiency was quantified by flow cytometry for GFP+ cell populations. Infection efficiencies under 50% were utilized to ensure an MOI of approximately one. Pool composition was measured at the beginning of the experiment, as well as following recovery from an LD90 doxorubicin drug dose. Untreated cells that had grown in culture for the duration of the experiment were used as controls. Hairpin 97mer sequences in the Mir30 context were:

shBid-1-
TGCTGTTGACAGTGAGCGCCACAGAAGATTCCATATCAAATAGTGAAGCCACAGATGTATT
TGATATGGAATCTTCTGTGATGCCTACTGCCTCGGA,

shBid-2-
TGCTGTTGACAGTGAGCGCCACAGAAGATTCCATATCAAATAGTGAAGCCACAGATGTATT
TGATATGGAATCTTCTGTGATGCCTACTGCCTCGGA.

shCaspase 8-
TGCTGTTGACAGTGAGCGAAACTATGACGTGAGCAATAAATAGTGAAGCCACAGATGTATT
TATTGCTCACGTCATAGTTCTGCCTACTGCCTCGGA

Background distribution analysis for *in vivo* screening data

454 sequencing data used to determine CV thresholds is available from the GEO database (accession number GSE16090). Coefficients of variation were calculated by dividing the standard deviation of the fold change in read number (for any hairpin with >4 reads) by the mean of the fold change. To be included in this analysis hairpins had to be present at high enough quantities to have at least 4 reads. Previously validated hit CVs (13) included IL-6, Lyn, Rac2, Twf, and CrkL and were compared to the background distribution by t-test. Cumulative distributions were plotted in Matlab using the dfittool.

***In vivo* screening**

6-week old C57BL/6J mice (Jackson Laboratories) were tail vein injected with 2 million *Eμ-Myc p19*$^{ARF-/-}$ lymphoma cells expressing the 22 shRNAs targeting the Bcl-2 family. Infection was optimized such that each tumor cell expressed a single shRNA. We sampled pool composition before injection, upon the development of a palpable tumor burden, and upon relapse following IP injection of 8mg/kg of doxorubicin. For *in vivo* screen validation, pure populations of cells expressing shRNAs were isolated by GFP sorting using a FACS ARIA cell

sorter. 2 million cells transduced with a vector control or specific shRNAs were injected into syngeneic recipient mice. At the presentation of palpable lymphomas, mice were treated with 10mg/kg doxorubicin and disease free survival/tumor free progression were monitored.

Screening analysis

Luminex intensities for serial dilutions of PCR samples from pooled hairpin libraries were compared by calculating a curve fit for a given sample using the equation (Y=a*(1-exp(-b*x)). Sample integrals were then calculated, and these integral scores were compared after subtracting the initial from the final integral score. All independent Luminex runs were normalized to the maximum signal intensity and all runs performed on different days contained internal standards for day-to-day normalization. Scoring shRNAs were identified following a three-step process. First, in order to eliminate a systematic error for depleting hairpins, we transformed all the data by adding the hairpin mean to all *in vivo* measurements. We then applied two filters. The first filter was based upon a comparison of the distribution of a given shRNA with the variation of neutral hairpins. We required our "hits" to have a coefficient of variation that was equal to or less than 0.4. This allowed us to threshold out approximately 80% of neutral hairpins. The second filter was based upon a comparison of treated samples with untreated hairpin samples. To progress to further validation efforts, we required our treated sample to be different at the 0.10 significance level versus untreated controls.

Data analysis

Linear fits were calculated using a least squares algorithm. Sequences were compared for overlap using the local alignment method of Smith-Waterman in the Matlab function localalign.m. Heat maps were generated in Matlab. Kaplan Meier analyses were performed using Graph Pad Prism software.

Acknowledgements

The authors would like to thank members of the Lauffenburger and Hemann labs for helpful comments and criticisms. M.T.H. is supported by NIH RO1 CA128803 and the Ludwig Foundation. J.R.P. is a Poitras Graduate Fellow, and J.R.P. and C. E. M. are supported by the MIT Department of Biology training grant. L. A. G. is supported by a Ludwig Fellowship. Additional funding was provided by the Integrated Cancer Biology Program grant 1-U54-CA112967 to D.A.L. and M.T.H.

References

1. Bartz SR, Zhang Z, Burchard J, Imakura M, Martin M, Palmieri A, et al. Small interfering RNA screens reveal enhanced cisplatin cytotoxicity in tumor cells having both BRCA network and TP53 disruptions. Mol Cell Biol. 2006;26:9377-86.

2. Berns K, Horlings HM, Hennessy BT, Madiredjo M, Hijmans EM, Beelen K, et al. A functional genetic approach identifies the PI3K pathway as a major determinant of trastuzumab resistance in breast cancer. Cancer Cell. 2007;12:395-402.

3. Huang S, Laoukili J, Epping MT, Koster J, Holzel M, Westerman BA, et al. ZNF423 is critically required for retinoic acid-induced differentiation and is a marker of neuroblastoma outcome. Cancer Cell. 2009;15:328-40.

4. Doles J, Hemann MT. Nek4 status differentially alters sensitivity to distinct microtubule poisons. Cancer Res. 2010;70:1033-41.

5. Burgess DJ, Doles J, Zender L, Xue W, Ma B, McCombie WR, et al. Topoisomerase levels determine chemotherapy response in vitro and in vivo. Proc Natl Acad Sci U S A. 2008;105:9053-8.

6. Smogorzewska A, Desetty R, Saito TT, Schlabach M, Lach FP, Sowa ME, et al. A genetic screen identifies FAN1, a Fanconi anemia-associated nuclease necessary for DNA interstrand crosslink repair. Mol Cell. 2010; 39:36-47.

7. Sharpless NE, Depinho RA. The mighty mouse: genetically engineered mouse models in cancer drug development. Nat Rev Drug Discov. 2006;5:741-54.

8. Hideshima T, Mitsiades C, Tonon G, Richardson PG, Anderson KC. Understanding multiple myeloma pathogenesis in the bone marrow to identify new therapeutic targets. Nat Rev Cancer. 2007;7:585-98.

9. Gilbert LA, Hemann MT. DNA damage-mediated induction of a chemoresistant niche. Cell. 2010; 143:355-66.

10. Nguyen DX, Bos PD, Massague J. Metastasis: from dissemination to organ-specific colonization. Nat Rev Cancer. 2009;9:274-84.

11. Bric A, Miething C, Bialucha CU, Scuoppo C, Zender L, Krasnitz A, et al. Functional identification of tumor-suppressor genes through an in vivo RNA interference screen in a mouse lymphoma model. Cancer Cell. 2009;16:324-35.

12. Zender L, Xue W, Zuber J, Semighini CP, Krasnitz A, Ma B, et al. An oncogenomics-based in vivo RNAi screen identifies tumor suppressors in liver cancer. Cell. 2008;135:852-64.

13. Meacham CE, Ho EE, Dubrovsky E, Gertler FB, Hemann MT. In vivo RNAi screening identifies regulators of actin dynamics as key determinants of lymphoma progression. Nat Genet. 2009;41:1133-7.

14. Adams JM, Cory S. Bcl-2-regulated apoptosis: mechanism and therapeutic potential. Curr Opin Immunol. 2007;19:488-96.

15. Cotter TG. Apoptosis and cancer: the genesis of a research field. Nat Rev Cancer. 2009;9:501-7.

16. Certo M, Del Gaizo Moore V, Nishino M, Wei G, Korsmeyer S, Armstrong SA, et al. Mitochondria primed by death signals determine cellular addiction to antiapoptotic BCL-2 family members. Cancer Cell. 2006;9:351-65.

17. Deng J, Carlson N, Takeyama K, Dal Cin P, Shipp M, Letai A. BH3 profiling identifies three distinct classes of apoptotic blocks to predict response to ABT-737 and conventional chemotherapeutic agents. Cancer Cell. 2007;12:171-85.

18. Letai AG. Diagnosing and exploiting cancer's addiction to blocks in apoptosis. Nat Rev Cancer. 2008;8:121-32.

19. Youle RJ, Strasser A. The BCL-2 protein family: opposing activities that mediate cell death. Nat Rev Mol Cell Biol. 2008;9:47-59.

20. Jiang H, Pritchard JR, Williams RT, Lauffenburger DA, Hemann MT. A mammalian functional-genetic approach to characterizing cancer therapeutics. Nat Chem Biol. 2011; 7:92-100.

21. Lu J, Getz G, Miska EA, Alvarez-Saavedra E, Lamb J, Peck D, et al. MicroRNA expression profiles classify human cancers. Nature. 2005;435:834-8.
22. Smith TF, Waterman MS. Identification of common molecular subsequences. J Mol Biol. 1981;147:195-7.

23. Adams JM, Harris AW, Pinkert CA, Corcoran LM, Alexander WS, Cory S, et al. The c-myc oncogene driven by immunoglobulin enhancers induces lymphoid malignancy in transgenic mice. Nature. 1985;318:533-8.

24. Jiang H, Reinhardt HC, Bartkova J, Tommiska J, Blomqvist C, Nevanlinna H, et al. The combined status of ATM and p53 link tumor development with therapeutic response. Genes Dev. 2009;23:1895-909.

25. Williams RT, Roussel MF, Sherr CJ. Arf gene loss enhances oncogenicity and limits imatinib response in mouse models of Bcr-Abl-induced acute lymphoblastic leukemia. Proc Natl Acad Sci U S A. 2006;103:6688-93.

26. Lindemann RK, Newbold A, Whitecross KF, Cluse LA, Frew AJ, Ellis L, et al. Analysis of the apoptotic and therapeutic activities of histone deacetylase inhibitors by using a mouse model of B cell lymphoma. Proceedings of the National Academy of Sciences of the United States of America. 2007;104:8071-6.

27. Villunger A, Michalak EM, Coultas L, Mullauer F, Bock G, Ausserlechner MJ, et al. p53- and drug-induced apoptotic responses mediated by BH3-only proteins puma and noxa. Science. 2003;302:1036-8.

28. Wang K, Yin XM, Chao DT, Milliman CL, Korsmeyer SJ. BID: a novel BH3 domain-only death agonist. Genes Dev. 1996;10:2859-69.

29. Li H, Zhu H, Xu CJ, Yuan J. Cleavage of BID by caspase 8 mediates the mitochondrial damage in the Fas pathway of apoptosis. Cell. 1998;94:491-501.

30. Zinkel SS, Hurov KE, Ong C, Abtahi FM, Gross A, Korsmeyer SJ. A role for proapoptotic BID in the DNA-damage response. Cell. 2005;122:579-91.

31. Kaufmann T, Tai L, Ekert PG, Huang DC, Norris F, Lindemann RK, et al. The BH3-only protein bid is dispensable for DNA damage- and replicative stress-induced apoptosis or cell-cycle arrest. Cell. 2007;129:423-33.

32. Ren D, Tu HC, Kim H, Wang GX, Bean GR, Takeuchi O, et al. BID, BIM, and PUMA are essential for activation of the BAX- and BAK-dependent cell death program. Science. 2010;330:1390-3.

33. Dickins RA, Hemann MT, Zilfou JT, Simpson DR, Ibarra I, Hannon GJ, et al. Probing tumor phenotypes using stable and regulated synthetic microRNA precursors. Nat Genet. 2005;37:1289-95.

34. Williams RT, den Besten W, Sherr CJ. Cytokine-dependent imatinib resistance in mouse BCR-ABL+, Arf-null lymphoblastic leukemia. Genes Dev. 2007;21:2283-7.

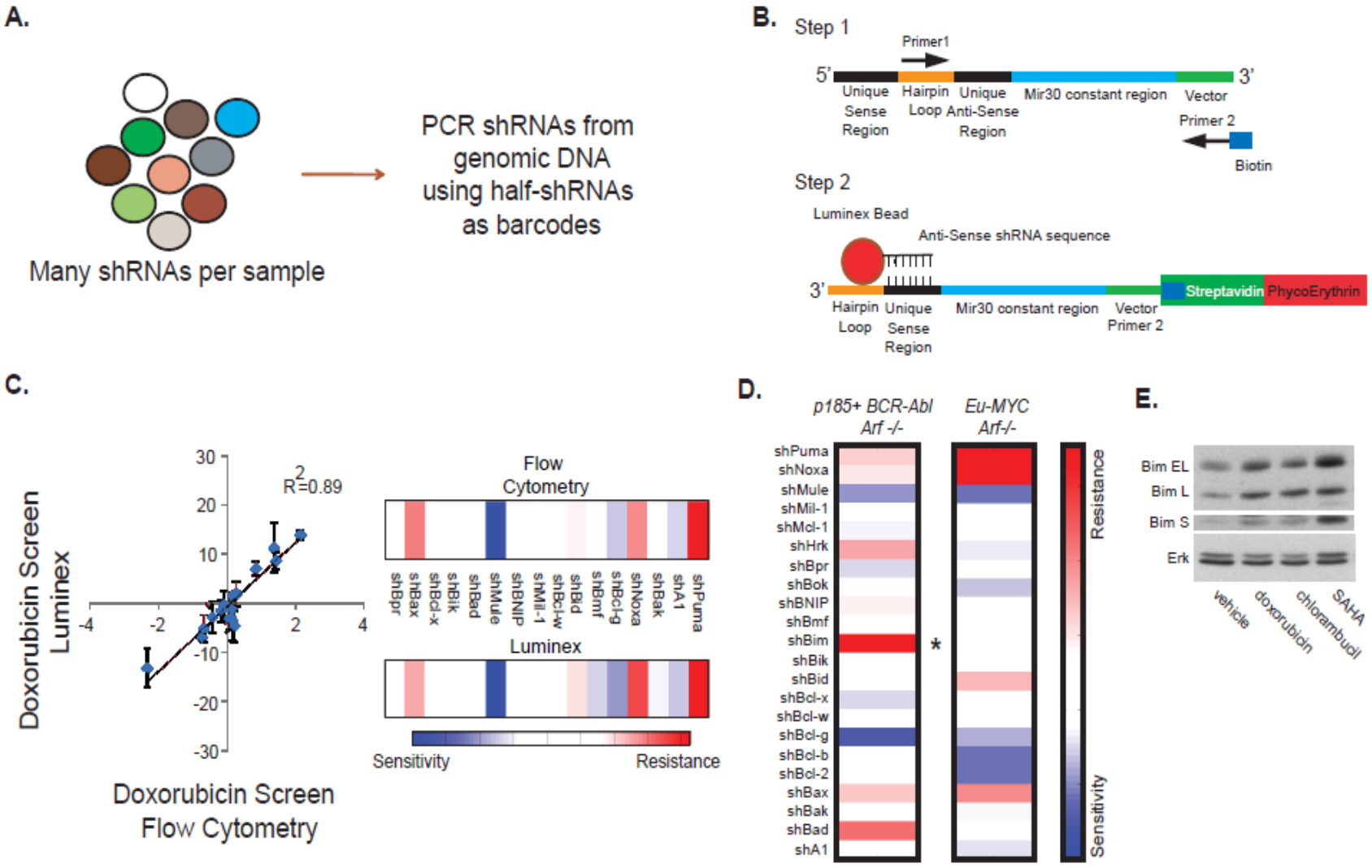
A.
Many shRNAs per sample
PCR shRNAs from genomic DNA using half-shRNAs as barcodes
B.
Step 1
Primer1
5'
3'
Unique Sense Region
Hairpin Loop
Unique Anti-Sense Region
Mir30 constant region
Vector
Primer 2
Biotin
Step 2
Luminex Bead
Anti-Sense shRNA sequence
3'
Hairpin Loop
Unique Sense Region
Mir30 constant region
Vector Primer 2
Streptavidin
PhycoErythrin
C.
Doxorubicin Screen Luminex
R2=0.89
Doxorubicin Screen Flow Cytometry
Flow Cytometry
shBpr
shBax
shBcl-x
shBik
shBad
shMule
shBNIP
shMil-1
shBcl-w
shBid
shBmf
shBcl-g
shNoxa
shBak
shA1
shPuma
Luminex
Sensitivity
Resistance
D.
p185+ BCR-Abl Arf -/-
Eu-MYC Arf-/-
shPuma
shNoxa
shMule
shMil-1
shMcl-1
shHrk
shBpr
shBok
shBNIP
shBmf
shBim
shBik
shBid
shBcl-x
shBcl-w
shBcl-g
shBcl-b
shBcl-2
shBax
shBak
shBad
shA1
*
Resistance
Sensitivity
E.
Bim EL
Bim L
Bim S
Erk
vehicle
doxorubicin
chlorambucil
SAHA

Figure 1 - Examining the role of the entire Bcl-2 family in therapeutic response. (A) A schematic depicting the difference between single and pool-based evaluation of shRNA composition**. (B)** A diagram illustrating the Luminex-based shRNA PCR strategy. PCR primers were designed from constant regions flanking all hairpins. After PCR amplification, a biotinylated primer is used to measure hairpin abundance, and the unique fluorescence of the luminex bead distinguishes hairpin identity. **(C)** A comparison of the bead-based quantification of hairpin representation following doxorubicin treatment with single cell flow cytometry measurements (20). (Left) Bead-based measurements are plotted against each corresponding single hairpin measurements. (Right) Heat maps comparing shRNA enrichment and depletion using bead-based and flow cytometry approaches. **(D)** A heat map comparing the impact of depleting each Bcl-2 family hairpin on the response to doxorubicin treatment in *Eμ-MYC p19*$^{Arf-/-}$ lymphomas and *p185 BCR-Abl+ p19*$^{Arf-/-}$ B-ALLs. The asterisk demarcates the differential impact of suppressing the BH3-only protein Bim on doxorubicin sensitivity in these two cell types. **(E)** *p185 BCR-Abl+ p19*$^{Arf-/-}$ cells were treated for 12 hrs at an LD90 of the indicated compounds and analyzed for Bim levels by western blot.

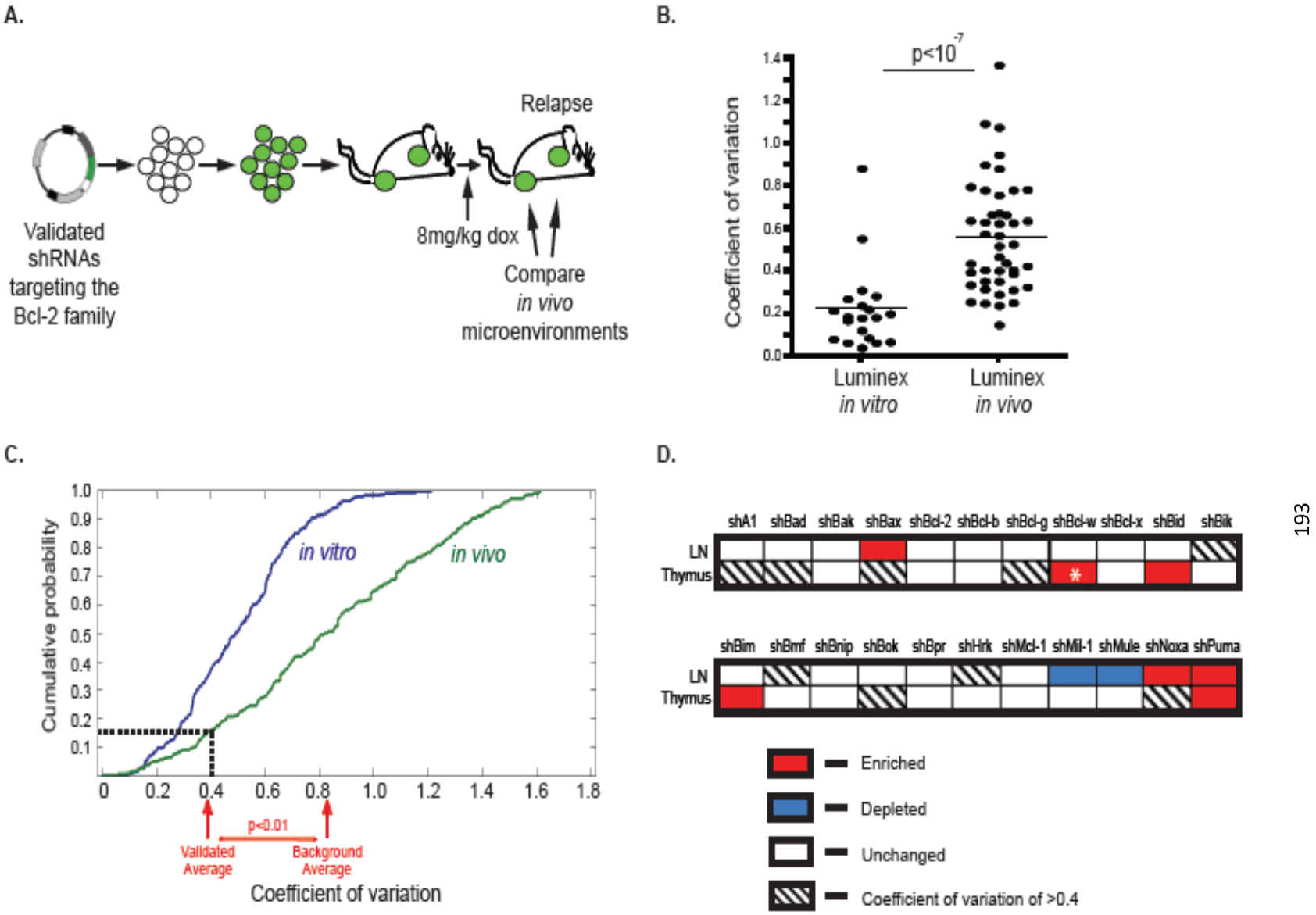
A.
Relapse
Validated shRNAs targeting the Bcl-2 family
8mg/kg dox
Compare in vivo microenvironments
B.
p<10-7
Coefficient of variation
Luminex in vitro
Luminex in vivo
C.
Cumulative probability
in vitro
in vivo
p<0.01
Validated Average
Background Average
Coefficient of variation
D.
shA1 shBad shBak shBax shBcl-2 shBcl-b shBcl-g shBcl-w shBcl-x shBid shBik
LN
Thymus
shBim shBmf shBnip shBok shBpr shHrk shMcl-1 shMil-1 shMule shNoxa shPuma
LN
Thymus
Enriched
Depleted
Unchanged
Coefficient of variation of >0.4

Figure 2 - An *in vivo* shRNA screen for modulators of doxorubicin response. **(A)** A diagram depicting the *in vivo* screening strategy. Pooled shRNAs targeting Bcl-2 family members were retrovirally transduced into *Eμ-MYC p19*$^{Arf-/-}$ lymphomas. shRNA composition was measured either following the presentation of palpable tumor burden or following tumor relapse after treatment with 8mg/kg doxorubicin. **(B)** A comparison of the coefficient of variation (CV) for hairpins targeting the Bcl-2 family in cell culture versus *in vivo* screens using a Luminex measurement methodology. **(C)** An analysis of the distribution of shRNA CV values for a large *in vitro* versus *in vivo* screening data set generated by high-throughput sequencing. The vertical line represents the CV threshold used to filter *in vivo* data. The arrows denote averages for validated hairpins relative to all hairpins **(D)** Bcl-2 family "hits" following filtering for CV and enrichment criteria and separated by anatomical niche. The asterisk denotes a Bcl-w shRNA that scored as enriched in the thymus, but was excluded due to the lack of Bcl-w expression in this context.

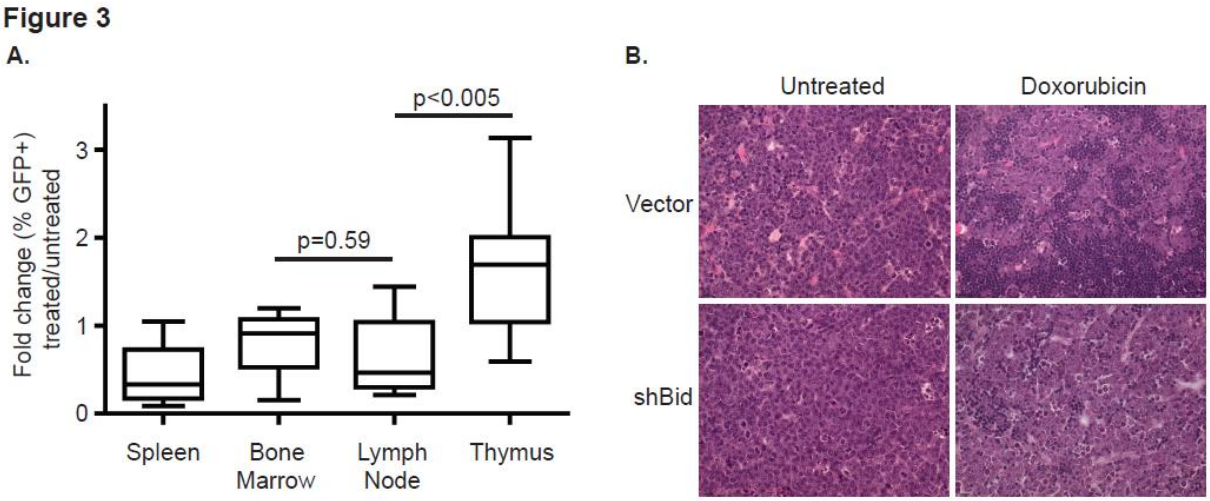

Figure 3 - **Bid potentiates doxorubicin efficacy in the thymus**. **(A)** A graph depicting an *in vivo* GFP competition assay in lymphoma cells partially transduced with shBid-1. Mice were injected with partially transduced lymphoma populations. At tumor onset all mice were treated

with 10mg/kg doxorubicin. 72 hours after treatment, mice were sacrificed and surviving lymphoma populations were harvested. Fold change in GFP percentage was assessed 48 hours later (n≥4). **(B)** H&E stained sections from mice bearing vector control or shBid thymic lymphomas. Mice were treated with 10mg/kg doxorubicin and sacrificed 48 hours later. Representative fields from treated and untreated are shown at 25x magnification. Dark patches in treated vector control tumors indicate sites of normal lymphocyte infiltration.

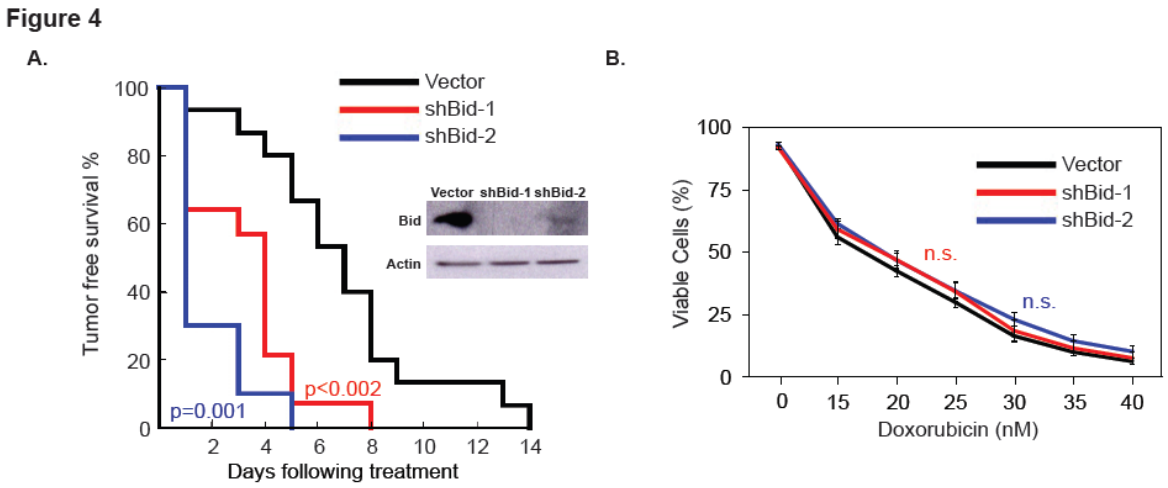

Figure 4 - Bid status affects therapeutic outcome *in vivo*, but not *in vitro*.

(A) A Kaplan-Meier curve showing tumor free survival in mice bearing vector or shBid lymphomas. All mice were treated with a single dose of 10mg/kg doxorubicin (n≥10). (Inset) A western blot showing Bid protein levels in the presence of Bid shRNAs. **(B)** A dose response curve showing the relative viability of lymphoma cells treated with doxorubicin *in vitro* for 48 hours. Lymphoma cells were transduced with either a vector control or an shRNA targeting Bid.

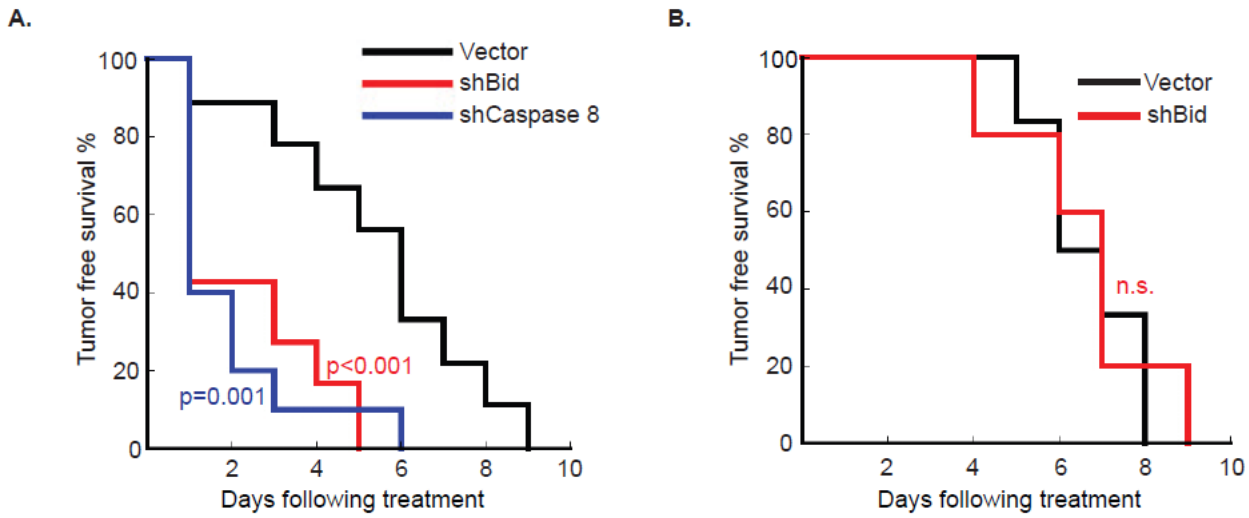

Figure 5 - The extrinsic death pathway mediates doxorubicin response in the thymus. **(A)** A Kaplan-Meier curve showing tumor free survival of mice bearing vector, shBid or shCaspase 8 expressing lymphomas. All mice were treated with a single dose of 10mg/kg doxorubicin (n≥10). **(B)** A Kaplan-Meier curve showing the tumor free survival of thymectomized mice transplanted with pure populations of lymphoma cells transduced with shBid or a vector control. All mice were treated with a single dose of 10mg/kg doxorubicin (n=6 for both cohorts).

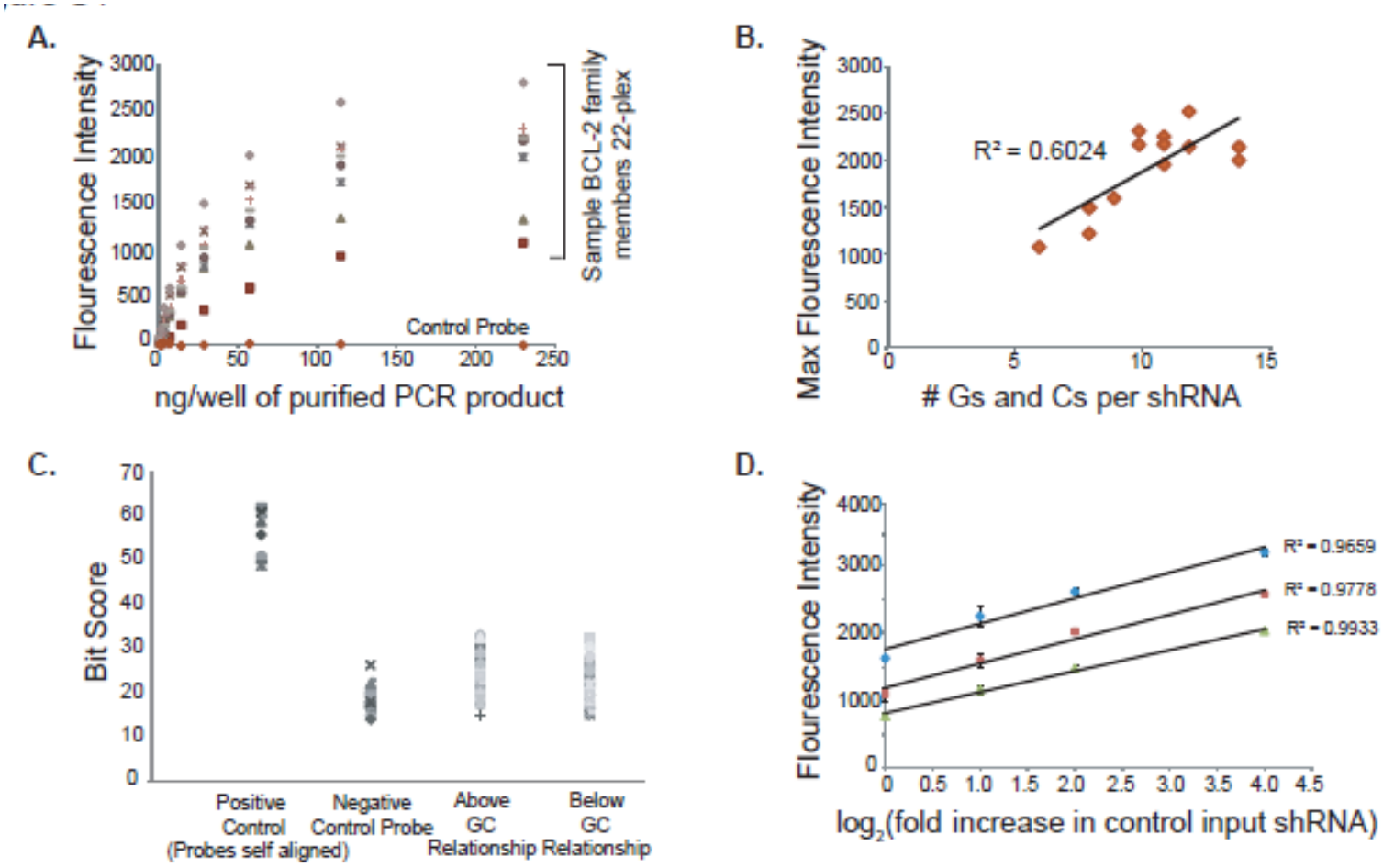

Supplemental Figure S1 - Analysis of the variation in probe maximum flourescence intensity. (A) Representative curves show the range of measurement for shRNAs targeting multiple members of the BCL-2 family in a 22-plex experiment with pooled plasmid DNA. A control sequence that is not in the 22-plasmid mixture shows little signal.(B) A graph showing the relationship between GC content and the variation maximum flourescence intensity for a given probe. (C) Outliers deviating significantly above and below the relationship depicted in (A) were analyzed for local sequence alignments with the entire shRNA library. These values were compared to values for probes with high local sequence alignments (self aligned probes) and the negative control probe from Figure 1C (D)Purified single hairpin DNA mixed at known ratios was used to examine the measurement resolution of single hairpins in a complex shRNA pool.

shPuma DNA was introduced at 10-80% of the total pool composition. The fluorescence readings of hairpin abundance are plotted against the known fold enrichment. The different linear fits encompass analogous measurements across an 8-fold range of sample concentrations (increasing bottom to top).

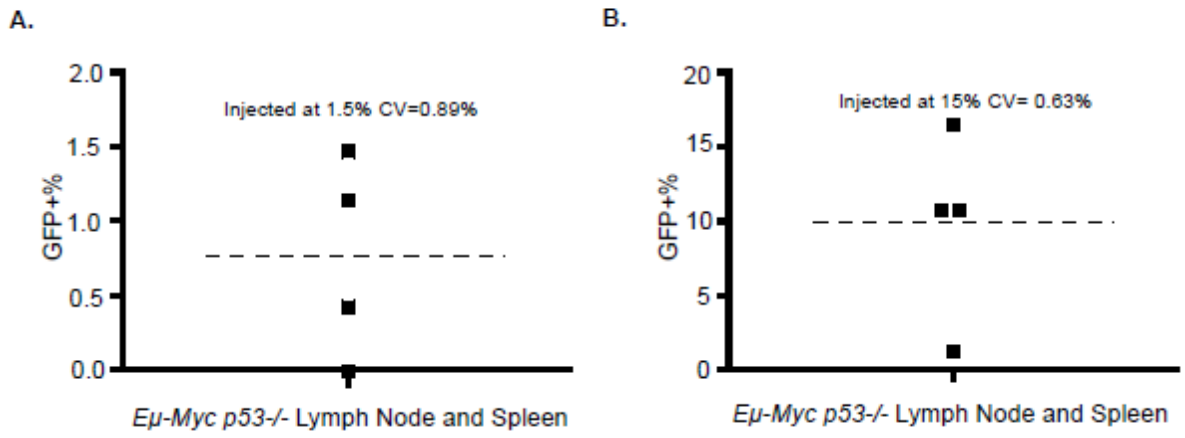

Supplementary Figure S2 - An analysis of the variation in the population of cells expressing a control vector following vincristine treatment in vivo (A) A graph showing the percentage of GFP positive Eμ-Myc p53-/- lymphoma cells following treatment with 1.5mg/kg vincristine in vivo. The input population was infected to (A) 1.5% or (B) 15%. At the presentation of palpable disease, tumors were harvested and analyzed in triplicate. The CV is indicated above each graph and the mean is demarcated with a dashed line.

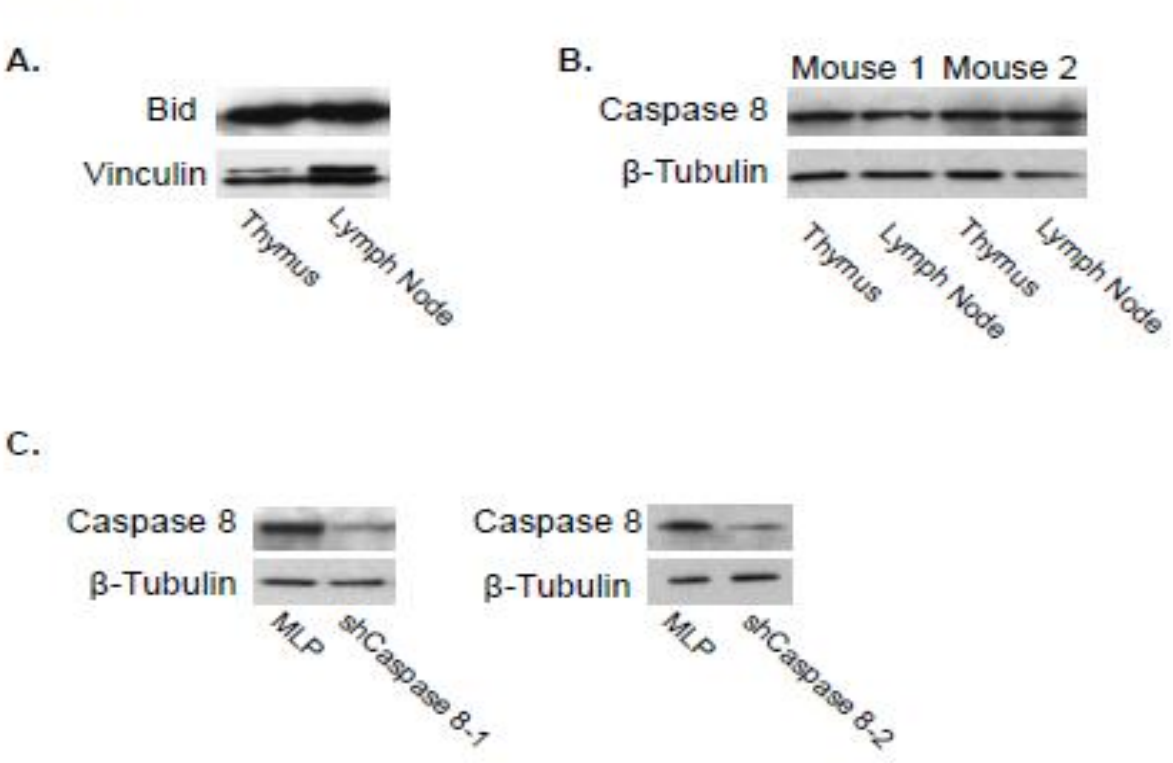

Supplementary Figure S3 - Western blots showing protein levels in distinct tumor sites. (A) A western blot showing Bid levels in tumor-bearing lymph node and thymus. (B) A western blot Caspase 8 levels in tumor-bearing lymph node and thymus. (C) Examination of the protein knockdown conferred by two shRNAs targeting Caspase 8.

Supplementary Figure 4 - Western blots showing shRNA-induced protein knockdown for three pro-apoptotic Bcl-2 family members. A) Western blots of Eμ-Myc lymphoma cells expressing the indicated shRNAs. B) A western blot showing Bim suppression in B-ALL cells.

Lymph Node	Change vs. Untreated	Untreated Integral Score	Treated Integral Score	CV
shNoxa	8.3	32.7	41	0.2
shPuma	8	26.9	34.9	0.24
shBax	5.1	25.9	31	0.4
shMule	-3.5	16.5	13	0.3
shMil1	-4.3	24	19.7	0.25
Thymus				
shBid	11	13.1	24.1	0.4
shBim	10.3	18.7	29	0.25
shPuma	5.4	15.7	21.1	0.33

Supplementary Table S1 - A list of top scoring shRNAs meeting the hit criteria separated by anatomical location. The change versus untreated represents the level of enrichment/depletion, and the coefficient of variation is the mean divided by the standard deviation for the doxorubicin treated cohort.

Conclusions

Annotating the mechanism by which a small molecule exerts a defined effect in a biological system is a difficult and classic problem in both drug discovery and biological research. At a basic level there are two very important sides of this issue that must be simultaneously considered; the spectrum of biochemical interactions elicited by a particular small molecule, and the phenotype of the small molecule. The more resolution and information on both sides of this important problem, the more likely you are to understand the connection between a drug and a phenotype.

In this thesis we explored different ways of interpreting drug mechanisms of action in a multivariate manner. I used phosphoprotein signaling measurements, and RNAi derived phenotypes coupled with supervised and unsupervised learning techniques. In the first chapter we found that a highly pleiotropic compound,17AAG , that interacts with approximately 1-10% of the proteome and exhibits pro and anti-apoptotic functions, can be reverse-engineered by analyzing pro-apoptotic signaling and recreating a select set of these pro-apoptotic effects with more specific kinase inhibitors. In the second chapter, as part of a collaboration, we developed a targeted method utilizing RNAi suppression of key cell death genes to modify therapeutic response and predict mechanisms of action. Later, using that same methodology, I attempted to define a specific concept, “combination drug mechanism of action” where I examined how drugs combine to form combinations of effects. Do they accentuate a single drug’s mechanism of action? Do they elicit a combination of effects? Or do they work in entirely novel ways? I found that highly synergistic combinations potentiated the action of a single drug component compound, and that non-synergistic combinations average extant genetic variation. Interestingly, we never saw a combination with an entirely new mechanism of action. This indicated a surprising simplicity to combination therapy, and suggested that most combinations can be interpreted by single drug genetic differences. As an important extension to other

systems, we found that this averaging affect can be extended to distinct oncogenes, spontaneous mouse models of cancer, and clinical genomics datasets. Finally, we extended our genetic profiling techniques to *in vivo* systems to examine the microenviroment dependence of the frontline chemotherapeutic doxorubicin, and found that the BH3 only family member Bid specifically mediates therapeutic response in the thymus.

In recent years advances in measurement technologies (transcriptomics, proteomics, genomics, metabolomics) have led to higher resolution measurements of drug phenotype. In general for this thesis we have strictly focused on phenotype. Molecular phenotypes are becoming more and more prevalent in both biological and drug discovery. The majority of these approaches have used gene expression analysis and other high dimensional measurements to define novel molecular phenotypes representing a unique gene expression state. These states can be correlated with other biological phenotypes but are not causal descriptions of drug or gene function. I have focused on developing genetic signatures that can causally describe drug function in a manner that is more specific than cell viability. Systematic loss or gain of function can, in principle, be used to alter any phenotype of interest following any perturbation (i.e.cell death, development, inflammatory cytokine release, transcription factor activity). Thus, our approach is extendable to other systems and phenotypes, but for cancer drug discovery we have been primarily interested in cell death. Thus, the pattern that shRNA mediated suppression has on small molecule induced cell death can form a high resolution signature that is causally associated with a phenotype of interest. This molecular phenotype does not just correlate with cell death, but can more specifically define cell death with a higher resolution description of genetic events that perturb it in response to a small molecule. These descriptions allow more specific distinctions in the type of cell death that can occur following drug treatment, suggesting that molecular signatures of causal alterations provide high resolution signatures of drug action. I would propose that the extension of genetic phenotype profiling to other areas of

cell and molecular biology should facilitate important distinctions in many common phenotypes and could accelerate mechanistic discovery by providing higher resolution.

Unfortunately, a more specific description of the mammalian cell death phenotype, though it may be used to predict mechanism of action, does not suggest a biochemical mechanism in the absence of a reference set. Therefore, molecular phenotyping and comprehensive biochemical datasets will need to be used in tandem to identify the relevant molecular events for a specific cell death phenotype involving un-characterized compounds. For instance, databases involving kinase activity assays/binding assays for large fractions of the kinome are now publically available [1,2]. These datasets provide a rich resource for understanding the spectrum of the biochemical events that a drug can have. However, in order to understand which biochemical events lead to a cell death phenotype, functional signatures may provide mechanistic groupings between compounds which can then be explored for common biochemical effects. For instance, in chapter 2 we showed that kinase inhibitors work by at least three distinct mechanisms in E*u-Myc*$^{Arf\ -/-}$ lymphoma cells. These 3 functionally distinct mechanisms are probably the result of three independent modalities of kinase inhibition. Mining comprehensive kinase datasets may provide biochemical resolution and help identify a kinase or a set of kinases that can be utilized to produce these functionally distinct biological phenotypes in a manner that is somewhat analogous to chapter one.

Biological investigation or high throughput screening using our shRNA signatures may require us to enhance our phenotypic resolution and our informatics approach. This would be important to both define new drug categories and subdivivde established categories. From a bioinformatic perspective, when analyzing groups with unknown parameters there are many difficulties and questions:(what is the true drug category definition in shRNA space?). It is likely impossible to decide from first principles, or even on a global statistical basis how to accurately subdivide or create specific drug category definitions. As such, data driven methodologies will

have an important place in iteratively deriving the boundaries of a functional category. Furthermore, the goal will likely be to find local solutions (around particular drug mechanisms) using unsupervised methodologies and clustering statistics. This may provide arguments in favor of the alteration of a functional definition, however, co-identification of cohesive biochemical signatures in other large data sets may provide secondary criteria to further sharpen mechanistic boundaries.

From a biological perspective, we lack some degree of biological resolution in many categories. Taxol a tubulin hyperstabilizing agent and Vincristine a tubulin destabilizing agent cluster together (chapter 2, figure 1). Though they both act on the mitotic spindle, they have opposite biochemical effects on their predominant target. Though their mechanisms of cell death may be more similar than other cytotoxic categories, it may be desirable to add resolution between these two types of drugs in the future. Furthermore, in spite of the diverse HDAC binding profiles of HDAC inhibitors, all HDAC inhibitors belong to a single category that is shared with DNA methyl transferase inhibitors like decitabine. Finally, kinase inhibitors may require activated alleles to demonstrate resolution if a kinase target is not expressed in a certain cell line. To this end I would propose that a combination of new model generation, and high throughput screening for hairpins associated with drug category specific effects should allow for the tailored enhancement of current categories when resolution over a drug category becomes a problem.

It may also be possible to add predictors and biological readouts of a non genetic nature. Recently the Stockwell group utilized an approach that they call “modulatory profiling” in their work they examine compound dose response relationships in the presence of a “modulatory” compound [3]. While they lacked considerable resolution amongst DNA damage drugs, they did have considerable success with compounds that worked through non-canonical death

pathways. Interestingly, their approach is similar to work by the Kishony group who showed that drug interactions successfully predicted known drug categories in E. coli. Their data was particularly striking and coherent. All epistatic relationships between one category and another category were entirely uniform in their synergy or antagonism [4]. As such I would also propose that at times, categories that prove problematic may be investigated with small molecule "tool" compounds that have well studied mechanisms affecting diverse biological processes.

In deriving a strategy for defining combination drug mechanisms of action we have combined RNAi based interrogation of biological pathways, and multiple informatics techniques that together demonstrate a simple strategy to compare a signature of a combination of drug's relative to all other single drug signatures. We have used this strategy to investigate long standing hypotheses about combination drug action, and we find that these comparisons yield strikingly simple mechanisms of action. The extremely potent synergies that we examined act like single drugs, and combinations that are pervasive across cytotoxic regimens in a variety of cancers average single drug signatures. Furthermore, this averaging phenotype extends to an unbiased 10,000 shRNA library as well as natural variation in mouse models of cancer and produces diminishing resolution in human clinical data. At its most basic level our data shows a surprising simplicity in "combination drug mechanisms of action". Furthermore, drug averaging implies a simple predictive power in combination signatures. Complex mixtures of diverse population structures with 1- 10,000 alterations in 2 distinct oncogenic contexts effectively average differences in therapeutic response as a weighted sum of their dose contribution. This is not the result of having an absence of an effect, since the depletion of an shRNA in response to a drug can counterbalance the enrichment of an shRNA in response to a second drug and allow for the higher dosing and the suppression of an shRNA phenotype. This result is even more surprising in light of the fact that many of these drugs activate and signal through overlapping sets of stress response cascades, their direct molecular events occur with variable

pharmacokinetics, and the cellular arrest in response to stress occurs at a variety of cell cycle stages. Therefore, the potential combinatorial complexity of combination therapy dosings, and the myriad of molecular events downstream of drug action can lend themselves to unexpectedly simple principles for the interpretation of combination drug mechanisms of action that are true across oncogenic backgrounds even if particular dependencies are cell line specific.

Specifically, our averaging data suggests a surprising simplicity to multidrug mechanisms of action and response to mixed populations at many scales. We propose that given a vector N describing all *i* variants in a population [N_1…….N_i] and a vector F_d describing the relative fitness advantage of the *i* variants for a given drug d_i [F_1……F_i], that many combinations, and even clinically used regimens simply average F_d across different drugs. Furthermore, this average is weighted based upon the total contribution to overall killing by a given combination, such that for the N_1 variant its fitness F_1 in the case of a drug combination C_d and is the sum of the proportional killing contributed by each individual drug in the combination. Thus the fate of N_1 is just fractional contribution of each drug in *C* times F_1. Furthermore the weightings implied by *C* appear to be the same for most shRNAs examined. Thus the solution is similar for the entire population of variants. Finally, given a different oncogene with a new F vector the average tends to follow the same relationship. Finally, even highly synergistic combinations that tend to polarize cellular response pick a vector F_d for any given drug. This suggests that the relationship governing the response of a variant in a mixed population is predominantly the same across all hairpins.

Numerous recent and ongoing large-scale efforts have sought to systematically delineate synergistic combinations of drugs for cancer therapy [5]. Yet, despite their ability to identify synergy in cell-based studies, synergistic compounds might fail for a variety of reasons.

They may be synergistic in both tumor and normal cells, leading to toxicity and the absence of a therapeutic window. However, they may also be highly specific to the set of alterations present in a tumor cell [6]. Our functional signatures support the latter conclusion. Synergistic combinations appear to polarize drug response, resulting in shRNA dependencies that favor the mechanism of action of a single drug. The specificity of highly synergistic drug combinations suggests that functional biomarkers of single drug action will help large randomized clinical trials succeed in the face of the heterogeneity in patient populations.

Effective combination therapies have been argued to act by; the minimization of acquired resistance, the existence of cell intrinsic drug synergy, and the maximization of the cumulative drug dose. While increases in the tolerated cumulative drug dose have been demonstrated to be critical to combination success in a variety of cancers [7-9], it is impossible to distinguish dose effects from other proposed mechanisms of action in clinical settings.

The rationale that combination therapies minimize the acquisition of resistance in heterogeneous populations of cells has its roots in the Luria-Delbruck fluctuation experiments of the 1940's[10-13]. If two drugs work independently through distinct mechanisms of action, then resistance requires the acquisition of mutations in distinct drug targets. Consistent with this idea, in tuberculosis and HIV, sequencing studies in drug resistant clinical isolates have shown that pathogens treated with clinical combination regimens tend to follow this path to drug resistance [14,15]. However, genomic and sequencing studies in pre-treatment and relapsed leukemias treated with conventional chemotherapeutic regimens suggest a distinct picture. Relapsed leukemias rarely harbor alterations in genes that are direct biochemical targets of drug action, and selection seems to favor multi-drug resistant cell states [16-18]. In the context of our study, when the suppression of wildtype gene function by RNAi in single versus combination

dosing leads to distinct therapeutic phenotypes, these distinctions are averaged. This averaging occurs for shRNAs that confer either resistance or sensitivity. Our data suggests that downstream mechanisms of cell death are often shared between “independent compounds” and combinations that average genetic dependencies minimize the relative resistance between two drugs, but they also minimize the relative sensitivities.

The basic averaging mechanisms for combination drugs in the face of both introduced and spontaneous variation may represent an unintended consequence of clinical trial design. Genetically unstratified cohorts that are randomly assigned to experimental or control groups are often used to iteratively define combinations that perform better than the previous generation of treatment. While these regimens manifest some of the greatest success stories in decades of cancer research, the lack of relevant molecular information during their inception has served to shape regimens that are broadly useful across diverse patients rather than tailored to “driving” cancer lesions. We suggest that some subsets of patients may only respond to subsets of drug regimens. An implication of this is that averaging combinations may have a fundamental incompatibility with personalized medicine. This hypothesis is further supported by our analysis of microarray data from large clinical cohorts.

Our data suggest some very specific ideas for combination therapy. The first is that highly synergistic combinations will require a companion biomarker to maximize the likelihood of success in a clinical trial. Though this seems difficult given the relative lack of drug efficacy biomarkers, our data suggests a parsimony to biomarker discovery: biomarkers of single drugs will be sufficient to stratify combination therapy response. The predictive nature of the averaging phenotype suggests a similar simplicity in combination therapy: that combinations may be designed to account for this averaging phenomena, and that single drug genetic dependencies will be sufficient for regimen design.

We think the principles governing combination action create entirely new opportunities in personalized medicine. Beyond giving the right drug to the right patient, the predictability of mixed populations of cells in response to combinations of drugs allows for the explicit calculation of the trajectory of a population of cancer cells in response to a combination therapy. Given equally potent drugs and a heterogeneous population of cancer cells with known single drug responses, we expect that it will be possible to compute solutions that can minimize drug resistance over all variants of that population, or that purposely select for a particular mode of resistance to combination therapy. This is especially interesting in light of the fact that resistance to therapy can be detected at diagnosis [16,18] [19,20]since the detection of resistant subpopulations prior to therapy, and single drug responses average for most combinations, it may be possible to give the personalized combinations that minimize the outgrowth of resistant clones at the outset of diagnosis.

Finally in chapter 4 we examined the influence of the microenvironment on genetic signatures. Interestingly, across multiple genotypes and microenvironments, we always noted a dependence on an activating BH3 family member (Bid, Bim, or Puma) These microenvironmental screens gave snapshots of the relevant BCL-2 family players in the thymic microenviroment. Though we were not able to identify the cell type or cytokine responsible for Bid activation in the thymus, we were able to show the thymic specificity of the genetic effect (chapter 4). The emergence of a BH-3 only domain BCL-2 family dependency is especially interesting in light of two findings: 1. The thymus has a net pro-survival effect for the cancer cells residing inside of it, such that ablation of the thymus improves therapeutic response [21] and 2. the removal of the thymus eliminates Bid's effect on tumor free survival. Clearly these results suggest a balance of pro and anti-apoptotic factors regulate response to therapy in the thymic niche. Disrupting the balance either way can affect therapeutic response, but it is interesting to note that pro survival thymic signals upregulate BCL-xL. Therefore it is intriguing to speculate

that altering the anti-apoptotic load may reveal new BCL-2 family genetic dependencies that are not measurable at the basal state, and require an intact *in vivo* niche.

Importantly, in reference to the discussion regarding the predictable effects of drug combinations in chapter 3, it will be critical to examine the genetic principles by which combinations of drugs interact *in vivo.* The emergence of a Bid phenotype specifically *in vivo*, suggests that the microenvironment creates neomorphic effects in drug signatures. Direct studies of combination drug effects on genetic variants *in vivo* will be necessary to understand whether the genetic principles of combination action that we derived *in vitro* extend to genetic dependencies that are created by treatment in specific microenvironmental niches *in vivo*.

References

1 Anastassiadis, T., Deacon, S. W., Devarajan, K., Ma, H. & Peterson, J. R. Comprehensive assay of kinase catalytic activity reveals features of kinase inhibitor selectivity. *Nature biotechnology* **29**, 1039-1045, doi:10.1038/nbt.2017 (2011).

2 Davis, M. I. *et al.* Comprehensive analysis of kinase inhibitor selectivity. *Nature biotechnology* **29**, 1046-1051, doi:10.1038/nbt.1990 (2011).

3 Wolpaw, A. J. *et al.* Modulatory profiling identifies mechanisms of small molecule-induced cell death. *Proceedings of the National Academy of Sciences of the United States of America* **108**, E771-780, doi:10.1073/pnas.1106149108 (2011).

4 Yeh, P., Tschumi, A. I. & Kishony, R. Functional classification of drugs by properties of their pairwise interactions. *Nature genetics* **38**, 489-494, doi:10.1038/ng1755 (2006).

5 Borisy, A. A. *et al.* Systematic discovery of multicomponent therapeutics. *Proceedings of the National Academy of Sciences of the United States of America* **100**, 7977-7982, doi:10.1073/pnas.1337088100 (2003).

6 Lehar, J., Krueger, A. S., Zimmermann, G. R. & Borisy, A. A. Therapeutic selectivity and the multi-node drug target. *Discov Med* **8**, 185-190 (2009).

7 Frei, E., 3rd, Elias, A., Wheeler, C., Richardson, P. & Hryniuk, W. The relationship between high-dose treatment and combination chemotherapy: the concept of summation dose intensity. *Clinical cancer research : an official journal of the American Association for Cancer Research* **4**, 2027-2037 (1998).

8 Budman, D. R. *et al.* Dose and dose intensity as determinants of outcome in the adjuvant treatment of breast cancer. The Cancer and Leukemia Group B. *Journal of the National Cancer Institute* **90**, 1205-1211 (1998).

9 Frei, E., 3rd. Curative cancer chemotherapy. *Cancer research* **45**, 6523-6537 (1985).

10 Luria, S. E. & Delbruck, M. Mutations of Bacteria from Virus Sensitivity to Virus Resistance. *Genetics* **28**, 491-511 (1943).

11 Newcombe, H. B. & Hawirko, R. Spontaneous Mutation to Streptomycin Resistance and Dependence in Escherichia Coli. *J Bacteriol* **57**, 565-572 (1949).

12 Law, L. W. Origin of the resistance of leukaemic cells to folic acid antagonists. *Nature* **169**, 628-629 (1952).

13 Frei, E., 3rd *et al.* A comparative study of two regimens of combination chemotherapy in acute leukemia. *Blood* **13**, 1126-1148 (1958).

14 Almeida Da Silva, P. E. & Palomino, J. C. Molecular basis and mechanisms of drug resistance in Mycobacterium tuberculosis: classical and new drugs. *J Antimicrob Chemother* **66**, 1417-1430, doi:10.1093/jac/dkr173 (2011).

15 Durant, J. *et al.* Drug-resistance genotyping in HIV-1 therapy: the VIRADAPT randomised controlled trial. *Lancet* **353**, 2195-2199 (1999).

16 Mullighan, C. G. *et al.* Genomic analysis of the clonal origins of relapsed acute lymphoblastic leukemia. *Science* **322**, 1377-1380, doi:10.1126/science.1164266 (2008).

17 Mullighan, C. G. *et al.* CREBBP mutations in relapsed acute lymphoblastic leukaemia. *Nature* **471**, 235-239, doi:10.1038/nature09727 (2011).

18 Ding, L. *et al.* Clonal evolution in relapsed acute myeloid leukaemia revealed by whole-genome sequencing. *Nature* **481**, 506-510, doi:10.1038/nature10738 (2012).

19 Nardi, V. *et al.* Quantitative monitoring by polymerase colony assay of known mutations resistant to ABL kinase inhibitors. *Oncogene* **27**, 775-782, doi:10.1038/sj.onc.1210698 (2008).

20 Snuderl, M. *et al.* Mosaic amplification of multiple receptor tyrosine kinase genes in glioblastoma. *Cancer Cell* **20**, 810-817, doi:10.1016/j.ccr.2011.11.005 (2011).

21 Gilbert, L. A. & Hemann, M. T. DNA damage-mediated induction of a chemoresistant niche. *Cell* **143**, 355-366, doi:10.1016/j.cell.2010.09.043 (2010).